Vol. 289, No. 1, April 20, 1994

ISSN 0003-2670

ANALYTICA CHIMICA ACTA

An international journal devoted to all branches of analytical chemistry

Editors: Harry L. Pardue (West Lafayette, IN, USA)
Alan Townshend (Hull, Great Britain)
J.T. Clerc (Berne, Switzerland)
Willem E. van der Linden (Enschede, Netherlands)
Paul J. Worsfold (Plymouth, Great Britain)

Associate Editor: Sarah C. Rutan (Richmond, VA, USA)

Editorial Advisers:

F.C. Adams, Antwerp
M. Aizawa, Yokohama
W.R.G. Baeyens, Ghent
C.M.G. van den Berg, Liverpool
A.M. Bond, Bundoora, Vic.
M. Bos, Enschede
J. Buffle, Geneva
R.G. Cooks, West Lafayette, IN
P.R. Coulet, Lyon
S.R. Crouch, East Lansing, MI
R. Dams, Ghent
P.K. Dasgupta, Lubbock, TX
Z. Fang, Shenyang
P.J. Gemperline, Greenville, NC
W. Heineman, Cincinnati, OH
G.M. Hieftje, Bloomington, IN
G. Horvai, Budapest
T. Imasaka, Fukuoka
D. Jagner, Gothenburg
G. Johansson, Lund
D.C. Johnson, Ames, IA
A.M.G. Macdonald, Birmingham
D.L. Massart, Brussels
P.C. Meier, Schaffhausen
M. Meloun, Pardubice
M.E. Meyerhoff, Ann Arbor, MI
H.A. Mottola, Stillwater, OK
M. Otto, Freiberg
D. Pérez-Bendito, Córdoba
A. Sanz-Medel, Oviedo
T. Sawada, Tokyo
K. Schügerl, Hannover
M.R. Smyth, Dublin
R.D. Snook, Manchester
J.V. Sweedler, Urbana, IL
M. Thompson, Toronto
G. Tölg, Dortmund
Y. Umezawa, Tokyo
J. Wang, Las Cruces, NM
H.W. Werner, Eindhoven
O.S. Wolfbeis, Graz
Yu.A. Zolotov, Moscow
J. Zupan, Ljubljana

ELSEVIER

ANALYTICA CHIMICA ACTA

Scope. *Analytica Chimica Acta* publishes original papers, rapid publication letters and reviews dealing with every aspect of modern analytical chemistry. Reviews are normally written by invitation of the editors, who welcome suggestions for subjects. Letters can be published within **four months** of submission. For information on the Letters section, see inside back cover.

Submission of Papers

Americas

Prof. Harry L. Pardue
Department of Chemistry
1393 BRWN Bldg, Purdue University
West Lafayette, IN 47907–1393
USA

Tel:(+1-317) 494 5320
Fax:(+1-317) 496 1200

Computer Techniques

Prof. J.T. Clerc
Universität Bern
Pharmazeutisches Institut
Baltzerstrasse 5, CH-3012 Bern
Switzerland

Tel:(+41-31) 6314191
Fax:(+41-31) 6314198

Prof. Sarah C. Rutan
Department of Chemistry
Virginia Commonwealth University
P.O. Box 2006
Richmond, VA 23284-2006
USA
Tel:(+1-804) 367 1298
Fax:(+1-804) 367 7517

Other Papers

Prof. Alan Townshend
Department of Chemistry
The University
Hull HU6 7RX
Great Britain

Tel:(+44-482) 465027
Fax:(+44-482) 466410

Prof. Willem E. van der Linden
Laboratory for Chemical Analysis
Department of Chemical Technology
Twente University of Technology
P.O. Box 217, 7500 AE Enschede
The Netherlands
Tel:(+31-53) 892629
Fax:(+31-53) 356024

Prof. Paul Worsfold
Dept. of Environmental Sciences
University of Plymouth
Plymouth PL4 8AA
Great Britain

Tel:(+44-752) 233006
Fax:(+44-752) 233009

Submission of an article is understood to imply that the article is original and unpublished and is not being considered for publication elsewhere. *Anal. Chim. Acta* accepts papers in English only. There are no page charges. Manuscripts should conform in layout and style to the papers published in this issue. See inside back cover for "Information for Authors".

Publication. *Analytica Chimica Acta* appears in 16 volumes in 1994 (Vols. 281–296). *Vibrational Spectroscopy* appears in 2 volumes in 1994 (Vols. 6 and 7). Subscriptions are accepted on a prepaid basis only, unless different terms have been previously agreed upon. It is possible to order a combined subscription (*Anal. Chim. Acta* **and** *Vib. Spectrosc.*).
Our p.p.h. (postage, packing and handling) charge includes surface delivery of all issues, except to subscribers in the U.S.A., Canada, Australia, New Zealand, China, India, Israel, South Africa, Malaysia, Thailand, Singapore, South Korea, Taiwan, Pakistan, Hong Kong, Brazil, Argentina and Mexico, who receive all issues by air delivery (S.A.L.–Surface Air Lifted) at no extra cost. For Japan, air delivery requires 25% additional charge of the normal postage and handling charge; for all other countries airmail and S.A.L. charges are available upon request.

Subscription orders. Subscription prices are available upon request from the publisher. Subscription orders can be entered only by calendar year and should be sent to: Elsevier Science B.V., Journals Department, P.O. Box 211, 1000 AE Amsterdam, The Netherlands. Tel: (+31-20) 5803 642, Telex: 18582, Telefax: (+31-20) 5803598, to which requests for sample copies can also be sent. Claims for issues not received should be made within six months of publication of the issues. If not they cannot be honoured free of charge. Readers in the U.S.A. and Canada can contact the following address: Elsevier Science Inc., Journal Information Center, 655 Avenue of the Americas, New York, NY 10010, U.S.A. Tel: (+1-212) 6333750, Telefax: (+1-212) 6333990, for further information, or a free sample copy of this or any other Elsevier Science journal.
Advertisements. Advertisement rates are available from the publisher on request.

US mailing notice – Analytica Chimica Acta (ISSN 0003-2670) is published 3 times a month (total 48 issues) by Elsevier Science B.V. (Molenwerf 1, Postbus 211, 1000 AE Amsterdam). Annual subscription price in the USA US$ 3035.75 (valid in North, Central and South America), including air speed delivery. Second class postage paid at Jamaica, NY 11431. *USA Postmasters*: Send address changes to Anal. Chim. Acta, Publications Expediting, Inc., 200 Meacham Av., Elmont, NY 11003. Airfreight and mailing in the USA by Publication Expediting.

ANALYTICA CHIMICA ACTA

An international journal devoted to all branches of analytical chemistry

(Full texts are incorporated in CJELSEVIER, a file in the Chemical Journals Online database available on STN International; Abstracted, indexed in: Aluminum Abstracts; Anal. Abstr.; Biol. Abstr.; BIOSIS; Chem. Abstr.; Curr. Contents Phys. Chem. Earth Sci.; Engineered Materials Abstracts; Excerpta Medica; Index Med.; Life Sci.; Mass Spectrom. Bull.; Material Business Alerts; Metals Abstracts; Sci. Citation Index)

VOL. 289 NO. 1 CONTENTS APRIL 20, 1994

(Continued overleaf)

4 ม.ค. 2537

Contents (continued)

ANALYTICA CHIMICA ACTA
VOL. 289 (1994)

ANALYTICA CHIMICA ACTA

An international journal devoted to all branches of analytical chemistry
Revue internationale consacrée à tous les domaines de la chimie analytique
Internationale Zeitschrift für alle Gebiete der analytischen Chemie

Editors: Harry L. Pardue (West Lafayette, IN, USA)
Alan Townshend (Hull, Great Britain)
J.T. Clerc (Berne, Switzerland)
Willem E. van der Linden (Enschede, Netherlands)
Paul J. Worsfold (Plymouth, Great Britain)

Associate Editor: Sarah C. Rutan (Richmond, VA, USA)

Editorial Advisers:

F.C. Adams, Antwerp
M. Aizawa, Yokohama
W.R.G. Baeyens, Ghent
C.M.G. van den Berg, Liverpool
A.M. Bond, Bundoora, Vic.
M. Bos, Enschede
J. Buffle, Geneva
R.G. Cooks, West Lafayette, IN
P.R. Coulet, Lyon
S.R. Crouch, East Lansing, MI
R. Dams, Ghent
P.K. Dasgupta, Lubbock, TX
Z. Fang, Shenyang
P.J. Gemperline, Greenville, NC
W. Heineman, Cincinnati, OH
G.M. Hieftje, Bloomington, IN
G. Horvai, Budapest
T. Imasaka, Fukuoka
D. Jagner, Gothenburg
G. Johansson, Lund
D.C. Johnson, Ames, IA
A.M.G. Macdonald, Birmingham
D.L. Massart, Brussels
P.C. Meier, Schaffhausen
M. Meloun, Pardubice
M.E. Meyerhoff, Ann Arbor, MI
H.A. Mottola, Stillwater, OK
M. Otto, Freiberg
D. Pérez-Bendito, Córdoba
A. Sanz-Medel, Oviedo
T. Sawada, Tokyo
K. Schügerl, Hannover
M.R. Smyth, Dublin
R.D. Snook, Manchester
J.V. Sweedler, Urbana, IL
M. Thompson, Toronto
G. Tölg, Dortmund
Y. Umezawa, Tokyo
J. Wang, Las Cruces, NM
H.W. Werner, Eindhoven
O.S. Wolfbeis, Graz
Yu.A. Zolotov, Moscow
J. Zupan, Ljubljana

Anal. Chim. Acta, Vol. 289 (1994)

ELSEVIER, Amsterdam–London–New York–Tokyo

© 1994 ELSEVIER SCIENCE B.V. ALL RIGHTS RESERVED

0003-2670/94/$07.00

No part of this publication may be reproduced, stored in a retrieval system or transmitted in any form or by any means, electronic, mechanical, photocopying, recording or otherwise, without the prior written permission of the publisher, Elsevier Science B.V., Copyright and Permissions Dept., P.O. Box 521, 1000 AM Amsterdam, The Netherlands.

Upon acceptance of an article by the journal, the author(s) will be asked to transfer copyright of the article to the publisher. The transfer will ensure the widest possible dissemination of information.

Special regulations for readers in the U.S.A. – This journal has been registered with the Copyright Clearance Center, Inc. Consent is given for copying of articles for personal or internal use, or for the personal use of specific clients. This consent is given on the condition that the copier pays through the Center the per-copy fee for copying beyond that permitted by Sections 107 or 108 of the U.S. Copyright Law. The per-copy fee is stated in the code-line at the bottom of the first page of each article. The appropriate fee, together with a copy of the first page of the article, should be forwarded to the Copyright Clearance Center, Inc., 27 Congress Street, Salem, MA 01970, U.S.A. If no code-line appears, broad consent to copy has not been given and permission to copy must be obtained directly from the author(s). The fee indicated on the first page of an article in the issue will apply retroactively to all articles in the journal, regardless of the year of publication. This consent does not extend to other kinds of copying, such as for general distribution, resale, advertising and promotion purposes, or for creating new collective works. Special written permission must be obtained from the publisher for such copying.

No responsibility is assumed by the publisher for any injury and/or damage to persons or property as a matter of products liability, negligence or otherwise, or from any use or operation of any methods, products, instructions or ideas contained in the material herein.

Although all advertising material is expected to conform to ethical (medical) standards, inclusion in this publication does not constitute a guarantee or endorsement of the quality or value of such product or of the claims made of it by its manufacturer.

This issue is printed on acid-free paper.

PRINTED IN THE NETHERLANDS

ELSEVIER

Analytica Chimica Acta 289 (1994) 1–13

ANALYTICA CHIMICA ACTA

Plasticizers for liquid polymeric membranes of ion-selective chemical sensors

Rudolf Eugster, Thomas Rosatzin, Bruno Rusterholz *, Barbara Aebersold, Urs Pedrazza, Denise Rüegg, Angela Schmid, Ursula E. Spichiger, Wilhelm Simon [1]

Department of Organic Chemistry, Swiss Federal Institute of Technology (ETH), Universitätstrasse 16, CH-8092 Zürich, Switzerland

(Received 14th September 1993)

Abstract

A variety of 55 different plasticizers based on various structural elements were investigated in respect to their applicability in liquid polymeric membranes of chemical sensors. The plasticizers and the overall performance of the membrane were judged in respect to the properties of lipophilicity, solubility, exudation and selectivity, respectively. A strategy for the design of plasticizers is derived from theoretical considerations and verified by experiments. The selectivity data were obtained by measurements with a standard Mg^{2+} selective electrode optimized for clinical applications. A plasticizer needs several large alkyl and/or aryl residues to exhibit sufficient lipophilicity. In order to avoid crystallization or exudation, the use of branched alkyl chains as well as the link or the substitution of the structural elements by an adequate number of polar or polarizable groups is encouraged. However, to ensure high selectivities, plasticizers should not contain functional groups which may act as coordination sites and therefore compete with the carrier. In contrast to earlier publications it was observed that other properties than the dielectric constant of the plasticizer are more important for the selectivity of the membrane. A correlation between selectivity coefficient and the dielectric constant of the plasticizer could not be found.

Key words: Sensors; Plasticizers; Liquid polymeric membranes; Ion-selective chemical sensors

1. Introduction

The introduction of high molecular poly(vinylchloride) (PVC) as matrix for the preparation of membranes for ion-selective electrodes [1,2] was a milestone in the development of membrane technology for chemical sensors. This step was subsequently connected with the takeover of many plasticizers known from the industrial PVC processing. In this context several mechanisms for the interaction of the plasticizer with the polymer were offered [3–5]. At that time only little effort was made to adjust the properties of the plasticizers to the requirements of the recognition process. Morf [6] and Simon et al. [7] postulated the impact of the dielectric constant of the membrane on the selectivity (Eq. 1) and therefore introduced *o*-NPOE to enhance the preference

* Corresponding author.

[1] Author deceased, November 1992.

0003-2670/94/$07.00 © 1994 Elsevier Science B.V. All rights reserved
SSDI 0003-2670(94)00018-H

of divalent over monovalent cations of the same radius [6,8].

$$\Delta \log K^{pot}_{MgNa} = \left(\Delta\frac{1}{\epsilon}\right)\frac{Ne^2}{RT \ln 10} \times\left(-\frac{2z^2_{Na}}{2r_{NaS}}+\frac{z^2_{Mg}}{2r_{MgS}}\right) \quad (1)$$

where $\log K^{pot}_{MgNa}$ = selectivity coefficient [(mol $l^{-1})^{-1}$]; N = Avogadro constant ($6.022 \cdot 10^{23}$ mol l^{-1}); ϵ = dielectric constant of the membrane (A^2 s^4 m^{-3} kg^{-1}); e = elementary charge ($1.602 \cdot 10^{-19}$ C); z_{Na} = charge of Na^+ (dimensionless); z_{Mg} = charge of Mg^{2+} (dimensionless); r_{NaS} = radius of the Na^+–ligand complex (m); r_{MgS} = radius of the Mg^{2+}–ligand complex (m); R = gas constant (8.314 J K^{-1} mol^{-1}); and T = absolute temperature (K). In the case of the preference of Mg^{2+} over Ca^{2+}, the dependence on the dielectric constant of the membrane was derived on the basis of the Born equation [9,10].

$$\Delta \log K^{pot,sel}_{MgCa} = \left(\Delta\frac{1}{\epsilon_r}\right)\frac{2Ne^2}{4\pi\epsilon_0 RT \ln 10} \times\left(-\frac{1}{r_{CaS}}+\frac{1}{r_{MgS}}\right) \quad (2)$$

where $K^{pot,sel}_{MgCa}$ = selectivity constant (mol^{-1} l); ϵ_r = relative dielectric constant of the membrane (dimensionless); and ϵ_0 = electrical field constant ($8.854 \cdot 10^{-12}$ A^2 s^4 m^{-3} kg^{-1}). Eq. 2 suggests an increase of the discrimination of larger ion–ligand complexes as ϵ_r increases. Since Ca^{2+} tends to form more voluminous ion–ligand complexes than Mg^{2+} due to its higher complex stoichiometry and its larger ionic radius, plasticizers with high dielectric constants should improve the preference of Mg^{2+} over Ca^{2+}. For example, an increase of ϵ_r from 4 to 18 theoretically induces a change of the selectivity constant $\Delta \log K^{pot,sel}_{MgCa} = -1.32$ for $r_{CaS} = 1.9$ nm and $r_{MgS} = 1.5$ nm (total volume assumption).

In general, the basic requirements for an adequate plasticizer are given by at least four criteria. On one hand a plasticizer must exhibit sufficient lipophilicity, no crystallization in the membrane phase and no exudation in order to guarantee a good membrane performance. On the other hand an optimisation of the selectivities should be achieved for each application.

Oesch and Simon [11] and Dinten et al. [12,13] realized that the lipophilicity of a plasticizer is a critical parameter which may limit the lifetime of a sensor by leaching from the membrane into the surrounding media. Therefore, a start was made to prepare plasticizers of high lipophilicity [14].

In this paper we report on a strategy to build up suitable plasticizers which fulfill all four criteria mentioned above. The syntheses of different compounds are described. They contain structural elements such as branched carbon chains or aromatic rings and/or polar or polarizable groups. Since clinical chemists feel a strong demand for improved Mg^{2+} sensors, a standard Mg^{2+} selective electrode (composition of the membrane see experimental) was chosen to measure the influence of the plasticizer on the selectivity. For this membrane the preference for Mg^{2+} over Na^+, K^+ and H^+ is sufficient for assays in the physiological range whereas a chemometrical correction is still necessary for the calcium interference of about 10% [15]. All data on the structure, nomenclature, synthesis and physical data of the plasticizers as well as their membrane performance and selectivity coefficient are summarized in the Appendix. A thorough discussion of the results is given in respect to earlier explanations.

2. Experimental

2.1. Reagents

For all experiments, doubly quartz-distilled water and chemicals of puriss. or p.a. grade were used. For the preparation of all aqueous salt solutions metal chlorides were used.

2.2. Membrane preparation

The solvent polymeric membranes were prepared according to [16] using 1 wt.% carrier ETH 7025 ([15], Selectophore, Fluka, Buchs), 155 mol% (relative to the ligand) lipophilic anionic sites, 33 wt.% poly(vinyl chloride) (PVC; high molecular

weight; purum p.a., Fluka) and 65–0 wt.% plasticizer and 0–65 wt.% *o*-nitrophenyl octyl ether (*o*-NPOE; Selectophore, Fluka). As lipophilic anionic sites, potassium tetrakis(*p*-chlorophenyl) borate (KTpClPB; purum p.a., Fluka) was incorporated. Commercially available plasticizers were purchased (see Appendix B). The syntheses of the plasticizers which are liquid at room temperature, are given in Appendix B.

2.3. emf Measurements

emf Measurements were carried out at 21 ± 1°C with cells of the following type:

$$Hg\,|\,Hg_2Cl_2\,|\,KCl\ (satd.)\,|\,3\ M\ KCl\,\|\,sample\ solution\,\|\,membrane\,\|\,0.1\ M\ MgCl_2\,|\,AgCl\,|\,Ag$$

For all measurements the membranes were fixed into Philips (Eindhoven) IS 560 electrode bodies. The external half cell was a free-flowing free-diffusion liquid-junction calomel reference electrode [17]. The equipment used for the potentiometric measurements was specified earlier [18]. The measured emf values were corrected for changes in the liquid-junction potential by applying the Henderson formula [19]. The activity coefficients used are described earlier [20]. Selectivity coefficients log K^{pot}_{MgJ} were determined according to the separate solution method (SSM) in 0.1 M unbuffered solutions of the corresponding chloride salts [21].

2.4. Lipophilicity

The lipophilicity, log P, of the plasticizers was determined by thin-layer chromatography (TLC) on reversed-phase silica plates according to the procedure described previously [11,13]. The log P_{TLC} values obtained by this method are closely related to water–*n*-octan-1-ol partition coefficients.

3. Results and discussion

3.1. Physical properties

Plasticizers need to fulfill the four principal criteria mentioned already earlier: high lipophilicity, solubility in the polymeric membrane (no crystallization) as well as no exudation (one phase system) and good selectivity behaviour of the resulting membrane. As documented with a large set of data, the lipophilicity log P_{TLC} of the plasticizers can be enhanced by lengthening the alkyl residues. The hereby induced increase of the melting point and the subsequently observable tendency to crystallize in the membrane at room temperature can to a certain degree be avoided by using branched alkyl residues (compare ETH 5367 or ETH 4302 and ETH 2480 or ETH 4358, respectively, in Appendix C). However, these compounds usually showed exudation (e.g., ETH 5373).

The introduction of alkyl residues with halogen atoms (R_xH_yX) or several functional groups with favourable dipole moments did occasionally lead to compounds with melting points above room temperature (see Appendix A). These plasticizers subsequently always crystallized in the membrane phase (see Appendix C) and were therefore useless. However, a large variety of compounds that fulfill all four criteria mentioned above could be synthesized and are perfectly suitable as plasticizers in membranes of ion-selective chemical sensors.

3.2. Selectivity

All plasticizers containing a carboxylic acid ester preferred monovalent cations, especially Na^+, over Mg^{2+}, except for ETH 5372 (see Appendix C). The same effect can be observed for the discrimination of Ca^{2+} over Mg^{2+} as compared to a reference membrane with *o*-NPOE as plasticizer, except for DOS. Plasticizers containing a hydroxyl group exhibited a similar behaviour. The increase of the plasticizer to *o*-NPOE ratio corresponding to an increase of the concentration of the functional groups usually causes a loss of selectivity, as shown in the case of ETH 264 and ETH 4190 (see Appendix C). The nitric acid ester ETH 8053 showed similar selectivities as membranes with *o*-NPOE. TEHP turned out to prefer alkali ions, especially Li^+. Chloroparaffin and Mesamoll (see Appendix A)

induce selectivity coefficients which are slightly worse than those obtained with *o*-NPOE.

In contrast to alcohols and esters, *o*-nitrophenyl ethers show very good selectivities for Mg^{2+} over Ca^{2+}, Na^+ and K^+. ETH 5373, for example, exhibits a remarkable discrimination of calcium ($\log K^{pot}_{MgCa} = -1.5$). An improvement of the selectivity coefficients can be achieved by increasing the length of the alkyl chains which at the same time increased the lipophilicity.

Unfortunately, the restrictions mentioned above (crystallization, exudation) set a clear limit to the selectivity that can be achieved with this class of plasticizer. However, the examples ETH 5373, ETH 5393 and ETH 2480 demonstrate that mixtures of these extremely lipophilic plasticizers with *o*-NPOE up to a ratio of 4:6 do not exude. A part of the selectivity gain induced by the plasticizer is, however, lost and a selectivity maximum of about $\log K^{pot}_{MgCa} = -1.25$ can be obtained.

As shown with compounds such as FNDPE (see Appendix B) or even chloroparaffin, the introduction of halogens to the molecule does not worsen the membrane performance and this group of plasticizers might therefore carry some potential for improvement.

The following model is proposed to account for the main effects observed so far. Plasticizers may compete with the carrier. They should therefore not contain functional groups which may act as competitive coordination sites. Plasticizers with long alkyl chains are able to separate the polymer chains. That is why they are thought to be excellent plasticizers but on the other hand the weak interaction with the polymer chain is responsible for their tendency to exude. For that reason the use of polymers with less intermolecular interaction or the substitution of the alkyl chains of the plasticizer by polar or polarizable groups is proposed. However, the substitution of PVC by other polymers, e.g., polystyrene–butadiene (PSB), leads to other restrictions such as an increase of the membrane resistance by a factor of 10 or more. In further work we used alkyl chains containing a polar or polarizable group (e.g., phenyl group, multiple bond, halogen) to prevent exudation.

Since a correlation of the selectivity behaviour and the dielectric constant of the membrane was postulated ([6], Eqs. 1 and 2) and since the dielectric constant of a plasticizer corresponds approximately to the square of its dipole moment, plasticizers based on the compounds shown in Table 1 were synthesized. They were expected to show higher dielectric constants than *o*-NPOE. Therefore membranes prepared from those plasticizers should show increasing selectivity coefficients (see Table 1). The results show that ETH 4358 and ETH 8032 which are supposed to exhibit relative dielectric constants in the range of 50 and 30 induce a less distinctive preference of Mg^{2+} over Ca^{2+}, Na^+ and K^+ (see Appendix C). Hence such a simple correlation could not be confirmed.

Even if higher dipole moments are strived for, molecules with the features of an amphoteric ion (e.g., *o*-benzbetaine, dipole moment $\mu = 13.2$ D) may be used. Substitution of the benzene ring is always possible in order to increase the dipole moment [23]. Remembering even the small selectivity loss when changing from *o*-NPOE to chloroparaffin or Mesamoll, one has to question the applicability of Eqs. 1 and 2.

Three reasons should be kept in mind. First, the dielectric constant of the membrane does not necessarily have to correspond exactly to the dielectric constant of the plasticizer due to molecular interaction in the membrane phase [24,25] and ion-pairing. The latter effect, however, does not seem to occur in membranes of high dielectric constants [26]. Secondly, it might be that other effects caused by structural differences of the plasticizer dominate the effects expressed by Eqs. 1 and 2. Thirdly, the only polar membrane solvents used in earlier contributions were nitrophenyl ether compounds whereas the apolar plasticizers always contained other functional groups with potential coordination sites which might compete with the carrier. Therefore, it can not be excluded that the dependence of the selectivity coefficient on the dielectric constant of the membrane, as published by other workers [6–8], was actually caused by the influence of the competing functional groups of the plasticizer used. Nevertheless, Eq. 1 was introduced to explain the facilitated dehydration and generation of the ion–car-

Table 1
Dipole moments, μ, of some selected compounds [22] [the μ values are given in Debye units (1 Debye = $3.33 \cdot 10^{-30}$ Cm)]

Compound	μ (D)	Plasticizer, ETH No. or acronym
3,4-Dinitroaniline	8.9	–
N,*N*-Dimethyl-*p*-nitroaniline	7.1	4332
3,4-Dinitrophenol	7.0	4358
2-Methoxy-4-nitrophenol	6.0	4315
N,*N*-Dimethyl-*p*-toluene-sulfonamide	5.6	8032
Methyl *p*-toluenesulfonate	5.2	8028
Methyl phenyl sulfone	5.0	–
o-Nitroanisol	4.8	*o*-NPOE [a]

[a] Commercially available.

rier complex by a high dielectric constant of the membrane phase and thus makes sense in this respect.

The introduction of polar or polarizable groups prevents these plasticizers from exuding but they all induce somewhat worse selectivities than the analogues without such groups. In the future attention must be paid that only a minimum of polar or polarizable groups is introduced which is necessary to avoid exudation. The more numerous such groups are the more the discrimination of interfering ions decreases. Neither by optimizing plasticizers (see ETH 8045) nor by using mixtures with *o*-NPOE (see ETH 5373), selectivity coefficients for calcium below $\log K^{\text{pot}}_{\text{MgCa}} = -1.25$ could be obtained with membranes which are suitable for a realistic longterm monitoring. However, the selectivity coefficient may be improved to $\log K^{\text{pot}}_{\text{MgCa}} = -1.5$ with the plasticizer ETH 5373. It is noteworthy that the sidechain of this plasticizer is the hydrogenated derivative of the natural phytyl sidechain of chlorophyll *a* and *b* which contribute to a high lipid solubility of chlorophyll. In contrast to BTCU (ETH 2041, see Appendix B), several compounds such as ETH 8045 or ETH 5462 underline the feasibility of increasing the lipophilicity without introducing disturbing functional groups.

Since the experimental results do not depend on the transformation technique used (i.e., potentiometric transformation) the conclusions are valid for all systems based on the same membrane technology and/or the same recognition process.

The correlation between the lipophilicity and the dielectric constant of the plasticizer as well as the dielectric constant of the membrane and the induced selectivities on the other hand, are the topic of a further investigation [27].

4. Conclusions

Based on a large set of examples, simple empirical rules are given to plan the syntheses of plasticizers which fulfill the demands of high lipophilicity, no exudation and no crystallization in PVC membranes. The selectivity can be improved to a large extent by using plasticizers which do not contain functional groups that might compete with the carrier.

More detailed studies are needed which document the correlation between the dipole moment of a functional group and the dielectric constant of the plasticizers. Further clarification may be provided by a thorough investigation of the correlation between the dielectric constant of the whole membrane and the selectivity coefficients measured with it. Up to now, no simple rule can account for all the selectivity modifying effects.

5. Acknowledgements

This work was partly supported by the Swiss National Science Foundation and by Ciba-Corning Diagnostics Co.

6. Appendix A

Structures and physical data of the plasticizers [a] (for the IUPAC nomenclature see Appendix B)

Compound (H substituents not indicated)	Acronym or ETH No.	Substituents	ϵ [b]	log P_{TLC}	m.p. (°C)
Halogen alkanes	Chloroparaffin (ClP)	1-Chloroalkanes	7.9	6.4–9.3	< 25
Alcohol	4190	Dihydrophytol			
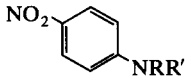	4332	R = methyl, CH_3 R' = decyl, n-$C_{10}H_{21}$			74–76
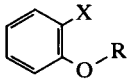	5406	R = octyl, n-C_8H_{17}; X = CF_3			
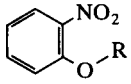 R = C_xH_y	o-NPOE	Octyl, n-C_8H_{17}	23.9	5.8 ± 0.4	
	o-NPPE	Phenyl, C_6H_5			
	217	Dodecyl, n-$C_{12}H_{25}$		8.2 ± 0.6	
	220	Pentadecyl, n-$C_{15}H_{31}$		15 ± 0.1	30–31
	2480	2-Octyldodecyl, $C_{18}H_{37}$			
	2481	2-Octyleicosyl, $C_{28}H_{57}$			
	4314	12-Phenyldodecyl, $C_{18}H_{29}$		11.2 ± 1.5	
	5367	Octadecyl, n-$C_{18}H_{37}$			44–45
	5373	2-(3,7-Dimethyloctyl)-5,9-dimethyldodecyl, $C_{20}H_{41}$		13.5 ± 0.5	
	5382	5-Cholesten, $C_{27}H_{45}$			113–113.5
	5389	Dimethylpentyl, C_7H_{15}			
	5392	3,7,11,15-Tetramethylhexadecyl, $C_{22}H_{45}$			
	8036	4-(*tert.*-Butyl)benzyl, $C_{11}H_{15}$			
	8045	12-(4-Ethylphenyl)dodecyl, $C_{20}H_{33}$		12.8 ± 2	
	8050	2-[(4-*tert.*-Butyl)benzyl]decyl, $C_{21}H_{34}$			
	8059	13,13-Diphenyltridecyl, $C_{25}H_{35}$			
	8063	12-(4-Butylphenyl)dodecyl, $C_{22}H_{37}$			
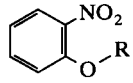 R = C_xH_yX	FNDPE	o-Fluorophenyl, C_6H_4F		2.9 ± 0.2	
	4306	12-Bromododecyl, $C_{12}H_{24}Br$		8.7 ± 1	
	4354	12-Cyanododecyl, $C_{13}H_{24}N$			40–45
	5402	12-(o-Nitrophenoxy)dodecyl, $C_{18}H_{28}NO_2$			65–67
	5408	80 mol% 12-bromooctadecyl, $C_{18}H_{36}Br$ 20 mol% octadecenyl, $C_{18}H_{35}$			
	5462	6-{phenyl[3,5-bis(6-iodohexyl)]}hexyl, $C_{24}H_{39}I_2$		16.1 ± 3	
	8030	12-Iodododecyl, $C_{12}H_{24}I$			38–39
	8031	10-Chlorodecyl, $C_{10}H_{20}Cl$			
	8034	2,6-Dichlorobenzyl, $C_7H_5Cl_2$			129–130
	8035	12-Fluorododecyl, $C_{12}H_{24}F$			
	8037	4-Bromobenzyl, C_7H_6Br			69–70
	8055	12-Nitrododecyl, $C_{12}H_{24}NO_2$			
	8057	12-(4-Octyloxyphenyl)dodecyl, $C_{26}H_{45}O$			
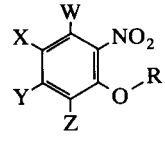	5401	R = dodecyl, n-$C_{12}H_{25}$; X = NO_2			49–51
	7132	R = dodecyl, n-$C_{12}H_{25}$; Y = CF_3		9.7 ± 2	
	8064	R = 12-(4-butylphenyl)dodecyl, $C_{22}H_{37}$; Z = isopropyl, C_3H_7			
	8065	R = 12-(2-isopropyl-6-nitrophenoxy)dodecyl, $C_{21}H_{34}NO_2$; Z = isopropyl, C_3H_7			

Appendix A (continued)

Compound (H substituents not indicated)	Acronym or ETH No.	Substituents	ϵ [b]	log P_{TLC}	m.p. (°C)
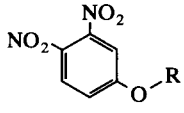	4302	R = dodecyl, n-$C_{12}H_{25}$			49–49.5
	4358	R = 2-(3-methylbutyl)5-methylhexyl, $C_{12}H_{25}$			
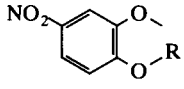	4315	R = dodecyl, n-$C_{12}H_{25}$			53–55
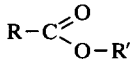	BBPA	Bis(1-butylpentyl) adipate		9.3 ± 0.6	
	DBP	Dibutylphthalate		4.7 ± 0.3	
	DOS	Bis(2-ethylhexyl) sebacate	3.9	11 ± 1	
	264	R = 10-hydroxydecyl R′ = butyl			
	2041	Tetra-n-undecyl benzophenone-3,3′,4,4′-tetracarboxylate	4.9	22 ± 4	
	5372	11-(2-Nitrophenyloxy) undecanoic acid 1-butylpentylester			
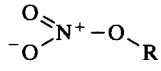	8053	R = 12-(2-nitrophenyloxy)dodecyl, $C_{18}H_{28}NO_3$			
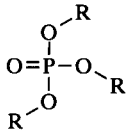	TEHP	R = 2-ethylhexyl, C_8H_{17}	4.8	10.2 ± 0.9	
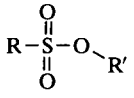	Mesamoll	R = $C_{13}H_{27}$–$C_{17}H_{35}$ R′ = phenyl, C_6H_4		8.1 ± 0.6	
	2485	R = hexadecyl, n-$C_{16}H_{33}$; R′ = 2-nitrophenyl, $C_6H_4NO_2$			58–60
	4305	R = 2-nitrophenyl, $C_6H_4NO_2$; R′ = dodecyl, n-$C_{12}H_{25}$			49.5–51.5
	8028	R = 4-methylphenyl, C_7H_7; R′ = 2-nitrophenyloxydodecyl, $C_{18}H_{28}NO_3$			38–39
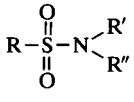	8032	R = 4-methylphenyl, C_7H_7; R′ = methyl, CH_3; R″ = heptyl, n-C_7H_{15}			< 25
	8033	R = 4-methylphenyl, C_7H_7; R′ = H; R″ = dodecyl, n-$C_{12}H_{25}$			73–74

[a] The order is chosen according to increasing number of oxidation, the acronym (alphabetically) and the ETH number (numerically).

[b] All data from [12].

7. Appendix B

The nomenclature of all plasticizers is given below. Furthermore for all not commercially available plasticizers, which are liquid at room temperature (m.p. < 30°C) and show no signs of crystallization in the membrane phase, the syntheses and the data of the elemental analysis are given. The constitutions of all synthesized plasticizers were confirmed by ^{1}H NMR ($CDCl_3$), IR ($CHCl_3$) and mass spectrometry.

Chloroparaffin (Hüls, Marl, Germany) (ClP); 60 wt.% Cl, $\overline{C} = 11.5$.

Bis(1-butylpentyl) adipate (Selectophore, Fluka) (BBPA).

Bis(2-ethylhexyl) sebacate (Selectophore, Fluka) (DOS).

Dibutylphthalate (Selectophore, Fluka) (DBP).

2′-Fluoro 2-nitrodiphenyl ether (Selectophore, Fluka) (FNDPE).

Mesamoll H81 (Bayer, Leverkusen) (alkylsulfonic acid phenyl ester); alkyl chain length $\overline{C} = 13–17$.

o-Nitrophenyl octyl ether (Selectophore, Fluka) (*o*-NPOE).

o-Nitrophenyl phenyl ether (Selectophore, Fluka) (*o*-NPPE).

Tris(2-ethylhexyl) phosphate (Selectophore, Fluka) (TEHP).

ETH 217 (*o*-NPDDE, 2-nitrophenyl dodecyl ether); prepared according to the procedure given for ETH 5373. Anal. calculated for $C_{18}H_{29}NO_3$ (307.43): C 70.32, H 9.51, N 4.56; found C 70.28, H 9.56, N 4.62.

ETH 220 (*o*-NPPDE, 2-nitrophenyl pentadecyl ether); prepared according to the procedure given for ETH 5373. Anal. calculated for $C_{21}H_{35}NO_3$ (349.51): C 72.17, H 10.09, N 4.01; found C 71.92, H 10.11, N 4.19.

ETH 264 (BHDE, butyric acid 10-hydroxydecyl ester); obtained by the reaction of butyric acid chloride (Fluka, purum) with 1,10-dihydroxydecane (Fluka, pract.). Anal. calculated for $C_{14}H_{28}O_3$ (244.37): C 68.81, H 11.55; found C 68.85, H 11.37.

ETH 2041 (Selectophore, Fluka) (BTCU, tetra-*n*-undecyl benzophenone-3,3′,4,4′-tetracarboxylate).

ETH 2480 (2-nitrophenyl 2-octyldecyl ether); prepared according to the procedure given for ETH 8050. Anal. calculated for $C_{24}H_{41}NO_3$ (391.60): C 73.61, H 10.55, N 3.58; found C 73.41, H 10.39, N 3.34.

ETH 2481 (2-nitrophenyl 2-octyleicosyl ether); prepared according to the procedure given for ETH 8050. Anal. calculated for $C_{34}H_{61}NO_3$ (531.87): C 76.78, H 11.56, N 2.63; found C 76.78, H 11.74, N 2.77.

ETH 2485 (hexadecanesulfonic acid 2-nitrophenyl ester).

ETH 4190 (DHP, dihydrophytol, 3,7,11,15-tetramethylhexadecan-1-ol); to a solution of 16.0 g (54 mmol) distilled 3,7,11,15-tetramethyl-2-hexadecen-1-ol (phytol; Fluka, pract.) in 350 ml ethanol (Fluka, puriss. p.a.) 0.14 g platinum(IV) oxide hydrate (≈ 80% Pt; Fluka, puriss.) was added. During 4 h a slow stream of hydrogen was introduced. Then the catalyst was filtered off and the solvent evaporated. The crude product was purified by Kugelrohr distillation (140–150°C, 0.04 Torr) to yield 11.3 g (37.8 mmol. 70.1%) of the product. Anal. calculated for $C_{20}H_{42}O$ (298.55): C 80.46, H 14.18; found C 80.54, H 14.24.

ETH 4302 (3,4-dinitrophenyl dodecyl ether).

ETH 4305 (2-nitrobenzenesulfonic acid dodecyl ester).

ETH 4306 (12-bromododecyl 2-nitrophenyl ether); prepared according to the procedure given for ETH 5373. Anal. calculated for $C_{18}H_{28}NO_3Br$ (386.33): C 55.96, H 7.31, N 3.63; found C 56.09, H 7.43, N 3.46.

ETH 4314 (2-nitrophenyl 12-phenyldodecyl ether); a solution of 7.8 g (50 mmol) bromobenzene (Fluka, puriss.) in 100 ml THF (Fluka, puriss. p.a.) was added dropwise to 1.22 g (50 mmol) magnesium grit (Fluka, purum, 30–55 mesh) at such a rate that the solvent was gently boiling. After additional refluxing for 1.5 h all magnesium had disappeared. Then a solution of 16.41 g (50 mmol) 1,12-dibromododecane (Fluka, puriss.) in 100 ml THF was added dropwise to the reaction mixture and refluxing was continued for 2 h. To complete the reaction a catalytic amount of copper(II) bromide (Fluka, puriss. p.a.) was added and refluxing was continued for 5 h. Then the reaction mixture was diluted with CH_2Cl_2 and washed twice with 0.1 M HCl and H_2O. The

organic phase was dried over $MgSO_4$ and the solvent evaporated. A solution of the crude product (14.9 g), 19.8 g (142 mmol) 2-nitrophenol (Fluka, puriss. p.a.) and 46.3 g (142 mmol) cesium carbonate (Fluka, puriss. p.a.) in 250 ml *N,N*-dimethylformamide (Fluka, puriss. p.a.) was stirred for 4.5 h at 110°C. After cooling to room temperature the reaction mixture was diluted with CH_2Cl_2 and washed several times with 1 M NaOH and H_2O. The organic phase was dried over $MgSO_4$ and the solvent evaporated. The crude product was purified by flash chromatography (550 g silica gel, hexane–ethyl acetate, 9:1) and Kugelrohr distillation (160°C, 0.08 Torr) to yield 3.1 g (8.1 mmol, 17.9%) of pure ETH 4314. Anal. calculated for $C_{24}H_{33}NO_3$ (383.53): C 75.16, H 8.67, N 3.65; found C 74.92, H 8.79, N 3.41.

ETH 4315 (dodecyl 2-methoxy-4-nitrophenyl ether).

ETH 4332 (*N*-decyl-*N*-methyl-4-nitroaniline).

ETH 4354 (12-cyanododecyl 2-nitrophenyl ether).

ETH 4358 [5-methyl-2-(3-methylbutyl)hexyl 3,4-dinitrophenyl ether]; prepared according to the procedure given for ETH 8050. Anal. calculated for $C_{18}H_{28}N_2O_5$ (352.43): C 61.34, H 8.01, N 7.95; found C 62.93, H 8.28, N 7.41.

ETH 5367 (*o*-nitrophenyl octadecyl ether, *o*-NPODE).

ETH 5372 [11-(2-nitrophenyloxy)undecanoic acid 1-butylpentyl ester]; prepared according to the procedure given for ETH 5373 (the synthesis of 11-bromo-(1-butylpentyl)undecanoate is described in [28]). Anal. calculated for $C_{26}H_{43}NO_5$ (467.54): C 69.45, H 9.64, N 3.12; found C 69.51, H 9.70, N 2.99.

ETH 5373 (3,7,11,15-tetramethylhexadecyl 2-nitrophenyl ether); a mixture of 7.0 g (19 mmol) 1-bromo-3,7,11,15-tetramethylhexadecane (prepared from DHP according to standard literature procedure [29], 2.6 g (19 mmol) 2-nitrophenol (Fluka, puriss. p.a.) and 6.2 g (19 mmol) cesium carbonate (Fluka, puriss. p.a.) in 150 ml *N,N*-dimethylformamide (Fluka, puriss. p.a.) was stirred for 2 h at 110°C. After cooling to room temperature the reaction mixture was diluted with CH_2Cl_2 and washed several times with H_2O. The organic phase was dried over $MgSO_4$ and the solvent evaporated. The crude product was purified by flash chromatography (250 g silica gel, hexane–ethyl acetate, 95:5) to yield 5.5 g (13.1 mmol, 69.0%) of pure ETH 5373. Anal. calculated for $C_{26}H_{45}NO_3$ (419.65): C 74.42, H 10.81, N 3.34; found C 74.35, H 11.04, N 3.21.

ETH 5382 [3-β-(2-nitrophenyloxy)-cholest-5-ene].

ETH 5389 (1,1-dimethylpentyl 2-nitrophenyl ether); prepared according to the procedure given for ETH 5373.

ETH 5392 [2-(3,7 dimethyloctyl)-5,9-dimethyldecyl 2-nitrophenyl ether]; prepared according to the procedure given for ETH 5373. Anal. calculated for $C_{28}H_{49}NO_3$ (447.71): C 75.12, H 11.03, N 3.13; found C 75.52, H 11.08, N 2.85.

ETH 5401 (2,4-dinitrophenyl dodecyl ether).

ETH 5402 [2-nitrophenyl-12-(2-nitrophenyloxy) dodecyl ether].

ETH 5406 (octyl 2-trifluoromethylphenyl ether); prepared according to the procedure given for ETH 5373. Anal. calculated for $C_{15}H_{21}OF_3$ (274.32): C 65.68, H 7.72; found C 65.66, H 7.97.

ETH 5408 (12-bromooctadecyl 2-nitrophenyl ether); prepared according to the procedure given for ETH 5373 {1,12-dibromooctadecane was prepared by reducing 12-hydroxyoctadecanoic acid (Fluka, techn.) with $LiAlH_4$ to 1,12-octadecandiol and convertion of this diol to the corresponding dibromide using the method described in [30]}. Anal. calculated for $C_{24}H_{40}NO_3Br$ (470.49): C 61.27, H 8.57, N 2.98; found C 63.12, H 8.92, N 2.89 (The ^1H NMR as well as the elemental analysis showed approximately 20 mol% of 2-nitrophenyl octadecenyl ether).

ETH 5462 [3,5-bis(6-iodohexyl)phenylhexyl 2-nitrophenyl ether]; prepared according to the procedure given for ETH 5373. {1,3,5-Tris(6-iodohexyl)benzene was synthesized according to the method described in [31]}. Anal. calculated for $C_{30}H_{43}NO_3I_2$ (719.49): C 50.08, H 6.02, N 1.95; found C 50.20, H 6.20, N 1.69.

ETH 7132 (dodecyl 2-nitro-5-trifluoromethylphenyl ether); prepared according to the procedure given for ETH 5373. Anal. calculated for $C_{19}H_{28}NO_3F_3$ (375.42): C 60.79, H 7.52, N 3.73; found C 60.75, H 7.66, N 3.73.

ETH 8028 [4-toluenesulfonic acid 12-(2-nitrophenyloxy)dodecyl ester].

ETH 8030 (12-iodododecyl 2-nitrophenyl ether).

ETH 8031 (10-chlorodecyl 2-nitrophenyl ether); prepared according to the procedure given for ETH 5373. Anal. calculated for $C_{16}H_{24}NO_3Cl$ (315.84): C 61.24, H 7.71, N 4.46; found C 61.33, H 7.72, N 4.36.

ETH 8032 (*N*-heptyl-*N*-methyl-4-toluenesulfonamide); obtained by the reaction of toluene-4-sulfonic acid chloride (Fluka, puriss. p.a.) with *N*-heptyl-*N*-methylamine (Fluka, purum). Anal. calculated for $C_{15}H_{25}NO_2S$ (283.43): C 63.56, H 8.89, N 4.94; found C 63.70, H 8.96, N 4.90.

ETH 8033 (*N*-dodecyl 4-toluenesulfonamide).

ETH 8034 (2,6-dichlorobenzyl 2-nitrophenyl ether).

ETH 8035 (12-fluorododecyl 2-nitrophenyl ether).

ETH 8036 (4-*tert.*-butylbenzyl 2-nitrophenyl ether); prepared according to the procedure given for ETH 5373. Anal. calculated for $C_{17}H_{19}NO_3$ (386.14): C 71.56, H 6.71, N 4.91; found C 71.50, H 6.72, N 4.88.

ETH 8037 (4-bromobenzyl 2-nitrophenyl ether).

ETH 8045 [12-(4-ethylphenyl)dodecyl 2-nitrophenyl ether]; prepared according to the procedure given for ETH 4314. Anal. calculated for $C_{26}H_{37}NO_3$ (411.58): C 75.87, H 9.06, N 3.40; found C 76.11, H 9.36, N 3.24.

ETH 8050 [2-(4-*tert.*-butylbenzyl)decyl 2-nitrophenyl ether]; malonic acid diethyl ester (Fluka, puriss.) was reacted with freshly prepared sodium ethanolate and one mol equivalent of 1-octylbromide (Fluka, purum) to give 2-octylmalonic acid diethyl ester. By repeating the same procedure using 4-*tert.*-butylbenzylbromide (Fluka, pract.) instead of 1-octylbromide, 2-(4-*tert.*-butylbenzyl)-2-octylmalonic acid diethyl ester was obtained. Saponification of the diester and decarboxylation gave 2-(4-*tert.*-butylbenzyl)decanoic acid which was reduced with $LiAlH_4$ to the corresponding alcohol. Then the procedure described for ETH 5373 was used to obtain the final product. Anal. calculated for $C_{27}H_{39}NO_3$ (425.61): C 76.20, H 9.24, N 3.29; found C 76.05, H 9.51, N 3.08.

ETH 8053 [nitro-2-(12-nitrooxydodecyloxy)benzene]; 2-nitrophenyl 12-hydroxydecyl ether [prepared by reaction of 2-nitrophenol (Fluka, puriss. p.a.) with 1-bromo-12-dodecanol (Fluka, purum) according to ETH 5373] was reacted with 4-toluenesulfonic acid chloride (Fluka, puriss., p.a.) to give 4-toluenesulfonic acid 12-(2-nitrophenyloxy)dodecyl ester. Reaction of this ester with sodium iodide (Fluka, puriss. p.a.) and silver nitrate (Fluka, puriss. p.a.) in a second step gave the product. Anal. calculated for $C_{18}H_{28}N_2O_6$ (368.43): C 58.68, H 7.66, N 7.60; found C 58.95, H 7.39, N 7.49.

ETH 8055 (12-nitrododecyl 2-nitrophenyl ether).

ETH 8057 [2-nitrophenyl 12-(4-octyloxyphenyl) dodecyl ether]; prepared according to the procedure given for ETH 5373. Anal. calculated for $C_{32}H_{49}NO_4$ (511.75): C 75.11, H 9.65, N 2.74; found C 75.20, H 9.82, N 2.61.

ETH 8059 (13,13-diphenyltridecyl 2-nitrophenyl ether); prepared according to the procedure given for ETH 5373. For the preparation of 1-bromo-13,13-diphenyltridecane see [32]. Anal. calculated for $C_{31}H_{39}NO_3$ (473.66): C 78.61, H 8.30, N 2.96; found C 78.59, H 8.43, N 3.12.

ETH 8063 [12-(4-butylphenyl)dodecyl 2-nitrophenyl ether]; prepared according to the procedure given for ETH 4314. Anal. calculated for $C_{28}H_{41}NO_3$ (439.64): C 76.50, H 9.40, N 3.19; found C 76.25, H 9.51, N 2.92.

ETH 8064 [12-(4-butylphenyl)dodecyl 2-(1-methylethyl)-6-nitrophenyl ether]; prepared according to the procedure given for ETH 4314. Anal. calculated for $C_{31}H_{47}NO_3$ (481.72): C 77.29, H 9.83, N 2.91; found C 77.43, H 9.68, N 2.68.

ETH 8065 {2-(1-methylethyl)-6-nitrophenyl 12-[2-(1-methylethyl)-6-nitrophenyloxy]dodecyl ether}; prepared according to the procedure given for ETH 5373. Anal. calculated for $C_{30}H_{44}N_2O_6$ (528.69): C 68.16, H 8.39, N 5.30; found C 68.44, H 8.04, N 5.05.

8. Appendix C

Properties of the standard Mg^{2+} selective membranes containing the plasticizers shown in Appendix A (composition see Experimental)

ETH No. or acronym [a]	*X*% of 65 wt.% plasticizer [b]	Exudation	Crystallization [c]	log K^{pot}_{MgJ}		
				Ca^{2+} (−2.3) [d]	Na^{+} (−3.7) [d]	K^{+} (−1.0) [d]
Chloroparaffin (ClP)	100	–	–	−0.7	−3.2	−2.6
4190	6	–	–	−0.4	−3.5	−2.2
	15	–	–	+0.1	−2.7	−1.7
	44	–	–	+0.3	−2.5	−1.5
4332	100	–	+	–	–	–
5406	100	+	–	–	–	–
o-NPOE	100	–	–	−1.0	−4.2	−2.8
o-NPPE	100	–	–	−0.8	−3.9	−2.4
217	100	+	–	−1.1	−4.5	−3.1
220	100	–	+	−1.4	−4.5	−3.2
2480	100	+	–	−1.4	−5.1	−3.6
	60	+	–	−1.2	−4.5	−3.4
	25	–	–	−1.2	−4.5	−3.0
2481	100	+	–	–	–	–
4314	100	–	–	−1.1	−4.6	−2.5
5367	100	–	+	–	–	–
5373	100	+	–	−1.5	−5.1	−3.4
	40	+	–	−1.3	−4.9	−3.2
	10	–	–	−1.2	−4.9	−3.0
5382	100	–	+	–	–	–
5389	100	–	–	−1.0	−4.4	−2.8
5392	100	+	–	–	–	–
	50	+	–	−1.3	−5.0	−3.4
	20	–	–	−1.2	−4.8	−3.3
8036	100	–	–	+0.8	−1.0	+1.2
8045	100	–	–	−1.3	−4.5	−3.3
8050	100	+	–	−0.9	−4.1	−3.0
8059	100	–	–	−0.6	−3.2	−1.8
8063	100	+	–	−1.2	−4.3	−3.0
FNDPE	100	–	–	−0.7	−3.9	−2.1
4306	100	–	–	−1.1	−4.8	−3.5
4354	–	+				
5402	100	–	+	–	–	–
5408	100	+	–	−1.2	−4.5	−3.7
5462	100	–	–	−1.0	−4.1	−3.0
8030	100	–	+	–	–	–
8031	100	–	–	−0.9	−4.3	−2.9
8034	100	–	+	–	–	–
8035	100	–	+	–	–	–
8037	100	–	+	–	–	–
8055	100	–	+	–	–	–
8057	100	+	–	−1.0	−4.1	−3.0
5401	100	–	+	–	–	–
7132	100	+	– rather stiff	−1.1	−4.5	−3.0

Appendix C (continued)

ETH No. or acronym [a]	X% of 65 wt.% plasticizer [b]	Exudation	Crystallization [c]	log K^{pot}_{MgJ}		
				Ca^{2+} (−2.3) [d]	Na^{+} (−3.7) [d]	K^{+} (−1.0) [d]
8064	100	+	− inhomogenous	−0.6	−3.2	−2.1
8065	100	−	−	−0.2	−2.3	−0.9
4302	100	−	+	−	−	−
4358	100	−	−	0	−3.2	−2.8
4315	100	−	+	−	−	−
BBPA	100	−	−	+0.0	+2.2	+3.1
DBP	100	−	−	+0.1	+0.8	+2.0
DOS	100	−	−	−1.5	+3.0	+4.0
264	50	−	−	+0.4	+0.6	+1.1
	15	−	−	+0.1	−1.3	−0.3
	5	−	−	−0.2	−2.9	−1.4
2041	100	−	−	−0.2	+1.8	+3.6
5372	100	+	−	−0.2	−2.4	−0.9
8053	100	−	−	−1.1	−4.2	−2.6
TEHP	100	−	−	+1.0	+2.0	+0.8
Mesamoll	100	−	−	−0.8	−3.8	−2.2
2485	100	−	+	−	−	−
4305	100	−	+	−	−	−
8028	100	−	+	0	+1.2	+3.2
8032	100	−	−	−0.2	−2.8	−1.5
8033	100	−	+	−	−	−

[a] For the nomenclature of the plasticizers see Appendix B.
[b] Standard membranes always contained a total amount of 65 wt.% plasticizers; mixtures were made with *o*-NPOE (see Experimental).
[c] +(−) with (without) exudation or crystallization in the given membrane composition.
[d] Required selectivity coefficient for measurements in human blood serum with calibration solutions containing a physiological ion background.

9. References

[1] R. Bloch, A. Shatkay and H.A. Saroff, Biophys. J., 7 (1967) 865.
[2] G.J. Moody, R. Oke and R.B. Thomas, Analyst, 95 (1970) 910.
[3] R. Gächter and H. Müller (Eds.), Taschenbuch der Kunststoff-Additive, Carl Hanser Verlag, München, Wien, 3rd edn., 1986, Chap. 5.
[4] H. Gnamm and G. Fuchs (Eds.), Lösungsmittel und Weichmachungsmittel, Vol. I, Wissenschaftliche Verlag, 8th edn., Stuttgart, 1986.
[5] J.K. Sears and J.R. Darby (Eds.), The Technology of Plasticizers, Wiley, New York, 1982.
[6] W.E. Morf (Ed.), The Principles of Ion-Selective Electrodes and of Membrane Transport, Akadémiai Kiadó, Budapest, 1981.
[7] W. Simon, W.E. Morf and P.C. Meier, Struct. Bonding, 16 (1973) 113.
[8] U. Fiedler, Anal. Chim. Acta, 89 (1977) 111.
[9] M. Born, Z. Phys., 1 (1920) 45.
[10] R. Eugster, Ph.D. Thesis, ETH 9977, Zürich, 1992.
[11] U. Oesch and W. Simon, Anal. Chem., 52 (1980) 692.
[12] O. Dinten, Ph.D. Thesis, ETH 8591, Zürich, 1988.
[13] O. Dinten, U.E. Spichiger, N. Chaniotakis, P. Gehrig, B. Rusterholz, W.E. Morf and W. Simon, Anal. Chem., 63 (1991) 596.
[14] U. Oesch, A. Xu, Z. Brzózka, G. Suter and W. Simon, Chimia, 40 (1986) 351.

[15] R. Eugster, B. Rusterholz, A. Schmid, U.E. Spichiger and W. Simon, Clin. Chem., 39 (1993) 855.
[16] U. Oesch, Z. Brzózka, A. Xu, B. Rusterholz, G. Suter, H.V. Pham, D.H. Welti, D. Ammann, E. Pretsch and W. Simon, Anal. Chem., 58 (1986) 2285.
[17] R.E. Dohner, D. Wegmann, W.E. Morf and W. Simon, Anal. Chem., 58 (1986) 2585.
[18] U. Schefer, D. Ammann, E. Pretsch, U. Oesch and W. Simon, Anal. Chem. 58 (1986) 2282.
[19] P.C. Meier, D. Ammann, W.E. Morf and W. Simon, in M. Koryta (Ed.), Medical and Biological Application of Electrochemical Devices, Wiley, New York, 1980.
[20] P.C. Meier, Anal. Chim. Acta, 136 (1982) 363.
[21] IUPAC, Pure Appl. Chem., 148 (1976) 127.
[22] A.L. McClellan, Tables of Experimental Dipole Moments, Freeman, San Francisco, CA, 1963.
[23] V.J. Minkin, O.A. Osipov and Y.A. Zhdanov, Dipole Moments in Organic Chemistry, Plenum Press, New York, 1970.
[24] R.M. Fuoss, J. Am. Chem. Soc., 61 (1939) 2334.
[25] R.D. Armstrong, A.K. Covington and W.G. Proud, J. Electroanal. Chem., 257 (1988) 155.
[26] R.D. Armstrong, H. Wang and M. Todd, J. Electroanal. Chem., 266 (1989) 173.
[27] M. Nägele, Ph.D. Thesis, Swiss Federal Institute of Technology, Zürich, in preparation.
[28] E. Bakker, M. Lerchi, T. Rosatzin, B. Rusterholz and W. Simon, Anal. Chim. Acta, 278 (1993) 211.
[29] Organikum, Berlin, 18th edn., 1990, p. 188.
[30] A.R. Katritzky, B. Nowak-Wydra and C.M. Marson, Chem. Scr., 27 (1987) 477.
[31] J. O'Donnell, H. Li, B. Rusterholz, U. Pedrazza and W. Simon, Anal. Chim. Acta, 281 (1993) 129.
[32] D. Jagner and J.P. Østergaard-Jensen, Anal. Chim. Acta, 80 (1975) 9.

ELSEVIER

Analytica Chimica Acta 289 (1994) 15–20

ANALYTICA CHIMICA ACTA

A permselective-membrane electrode for the electrochemical study of redox proteins. Application to cytochrome c_{552} from *Thiobacillus ferrooxidans*

Jean Haladjian [a,*], Pierre Bianco [a], Frédéric Nunzi [b], Mireille Bruschi [b]

[a] *Laboratoire de Chimie et Electrochimie des Complexes – Laboratoire de Chimie Bactérienne du C.N.R.S. Case 57, Université de Provence, Place Victor-Hugo, 13331 Marseille Cedex 3, France*

[b] *Laboratoire de Chimie Bactérienne du C.N.R.S., BP 71, 13277 Marseille Cédex 9, France*

(Received 19th July 1993; revised manuscript received 9th November 1993)

Abstract

A simple and effective procedure for electrode construction, based on casting a permselective membrane onto a gold electrode surface is described. A redox protein solution is entrapped between the permselective membrane and the electrode surface. The so-mounted permselective-membrane electrode placed in an electrolyte solution is used to study horse heart cytochrome *c* as a test system. The measured formal potential and the pH dependence profile are in accordance with the literature data. The permselective-membrane electrode is also used to investigate the electrochemistry of cytochrome c_{552} from *Thiobacillus ferrooxidans* and the pH dependence of its formal potential. The performance of this electrode makes it very attractive for studying redox proteins present in limited amounts only.

Key words: Permselective-membrane electrode; Cytochrome *c*; Cytochrome c_{552}; *Thiobacillus ferrooxidans*

1. Introduction

Recent developments [1,2] have shown that electrochemical techniques are powerful means for characterizing electron-transfer properties of biological systems. Metalloproteins and redox enzymes are molecules of particular interest in bioelectrochemistry. Significant advances have been gained especially for direct electron-transfer reactions. Nevertheless, in several cases, a major obstacle can be the very small volumes of protein sample available for investigations. Thin-layer electrochemistry has proved helpful in quantitative studies of electrode reactions with small heterogeneous rate constants [3]. Alternatively, great economy with regard to sample size is afforded if miniaturized cells are used. In this case, the geometry of the cell body and electrode, as well as the position of the electrode within the cell are important factors contributing to overall cell performance.

This article describes the construction, performance and advantages of a permselective-mem-

* Corresponding author.

0003-2670/94/$07.00 © 1994 Elsevier Science B.V. All rights reserved
SSDI 0003-2670(93)E0628-K

brane electrode (PME), in which a small volume of redox protein solution is entrapped between a permselective membrane and the electrode surface. The resulting PME couples the advantages of miniaturization with ease of fabrication and low cost. The analytical performance and reliability of this PM electrode are first evaluated by investigating the electrochemistry of well-known horse heart cytochrome *c* (MW 12 384) as test system. Secondly, our goal was to utilize the PME in an approach to the electron-transfer reactions of another monohemic cytochrome, cytochrome c_{552} extracted from the acidophilic chemolithotrophic bacterium *Thiobacillus ferrooxidans*. This organism is a member of the *Thiobacilli* group of sulfur bacteria and it is considered as the most efficient microorganism used in the commercial extraction of copper and uranium from ores by bioleaching process. *Thiobacillus ferrooxidans* derives its energy from the oxidation of Fe(II) by oxygen at pH 2. The iron oxidation involves an electron transport chain localized in the periplasmic space of the cell [4]. This chain includes several metalloenzymes, among them a *c*-type cytochrome, cytochrome c_{552} (MW 14 000), has been characterized [5]. The midpoint of this protein (measured from potentiometric titrations) is +0.36 V at pH 7.0 [5] but no data exist concerning the voltammetric determination of this cytochrome, especially the pH dependence of the redox potential. Considering the small quantities of available cytochrome c_{552} samples, a good opportunity was offered to investigate the electrochemistry of this protein using the here reported PM electrode.

2. Experimental

2.1. Materials

Horse heart cytochrome *c* (type VI) from Sigma was purified by chromatography on carboxymethylcellulose (CM-52, Whatman) after a published procedure [6]. *Thiobacillus ferrooxidans* cytochrome c_{552} is unstable at neutral pH; therefore, the purification procedure was performed at acidic pH and all steps were carried out at +4°C. The bacterial extract (106 g wet weight) was treated three times with a French press cell and centrifuged at 135 000 *g* for 45 min. The resulting supernatant was dialyzed against 10 mM sodium phosphate buffer at pH 4.8. The dialyzed solution was applied on a carboxymethylcellulose (CMC Waters) (2.5 × 10 cm) equilibrated in the same buffer. Proteins were eluted with 10 mM sodium phosphate + 1 M NaCl buffer at pH 4.8. The resulting fraction was subjected to an hydroxyapatite column (Bio-Gel HTP)(2 × 5 cm) equilibrated with 10 mM sodium phosphate +1 M NaCl buffer at pH 4.8. The elution was performed with 1 M sodium phosphate + 1 M NaCl buffer at pH 4.8. The fraction containing cytochrome c_{552} was loaded onto a Sephadex G50 column (1.2 × 120 cm) equilibrated with 10 mM sodium phosphate + 1 M NaCl buffer at pH 4.8. The cytochrome fraction was dialyzed against 10 mM sodium phosphate buffer to pH 7 and applied to a CMC column equilibrated with the same buffer. The cytochrome (3 mg) was eluted with 25 mM sodium phosphate buffer at pH 7. The pH of the solution was immediately readjusted at 6. The cytochrome was judged to be

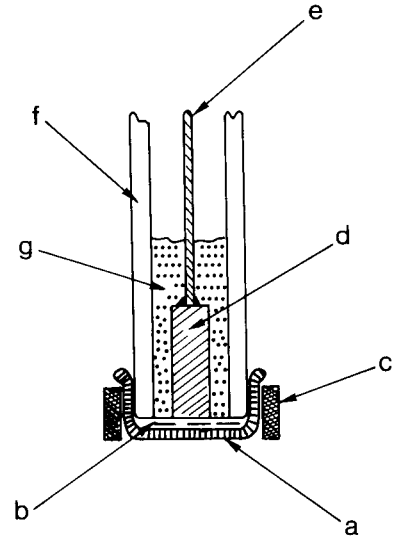

Fig. 1. Scheme of the permselective-membrane working gold electrode. a, permselective membrane; b, entrapped protein solution; c, rubber ring; d, gold cylinder; e, copper wire sealed to the gold cylinder; f, glass tube; g, resin sheath.

pure by sodium dodecyl sulfate polyacrylamide gel electrophoresis and N-terminal sequence determination. The absorption ratio, $A_{552nm(red.)}/A_{280nm(ox.)}$, was 1.05 and the millimolar extinction coefficient at the peak was determined to be 27 mM^{-1} cm^{-1}.

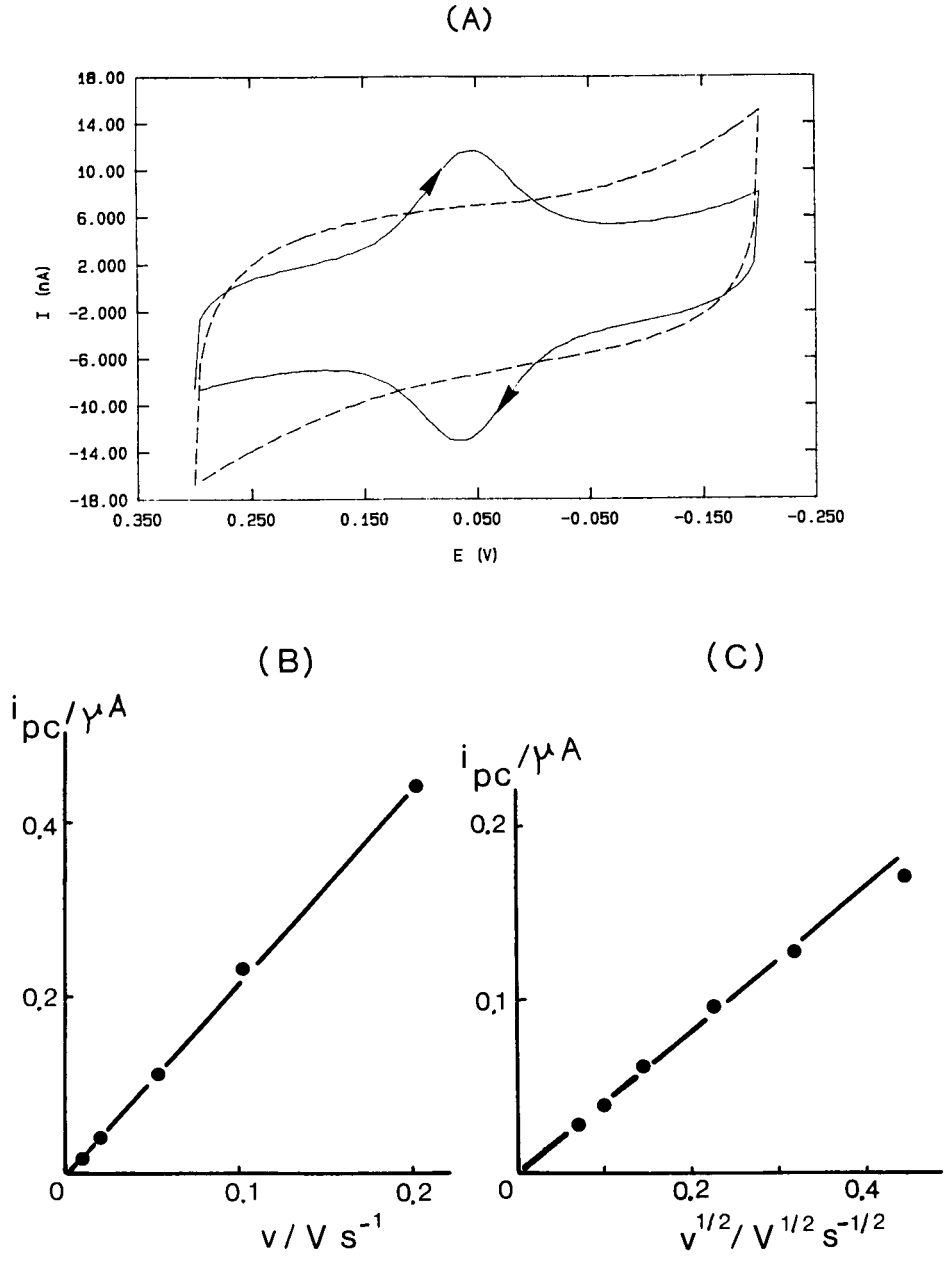

Fig. 2. (A) Cyclic voltammogram at the permselective-membrane gold electrode (modified by 6-mercaptopurine) of 230 μM cytochrome *c*. (– – –) Background solution: 0.1 M phosphate buffer pH 7.5. Scan rate: 10 mV s^{-1}. (B) Scan rate-dependence of the cathodic peak height i_{pc} (see Fig. 2A) at the PME. (C) Scan rate-dependence of the cathodic peak height i_{pc} when the 6-mercaptopurine-modified gold electrode was dipped in the cytochrome *c* solution (without PM).

All other chemicals were reagent grade. Distilled demineralized water was used to prepare all solutions.

2.2. Apparatus

Cyclic (CV) and square-wave (SW) voltammetry experiments were carried out using an EG&G 273A potentiostat modulated by a Hyundai super 386-SE microcomputer with EG and G PARC M270/250 software. SW voltammograms were obtained using SW frequency of 0.25 Hz, scan increment of 10 mV and pulse height amplitude of 25 mV. A three-electrode system consisting of a Metrohm Ag/AgCl (saturated NaCl) electrode, a platinum wire auxiliary and the PM working electrode were used throughout. Unless otherwise specified, all potentials reported are referred to the Ag/AgCl (saturated NaCl) reference electrode; potentials vs. the standard hydrogen electrode (SHE) can be obtained by adding 0.210 V.

The solutions were deoxygenated by bubbling with high-purity nitrogen. All experiments were carried out at room temperature (ca. 25°C).

2.3. Electrode preparation

The permselective-membrane electrode was prepared in a manner very close to that described in [7]. The working gold-disk electrode constructed by inserting a gold wire into a resin casting (exposed area 0.008 cm^2) was first polished with ultrafine emery paper, then modified when necessary using 6-mercaptopurine as promoter (as described in previous work [8]). A small volume (ordinarily 2 μl) of the protein solution was deposited on the electrode surface and covered up with a piece (about twice the diameter of the electrode sensor) of permselective membrane (dialysis membrane Visking PM 6000/8000, 30 μm thick). A rubber ring having a diameter that fitted the electrode snugly was gently pushed around the electrode body so that the entrapped protein solution formed a uniform layer on the electrode surface (Fig. 1). Then the PM electrode was placed into the three-electrode cell containing the supporting electrolyte. Small ions were allowed to diffuse through the permselective membrane but the relatively large molecules of cytochrome remained entrapped in the close vicinity of the gold surface.

3. Results and discussion

3.1. Study of cytochrome c at the PME

A typical cyclic voltammogram obtained at the PME is shown in Fig. 2A for the 230 μM cytochrome *c* solution entrapped between the permselective membrane and the gold electrode. The PME is immersed in 0.1 M phosphate buffer at pH 7.5. The gold surface was modified beforehand using 6-mercaptopurine (see the experimental section). Both cathodic (E_{pc} = +0.056 V) and anodic (E_{pa} = +0.065 V) peaks are symmetrical, the Faradaic current drops to zero after the potential passes through peak potential E_p. The peak current i_{pc} increases linearly with increasing scan rate, v (Fig. 2B), in contrast to the diffusion-controlled behavior (linear $i_{pc} - v^{1/2}$ plot) observed when the modified gold electrode (without the permselective membrane) is simply dipped in the same solution (Fig. 2C). The peak

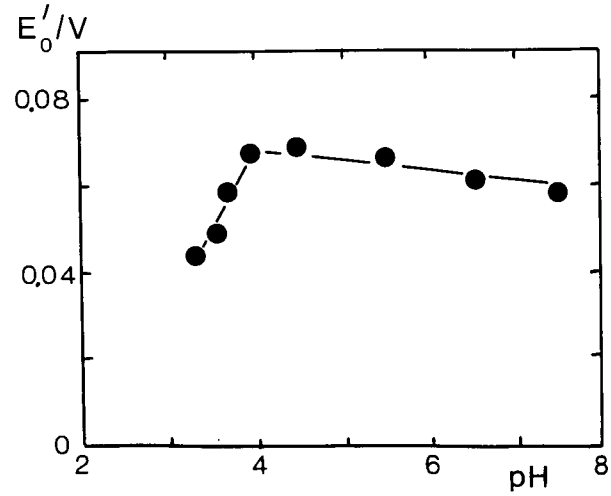

Fig. 3. pH-dependence of the formal potential E_0' of cytochrome *c*. Volume of cytochrome *c* solution deposited on the permselective membrane: 2 μl (see Experimental section).

separation ΔE_p is independent of the cytochrome c concentration and tends to zero when the scan rate decreases, in contrast to the limit value of ≈ 59 mV observed for the diffusion-controlled system. The formal potential evaluated as the mean of E_{pc} and E_{pa} is $E_0' = +0.060$ V in agreement with previous data [9]. These results resemble those obtained in thin-layer voltammetry experiments for fully reversible electrode reaction [3]. Consequently, the concepts of thin-layer voltammetry can be reasonably applied also to voltammetry at the here reported PME. Using the relationship [10]

$$i_p = (9.39 \times 10^5) n^2 v V c$$

a typical volume, V, of 5×10^{-3} μl can be evaluated for the effectively electrolyzed solution. This volume corresponds to a typical layer thickness of approx. 5 μm. In fact this value is only indicative and depends on experiments.

The PME has also been used to investigate the pH-dependence of the redox potential E_0' in the pH range 3–7.5. The peak separation ΔE_p increases when the pH is decreased and poorly-defined voltammograms are attained when the pH is lowered to ~ 3. Our results (Fig. 3) are in good agreement with previous data [8] and confirm that E_0' decreases for pH $\leqslant 4$. It has been proposed that such a behavior results from structural changes in cytochrome c molecule.

3.2. Study of cytochrome c_{552} from T. ferrooxidans at the PME

The preceding approach has been used also for investigating the electrochemical behavior of *T. ferrooxidans* cytochrome c_{552}. A typical cyclic voltammogram and the corresponding SW curve for a 70 μM solution are given in Fig. 4A and B, respectively. In contrast to the case of cytochrome c, it is worth noting that the gold surface does not need to be modified by 6-mercaptopurine for obtaining well-defined voltammograms. Since the peak separation ΔE_p is 35 mV (at 10 mV s $-$ *1*), it can be concluded that cytochrome c_{552} is a quasi-reversible electrochemical system. The mean of cathodic ($E_{pc} =$ $+0.150$ V) and anodic ($E_{pa} = +0.185$ V) CV peak potentials (Fig. 4A) and SWV peak potential ($+0.165$ V) (Fig. 4B) yields a common value of $+0.165$ V (i.e., $+0.375$ V vs. SHE) for the formal potential E_0' of cytochrome c_{552}.

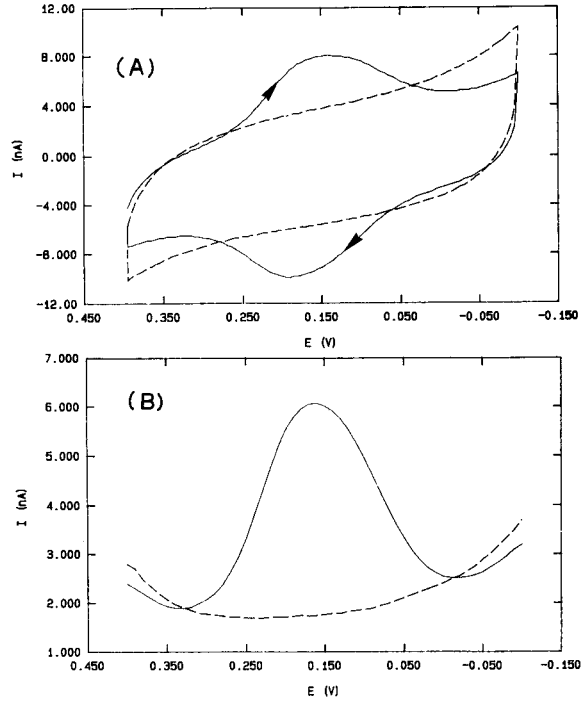

Fig. 4. Cyclic voltammogram (A) and square-wave voltammogram (B) at the permselective-membrane gold electrode of 70 μM cytochrome c_{552} from *Thiobacillus ferrooxidans*. (– – –) Background solution: 0.01 M phosphate buffer pH 6.1. CV scan rate: 10 mV s^{-1}.

The PME was also used for exploring the pH effects (Fig. 5). When pH is decreased from 7 to 4.5, a linear dependence of the formal potential is observed with a slope of 30 mV per pH unit. For a number of c-type cytochromes, changes in redox potential with pH have been observed and interpreted as due to ionizations and/or some structural changes. In the case of cytochrome c_{552}, the slope of the (E_0'–pH) variation is rather unusual and cannot be explained simply in terms of protein chemistry. Our knowledge on the cytochrome c_{552} structure and behavior are at present too limited and require additional data for a satisfactory explanation.

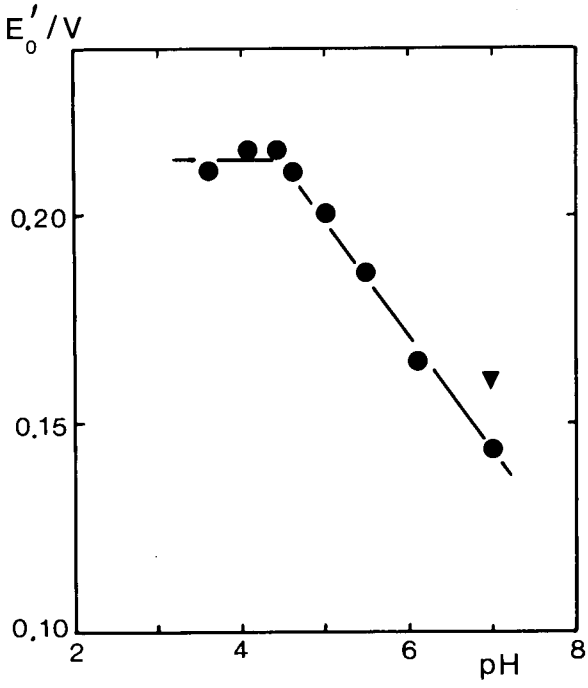

Fig. 5. pH-dependence of the formal potential E_0' of cytochrome c_{552} from *Thiobacillus ferrooxidans*. (▼) Value obtained by Sato et al. [5] from potentiometric measurements.

A constant value is observed for E_0' in the pH range 3.5–4.5 ($E_0' = +0.215$ V). No electrode response is detected at pH $\leqslant 3.5$ but the signals are restored when pH is raised above 3.5. In contrast, the signals tend to disappear for pH values superior to ≈ 7.5 and are not reestablished when coming back to acid pH values, suggesting that cytochrome c_{552} is irreversibly denatured at pH $\leqslant 7.5$. The value given by Sato et al. [5] for E_0' from potentiometric measurements (Fig. 5) is in agreement with the present data.

In conclusion, the here reported PME has been shown to be well-suited for studying very small volumes of solution, and, as a consequence, low amounts of redox protein sample (≈ 1 μg). It offers advantages of miniaturization, simplicity of construction and stability and can operate as a thin-layer cell for the study of other redox protein systems. Studies in this direction are in progress.

4. Acknowledgements

This work was supported by grants from l'Agence de l'Environnement et de la Maîtrise de l'Energie (ADEME, Paris, France), le Bureau des recherches Géologiques et Minières (BRGM, Orléans, France) and la COGEMA (Paris, France). F.N. acknowledges a scholarship from ADEME.

5. References

[1] L.H. Guo and H.A.O. Hill, Adv. Inorg. Chem., 36 (1991) 341.
[2] F.A. Armstrong, Perspect. Bioinorg. Chem., 1 (1991) 141.
[3] A.T. Hubbard and F.C. Anson, in A.J. Bard (Ed.), Electroanalytical Chemistry, Vol. 4, Marcel Dekker, New York, 1970, p. 129.
[4] W.J. Ingledew, Biochim. Biophys. Acta, 683 (1982) 89.
[5] A. Sato, Y. Fukumori, T. Yano, M. Kai and T. Yamanaka, Biochim. Biophys. Acta, 976 (1989) 129.
[6] D.L. Brautigan, S. Ferguson-Miller and E. Margoliash, Methods Enzymol., D53 (1978) 131.
[7] G.G. Guilbault, Methods Enzymol., 137 (1988) 14.
[8] I. Taniguchi, N. Higo, K. Umekita and K. Yasukouchi, J. Electroanal. Chem., 206 (1986) 341.
[9] R.E. Dickerson and R. Timkovich, in P.D. Boyer (Ed.), The Enzymes, Vol. XI-A, Academic Press, New York, 1975, p. 397.
[10] A.J. Bard and L.R. Faulkner, Electrochemical Methods, Fundamentals and Applications, Wiley, Chichester, 1980.

ELSEVIER

Analytica Chimica Acta 289 (1994) 21–26

ANALYTICA CHIMICA ACTA

Potentiometric selective determination of hydrogen sulfide by an electropolymerized membrane electrode based on binaphthyl-20-crown-6

Yi Long Ma [a,1], Ahmed Galal [a,2], Hans Zimmer [a], Harry B. Mark, Jr. *[,a], Zai Fu Huang [b], Paul L. Bishop [c]

[a] *Department of Chemistry, University of Cincinnati, Cincinnati, OH 45221, USA;* [b] *Department of Environmental Science, Wuhan University, Wuhan, Hubei 430072, China;* [c] *Department of Civil and Environmental Engineering, University of Cincinnati, Cincinnati, OH 45221, USA*

(Received 23rd August 1993; revised manuscript received 11th October 1993)

Abstract

A novel potentiometric selective determination method for hydrogen sulfide (HS^-) by an electropolymerized membrane electrode based on a neutral anion carrier, binaphthyl-20-crown-6, has been developed. The potentiometric response is highly dependent on the pH of the solution and the nature of the buffer medium. The response of the polybinaphthyl-20-crown-6 electrode to HS^- has a linear dynamic range between 2×10^{-7} and 2×10^{-5} M with a "super-Nernstian" slope of about 110 mV/decade concentration and a detection limit of 6×10^{-8} M in phosphate buffer (0.1 M, pH 7.5). Other inorganic anions do not interfere with the determination of HS^- and those interfering problems encountered by potentiometric sulfide ion selective electrode have been circumvented. The potentiometric response mechanism towards hydrogen sulfide (HS^-) is discussed and a mechanistic model of the electrode response is given.

Key words: Potentiometry; Hydrogen sulfide; Binaphthyl-20-crown-6; Electropolymerization

1. Introduction

Carriers are used as active membrane components in the design of novel potentiometric selective electrodes for inorganic anions, namely, various derivatives of vitamin B_{12} [1,2] and metalloporphyrins [3–9]. Recently, two potentiometric electrodes based on conducting poly(3-methylthiophene) and poly(tetrakis(*p*-aminophenyl)porphyrin polymer films for iodide were reported [10,11]. Also electrodes developed for organic anions, which are based on lipophilic derivatives of macrocyclic polyamines and calixarene compounds, have been reported [12–14]. Our previous efforts to utilize electropolymerized bi-

* Corresponding author.

[1] Permanent address: Institute of Environmental Medicine, Tongji Medical University, Wuhan, Hubei 430030, China.

[2] Permanent address: The Department of Chemistry, College of Sciences, University of Cairo, Giza, Egypt.

0003-2670/94/$07.00 © 1994 Elsevier Science B.V. All rights reserved
SSDI 0003-2670(93)E0649-R

naphthyl-20-crown-6 as the membrane component in the design of a novel molecule selective electrode have yielded a sensor that exhibited unique and analytically useful selectivity responses for molecules containing 1,2-dihydroxybenzene moieties, such as catecholamines [15,16]. In the present study, we have found that an electrode coated with an electropolymerized binaphthyl-20-crown-6 membrane has an excellent capability of potentiometric selective response to HS^- ion, and it can serve as a promising method to determine hydrogen sulfide gas or sulfide ion in environmental monitoring. The detection technique described in this work is based on potentiometry, a simpler approach than those reported earlier [17].

2. Experimental

2.1. Reagents

The lipophilic macrocyclic crown ether, binaphthyl-20-crown-6 was synthesized in our lab and verified by IR and ^1H NMR [16]. The tetrabutylammonium tetrafluoroborate (TBATFB) was purchased from Aldrich and used as is. The acetonitrile was dried by double distillation over calcium hydride. The phosphate buffer stock solution (pH 7.5, 0.5 M) was prepared with potassium dihydrogenphosphate and the pH was adjusted by addition of KOH or H_2SO_4. The series of standard solutions of sodium sulfide were prepared daily before use.

All chemicals used in the present study were of reagent grade. Deionized water of 17.8 MΩ electrical resistance was used throughout.

2.2. Fabrication of the electrode

The details of the electrode preparation have been described in a previous paper [15]. Briefly, a stationary platinum disk electrode with a 1.6 mm diameter (MF-2012, Bioanalytical Systems) was used as a basic substrate matrix. The polymerization of binaphthyl-20-crown-6 on the platinum electrode was carried out in a three electrode single compartment cell containing 20 mM of binaphthyl-20-crown-6 and 200 mM TBATFB dissolved in freshly distilled acetonitrile. The above mentioned stationary platinum electrode was used as the working electrode, a platinum wire coil as the auxiliary electrode and an Ag/AgCl reference electrode. Electrochemical polymerization was performed with a PAR 175 potentiostat/galvanostat (EG&G Princeton Applied Research) with an applied potential of +3.2 V vs. Ag/AgCl electrode for 5 min. The polymerized electrode was then rinsed with acetone, air dried, and immersed in a three electrode single compartment cell containing a monomer free acetonitrile solution of TBATFB for about 25 min at an applied potential of 0.5 V vs. the Ag/AgCl electrode. This polymerized electrode was then rinsed with water and dried in air about 20 min before use.

2.3. Potential measurement

Potential measurements were made with an Orion Model 601A ionalyzer using a Calomel electrode (Mf-2055, BAS) as the reference electrode. The electrochemical cell used can be represented by: $Hg|Hg_2Cl_2$, KCl(sat.)|phosphate buffer(0.1 M)|polymer film|Pt. The electrode potential was measured in 25 ml of a 0.1 M phosphate buffer solution (pH 7.5) with stirring at 22°C and recorded with a chart recorder. The polymerized electrodes were preconditioned in stirred water until a steady potential was obtained before use. A stepwise addition method was used for the HS^- calibration.

3. Results and discussion

3.1. The pH dependence of the polycrown ether electrode response to sulfide

Fig. 1 shows the pH dependence of the observed potential of the polycrown electrode in 0.1 M potassium phosphate buffer in the presence of 10^{-6} M sodium sulfide. Stable response potentials were obtained in the pH range 6–9. Fig. 2 shows a series of calibration curves of the electrode in solutions of different pH values. As

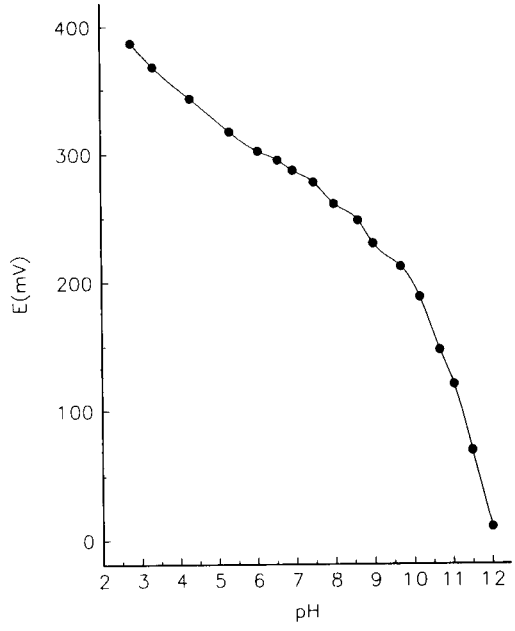

Fig. 1. pH dependence profile of the polybinaphthyl-20-crown-6 electrode (phosphate buffer: 0.1 M).

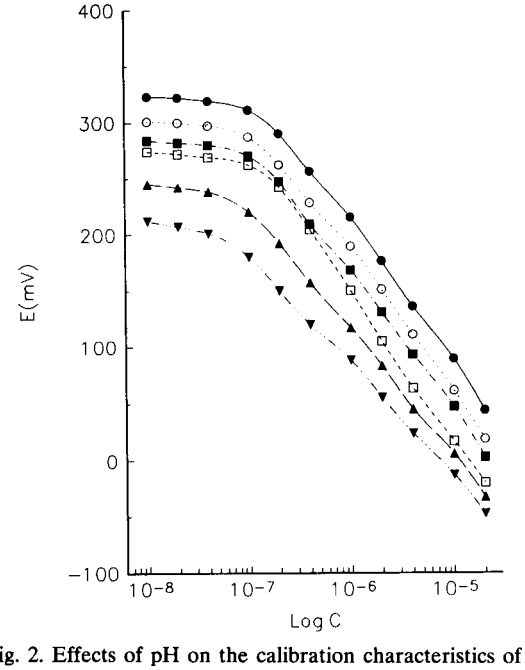

Fig. 2. Effects of pH on the calibration characteristics of the polybinaphthyl-20-crown-6 electrode (phosphate buffer: 0.1 M). ● = pH 6.5, ▲ = pH 8.5, ○ = pH 7.0, ▼ = pH 9.5, ■ = pH 7.5, □ = pH 8.0.

indicated in Fig. 2, the potential responses to the same concentration of sulfide decrease as the pH increases. The response time of the electrode and its recovery after usage improved with pH increases of the buffer. The electrode responded to OH^- at pH > 9.5 with a negative shift in potential reading (Fig. 1). Moreover, the calibration curve characteristics of the electrode showed poor linearity (Fig. 2). If the pH of the solution was lower than 7.0, the detection limit of electrode response was found to decrease. The "best" calibration curve of the electrode was obtained at pH 7.5. As discussed previously, such a high pH dependence suggested that the HS^- ion is the species interacting with the crown ether of the polybinaphthyl-20-crown-6, probably through a hydrogen bond [15].

3.2. Effects of buffer media on electrode response

Fig. 3 shows the effects of different buffer media at the same pH and concentration on the response behaviour of the electrode. This polybinaphthyl-20-crown-6 electrode had the best response performance in the phosphate buffer and the worst in the triethanolamine buffer. The order of preferable buffer media is: phosphate > NH3–NH_4Ac > Tris > DIPSO > triethanolamine. Both the detection limit and response slope of the electrode were found to decrease gradually in that order.

3.3. Performance of the polycrown ether electrode

A typical calibration curve of the electrode is shown in Fig. 4. The electrode has a linear response over the range of 2×10^{-7}–2×10^{-5} M with a super Nernstian response slope of about 110 mM/decade and a detection limit of 6×10^{-8} M.

The typical dynamic response time of the electrode (t_{95}) was about 2 min under stirred conditions as the concentration of sulfide was increased from 2×10^{-7} to 2×10^{-6} M. The steady state potential response after addition of sulfide standard solution remained constant for about 2–5 min, then increased in the positive direction and reached a final steady potential value. The

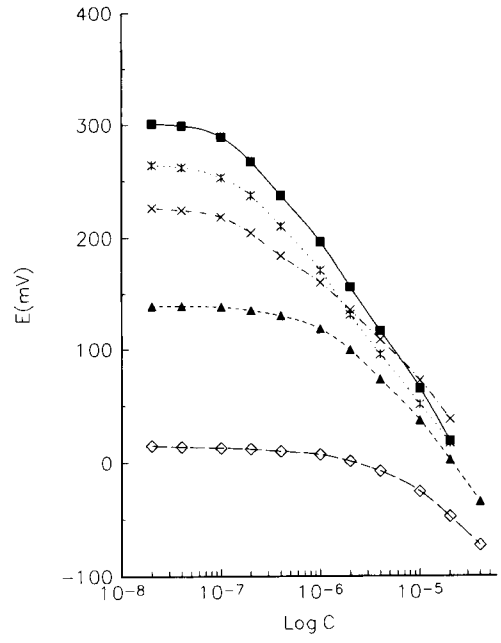

Fig. 3. Effects of different buffer media on the responses of the electrode to HS^{2-}. Buffers: 0.1 M pH 7.5, ■ = phosphate, ▲ = DIPSO, * = NH_3–NH_4Ac, ◇ = triethanolamine, × = Tris.

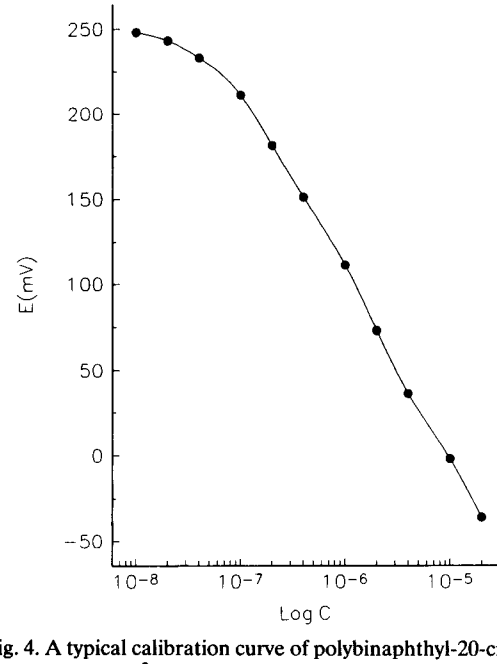

Fig. 4. A typical calibration curve of polybinaphthyl-20-crown-6 electrode for HS^{2-} (phosphate buffer: 0.1 M, pH 7.5).

first steady state responses were used in all experiments in the present study.

The selectivity coefficients of the polycrown ether electrode were determined by the matched potential method [18,19]. The conventional cations did not interfere with the determination of sulfide. The anion selectivity coefficients of the electrode are shown in Table 1.

The anions SCN^-, I^-, $S_2O_3^{2-}$ and Br^- exhibit some interference, but this electrode has excellent potentiometric selectivity toward other anions, F^-, Cl^-, HCO_3^-, Ac^-, No_3^-, NO^{2-}, ClO_4^-, $B_4O_7^{2-}$ and SO_4^{2-}. Compared to the conventional sulfide ion selective membrane electrodes, which used to exhibit serious interferences from the anions I^- and SCN^-, this polybinaphthyl-20-crown-6 electrode has circumvented those problems.

3.4. Possible response mechanism of the polybinaphthyl-20-crown-6 electrode towards hydrogen sulfide

As indicated above, the polybinaphthyl-20-crown-6 electrode has an optimal buffer condition of pH 7.5. Hydrogen sulfide has an acid dissociation constants of $pK_1 = 7.04$ and pK_2 11.96. The dominant form in the solution of pH 7.5 would be HS^-. Therefore, this electrode actually responds to anion HS^-. Fig. 1 has shown that the response of the polybinaphthyl-20-crown-6 electrode to HS^- is highly pH dependent just like its response to catecholamine molecules [15]. As discussed in our previous study, [15], the response mechanism of this electrode to the molecules containing 3,4-dihydroxylbenzene moieties was suggested to be relative to the formation of hydrogen bonds and mononegative charged anions between polycrown ether and guest molecules on the electrode surface. A similar hydrogen bond model is suggested in the present case.

In the case of conventional ion selective electrodes, monovalent ions ($n = 1$) have a Nernstian response slope of 59 mV/decade, and 29 mV/decade for divalent ions ($n = 2$). It corresponds to net charge effects on the surface of the electrode membrane which are one and two respectively. In other words, ion exchange or diffusion between

the membrane phase and the solution phase leads to an unbalanced charge distribution. If one monovalent ion is adsorbed in or out the membrane, it makes the membrane obtain or lose one charge. Thus, the electrode should have a Nernstian slope of 59 mV/decade. If one divalent ion is adsorbed in or out of the membrane, this results in the gain or loss of two charges and the electrode will have an approximate Nernstian slope of 29 mV/decade.

In the present case, the super Nernstian response to HS^- with a slope of 110 mV/decade suggests that the net charge effect on the electrode membrane surface should be one half of a charge, e.g., $n = 0.5$ in the Nernstian equation. Such a half charge effect can be explained as follows. If one ion diffuses into the ion or molecule selective membrane and occupies one ion exchange site (or one receptor molecule), the net charge effect on the membrane surface should be the same charge value. If two ion exchange sites combine with one ion and share one charge, the net charge effect on the membrane surface will be half of the ion charge. Then, we can propose that one HS^- diffuses into the polymer membrane and complexes with two crown ether rings, resulting in half of the net charge effect and a "double" Nernstian response slope.

Recently, Kliza and Meyerhoff [10] summarized four possible potentiometric anion response mechanisms of polyporphyrin derivatives electrodes: (1) ion-exchange process with the anion-doped polymer backbone, (2) ion-exchange resulting from entrapped quaternary ammonium ion supporting electrolyte, (3) redox response at the underlying electrode surface, and (4) redox response due to redox reaction within the conducting polymer. They suggested that the overall potentiometric anions response of the polyporphyrin electrode may result from a combination of each of four mechanisms. The second mechanism is not applicable here as a cationic species can not be present. If the third and/or fourth mechanisms are the dominant pathway, then some redox species may interfere with the potentiometric measurement of the electrode. In the present study, the polybinaphthyl-20-crown-6 electrode exhibits a very poor response towards many anions. Thus, the first mechanism is more likely to be the response mechanism (Fig. 5). EDA studies had previously shown that K^+ is incorporated in the crown as expected [15]. Thus, as HS^- diffuses into the polymer film, the hydrogen terminal of the HS^- forms the hydrogen bond with the oxygen of the crown ether and the sulfur terminal complexes with K^+ of another crown by ion pair, resulting in a double Nernstian response.

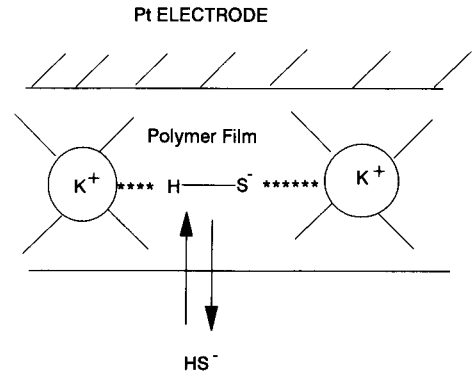

Fig. 5. A possible response mechanism model for HS^- response.

Table 1
Selectivity coefficients of hydrogen sulfide electrode

Anion	log K_{ij}^{pot}	Anion	log K_{ij}^{pot}
F^-	−5.0	SCN^-	−3.1
Cl^-	−4.5	NO_3^-	−4.1
Br^-	−3.7	NO_2^-	−4.1
I^-	−3.5	ClO_4^-	−6.4
HCO_3^-	−4.4	$B_4O_7^-$	−4.6
Ac^-	−4.0	$S_2O_3^-$	−3.6
		SO_4^-	−6.0

4. Acknowledgement

This research was supported in part by a grant under the Superfund Basic Research Program from the National Institute of Environmental Health Sciences and the Department of Chemistry of the University of Cincinnati.

5. References

[1] P. Schulthess, D. Ammann, B. Kraulter, C. Caderas, R. Stepanek and W. Simon, Anal. Chem., 57 (1985) 1397.
[2] P. Schulthess, D. Ammann, W. Simon, C. Caderas, R. Stepanek and B. Krautler, Helv. Chim. Acta, 67 (1984) 1027.
[3] N.A. Chaniotakis, A.M. Chasser, M.E. Meyerhoff and J.T. Groves, Anal. Chem., 60 (1988) 185.
[4] D. Ammann, H. Huser, B. Krautler, B. Rusterhoz, P. Schulthess, B. Lindemann, E. Halder and W. Simon, Helv. Chim. Acta, 69 (1986) 849.
[5] A. Hodinar and A. Jyo, Chem. Lett., 6 (1988) 993.
[6] N. Chaniotakis, S. Park and M. Meyerhoff, Anal. Chem., 61 (1989) 566.
[7] D. Brown, N. Chaniotakis, I. Lee, S. Ma, S. Park and M. Meyerhoff, Electroanalysis, 1 (1989) 477.
[8] S. Park, W. Matuszewski, M. Meyerhoff, Y. Liu and K. Kadish, Electroanalysis, 3 (1991) 909.
[9] S. Dounert, S. Wallace, A. Florido and L. Bachas, Anal. Chem., 63 (1991) 1676.
[10] D.M. Kliza and M.E. Meyerhoff, Electroanalysis, 4 (1992) 841.
[11] A.E. Karagozler, O.Y. Atama, A. Galal, Z.-L. Xue, H. Zimmer and H.B. Mark, Jr., Anal. Chim. Acta, 248 (1991) 163.
[12] Y. Umezawa, M. Kataoka, W. TaTakami, E. Kimura, T. Koike and H. Nada, Anal. Chem., 60 (1988) 2392.
[13] Y. Umezawa, M. Sugawara, M. Kataoka and K. Odashima, 5th Symposium on Ion-Selective Electrodes, Pergamon, Oxford, 1989, pp. 211–234.
[14] K. Odushima, K. Yagi, K. Tohda and Y. Umezawa, Anal. Chem., 65 (1993) 1074.
[15] Y.-L. Ma, A. Galal, H. Zimmer, H.B. Mark, Z.-F. Wang and P.L. Bishop, Anal. Chem., in press.
[16] F. Wang, Y.-L. Ma, X. Hu and Z.-F. Wang, Anal. Chem., (Chin.), in press.
[17] D.G. Taylor, NIOSH Manual of Analytical Methods, 3rd edn., U.S. Dept. of Health and Human Services, Washington, DC, 1984.
[18] K. Srinivasan and G.A. Rechnitz, Anal. Chem., 41 (1969) 1203.
[19] V.P.Y. Gadzekpo and G.D. Christia, Anal. Chim. Acta, 164 (1984) 279.

ELSEVIER

Analytica Chimica Acta 289 (1994) 27–34

ANALYTICA CHIMICA ACTA

Analysis of metabolites in sweat as a measure of physical condition

Kohji Mitsubayashi [1], Masayasu Suzuki [2], Eiichi Tamiya [3], Isao Karube *

R.C.A.S.T. (Research Center for Advanced Science and Technology), University of Tokyo, 4-6-1, Komaba, Meguro-ku, Tokyo 153, Japan

(Received 15th February 1993; revised manuscript received 15th November 1993)

Abstract

Sweat samples induced by heating, exhaustive exercise and endurance exercise, were collected from several healthy subjects. Analysis of the metabolites in sweat was performed using either amperometric biosensors, constructed from a dissolved oxygen sensor and immobilized enzyme membranes, or commercial ion-selective electrodes. The average concentrations of lactate and ammonium ion measured in sweat induced by exhaustive exercise were 115.8 and 90.5 mM respectively, 5.2 and 10.6 times higher than the results obtained from heat induced sweat. This contrasted with only a 2.0 and 3.0 fold increase following endurance exercise. The lactate concentration in sweat was found to be linearly related to the concentration of ammonium ion, with a slope of 1.07 ([ammonium ion]/[lactate], $r = 0.996$, lactate range of 16.1 to 110.3 mM). In view of these results, lactate and ammonium ion in sweat were shown to be related to an increase in anaerobic metabolism, involving the glycolysis pathway and purine nucleotide cycle (PNC). It was demonstrated that the analysis of both lactate and ammonium ion in sweat is an effective, non-invasive and convenient method for estimation of physical condition.

Key words: Ion selective electrodes; Biosensors; Lactate; Oxygen sensors; Sweat; Ammonium

1. Introduction

The increasing desire to naturally enhance the performance of sportsmen and athletes through evaluation of their training regime, requires an in situ estimation of physical and biochemical conditions. It is well known that the blood lactate concentration of an athlete undergoing exhaustive exercise, such as a 100-m sprint, increases following the onset of a more energy productive anaerobic metabolism. Once a certain level of lactate concentration is reached, however, exhaustion occurs and there is a rapid decline in exercise capacity [1–3]. The concentration of blood lactate is therefore an important index for estimating physical condition. Previously, lactate concentration has been monitored by taking blood

* Corresponding author.

[1] Also at Research Laboratories, Nippondenso Co., Ltd., 500-1, Minamiyama, Komenoki, Nisshin-cho, Aichi-gun, Aichi 470-01, Japan.

[2] Present address: Kyushu Institute of Technology, 680-4, Kawazu, Iizuka-shi, Fukuoka 820, Japan.

[3] Present address: Japan Advanced Institute for Science and Technology, Hokuriku (JAIST), 15, Asahidai, Tatsuguchi-cho, Nomi-gun, Ishikawa 923-12, Japan.

0003-2670/94/$07.00 © 1994 Elsevier Science B.V. All rights reserved
SSDI 0003-2670(93)E0636-L

samples from an athlete during exercise in an effort to improve performance [4,5].

More information on an athlete's physical condition can be obtained from monitoring the fluctuations in blood lactate concentration depending on the type of exercise performed and the effort applied [6]. Continuous collection of blood samples and the on-line analysis of the blood lactate concentration has been achieved using amperometric biosensors with an enzyme membrane [7–9]. Repeated collection of blood, however, involves insertion of a catheter or the use of an implantable biosensor. This can not only place a physical and mental strain on the subjects, but also presents a medical risk from infection. In view of this, a non-invasive, more convenient and safe monitoring method is required, for estimating an athlete's physical condition.

In this paper, the analysis of metabolites present in sweat is published as a safe, simple and continuous method for evaluating physical condition. Sweat samples of several healthy volunteers were collected and analyzed after some form of physical exercise or after heating. The analysis was conducted using either amperometric biosensors or commercial ion-selective electrodes. Based on our results, sweat lactate and ammonium ion concentrations are proposed to be related to an increase in anaerobic metabolism. The non-invasive monitoring of sweat contents for estimation of physical condition is also compared with previously reported data on blood and sweat analysis.

2. Experimental

2.1. Collection of sweat samples

Collection of sweat samples was carried out on several healthy, drug-free volunteers who did not have periodical physical exercise. Sweat production was induced either by heating the subjects in a hot-bath or by two forms of physical exercise. The first was a stair sprint which is an exhaustive exercise, the second being a 3000-m run which is a hard endurance exercise, but without exhaustion. Prior to the tests, the subjects had been allowed to rest for at least 3 h, but no food and drinks were supplied (for more than 3 h) until after the collections were completed.

Before starting the session, the upper surface of the subject's body was washed using distilled water and an 80% ethanol solution. During a heating session, the subjects sat in a hot bath (temperature maintained at 45°C) for about 5 min without any physical exertion, thus warming the body and inducing sweat production. The exhaustive exercise session involved running up and down five flights of stairs (first to fifth floor) three times. The endurance exercise session involved a 3000-m run on a flat course, at an average speed of 200 m min^{-1}. Physical exercises were carried out below 25°C to prevent sweat excretion by external heating. Each session was conducted on separate days in order to prevent any interfering effects from other sessions.

After taking either a hot-bath or exercise, sweat excreted from the skin was immediately wiped away for 2 min and discarded so that any substances not induced by the session were not subjected to analysis. The number of sweat glands in the upper body varies between 80 to 106 cm^{-2} [10]. To avoid the influence of different sweating rates from different parts of the body, therefore, a sweat sample of at least 20 ml was collected using petri dishes scraped over the entire upper surface of the subject's body. Collection was completely finished within 5 min. The collected samples were frozen immediately.

2.2. Sensor construction and analysis of sweat contents

Glucose, uric acid, Na^+, Cl^- and NH_4^+ were measured using either amperometric biosensors or commercially available ion-selective electrodes (ISEs).

The amperometric biosensors were constructed from a commercially available Clark-type dissolved oxygen sensor and an enzyme membrane, each containing the respective immobilized oxidase enzyme (lactate oxidase, EC 1.1.3.2, LOX-301-A, 33.0 U mg^{-1}, from *Pediococcus sp.*, Toyo Jozo, Tokyo; glucose oxidase, EC 1.1.3.4, G-7141, 100.0 U mg^{-1}, from *Aspergillus niger*, Sigma and uricase EC 1.7.3.3, UOD, 6.32 U mg^{-1}, from *Bacillus sp.*, Toyo Jozo).

Each enzyme was mixed with distilled water and photocrosslinkable poly(vinyl alcohol) (PVA-SbQ; degree of polymerization 1700, SbQ content 1.3 mol%, Toyo Gosei, Tokyo) in a weight ratio of 1:10:10. Dialysis membrane (part No. 157-0144-02, thickness = 15 μm, Technicon Chemical, Orcq) was used as a substrate for the enzyme membranes. The membrane was washed with distilled water, spread onto a flat glass plate and allowed to stand for approximately 1 h. The enzyme–PVA-SbQ mixture was placed onto the dialysis membrane and spread over the surface of the membrane until it had permeated completely (observed as a change in opacity of the membrane). Excess mixture was removed from the membrane and it was then placed in the dark at room temperature for 1 h. The membrane was then irradiated with a fluorescent light for 10 min [11]. The resulting enzyme membranes were stored on the glass plate below 10°C until required. The immobilized enzyme membranes, when stored in this way, retained their enzyme activity for greater than 3 months. When constructing the biosensors, the enzyme membranes were cut to the required dimensions using a scalpel, removed from the glass plate and fixed onto the sensor area of the dissolved oxygen electrode using a rubber O-ring.

The biosensors were used in a flow-injection measurement system (Fig. 1). Phosphate buffer (67 mM, pH 7.0) from the carrier reservoir was peristaltically pumped into the 0.2 ml reaction cell containing the biosensor.

The oxygen electrode consisted of a Pt working electrode and a Ag/AgCl counter electrode. A fixed voltage of −700 mV (vs. Ag/AgCl) was applied to the biosensor using a computer controlled potentiostat (HA-151, Hokuto Denko, Tokyo). Current output was monitored continuously on a computer display and saved on floppy disk for later analysis. 100 μl of sweat sample or calibration standards were injected into the flow system. The presence of the substrate was monitored as a decrease in the concentration of dissolved oxygen at the sensitive area of the oxygen sensor. The sweat sample was diluted with distilled water if necessary.

Sodium, chloride and ammonium ion concentrations were measured in a batch measurement cell (not the flow cell) using commercially available ISEs (sodium ISE, Type 7480, DKK, Tokyo; chloride ISE, Type 8002-06T, Horiba, Kyoto, and ammonium ISE, Type 7161, DKK) with ion meters (F-8L, Horiba, and IOL-50, DKK). The ISEs were calibrated using test solutions of varying concentration in a 50.0-ml batch measuring cell in accordance with manufacturer's instructions. The ISEs were then placed into the 50.0-ml batch measuring cell filled with distilled water, and a suitable volume of sweat sample was injected using a syringe. The output voltage was measured in quiescent solution following gentle stirring us-

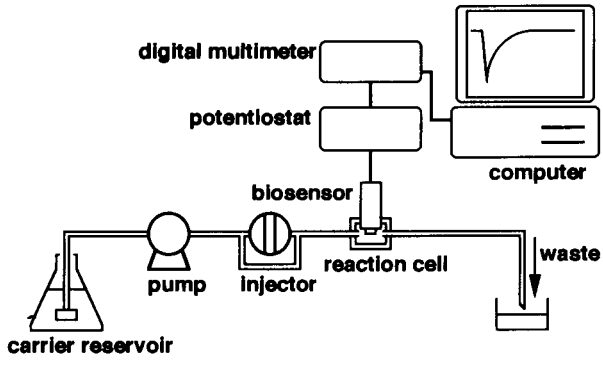

Fig. 1. Schematic diagram of the flow-injection measurement system.

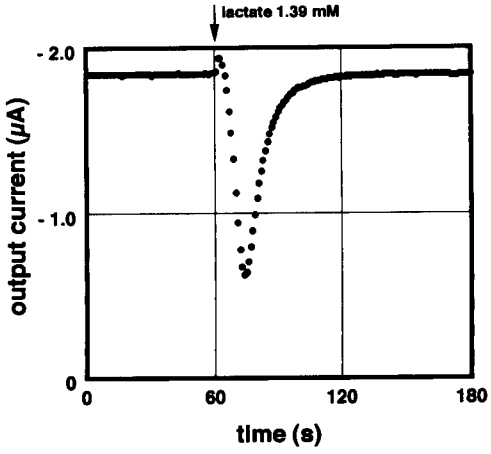

Fig. 2. Typical response of the lactate sensor using the flow-injection method. The arrow indicates injection of 100 μl of a 1.39 mM lactate solution.

ing a magnetic flea for several seconds. All sweat content analyses were performed at 25°C.

3. Results and discussion

3.1. Evaluation of the sensors

Fig. 2 shows the typical response of the lactate biosensor using the flow-injection measurement system. As the figure indicates, after the injection of 100 μl of calibration standard, the sensor current signal decreased rapidly, giving a peak approximately 14 s after injection and increased gradually to a steady state level. The difference between the steady state level and the peak current was regarded as the real output value derived from the concentration of the injected solution. Several flow rates were examined in the flow-injection measurement system, and a maximum peak height was obtained at a flow rate of 0.86 ml min^{-1}. All flow-injection analyses were therefore carried out at this flow rate.

Fig. 3 illustrates the calibration curve of the lactate sensor using the flow-injection method described above. The current decrease was found to be linearly related to the lactate concentration over the range 0.06 to 1.85 mM, with a correlation coefficient of 0.998. Calibration was also

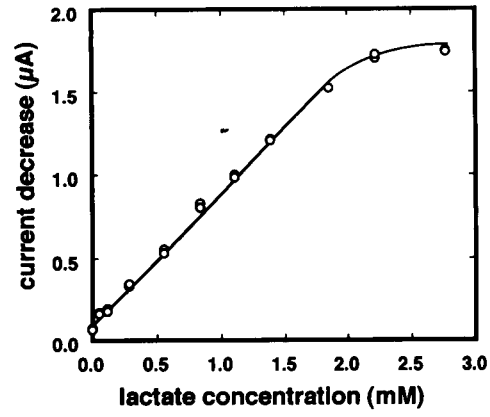

Fig. 3. Calibration curve of the lactate sensor. Injection of 100 μl of lactate solutions.

conducted for the other sensors, the biosensor for glucose had a linear range of 0.28 to 3.33 mM, and for the uric acid sensor the linear range was 0.06 to 0.59 mM.

For the ISEs, the sensor characteristics were obtained from a semi-logarithmic plot, giving a linear range for the sodium, chloride and ammonium ISEs of 10^{-4} to 10^{-1} M, 10^{-5} to 10^{-2} M, and 5.9×10^{-6} to 5.9×10^{-3} M, respectively. For sweat analysis, the sweat sample was diluted with distilled water if required.

3.2 The measurement of metabolites in sweat

Fig. 4 shows the comparison between the metabolites measured in sweat samples obtained

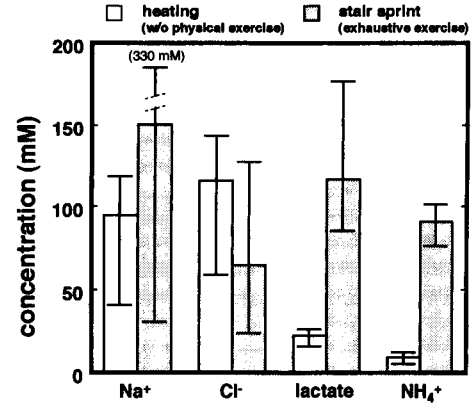

Fig. 4. Comparison of the metabolite concentrations in sweat induced by heating and stair sprint ($n = 4$).

from induced heating and the stair sprint exhaustive exercise. As this figure indicates, there was a wide variation in sodium and chloride concentration between subjects ($n = 4$). No correlation between the concentrations of these metabolites and physical condition could be clearly shown by these experiments.

The maximum concentrations of glucose and uric acid were 0.525 and 0.284 mM in the sweat samples induced by exhaustive exercise, but glucose and uric acid could not be detected in most of the sweat samples. As previously reported, the concentration levels of glucose and uric acid in sweat are low (glucose: 0 to 0.153 mM, uric acid: 0 to 0.09 mM) [12,13]. The effect of physical condition on these substances could also not be shown from these experiments. The reason for the occasional measurement of glucose and uric acid may possibly be caused by interference from redox active species present in the sweat samples.

As Fig. 4 also indicates, the concentrations of lactate and ammonium ion in sweat induced by the stair sprint exercise were 115.8 and 90.5 mM, an average of 5.2 fold (3.2 to 11.5) and 10.6 fold (6.0 to 16.5) higher respectively, than the concentrations in sweat induced by heating. The significant increases in the concentrations of these metabolites are considered to be caused by the effect of physical condition. The reason for the increase in concentration of lactate and ammonium ion in sweat is accounted for as follows.

Fig. 5 shows a schematic illustration of the metabolic pathway of ATP production. If oxygen and glycogen (glucose) are in sufficient supply, ATP can be produced continuously by aerobic metabolism (glycolysis, TCA cycle and respiratory chain). During an exhaustive exercise, such as the 100-m sprint or stair running, however, the increased physical load causes aerobic metabolism to be replaced by anaerobic glycolysis to yield ATP. Continued anaerobiosis leads to a deficiency in oxidized nicotinamide adenine dinucleotide (NAD^+), required for the breakdown of glucose to pyruvate, causing an imbalance in the relative levels of the adenine nucleotides (ATP, ADP, AMP). As a result, lactate is produced from pyruvate for the regeneration of NAD^+, and the purine nucleotide cycle (PNC) functions

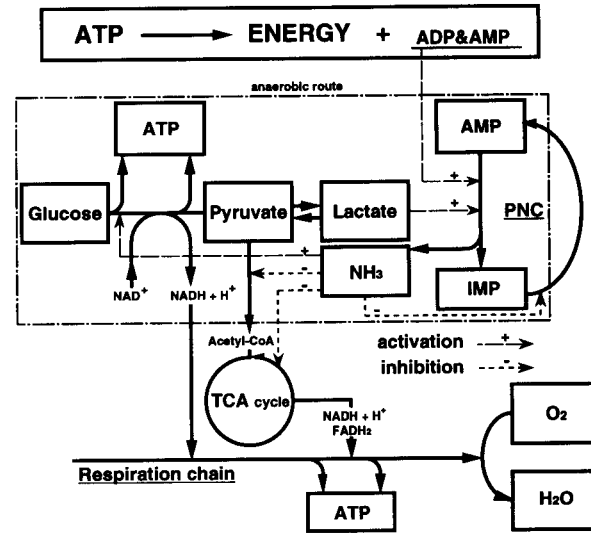

Fig. 5. Schematic diagram of ATP production pathway and the purine nucleotide cycle (PNC) illustrating the mechanisms of lactate and ammonia production during physical exercise.

to regulate the relative levels of the adenine nucleotides, producing ammonia as one of metabolites in the cycle.

Lactate and ammonia are not only produced as metabolites of the anaerobic route, but also activate this pathway themselves (as indicated by the arrows in Fig. 5). Namely, the lactate accumulation in skeletal muscle cells during anaerobiosis decreases the pH, thus improving the enzyme activity of adenylate deaminase, which is a key enzyme of the PNC [14]. In addition, the ammonia produced increases the rate of metabolite flux through glycolysis by directly increasing the activity of phosphofructokinase, one of the rate-limiting enzymes of glycolysis, without a change in the pH level [15], and also inhibits the respiratory activity of mitochondria and TCA activity [16]. The result of these combined effects is an increase in the availability of pyruvate [17].

The anaerobic pathway and the metabolites it produces operate synergistically to effect a sudden increase and accumulation of lactate and ammonia in the muscle cell, which is reflected as an increased concentration not only in the body fluids, but also in the sweat produced by the skin during exhaustive exercise. If the increased con-

centrations of lactate and ammonia in sweat during exhaustive exercise reflect a switch to anaerobic metabolism, then an aerobic exercise such as jogging, in which the oxygen supply is sufficient, would lead to a different result, namely, that the lactate and ammonia concentrations in sweat would be low.

This is born out by our analysis of the concentrations of lactate and ammonium in sweat induced by a 3000-m run, which were 2.0 and 3.0 fold higher respectively, than in sweat induced by heating, as compared with a 5.2 and 10.6 fold increase for the exhaustive session. These ratios are not related to the total energy consumption of the different physical exercises. The reason for the small increase in concentration for a non-exhaustive exercise is that the (instantaneous) energy requirement in the skeletal cell on endurance exercise can be supplied by the predominantly aerobic metabolism. Energy production occurs through a mixture of aerobic and anaerobic metabolisms resulting in only a moderate rise in the concentration of lactate and ammonium ions. These results are in agreement with those reported previously obtained from blood analysis [5].

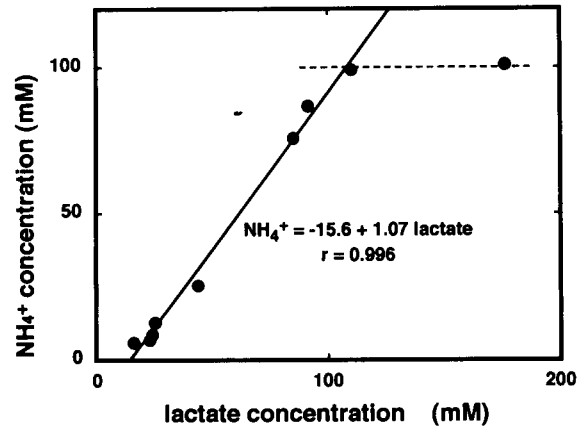

Fig. 6. Relationship between the lactate and ammonium ion concentrations in sweat under different physical conditions.

Fig. 6 shows the relationship between sweat lactate and sweat ammonium ion concentration following various forms of physical exercise. The ammonium ion concentration was found to be linearly related to the lactate concentration, over

Table 1
Mean concentrations of lactate and ammonium ion in the collected sweat samples, and previously reported concentrations in sweat and blood under various physical conditions

Contents	Physical condition			
	Rest (w/o exercise)	Endurance exercise	Exhaustive exercise	Ref.
Sweat	Heating	3000-m run	5-min stair sprint	
Lactate (mM)	22.1	43.7	115.8	This study
NH_4^+ (mM)	8.5	25.7	90.5	This study
	Pilocarpine sweating			
Lactate (mM)	4.0–40.0	–	–	[12]
NH_4^+ (mM)	3.3–6.1	–	–	[12]
Blood	Rest	30 min treadmill	V_{O2} max. exercise	
Lactate (mM)	-	3.9	11.1	[21]
NH_4^+ (μM)	37.6	70.0	77.6	[21]
Lactate (mM)	1.2	–	11.0	[22]
NH_4^+ (μM)	36.5	–	65.9	[22]
	Rest		12-min exh. exercise	
Lactate (mM)	–	–	12.5	[18]
NH_4^+ (μM)	(30)	–	120.8	[18]
	Rest	10 min max. work loads	5-min exh. exercise	
Lactate (mM)	1.3	4.3	12.3	[23]

the range 16.1 to 110.3 mM with a slope of 1.07 ([ammonium ion]/[lactate]) and a correlation coefficient of 0.996. This is in agreement with previously reported results which showed that blood lactate and blood ammonium ion are linearly related [1,18].

3.3. Sweat content analysis as an index for estimation of physical condition

Both experimental and theoretical approaches give a lactate concentration in blood of around 4 mM as being the critical value at which a switch from aerobic to anaerobic metabolism occurs [19,20].

Table 1 shows the average concentrations of lactate and ammonium ion obtained from our experiments and previously reported values measured in sweat and blood under different physical conditions. As is shown, our analysis gave a lactate concentration in sweat induced by exhaustive exercise of 115.8 mM, which is 5.2 times higher than the result obtained after heating, unlike the previously reported value in blood which is approximately 9 times higher.

The difference between sweat and blood lactate concentration may not only be due to the high permeability of the lactate molecule (mol.wt. 90.08) into the sebaceous gland, but may also be caused by additional production of lactate through the metabolic process of sweating, as reported previously [24]. However, since there is a significant increase in sweat lactate concentration (5.2 fold) following exhaustive exercise it could be utilized as an indicator for estimation of physical condition in a similar manner to blood lactate.

On the other hand, the ammonium ion concentration in sweat following exhaustive exercise is about 10.6 times higher than the concentration following heating, unlike in blood (approximately 2 fold). It is well established that the ammonia level in blood (50 to 80 μM) reflects the net flux of ammonium ions into and out of the blood circulation [25] and only indirectly reflects the actual tissue levels. 95% of ammonia exists in the ionized form, however this is poorly soluble in water or lipid at physiological pH levels [26]. Because blood pH is tightly maintained, NH_4^+ tends to accumulate and is trapped within the tissues [27]. During exercise, lactate produced by anaerobic metabolism lowers the muscle tissue pH from 7.0 to approximately 6.6, as compared with a drop in the blood pH value from 7.4 to 7.2 [28,29]. This situation leads to an increased accumulation of ammonium ion in the muscle tissues. Since the pH of sweat can decrease within the range of 4.0 to 6.8 [13], ammonium is easily solubilised and can be excreted in the sweat, resulting in the marked difference between blood NH_4^+ concentration and sweat NH_4^+ concentration following physical exercise. This difference is even more marked following exhaustive exercise because, as noted previously, ammonium ion is a product and synergistic effector of PNC metabolism. Since the concentration increase of ammonium ion in sweat is higher than the increase in blood, it is potentially an excellent non-invasive method for estimating physical condition.

The major cause of physical exhaustion is that the accumulated lactate lowers the muscle pH reducing the activity of the glycolysis enzymes and slowing down or stopping ATP production [5]. In several reports [30,31] however, ammonium ion has been mentioned as a cause of physical exhaustion. NH_4^+ can directly stimulate the tension output of frog sartorius muscle following substitution of sodium ions with NH_4^+ in the muscle extracellular fluid. With 30 mM NH_4^+ substitution, the average tension output increased during the 30 min exposure, whereas at higher concentrations (72, 90 and 120 mM), twitch tension was completely eliminated [30]. In short, a low NH_4^+ concentration has the effect of the stimulating muscle activity, while a high concentration terminates the muscle activity. This is in agreement with our values of 75.8 to 100.9 mM for the exhaustive session (see Fig. 6).

4. Conclusions

It has been shown that the concentrations of lactate and ammonium ion in even normal sweat are about 10 to 100 times higher than blood concentrations and can be detected using commercial ISEs or biosensors. The sweat sample can

be easily diluted so as to fall within the linear range of the sensor. One of the major effects on the stability and lifetime of a sensor applied to continuous analysis of clinical samples is that protein present in the sample can cause fouling of the sensor. Sweat, unlike blood which has a high protein content of between 67 to 83 g l^{-1}, has a very low protein content (0.20 to 0.77 g l^{-1}), and is therefore a better sample for continuous analysis. From a medical point of view, sweat analysis is a non-invasive method and is hence safer than blood analysis. In addition, it may be possible to target specific muscles, given that the concentration of metabolites in the sweat relates to the concentration in the underlying muscle tissue. This is different from blood analysis where the concentration of metabolites is equilibrated by the circulation. The analysis of both sweat lactate and NH_4^+ is an effective, simple and safe method for continuously monitoring the physical condition during exercise.

5. Acknowledgements

We wish to thank Dr. Jonathan M. Dicks (a Japan Society for the Promotion of Science research fellow, presently at RCAST) for his assistance in revising this manuscript.

6. References

[1] P. Babij, S.M. Matthews and M.J. Rennie, Eur. J. Appl. Physiol., 50 (1983) 405.
[2] H. Stegmann and W. Kindermann, Int. J. Sports Med., 3 (1982) 105.
[3] A.V. Hill, C.N.H. Long and H. Lupton, Proc. Roy. Soc. London, 97 (1924) 155.
[4] K. Wasserman, J.E. Hansen, D.Y. Sue and B.J. Whipp, Principle of Exercise Testing and Interpretation, Lea & Febiger, PA, 1987, p. 14.
[5] U. Mattner (Ed.), Lactate in Sports Medicine, Boehringer, Mannheim, 1988, p. 24.
[6] G.A. Noy, A.L.J. Buckle and K.G.M.M. Alberti, Clin. Chim. Acta, 89 (1987) 135.
[7] M. Mascini, S. Fortunati, D. Moscone, G. Palleschi, M. Massi-Benedetti and P. Fabietti, Clin. Chem., 31 (1985) 451.
[8] M. Mascini, F. Mazzei, D. Moscone, G. Calabrese and M.M. Benedetti, Clin. Chem., 33 (1987) 591.
[9] G. Palleschi, M. Mascini, L. Bernardi and P. Zeppilli, Med. Biol. Eng. Comput., 28 (1990) B25.
[10] M.F. Roberts, Am. J. Phys. Anthrop., 32 (1970) 395.
[11] K. Ichimura, J. Polym. Sci., 22 (1984) 2817.
[12] I.L. Schwartz, C.L. Comar and F. Bronner (Eds.), Mineral Metabolism, Vol. 1, Academic Press, New York, 1960, p. 346.
[13] S. Robinson and A.H. Robinson, Physiol. Rev., 34 (1954) 202.
[14] B. Setlow and J.M. Lowenstein, J. Biol. Chem., 242 (1967) 607.
[15] J.M. Lowenstein, Physiol. Rev., 52 (1972) 382.
[16] R. Klocke, K.A. Anderson, H. Rotman and R.E. Foster, Am. J. Physiol., 222 (1972) 1004.
[17] S. Schenker, P.W. McCandless, E. Brophy and M.S. Lewis, J. Clin. Invest., 46 (1967) 838.
[18] T. Tsutsumi, K. Aoki, Y. Goto and N. Kita, Bulletin of the Physical Fitness Research Institute, 63 (1986) 29.
[19] H. Heck, G. Hess and A. Mader, Dtsch. Z. Sportmed., 36 (1985) 19.
[20] A. Mader and H. Heck, Int. J. Sports Med., 7 (1986) 45.
[21] J.E. Wilkerson, D.L. Batterton and S.M. Horvath, Eur. J. Appl. Physiol., 34 (1975) 169.
[22] J.E. Wilkerson, D.L. Batterton and S.M. Horvath, Eur. J. Appl. Physiol., 37 (1977) 255.
[23] J. Karlesson, L. Nordesjo, L. Jorfeldt and B. Saltin, J. Appl. Physiol., 33 (1972) 199.
[24] R.S. Gordon, R.H. Thompson, J. Muenzer and D. Thrasher, J. Applied Physiol., 31 (1971) 713.
[25] B.J.C. Mutch and E.W. Banister, Med. Sci. Sports. Exerc., 15 (1983) 41.
[26] J.H. Lawrence, W.F. Loomis, C.A. Tobin and F.H. Turpin, J. Physiol. (London), 105 (1946) 197.
[27] R.A. Meyer, G.A. Dudley and R.L. Terjung, J. Appl. Physiol., 49 (1980) 1037.
[28] K. Sahlin, Acta. Physiol. Scand., 455 (1978) 1.
[29] K. Sahlin, R.C. Harris, B. Nylind and E. Hulman, Pfluegers Arch., 367 (1976) 143.
[30] D.E. Heald, Am. J. Physiol., 229 (1975) 1174.
[31] T. Tsutsumi, Y. Goto, N. Kita and K. Aoki, Bulletin of the Physical Fitness Research Institute, 68 (1988) 36.

ELSEVIER

Analytica Chimica Acta 289 (1994) 35–42

ANALYTICA CHIMICA ACTA

Electrochemical investigation of chloramine T

M. Hahn *,[a], A. Liebau [b], H.H. Rüttinger [b], R. Thamm [c]

[a] *ECH Elektrochemie Halle GmbH, Weinbergweg 23, 06120 Halle / S, Germany*
[b] *Martin-Luther-Universität Halle, Institut für Analytik und Umweltchemie, Weinbergweg 16, 06120 Halle, Germany*
[c] *Burnus Gesellschaft mbH, Rösslerstrasse 94, 64293 Darmstadt, Germany*

(Received 1st June 1993; revised manuscript received 23rd August 1993)

Abstract

Electrochemical measurement methods are suitable for examining the hydrolysis and reactivity of chloramine T. The individual species can be separated by means of capillary electrophoresis. Voltammetrical methods make it possible to judge selectively on the oxidation efficiency of individual substances. By coupling the coulometric determination with sample preparation techniques, e.g. stripping out, volatile chlorine can also be determined. The stability of chloramine T solutions was tested at various pH values and hydrolysis reactions are described. It is shown that chloramine T differs from other active chlorine donors and hypochlorite/chlorine with regard to its reactivity.

Key words: Electrophoresis; Voltammetry; Coulometry; Chloramine T

1. Introduction

Chloramine T (sodium salt of *N*-chlorotoluene sulphonamide) is a strong electrolyte; it is completely dissociated in water as the ions Na^+ and $CH_3C_6H_4SO_2NCl^-$. Its oxidative efficiency depends to a very considerable extent on the pH. Various intermediates are described as reactive species in the literature [1,2]: $R-SO_2-NCl^-$, $R-SO_2-NHCl$, $R-SO_2-NCl_2$, HOCl, OCl^-.

The formation of hypochlorite and toluene sulphonamide in alkaline solution according to

$$R-SO_2-NCl^- + H_2O \rightleftharpoons R-SO_2-NH_2 + ClO^- \quad (1)$$

($R = CH_3C_6H_4$) is discussed.

The protonated form of chloramine T is suggested as the intermediate according to reactions 2 and 3.

$$R-SO_2-NCl^- + H_2O \rightleftharpoons R-SO_2-NHCl + OH^- \quad (2)$$

$$R-SO_2-NHCl + OH^- \rightleftharpoons R-SO_2-NH_2 + ClO^- \quad (3)$$

Because of the pK_s value of 4.55, $R-SO_2-NHCl$ only exists in very small concentrations in alkaline solution. In acidic solution $R-SO_2-NHCl$ disproportionates according to

$$2R-SO_2-NHCl \rightleftharpoons R-SO_2-NH_2 + R-SO_2-NCl_2 \quad (4)$$

into toluene sulphonamide (solubility in water ca. 1×10^{-4} mol/l) and dichloramine T, which is

* Corresponding author.

0003-2670/94/$07.00 © 1994 Elsevier Science B.V. All rights reserved
SSDI 0003-2670(93)E0640-S

practically insoluble in water. At the same time $R-SO_2-NHCl$ hydrolyses according to

$$R-SO_2-NHCl + H_2O \rightleftharpoons R-SO_2-NH_2 + HOCl \quad (5)$$

with the formation of hypochlorous acid. HOCl exists in sulphuric acid medium, but in hydrochloric acid chlorine is produced

$$HOCl + Cl^- + H^+ \rightleftharpoons Cl_2 + H_2O \quad (6)$$

Since the redox potentials of chloramine T on the one hand and free chlorine or hypochlorite differ considerably from one another, both the oxidising and chlorinating powers are different. Furthermore, owing to the various pH-dependent equilibrium reactions, a very variable reactivity is to be expected.

In order to describe this behaviour it is necessary to know the concentrations of the individual components. With conventional titrimetric methods, however, it is only possible to determine the entire concentration of oxidising agents present, i.e. the sum of chloramine T (or the pH-dependent equilibrium concentrations) and free chlorine or hypochlorite. Thus in the iodimetric determination specified for determination of chloramine T content in DAB 9 (German Pharmacopoeia, 9th edn.), by adding iodide, the total available chlorine releases an equivalent quantity of iodine according to

$$\text{“}Cl_2\text{”} + 2I^- \rightarrow 2Cl^- + I_2 \quad (7)$$

This can subsequently be determined by titration with thiosulphate [3] or other back titration agents [4,5]. Differentiation of the “Cl_2” is impossible in this process.

In a similar way titration with Fe(II) also gives only the sum of the oxidising agents present [6,7]. Even with potentiometric determinations separation according to the different redox potentials is not possible [8]. A separate determination using OsO_4 as catalyst is possible through titration with arsenite [9,10]. Although a high sample flow rate and an extremely reproducible time regime can be achieved with the well-known flow-injection techniques, the determination still finishes with the known titrimetric methods [11].

With indirect spectrophotometric methods, reducing agents, e.g. Cr(II) [12], *o*-toluidine [13] or sulphanilamide [14] are used, but with these a differentiation between chlorine/ hypochlorite and chloramine T is not possible.

Degradative reactions of chloramine T cannot be examined by using direct spectrophotometric methods [15,16], which are based on the detection of the phenyl group. Characterisation of the individual equilibrium states therefore is extremely difficult and practically impossible.

For these reasons, the objective of the present investigation was to find methods which make it possible to differentiate between the individual species in equilibrium. In order to achieve this, either separation of the substances followed by non-specific detection or substance-specific direct determination is necessary. Electrochemical separation methods such as capillary electrophoresis [17], or electroanalytical methods, e.g. voltammetry [18] and coulometry [19], seem to be particularly suitable here.

2. Experimental

2.1. Capillary electrophoresis

A capillary electrophoresis instrument supplied by Dionex (CES I) with an integrated UV–visible spectrophotometric detector was used.

The ends of the capillary (fused silica, length 70 cm, $d_i = 75$ μm), which is filled with buffer solution, are immersed into two buffer vessels (10 mmol/l borax, pH 9.3). These also contain the electrodes. The sample is injected into the capillary by the force of gravity. This is carried out by immersing one capillary-end into the sample vessel and lifting it to a height of 10 cm for 10 s to produce a height difference which as a result has a hydrostatic flow of the sample solution into the capillary. After feeding the sample into the capillary a strong electrical field is applied (20 kV).

The species to be determined are then separated according to their rates of migration. Detection takes place at the other end of the capillary by UV absorption at 215 nm. For evaluation, the peaks were integrated. For identification pur-

poses comparison solutions of the corresponding substances of known concentrations are used, or standard solutions are added to the samples.

The electrical charge of the surface of the quartz capillary depends on the pH of the used buffer. As a result of this charge, a so-called electroosmotic flow occurs. This means, the entire contents of the capillary is transported in one direction. In the case of an uncoated capillary this flow is to the cathode side and increases with increasing pH. This influences the effective speed of the migrating ions correspondingly; in the case of the slower anions (e.g., phenolates, chloramine T) the direction of migration is actually reversed, so that detection on the cathode side is possible.

Fig. 1 shows a typical electropherogram of an alkaline chloramine T solution after 30 days of hydrolysis.

2.2. Measuring device for the determination of purgeable chlorine

By conventional direct iodimetric titration with a sodium thiosulphate solution it is not possible to differentiate between free chlorine/hypochlorite and that which is chemically bound to chloramine T.

Differentiation is possible, however, by determining the volatile, purgeable chlorine content (PCl) by stripping the free chlorine from the sample solution and determining it in a second absorber solution used as the titration solution. Fig. 2 shows the device for the measuring cell developed for this method.

The sample is introduced into the sample chamber via the dosing lock. The pH for stripping out can be altered, for example, by the reagent feed. The free chlorine is transferred to the electrolysis chamber by a stream of inert gas (N_2 or Ar). The electrolyte, which at the same time acts as absorber solution, consists of 0.1 M potassium iodide (in phosphate buffer, pH 4). Under these conditions, the chlorine, after stripping out, is absorbed quantitatively by the electrolyte, and liberates equimolar iodine concentrations from the iodide. Thus, the measured biamperometric detector signal is directly proportional to the transferred chlorine concentration.

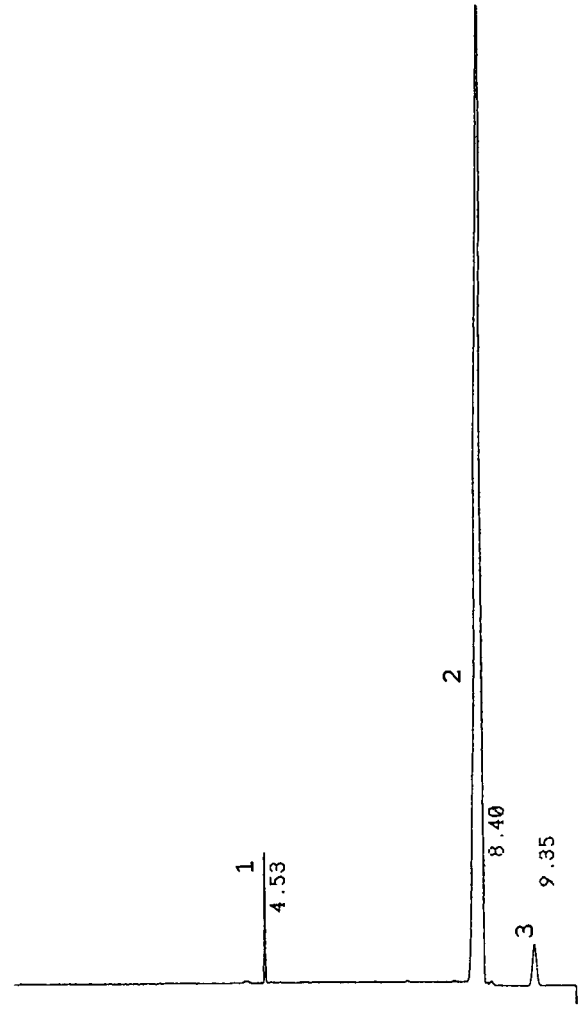

Fig. 1. Electropherogram of an alkaline chloramine T solution. Chloramine T: 1 mmol/l, 1 = *p*-Toluenesulfonamide, 2 = chloramine T, 3 = *p*-toluenesulfonic acid.

2.3. Voltammetric measurements

Comparable conclusions on the redox properties of different compounds can best be drawn from voltammetric measurements. The principle of this electrochemical method of measuring is that a definite potential is applied to an inert electrode. The current is then plotted as a function of the potential. The current flow is proportional to the rate of the electrochemical conversion at the electrode. Since, apart from the chemical kinetics, the rate of reaction is determined

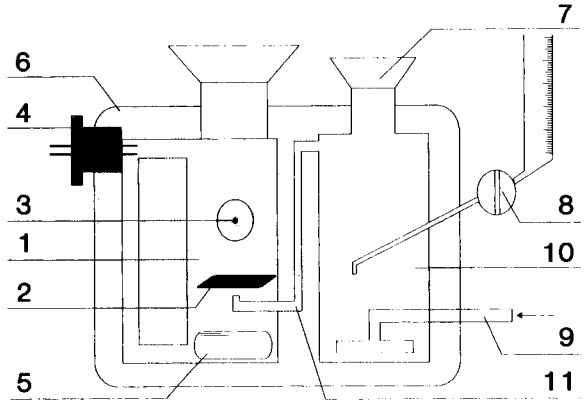

Fig. 2. Coulometric measuring cell for the determination of volatile chlorine, 1 = electrolysis chamber, 2 = generator electrode, 3 = auxilary electrode, 4 = biamperometric detector, 5 = magnetic stirrer, 6 = casing with temperature control, 7 = sample dosing lock, 8 = reagent feed inlet, 9 = inert gas inlet, 10 = sample chamber, 11 = transfer channel.

mainly by the transport processes at the electrode, a defined flow must be produced at the electrode in order to achieve stationary states. For this a rotating disk type electrode (40 revolutions/s).

Measurements were carried out (using a laboratory-made apparatus) in 16 ml of alkaline borax buffer solution (50 mmol/l, pH 9.2) at a potential changing rate of 13 mV/s. Measurements were made against a Ag/AgCl saturated reference electrode. Before each measurement the basic electrolyte solution was purged with argon to remove dissolved oxygen.

3. Results

3.1. Investigations into the rate of decomposition of chloramine T

Alkaline solution

Alkaline chloramine T solutions are very stable. No hydrolysis products are detectable in freshly prepared solutions. In order to investigate long-term stability, chloramine T solutions were prepared at intervals of 7 days and their decomposition followed by means of capillary electrophoresis. As shown in Fig. 3, the hydrolysis

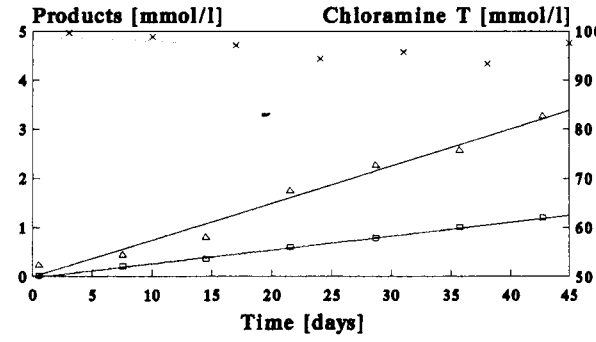

Fig. 3. Hydrolysis of chloramine T solutions at pH 12, c_{cat} = 100 mmol/l. △ = Toluene sulphonamide; □ = toluene sulphonic acid; × = chloramine T.

products toluene sulphonamide and toluene sulphonic acid can be found with increasing time. Other products were not detected. In no case was hypochlorite found. A reason may be the hypochlorite formed with the toluene sulphonamide according to reaction 3 is reduced instantly, accompanied by the formation of oxygen. The other possibility is that the available concentration is so small that it cannot be detected. The chloramine T content is reduced to the same extent as the hydrolysis products are formed.

Separately, hypochlorite was added gradually to alkaline, pure toluene sulphonamide solutions. Here a reaction of the toluene sulphonamide with hypochlorite takes place instantly and chloramine T is formed (Table 1). The amount of decrease of toluene sulphonamide concentration is identical to the amount of increase of chloramine T concentration. If toluene sulphonamide

Table 1
Conversion of toluene sulphonamide (TSA) with hypochlorite at pH 12 (toluene sulphonamide conc. = 2 mmol/l. CAT = Chloramine T)

Hypochlorite added (mmol/l)	TSA (mmol/l)	CAT (mmol/l)	Sum of TSA and CAT (mmol/l)
0	2.0	0	2.0
0.53	1.48	0.53	2.01
1.42	0.59	1.40	1.99
2.25	0	2.05	2.05
3.5	0	2.02	2.02

is present in the solution, no hypochlorite is to be found (see below).

After the quantitative conversion of the sulphonamide to chloramine T with hypochlorite has been completed, no formation of dichloramine T is to be observed when adding more hypochlorite. Chloramine T and hypochlorite then are found together in the alkaline solution. These results were obtained from voltammetric measurements.

Acid solution

In acid solution dichloramine T precipitates, so that practically no chlorine is available for reaction in the solution.

The protonated form $R-SO_2-NHCl$ is first formed from chloramine T in acid solution, H^+ being consumed in the reaction. This protonated form then disproportionates following reaction 4 to dichloramine T and toluene sulphonamide. Thus chloramine T acts as a buffer substance in acidic solution.

If the dichloramine T formed is filtered off and then redissolved in alkaline solution, chloramine T is reformed from the dichloramine T, together with a corresponding equimolar concentration of hypochlorite. Table 2 gives a data collection of the substances measured in the filtrate and residue.

In addition, toluene sulphonic acid was found in the residue. Probably, during precipitation, drying and redissolving the dichloramine T, decomposition is taking place. However, toluene sulphonamide could not be found after dissolution of dichloramine T.

Table 2
Determination of content of filtrate and residue of acidic chloramine T solutions (pH 1) (n.d. = not detectable; chloramine T conc. = 10 mmol/l)

	Exp. determined substance	Hydrochloric acid soln. (mmol/l)	Sulphuric acid soln. (mmol/l)
Filtrate	Chloramine T	2.26	2.35
	Toluene sulphonamide	2.85	3.07
	Toluene sulphonic acid	n.d.	n.d.
Residue	Chloramine T	1.90	1.84
	Toluene sulphonic acid	0.50	1.01
	Toluene sulphonamide	n.d.	n.d.

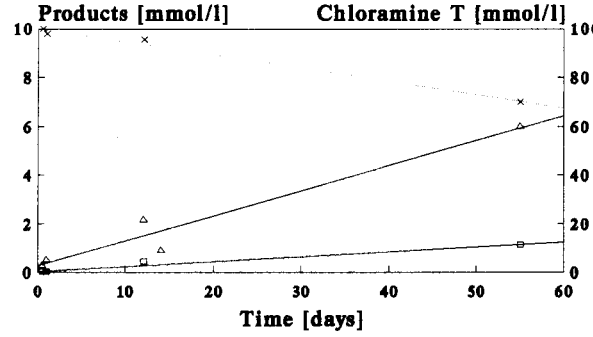

Fig. 4. Hydrolysis of chloramine T solutions at pH 7, $c_{cat} = 100$ mmol/l. Key to symbols as in Fig. 3.

Over a period of 109 h, no significant change in the active chlorine content in neutral and alkaline solutions was observed. In acidic solution the active chlorine content drops from 397 to 271 mg/l during these 109 h.

Neutral solution

When dissolving chloramine T in water, at first no formation of dichloramine T is observed in neutral solution. A noticeable clouding indicating precipitation of dichloramine T does not take place until hydrolysis has proceeded for 50 days.

The quantity of toluene sulphonamide formed is twice as much when compared to alkaline solutions. At the same time the chloramine T content, together with the active chlorine content, is reduced more quickly (Fig. 4). Toluene sulphonic acid is formed in the same concentration as in alkaline solution. Other products are also formed in smaller concentration ($< 0.5\%$ in 20 days). These are probably nucleus-chlorinated products of chloramine T. This assumption is confirmed by the fact that neutral and acid chloramine T solutions cause a slight increase in the content of adsorbable organic halogen compounds (AOX) (DIN 38409-14).

3.2. Electrochemical examination of oxidising power

Fig. 5 shows a typical voltammogram for chloramine T in alkaline solution. The cathodic cur-

rent at −616 mV against a saturated Ag/AgCl reference electrode corresponds to the reduction of the chloramine T and is proportional to its concentration.

In a separate test pure bleaching liquor solutions were measured. Hypochlorite/chlorine is already reduced at considerably more positive potentials (+185 mV). This means that, compared with bleaching liquor solution, chloramine T shows a lower reactivity.

Owing to their different potentials it is possible to distinguish between chloramine T and hypochlorite.

No hypochlorite could be detected in the chloramine T samples (detection limit: 2 μmol/l). In Fig. 6 no voltammetric wave in the curve is to be seen at 185 mV. If hypochlorite solution is added, no change in the shape of curve 2 can be observed until all of the toluene sulphonamide has been converted to chloramine T. A wave in the curve, proportional to the concentration, is not recognisable until a surplus of hypochlorite is present (curves 3–6). With voltammetric measurements small hypochlorite concentrations can be reliably determined, in the presence of a large excess of chloramine T.

In acidic solutions, too, no free chlorine is detectable, since hypochlorite/chlorine reacts with chloramine T at pH < 8 to form a precipitation of dichloramine T. Hypchlorite cannot be detected until an excess (above the stoichiometric

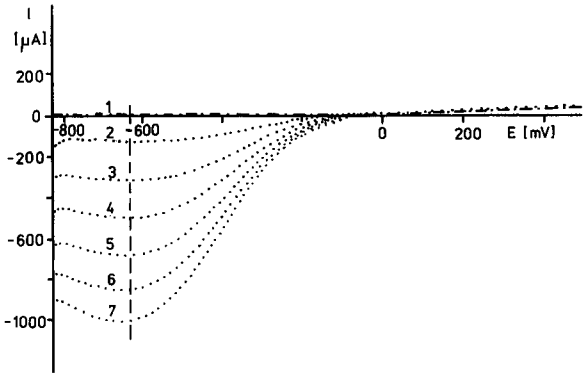

Fig. 5. Voltammogram of an alkaline chloramine T solution at different concentrations in the basic electrolyte solution. Basic electrolyte = 1. Chloramine T solutions (mmol/l): 2 = 0.31, 3 = 0.62, 4 = 0.93, 5 = 1.23, 6 = 1.54, 7 = 1.84.

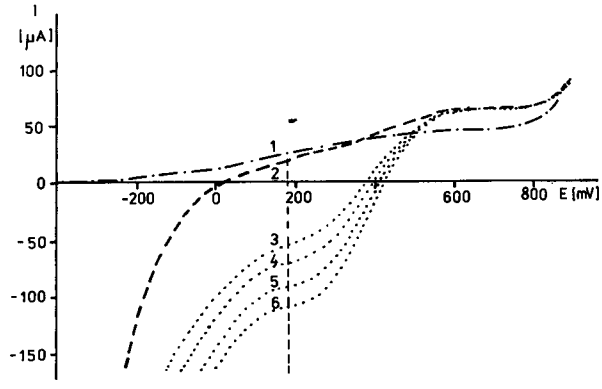

Fig. 6. Voltammogram of chloramine T after addition of hypochlorite. 1 = Basic electrolyte; 2 = chloramine T, 8.6 mmol/l. Hypochlorite excess: 3 = 0.34 mmol/l; 4 = 0.42 mmol/l; 5 = 0.51 mmol/l; 6 = 0.59 mmol/l.

quantity) of hypochlorite has been added (complete conversion of chloramine T to dichloramine T).

3.3. Availability of "active" chlorine; chlorinating power

In order to determine the available "active" chlorine in chloramine T solution the sample was brought into the sample chamber of the distillation measuring cell (Fig. 2) via the sample dosing lock. The pH can be adjusted by adding a reagent, e.g., by dosing buffer solutions. The chlorine liberated was transferred into the electrolysis chamber by inert gas and reacted with the iodide while liberating iodine. By controlling the biamperometric indication signal the purging process may be continuously monitored. The chlorine quantity which has been transferred is subsequently determined by means of coulometric titration of the iodine formed, using thiosulphate as excess reagent. In this way the biamperometric indication can be calibrated immediately.

The total chlorine content is determined by injecting the sample directly into the electrolysis chamber.

Fig. 7a–c shows the time-related purgeable chorine curves for bleaching liquor and two *N*-chloramines (sodium dichloroisocyanurate and chloramine T) at different pH values (hydrochlo-

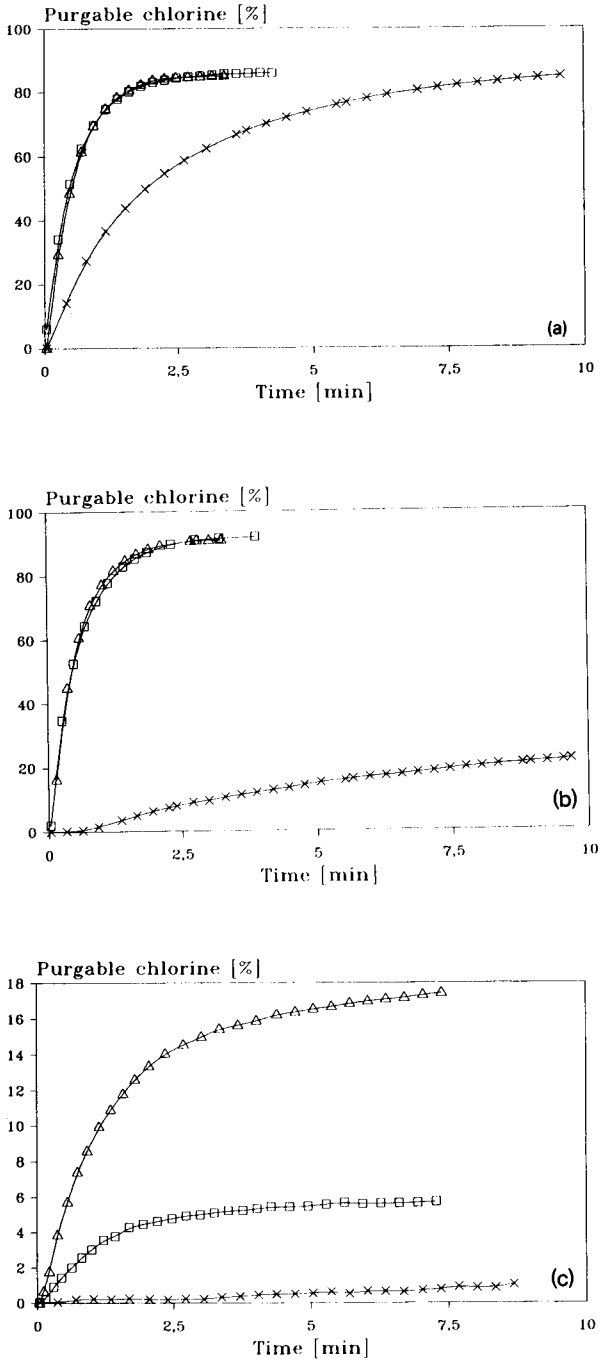

Fig. 7. Determination of volatile chlorine from chloramine T (×) and sodium dichloroisocyanurate (□) solutions in comparison with bleaching liquor (△). Chlorine content of solutions: 17.8 mg/l. Inert gas: argon flow = 550 ml/min. pH of sample chamber: a = 0, b = 1.3, c = 8.

ric acid solution), standardised to the total chlorine content. The concentrations of the available chlorine were identical for all three substances.

The results show that free chlorine is much more difficult to separate from chloramine T solutions than from chlorine or hypochlorite solutions. This means that, even in strong hydrochloric acid, the chlorine is mainly bound to chloramine T, or to the corresponding protonated form $R-SO_2-NHCl$ (reaction 2).

It is interesting to note that no chlorine can be stripped out of sulphuric acid solutions even at pH 0. This means that neither chloramine T (or its protonated form) nor dichloramine T can liberate chlorine, since the chlorine is present in oxidation step +1. Formation of chlorine according to reaction 6 can only take place as a subsequent reaction after chloride ions have been formed.

This assumption was confirmed by tests in which the chloride concentration in sulphuric acid solution was gradually increased by addition of KCl (Fig. 8). In this case chlorine can only be purged in significant quantities at pH 0 from 1 mol/l KCl solutions.

Conversely, even at high chloride concentrations (1 mol/l) no chlorine is purgeable if insufficient acid is present. Significant formation of chlorine is not noticeable until pH < 2. This means that the liberation of chlorine or the hypochlorite formation proceeds via the proto-

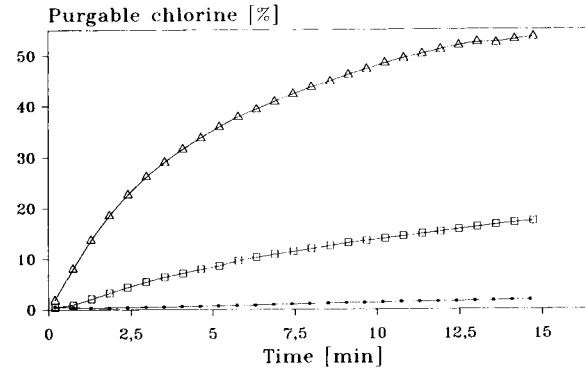

Fig. 8. Influence of chloride on purgable chlorine from sulphuric acid chloramine T solutions. Chloramine T: 1 mmol/l. Argon flow = 550 ml/min. □, small = 0.01 M KCl; □ = 0.1 M KCl; △ = 1 M KCl.

nated form $R-SO_2-NHCl$. On the other hand chlorine is driven out of bleaching liquor–chlorine solutions to the same extent, both in acid and neutral solutions.

4. Conclusions

It could be shown that chloramine T does not behave like the classical chlorine releasing compounds, e.g., Na-dichloroisocyanurate or hypochlorite/chlorine.

4.1. Equilibrium reactions

(1) Liberation of chlorine or HOCl from chloramine T can only take place from the protonated form (see also above):

$$R-SO_2-NCl^- + H^+ \rightleftharpoons R-SO_2-NHCl \quad (8)$$

$$R-SO_2-NHCl + H_2O \rightleftharpoons R-SO_2-NH_2 + HOCl \quad (9)$$

Since both positions of equilibrium are to the left, no hypochlorite is detectable in alkaline solution.

(2) Additional chloride ions are necessary to liberate (purge) the chlorine from acidic chloramine T solutions, i.e., HOCl is not purged.

(3) The concentration of dichloramine T formed in acid solution according to

$$R-SO_2-NHCl + HOCl \rightleftharpoons R-SO_2-NCl_2 + H_2O \quad (10)$$

depends on the pH, but not on the chloride concentration.

Furthermore, according to reactions 8–10, two protons are used up per molecule of dichloramine T formed.

Reaction 10 has the effect of removing HOCl from the equilibrium 9, which results in a shift of the equilibrium in the direction of toluene sulphonic acid until the equilibrium concentrations of HOCl in reactions 9 and 10 are identical. In the end, the equilibrium concentrations result from the (very low) solubility of dichloramine T.

Stoichiometric addition of hypochlorite to chloramine T in acidic solution results in its complete precipitation as dichloramine T. Hypochlorous acid is therefore practically nonexistent in acid chloramine T solutions.

4.2. Decomposition reactions of chloramine T

Aqueous chloramine T solutions do not have unlimited stability. On the one hand, a loss of chloramine T ("active" chlorine content) can be observed over a period of 60 days. A corresponding quantity of toluene sulphonamide is formed. Probably the hypochlorite, which is present only in very small concentrations in equilibrium 9, is subject to gradual decomposition (e.g., with formation of oxygen). On the other hand, toluene sulphonic acid is formed as a further decomposition product, i.e., by the hydrolysis of chloramine T accompanied by the splitting of the N–S bond. In the range examined, the rate of toluene sulphonic acid formation is pH-independent. The nitrogen which is split off is not oxidised to nitrate or nitrite, but probably N_2 is formed.

5. References

[1] M.C. Agraval and S.K. Upadhyay, J. Sci. Ind. Res., 49 (1990) 13.
[2] W. Gottardi, Hyg. Med., 16 (1991) 346.
[3] V.R.S. Rao, D. Venkappayya and G. Aravamudan, Talanta, 17 (1970) 770.
[4] B.C. Verma, K. Swaminathan and S. Kumar, Microchim. Acta, 2 (1978) 391.
[5] S. Sen, P.K. Porwal, A.K. Arora and A.V. Bajaj, Univ. Indore Res. J. Sci., 5 (1978) 22.
[6] J. Vulterin, Collect. Czech. Chem. Commun., 31 (1966) 4662.
[7] L. Erdey, G. Svehla and O. Weber, Fresenius' Z. Anal. Chem., 240 (1968) 91.
[8] W. Gottardi, Microchim. Acta, 1 (1982) 371.
[9] O.K. Norkus and S.P. Stulgiene, Zh. Anal. Khim., 22 (1967) 101.
[10] J. Vulterin, Sb. Vys. Sk. Chem.-Technol. Praze, Anal. Chem., 2 (1967) 37.
[11] D.F. Leggett, N.H. Chen and D.S. Mahadevappa, Fresenius' Z. Anal. Chem., 311 (1982) 687.
[12] K. Terada, H. Honnami and T. Kiba, Bull. Chem. Soc. Jpn., 50 (1977) 132.
[13] H. Thielemann, Pharmazie, 33 (1978) 767.
[14] N.W. Trieff, V.M.S. Ramanujam and G.C. Forti, Microchem. J., 22 (1977) 222.
[15] N.M.M. Gowda, V.M.S. Ramanujam and N.M. Trieff, Microchem. J., 25 (1980) 93.
[16] P.R. Beljaars and T.M.M. Rondags, J. Assoc. Off. Anal. Chem., 62 (1979) 1087.
[17] W.G. Kuhr, Anal. Chem., 62 (1990) 403R.
[18] F. Opekar and P. Beran, J. Electroanal. Chem., 69 (1976) 1.
[19] M. Hahn, Dissertation, University Halle, 1992.

ELSEVIER

Analytica Chimica Acta 289 (1994) 43–46

ANALYTICA CHIMICA ACTA

NADH sensor with electrochemically modified TCNQ electrode

A.S.N. Murthy *, Anita, R.L. Gupta

Department of Chemistry, Indian Institute of Technology, New Delhi-110 016, India

(Received 13th August 1993; revised manuscript received 13th October 1993)

Abstract

7,7,8,8-Tetracyanoquinodimethane (TCNQ) has been immobilized electrochemically on an edge plane pyrolytic graphite electrode. The electrode was immersed in a solution of TCNQ in acetonitrile and a voltage of 1.0 V vs. Ag/AgCl was applied for 25 min. The surface coverage was 5.3×10^{-10} mol cm^{-2}. The modified electrode catalyses the electron transfer from dihydronicotinamide adenine dinucleotide (NADH) and is potentially useful as a sensor for substrates enzymatically coupled to NAD^+/NADH.

Key words: Cyclic voltammetry; Sensors; NADH; TCNQ

1. Introduction

The oxidation of NADH is of special interest because of its practical application in the development of amperometric biosensors for NAD^+-dependent dehydrogenases [1]. Dehydrogenases depend on the soluble cofactor NAD^+/NADH. In order to lower the overpotential in the electrochemical oxidation of NADH, the use of several electron transfer mediators has been examined either in homogeneous solution or with mediator-modified electrodes. The subject has been reviewed recently [2]. A carbon paste electrode chemically modified with a polymer containing a covalently bound phenothiazene dye, toluidine blue [3] and poly(thionine) modified electrodes [4] have recently been suggested for electrocatalytic oxidation of NADH.

7,7,8,8-Tetracyanoquinodimethane (TCNQ) has been found to facilitate electron transfer from glucose oxidase to pyrolytic graphite electrode and the modified electrode (carbodiimide procedure) responded to glucose in the range up to 70 mM [5].

This paper reports on a voltage-facilitated immobilization procedure for TCNQ on an edge plane pyrolytic graphite electrode and the electrocatalytic activity of the modified electrode for NADH oxidation.

2. Experimental

2.1. Reagents

7,7,8,8-Tetracyanoquinodimethane (TCNQ, Aldrich) and NADH (Extra Pure for Biochemistry, SRL, India) were used as received. Acetonitrile was distilled over P_2O_5 before use. The standard buffer was 0.1 M phosphate buffer (pH

* Corresponding author.

0003-2670/94/$07.00 © 1994 Elsevier Science B.V. All rights reserved
SSDI 0003-2670(93)E0667-V

7.0) containing sodium perchlorate. All solutions were prepared in doubly distilled water and oxygen free conditions.

2.2. Apparatus

Cyclic voltammetry (CV) was carried out with a three electrode cell (BAS C-1B) with a working volume of 5 cm^3. The reference and counter electrodes were a sintered Ag/AgCl electrode and a platinum wire electrode, respectively. The working electrode was fabricated from 3 mm diameter edge plane pyrolytic graphite (EPG) supplied by Le Carbone (Lorraine, France). The EPG electrode was polished with 600 grit silicon carbide paper followed by 1 μm diamond paste. A BAS CV-27 voltammograph with a BAS X–Y recorder (Model No. MF 8050F) was used for the measurements. All experiments were carried out at 25 ± 0.1°C.

2.3. Immobilization procedure

TCNQ was immobilized on a clean EPG electrode by dipping it in a 10 mM solution of TCNQ in acetonitrile containing 0.1 M sodium perchlorate and applying a positive potential of 1.0 V vs. Ag/AgCl for 25 min. The electrode was washed with distilled water and stored in the phosphate buffer pH 7.0.

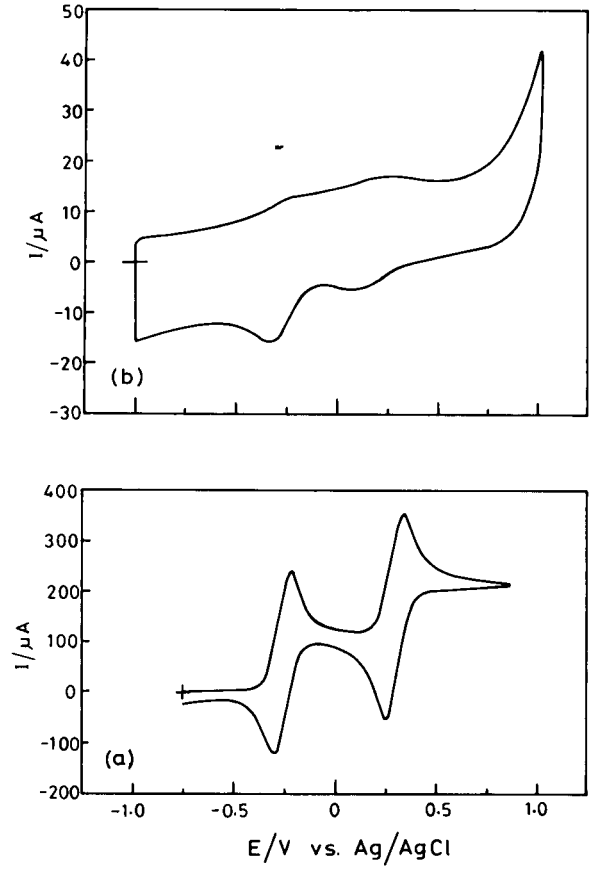

Fig. 1. Cyclic voltammograms of (a) TCNQ (10 mM) in CH_3CN and 0.1 M tetrabutylammonium perchlorate at the EPG electrode (b) a TCNQ-modified EPG electrode in phosphate buffer (pH 7.0); Scan rate: 50 mV s^{-1}.

3. Results and discussion

The CV of TCNQ in acetonitrile solution is shown in Fig. 1a. The two anodic peaks E_{pa1} and E_{pa2} (+0.250 and −0.313 V vs. Ag/AgCl) and the two cathodic peaks E_{pc1} and E_{pc2} (+0.325 and −0.200 V) correspond to the electrochemical processes $TCNQ \rightleftharpoons TCNQ^{\cdot -}$ and $TCNQ^{\cdot -} \rightleftharpoons TCNQ^{2-}$, respectively. These values are in fair agreement with those reported by Hendry and Turner [5] and Sharp [6]. The formal potentials are 0.288 V and −0.256 V, respectively. The CV of the EPG electrode modified with TCNQ in phosphate buffer is shown in Fig. 1b. E_{pa1} and E_{pa2} values are +0.250 and −0.225 V and E_{pc1} and E_{pc2} values are +0.100 and −0.325 V, respectively. The observed changes in the shape and position of the peaks are due to surface modifications. The peak positions are also slightly different from those observed for a TCNQ-modified electrode prepared by the dip coating method [7] possibly due to the presence of the sodium perchlorate supporting electrolyte. The surface coverage, as calculated from the voltammograms of the TCNQ-modified electrode at various scan rates using the equation [8]:

$$i_{p_a} = n^2F^2A\Gamma\nu/4RT$$

(where the parameters have their usual significance) is found to be 5.3×10^{-10} mol cm^{-2} and corresponds to a monolayer.

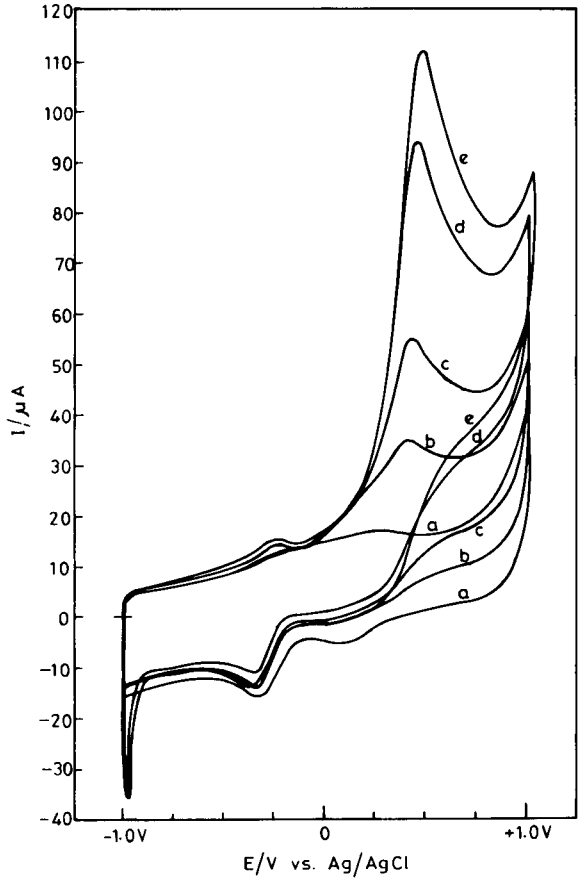

Fig. 2. Cyclic voltammograms of a TCNQ-modified EPG electrode in solutions containing (a) 0.0, (b) 1.0, (c) 2.0, (d) 4.0 and (e) 5.0 mM NADH; scan rate = 50 mV s^{-1}.

The CVs of an TCNQ-modified EPG electrode in the presence of varying concentrations of NADH at pH 7.0 are shown in Fig. 2. NADH is not stable below pH 7.0 [9]. While the peaks corresponding to $TCNQ^{\cdot -} \rightleftharpoons TCNQ^{2-}$ are unaffected, those due to $TCNQ \rightleftharpoons TCNQ^{\cdot -}$ change. The oxidation of NADH is accompanied by a shift of the 0.250 V peak to ca. 0.40 V and an increase in current (corresponding to $TCNQ^{\cdot -}$ oxidation) because the NADH in the solution diffuses towards the electrode and reduces the TCNQ produced electrochemically. As $TCNQ^{\cdot -}$ is regenerated by NADH during the scan, there is a resultant increase in the anodic current. Simultaneously, the cathodic current decreases. The overall reaction scheme may be depicted as follows:

$$TCNQ + NADH \xrightarrow{k} TCNQ^{\cdot -} + NAD^{+} + H^{+} + e^{-} \quad (1)$$

$$TCNQ^{\cdot -} \rightleftharpoons TCNQ + e^{-} \quad (2)$$

$$\text{Net: } NADH \rightarrow NAD^{+} + H^{+} + 2e^{-} \quad (3)$$

The amperometric response of a TCNQ-modified electrode to NADH in solution has been examined. A calibration graph was obtained by measuring the peak current at ca. 0.40 V upon addition of increasing amounts of NADH. The graph is linear over the range 1–10 mM with the equation $i_{p_a}(\mu A) = 19.1[NADH](mM) - 2.8$ (correlation coefficient = 0.999, $n = 7$).

The kinetic aspects of mediator modified electrodes are of interest [10]. An attempt has been made to determine an approximate rate of reaction 1 from analysis of the CVs. Andrieux and Saveant [11] have derived an expression relating the peak current and the concentration for the case when reaction 1 is extremely fast:

$$i_{p_a} = 0.496nFA(DnFv/RT)^{1/2}c \quad (4)$$

where the symbols have their usual significance. From our data on TCNQ modified electrode with a coverage of 5.3×10^{-10} mol cm^{-2}, the constant was found to be 0.326. Using this, and Fig. 1 of Ref. 11, the rate constant k for reaction 1 was calculated to be 4.8×10^{6} M^{-1} s^{-1}. A comparison of this value with other modified electrodes for NADH oxidation has shown that it is similar to that for a 4-[2-(2-naphthyl)vinyl]-catechol-coated electrode (ca. 2.0×10^{6} M^{-1} s^{-1}) [12]. Mention must be made that the values for rate constants obtained by CV or rotating disc experiments are about the same [12].

The results reported here demonstrate that a TCNQ-modified electrode can be effectively used for NADH sensing, up to at least 10 mM. The electrode is quite stable, and experiments concerning its use in for amperometric enzyme NAD^{+}/NADH systems are in progress.

4. Acknowledgements

R.L. Gupta is thankful to CSIR (India) for a Research Associateship and Anita to the authorities of IIT Delhi for the award of a fellowship.

5. References

[1] A.P.F. Turner, I. Karube and G.S. Wilson (Eds.), Biosensors, Fundamental and Applications, Oxford Univ. press, Oxford, 1987.
[2] W. Schuhamann and H.L. Schmidt, in A.P.F. Turner (Ed.), Advances in Biosensors Vol. 2, JAI Press, 1992.
[3] E. Dominguez, H.L. Lan, Y. Okamoto, P.D. Hale, T.A. Skotheim and L. Gorton, Biosensors Bioelectronics, 8 (1993) 167.
[4] T. Ohsaka, K. Tanaka and K. Tokuda, J. Chem. Soc. Chem. Commun., (1993) 222.
[5] S.P. Hendry and A.P.F. Turner, Horm. Metab. Res., Suppl. Ser., 20 (1988) 37.
[6] M. Sharp, Electrochim. Acta, 21 (1976) 973.
[7] A.S.N. Murthy and Anita, Bioelectrochem. Bioenerg., in press.
[8] M. Sharp, M. Petersson and K. Edstrom, J. Electroanal. Chem., 95 (1979) 123.
[9] H.K. Chenault and G.M. Whitesides, Appl. Biochem. Biotechnol., 14 (1987) 147.
[10] P.N. Bartlett, P. Tebbutt and R.G. Whitaker, Prog. React. Kinet., 16 (1991) 55.
[11] C.P. Andrieux and J.M. Saveant, J. Electroanal. Chem., 93 (1978) 163.
[12] H. Jaegfeldt, A. Torstensson, L. Gorton and G. Johansson, Anal. Chem., 53 (1981) 1979.

ELSEVIER

Analytica Chimica Acta 289 (1994) 47–55

ANALYTICA CHIMICA ACTA

Application of a surface acoustic wave sensor system for the detection of non-aqueous solutions and phase transitions in lipid multibilayers

Shouzhuo Yao *

New Material Research Institute, Hunan University, Changsha 410082, China

Kang Chen, Lihua Nie

Department of Chemistry and Chemical Engineering, Hunan University, Changsha 410082, China

(Received 14th June 1993; revised manuscript received 18th October 1993)

Abstract

A surface acoustic wave (SAW) sensor system utilizing a SAW resonator operating at 61 MHz and a pair of parallel electrodes in series was applied to the detection of organic mixtures. Linear frequency shifts were observed as the water content of organic solvents changed. The detection limit was 2 mg l^{-1}. The behaviour of the dielectric constant and conductivity of the lipid multibilayer during phase transition (from solid to liquid crystal) was measured with the SAW sensor system using polymer-coated electrodes. Large frequency changes were also observed for lecithin extracted from egg yolk at the phase transition temperature.

Key words: Acoustic methods; Sensors; Lipids; Phase transitions

1. Introduction

Surface acoustic wave (SAW) devices are very sensitive chemical sensors and most of the applications reported have been in the gas phase [1–7]. In these applications a thin layer of a chemically selective material is applied to the device surface and any physical changes caused by vapour or gas sorption in the film layer, such as deposited mass, elastic constant, electric conductivity and dielectric constant, will result in a shift of the resonator frequency of the device. Factors producing such an effect also include environmental temperature and pressure [8]. The extreme sensitivity of the SAW device makes it attractive as a gas sensor. Thé development of liquid-phase sensors is of interest in many areas, including biochemistry, immunology and electrochemistry. However, many problems arise when SAW sensors are applied in the liquid phase owing to the large energy loss in the propagation of the Rayleigh wave [9].

Most applications have employed SAW devices in the delay line configuration. An alterna-

* Corresponding author.

0003-2670/94/$07.00 © 1994 Elsevier Science B.V. All rights reserved
SSDI 0003-2670(93)E0635-K

tive SAW device configuration is the resonator, which has a narrower bandwidth, lower insert loss, higher Q values and hence lower noise levels than the delay line [10].

Recently, portable and remote sensors for water analysis have been rapidly developed, including dielectric and electrolytic chemical sensors [11,12], optic fibre sensors [13,14] and piezoelectric quartz crystal (PQC) and SAW sensors [1,15,16]. Among these sensors, the PQC and the SAW sensors are the most sensitive for detecting water because of their high mass sensitivity. However, most of the sensors for water analysis were restricted to gas-phase application.

The liquid-crystalline state has been discovered in a variety of biological materials, such as the cell membrane, Golgi apparatus, mitochondria, endoplasmic reticulum and chloroplast [17]. Phase-transition phenomena of lyotropic liquid crystals were studied using a quartz crystal microbalance (QCM) by Okahata and Ebato [18]. They investigated the contributions to frequency changes of fluidity or viscoelastic changes and phase transitions (slipping between layered structures) of multibilayer films in contact with a water phase. The electric conductivity of liquid-crystalline solutions has been repeatedly investigated, but the results are confusing and difficult to evaluate [19]. Dielectric measurements have also been applied to the observation of phase transitions [20]. However, the impedance properties of the phase transitions (from solid to liquid crystal) at high frequency have not been examined very closely.

We have introduced a modified type of SAW sensor system by combining an SAW resonator with a pair of parallel electrodes. We became interested in this sensor system because it can respond to any changes in the physical properties of the medium between the two electrodes that will cause variations in the loop parameters in the oscillation circuit. The SAW sensor system opens up new possibilities for SAW devices, as it was previously believed that these devices could respond only in the gas phase. Recently, we have observed linearity up to 0.02–0.03 mol l^{-1} and a slope of 2.30×10^4 Hz Ω m between the electrolytic conductivity and the SAW sensor system response. In addition, a capacitor (Csc) in series with the conductance cell significantly affects the sensitivity of the sensor system. We have also measured the total salt content in blood serum using the SAW sensor system [21].

In this work, the responses of the SAW sensor system utilizing a 61-MHz one-port resonator to dielectric constant changes were investigated and, as an example of its application, the results of determining the water content in organic solvents are reported. Results of monitoring the behaviour of the dielectric constant and electrolytic conductivity of lipid multibilayers during phase transition are also reported. The detection of the phase transition of lecithin extracted from egg yolk is also described.

2. Experimental

2.1. Materials

Cyclohexanone, benzyl alcohol, 1,2-dichloroethane, methyl acetate, ethyl acetate, propyl acetate, *n*-amyl acetate, tetrachloromethane, 1,4-dioxane, acetone, methanol, ethanol and tetrahydrofuran were of analytical-reagent grade and were dried before the experiments. The bilayer-forming amphiphile sodium dodecyl sulphate (SDS) was of analytical-reagent grade and used as received. Doubly distilled water was used throughout.

SDS was dissolved in water at 80°C, cooled gradually and kept at room temperature for 1 day before the experiments. Lecithin was extracted directly from egg yolk: a mixture of 80 ml of hot 95% ethanol and 15 g of fresh yolk was thoroughly stirred and centrifuged at 1000 rpm (500 *g*) for 10 min, the upper clear solution was then dried in a vacuum desiccator thermostated at 30°C and the light yellow, waxy residue of lecithin was purified by recrystallization twice from ethanol. The lecithin was stored in a refrigerator and protected from light and air to avoid oxidation.

2.2. Apparatus

The 61-MHz one-port resonator used was obtained from Zhuzhou Electronic Factory (Hunan),

with a y,z-cut $LiNbO_3$ crystal with aluminium metallization and mounted on round 5-pin TO-2 style package with epoxy and gold wire bands. The aluminium interdigital transducers (IDTs) were 13 000 Å thick. The resonators were designed with an acoustic aperture and a path length of several wavelengths. On the centre of each separate $LiNbO_3$ crystal chip there were 20 pairs of IDTs with 500 reflectors placed on each side of them. The nominal insertion loss of the resonator was 6.8 dB. The whole device was sealed from the atmosphere with an epoxied lid.

A schematic diagram of the experimental set-up is shown in Fig. 1. The oscillator circuitry allows the frequency to be monitored and the oscillating region may be slightly modulated by the tuning inductor on the oscillator board. Two platinum electrodes of dimensions 0.5×0.5 cm^2 were selected, ground with sandpaper and placed parallel in a detection cell at a fixed distance. The detection cell was suspended in a brass heat sink and the temperature of the circulating water was monitored and controlled by a WMZK-01 temperature controller (Medical Instruments, Shanghai). The electrical connections between the detection cell and the oscillator board were kept as short as possible. A 12 V d.c. power supply was provided by an adjustable dual-track d.c. power supply. The frequency was measured by using an Iwatsu SC7201 universal counter at a resolution of 1 Hz and data were collected at 6 points min^{-1}.

2.3. Procedures

A period of 30 min was needed to stabilize the whole set-up, including the frequency counter and power supply, before the oscillation frequency in air was measured (F_0). The baseline noise was determined by using frequency data collected for 5 min prior to the experiment. The detection cell was thermostated at 15 ± 0.1°C. Oscillation frequencies (F) of the SAW sensor system in organic solvents with different dielectric constants were measured. The procedure was repeated three or four times and the average frequency shifts was calculated as $\Delta F = F_0 - F$. Experiments on the response of the sensor system to water–organic and acetone–organic mixed solvent were conducted by serial additions of water or acetone to organic solvents with different dielectric constants. The response time, which depends mainly on the stirring speed, was less than 1 point (10 s).

The phase-transition phenomenon of SDS was detected by the SAW sensor system when the temperature of the detection cell was raised and lowered in the range 10–80°C at a rate of 12°C h^{-1}. During the experiment, the ambient temperature of the oscillator board, including the SAW

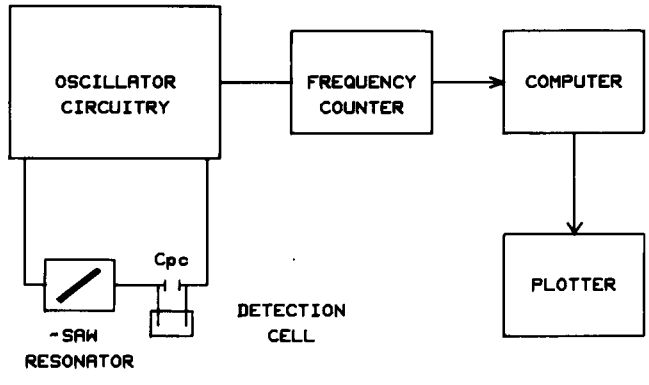

Fig. 1. Schematic diagram of the experimental set-up.

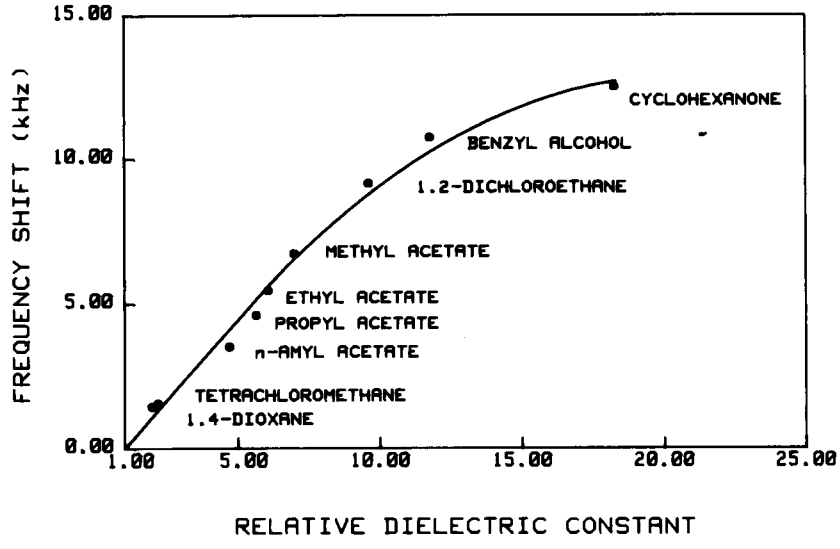

Fig. 2. Frequency responses of the SAW sensor system to organic solvents with different dielectric constants [22].

resonator, was maintained at 15°C. Comparisons were made between bare electrodes and electrodes with a coating of silicone rubber. The frequency behaviour of the response of the sensor system to an aqueous dispersion of lecithin was also measured.

3. Results and discussion

3.1. Response of the SAW sensor system to organic solvents

In a previous paper on the SAW sensor system [21], a frequency shift (ΔF)–electrolytic conduc-

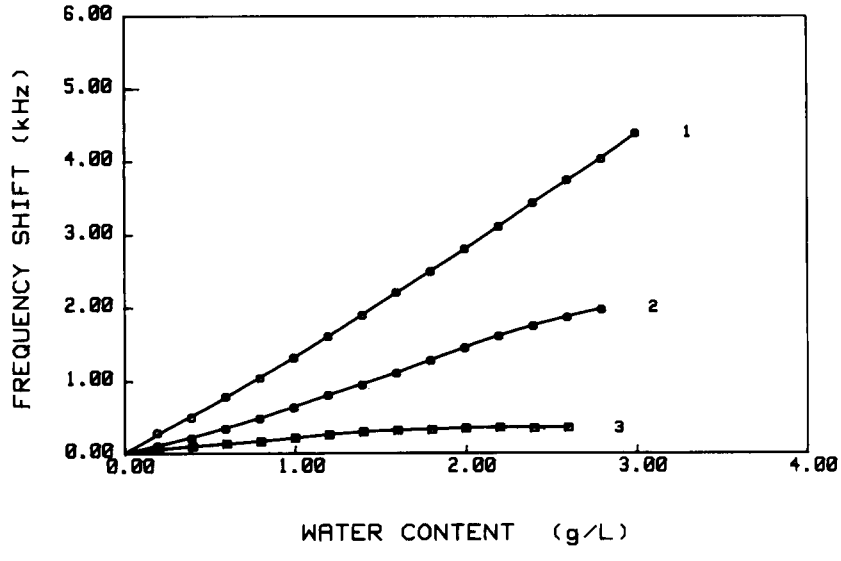

Fig. 3. Frequency shifts vs. water content in methanol with different capacitances (Cpc) in parallel with the detection cell: Cpc (1) < Cpc (2) < Cpc (3).

tivity (κ) correlation was presented:

$$\Delta F = a\kappa + b \quad (1)$$

where a and b are constants depending on the SAW device and the circuit used and other experimental conditions; a can be positive or negative depending on the series capacitor Csc. In this equation influence of the dielectric constant of the electrolyte solution on frequency was presumed to be negligible and was considered to be unchanged for different electrolyte concentrations. For a non-aqueous solution, variation of the dielectric constant becomes the major cause of frequency shifts. It was found that increases in dielectric constant and conductivity will cause a decrease in the oscillation frequency of the SAW sensor system.

The frequency shifts observed with different relative dielectric constants [22] of a variety of organic solvents are plotted in Fig. 2. It can be seen that over a certain range, the frequency shift varies linearly with the relative dielectric constant, i.e., the capacitance of the medium between the two electrodes, according to the following regression equation:

$$\Delta F = c\epsilon + d \quad (2)$$

where $c = 1.04$ (kHz), $d = -0.91$ (kHz) and $r = 0.9912$ in this work. In relating the frequency shift to the capacitance, it is worth noting that any displacement of the detection cell may change its natural capacitance and give rise to a significant deviation. This will limit the SAW sensor system to be used in a practical application because it is impossible to keep the whole experimental set-up absolutely unmoved during the experiment, so a set of parallel capacitors (Cpc) was introduced to adjust the oscillation frequency to a fixed value before each measurements (see Fig. 1). In later experiments, the Cpc was found to be very effective in obtaining a stable oscillation frequency.

We investigated the effect of the capacitance on the response of the SAW sensor system to water–methanol mixtures of different proportions. The results are shown in Fig. 3. The frequency shift data shown indicate that the greater the capacitance, the lower is the sensitivity of the sensor system.

For a binary mixture of a polar and non-polar substances, if there is no dipolar interaction between the two species, the dielectric constant (ϵ) can be calculated from the linear relationship [23]

$$\epsilon = \epsilon_1 p_1 + \epsilon_2 p_2 \quad (3)$$

where $p_1 + p_2 = 1$, p_1 and p_2 being the relative

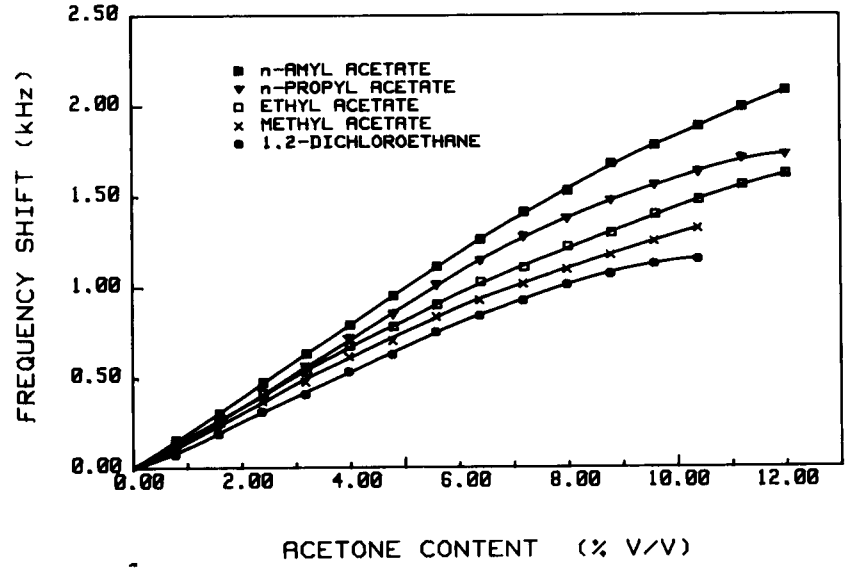

Fig. 4. Frequency shifts vs. acetone content in binary mixtures of acetone and organic solvents. Dielectric constants: (■) n-amyl acetate < (▼) n-propyl acetate < (□) ethyl acetate < (×) methyl acetate < (●) 1,2-dichloroethane.

volume fractions of each component. Although most systems do not behave ideally, in a binary mixture of acetone and organic solvent, if the acetone content (x) is small enough, there is still a linear relationship between the dielectric constant of the mixture and the acetone content:

$$\epsilon = \epsilon_1 + (\epsilon_2 - \epsilon_1)x \quad (4)$$

Hence acetone content can be measured by monitoring the oscillation frequency shift of the SAW sensor system. The sensitivity of the sensor system depends on the difference between the dielectric constants of acetone and the other organic solvent ($\epsilon_2 - \epsilon_1$). The oscillation frequency shift of the sensor system as a function of the acetone content in acetone–organic solvent mixtures with different dielectric constants is shown in Fig. 4. The sensitivities are in good agreement with the plot in Fig. 2 and Eqs. 3 and 4.

Fig. 5 shows the frequency shift versus the dielectric constant for water–organic solvent mixtures. The plots are curved concavely upwards. The differences in appearance and magnitude observed between the plots in Figs. 4 and 5 are probably due to the influences of the dielectric conductance and the dielectric loss in organic solvents with high dielectric constants. The contribution of the conductivity caused by the charge carrier must also be taken into account in mixtures with high water contents. As the plots are nearly linear when the water content is less than 1.5 g l^{-1}, the sensitivity of the SAW sensor system, which is defined as the incremental change in oscillation frequency occurring in response to an incremental change in water content, is 331.7 (1,4-dioxane), 624.2 (tetrahydrofuran), 1335.8 (methanol), 1620.8 (ethanol) and 3681.7 Hz l g^{-1} (acetone). With the lowest noise level of 2 Hz and a signal-to-noise ratio of 3, detection limits of 18, 10, 5, 4 and 2 mg l^{-1}, respectively, are obtained. This result suggests that the SAW sensor system is a promising sensor for the determination of low levels of water.

3.2. Response of the SAW sensor system to phase transition of multibilayer

SDS, the properties of which are well known [19,24], was selected. Owing to the large conductivity change of SDS during the phase transition [24], the oscillation stops at 57°C. When the electrodes were coated with a thin film of silicone

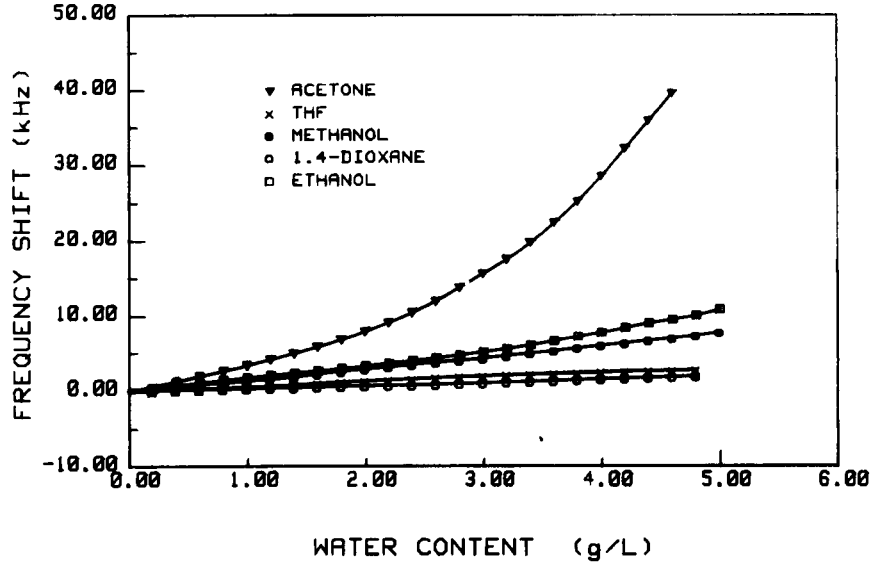

Fig. 5. Frequency shifts vs. water content in organic solvents with different dielectric constants. ▼ = Acetone; × = tetrahydrofuran; ● = methanol; ○ = 1,4-dioxane; □ = ethanol.

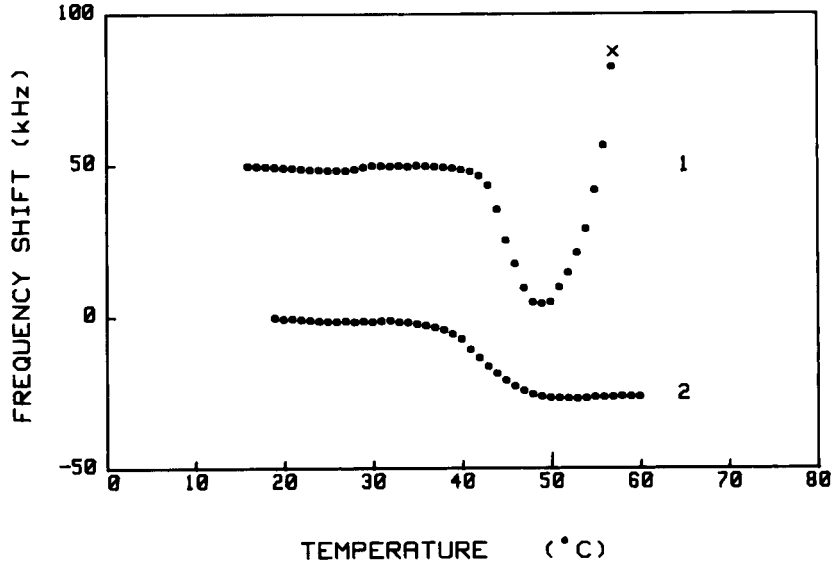

Fig. 6. Comparison between the frequency responses of the SAW sensor system with (1) two bare electrodes and (2) two polymer-coated electrodes to phase transition (from solid to liquid crystal) of 30% SDS.

rubber, a 50 kHz decrease in frequency of the sensor system response was observed. A comparison between the response of the SAW sensor system with polymer-coated electrodes and that with bare electrodes is shown in Fig. 6. Large differences in the frequency–temperature plots at higher temperature were observed. When the polymer film was cast on the electrodes, the sensor system gave much smaller frequency shifts but its oscillation could be maintained up to a higher

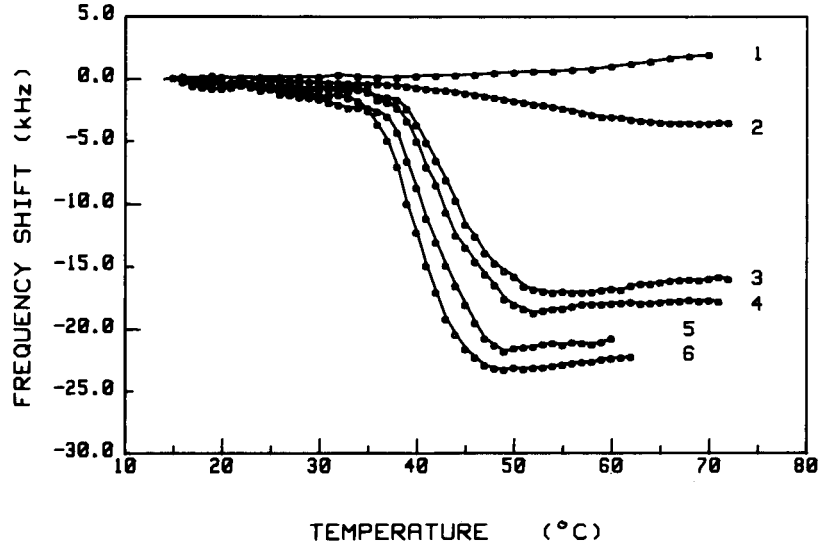

Fig. 7. Frequency behaviours of the SAW sensor system with respect to phase transition of SDS dispersions of (1) 0, (2) 0.1, (3) 25, (4) 30, (5) 35 and (6) 45 wt.%.

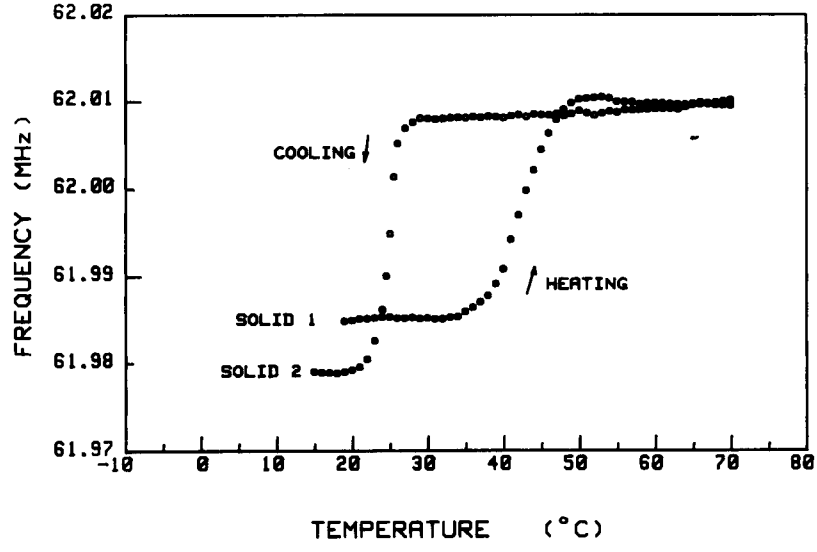

Fig. 8. Frequency behaviours of the SAW sensor system with respect to phase transition of 30% SDS with increasing and decreasing temperature.

temperature. Fig. 6 also shows that the temperature of the gel phase to liquid-crystalline phase transition coincides with the literature value of the phase-transition temperature, T_c. These results indicate that changes in conductivity and dielectric constant at T_c can be detected by the SAW sensor system.

Fig. 7 shows the frequency shift of different SDS dispersions. In a control experiment with water, the change in frequency representing the

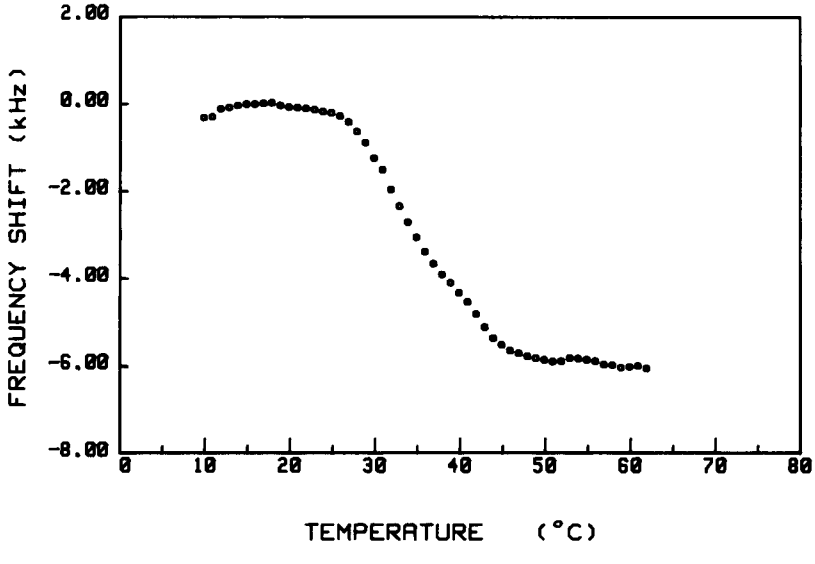

Fig. 9. Frequency response of the SAW sensor system to lecithin extracted from egg yolk.

inherent temperature drift of the device including polymer phase swelling, was linear or nearly so over the temperature range investigated (line 1). A 0.1% SDS solution is an isotropic micelle solution because there is no formation of a lamellar mesophase. The electric conductivity of the micelle solution is close to that of ordinary electrolytic salt solution (line 2). Frequency shifts occur over a temperature range from ca. 35°C to ca. 50°C for all other SDS dispersions (25–40%). No significant differences in the transition temperature for these dispersions were observed but the decrease in the frequency at T_c is greater in SDS dispersions of higher concentration.

Fig. 8 shows the frequency shift of a 30% SDS dispersion when the temperature was increased and decreased at a rate of 12°C h^{-1}. A 5-kHz frequency difference in the response of the sensor system was observed between the SDS solid 1 and solid 2. This was caused by the difference in the cooling procedures; solid 2 was cooled at a relatively faster rate than solid 1 (see Experimental).

3.3. Response of the SAW sensor system to phase transition of lecithin

The lamellar bilayer structure of lecithin enables the biological membrane to perform a wide range of important functions. Phase transition is primarily associated with melting of the hydrocarbon chains of lecithin, which is considered to be of importance for diffusion of the substance through the membrane. For this reason, egg yolk lecithin was selected. It was found that the SAW sensor system can give a clear response to the phase transition of lecithin (Fig. 9). The number of carbon atoms in the hydrocarbon chains of lecithin are different. The extract from egg yolk, still containing other phospholipids, also varies considerably in chemical composition. This may explain why the temperature of the crystal to liquid-crystalline transition, T_c, covers a wide range in this experiment.

4. Acknowledgement

This work was supported by funds from the National Science Foundation and Education Commission Fund of China.

5. References

[1] D.S. Ballantine and H. Wohltjen, Anal. Chem., 61 (1989) 704A.
[2] A. D'Amico and E. Verona, Sensors Actuators, 17 (1989) 55.
[3] C.G. Fox and J. F. Alder, Analyst, 114 (1989) 997.
[4] A.J. Ricco, S.J. Martin and T.E. Zipperian, Sensors Actuators, 8 (1985) 319.
[5] M.S. Nieuwenhuizen and A.J. Nederlof, Anal. Chem., 60 (1988) 236.
[6] D.S. Ballantine, S.L. Rose, J.W. Grate and H. Wohltjen, Anal. Chem., 58 (1986) 3058.
[7] A.W. Snow and H. Wohltjen, Anal. Chem., 56 (1984) 1411.
[8] W.M. Heckl, F.M. Marassi, K.M.R. Kallury, D.C. Stone and M. Thompson, Anal. Chem., 62 (1990) 32.
[9] G.S. Calabrese, H. Wohltjen and M.K. Roy, Anal. Chem., 59 (1987) 833.
[10] J.W. Grate and M. Klusty, Anal. Chem., 63 (1991) 1719.
[11] S.A. Stephen, Res. Dev., 2 (1989) 169.
[12] T. Hirschfeld, Chemtech., 16 (1986) 118.
[13] F. Boltinghouse and K. Abel, Anal. Chem., 61 (1989) 1863.
[14] C. Zhu, F.V. Bright, W.A. Watt and G.M. Hieftje, Proc. Electrochem. Soc., 87 (1987) 476.
[15] S.Z. Yao and L.H. Nie, Anal. Proc., 24 (1987) 336.
[16] P.H. Hung, IEEE Trans. Electron Devices, 35 (1988) 744.
[17] G.H. Brown and J.J. Wolken, Liquid Crystals and Biological Structures, Academic Press, New York, 1979.
[18] Y. Okahata and H. Ebato, Anal. Chem., 59 (1989) 2185.
[19] H. Kelker and R. Hatz, Handbook of Liquid Crystals, Verlag Chemie, Weinheim, 1980.
[20] A.V. Lobastova and Y.F. Deinega, Usp. Kolloidn. Khim., (1973) 300.
[21] S. Yao, K. Chen, F. Zhu, D. Shen and L. Nie, Anal. Chim. Acta, 287 (1994) 65.
[22] R.C. Weast, M.J. Astle and W.H. Beyer (Eds.), CRC Handbook of Chemistry and Physics, 65th edn., CRC Press, Boca Raton, FL, 1984, p. E-49.
[23] B.W. Thomas, in M. Kolthoff and P.J. Elving (Eds.), Treatise on Analytical Chemistry, Part I, Wiley, New York, Vol. 4, 1963, p. 2641
[24] L. Wang and S. Liao, Chemistry of Liquid Crystals, Science Press, Beijing, 1986 (in Chinese).

ELSEVIER

Analytica Chimica Acta 289 (1994) 57–67

ANALYTICA CHIMICA ACTA

Effects of contaminants and charge transfer on the molar absorptivities of fullerene solutions

Rhys N. Thomas

Chemistry Department, University of Missouri-Columbia, Columbia, MO 65211, USA

(Received 28th July 1993)

Abstract

Fullerene molar absorptivities in the visible region for C_{60} and C_{70} in toluene are given, along with methods of estimating mass fractions, contamination, and charge exchange in mixed fullerene solutions. Molar absorptivities for C_{60} in the UV and visible and that of ethyl carbazole in the UV are also reported.

Key words: UV–Visible spectrophotometry; Fullerenes; Molar absorptivity of fullerenes

1. Introduction

Solution chemistry of fullerenes usually is performed on mixtures of homologues of only approximately known composition in order to save the considerable expense of using pure samples. However, knowledge of the composition can become quite important to those involved in separations, and to those searching for reactions which show a preference for a particular fullerene. Further, reaction mixtures of fullerenes with other compounds are often difficult to separate, so a routine method of estimation of quantities of reactants and products would be quite useful. But, since fullerenes have broad absorption maxima and numerous shoulders over a huge wavelength range, separating features of reactants and products for kinetic measurements has proven to be very difficult.

A contributing difficulty was found in that molar absorptivities for the various fullerenes have been slow of publication. While much of the work reported to date requires that such constants be generated [e.g., when reporting the composition of a fullerene mixture as determined by liquid chromatography (LC)], the constants have been omitted from the final reports, requiring that many researchers repeat the same mundane experiments. Those which have been published [1–4] were only for absorption maxima for a particular fullerene. But, in order to determine the composition of a mixture or quantitate a spectrophotometrically detected liquid chromatogram, molar absorptivities at the same wavelength(s) must be known for all analytes.

Since several experiments were planned using mixed fullerenes in toluene, molar absorptivities were required for both C_{60} and C_{70} in that solvent. Other experiments were planned using ethylcarbazole and pure C_{60} in hexanes, requiring those constants as well. The molar absorptivities of the major maxima and shoulders of C_{60} in

0003-2670/94/$07.00 © 1994 Elsevier Science B.V. All rights reserved
SSDI 0003-2670(93)E0624-G

hexane were available in the literature, but values at all wavelengths in the UV–visible range were required. Those constants for ethylcarbazole, C_{60}, and C_{70} are reported here as a reference point for describing simple methods for (1) quantitating the C_{60} and C_{70} content of a mixture, (2) obtaining a qualitative estimate of the absorbing impurities, (3) allowing for the triplet-state absorbance, and (4) identifying the occurrence of charge transfer events between C_{60} and other analytes or solvent molecules.

2. Experimental

The concentrations were computed from masses of fullerene powders (from 1 to 4 mg per sample by difference) weighed on a balance having a calibrated precision of ± 0.01 mg. The powders were baked under nitrogen overnight at 150°C to drive off trace quantities of solvents in the powder. The concentrations of the solutions had standard deviations of 1.4% (C_{60} and ethylcarbazole), and 0.8% (C_{70}).

To investigate purity, mass spectra of the fullerene samples were taken on an Extrel 2000 fourier transform mass spectrometer (FTMS) using laser desorption at 50 lamp joules at 258 nm. Both positive and negative ion collection were used. The positive ion mode was further enhanced by ejecting 720 m/z in order to better observe the background.

UV–Visible absorption measurements to be used for molar absorptivities of C_{60} and C_{70} in toluene were taken on a Beckman 101A UV–visible spectrometer, using a 1.0 nm effective bandwidth, a medium response factor, and a 60 nm/min monochromator speed. The C_{60} sample was measured at 13 different dilutions ranging from 1.845 mM to 0.306 mM. The C_{70} sample was measured at 23 different dilutions ranging from 1.100 mM to 0.020 mM. To stay within the limits of the spectrometer and Beer's Law, only absorbances between 0.100 and 1.500 (± 0.0005) were used, resulting in at least 7 data points per molar absorptivity. Standard deviations for the slopes (σ_β) which generated the reported absorptivities were less than 1% at all but a very few wavelengths. The less precise values ($\sigma_\beta < 5\%$) were all located on steep absorption slopes, where reproducible measurements were much more difficult.

To test the ability of these coefficients to accurately indicate the relative quantities of C_{60} and C_{70} in a toluene solution, a set of solutions of 7 different proportions (47.5, 35.2, 25.8, 18.5, 12.5, 7.6 and 3.5% C_{70}) were mixed from the pure standards and their absorbances were measured at five wavelengths (407, 474, 540, 594 and 640 nm). These were chosen because the mixed fullerene spectrum had easily discernible peaks or shoulders at these wavelengths, allowing better reproducibility.

UV–Visible spectra of four mixtures of fullerenes of unknown composition from different sources were measured in order to determine the effect of trace amounts of higher fullerenes on fullerene-ratio calculations. Three of the mixture samples were gifts: one from Mustapha Diack of the University of Tennessee – Knoxville and Oak Ridge National Laboratory, one from ABC Laboratories of Columbia, MO, and one from Aldrich, purchased by the Analytical Chemistry Division of Oak Ridge National Laboratory. The fourth sample was an aliquot of the Diack solution after a reaction, containing substantially less C_{70} and a significant fraction of substituted C_{60}. Each of these mixtures was analyzed by FTMS to verify the presence of higher fullerenes.

To compare the effects of monochromatic versus white light excitation, spectra were obtained of C_{60} in toluene on a Perkin-Elmer 576 UV–visible spectrometer (1.0 nm effective bandwidth), and an HP 8452A diode array spectrometer (2 nm per channel). The same sample and reference solutions and quartz cells were used in each measurement, the two spectra being produced a few minutes apart.

To assess the effects of charge transfer on the visible spectrum of fullerenes, solutions of mixed fullerenes were made in methylene chloride, *tert.*-butylbenzene, aniline, nitrobenzene and bromobenzene. Spectra of these were taken immediately after making the solutions, and again after 3 and 33 days.

UV–Visible absorption measurements for cal-

culating the molar absorptivities of ethylcarbazole and C_{60} in hexane were performed on an HP 8452A diode array spectrometer (2 nm per channel). The C_{60} sample was measured at 14 different dilutions from 31 μM to 4.4 μM; the ethyl carbazole at 23 different dilutions from 8.8 μM to 1.1 μM, using the absorbances from 0.100 to 1.500, resulting in at least 7 data points per molar absorptivity. The standard deviations of the slopes (σ_β) were generally less than 1%, except in regions of steep absorbance slope.

3. Results

Under laser desorption in positive ion mode with mass 720 ejected, FTMS analysis of the C_{60} sample showed a C_{70} peak (840 m/z) which was about the same height as the C_{50}^+ fragmentation peak, demonstrating that the solution was essentially pure (Fig. 1). Without the ejection of 720 m/z, no signal for C_{70} was discernible. The

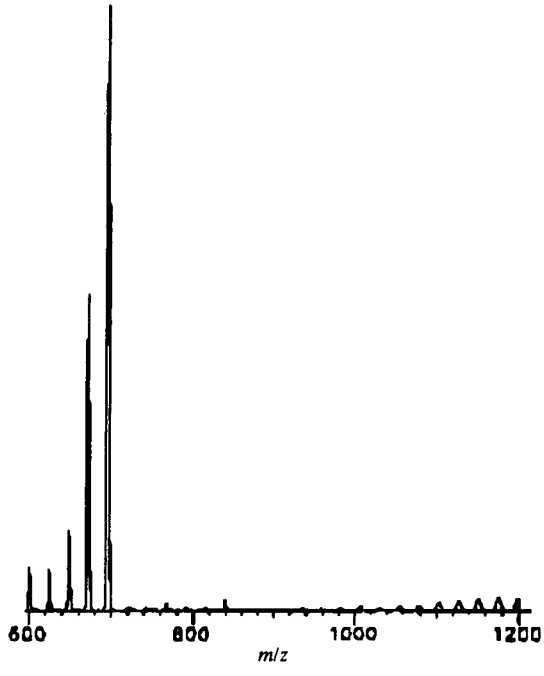

Fig. 1. FTMS of the pure C_{60} sample using positive ion mode, Q-switched laser desorption, ejecting 720 m/z to reveal the background.

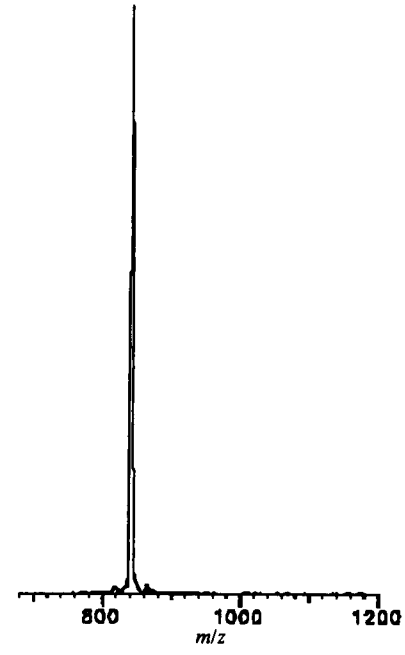

Fig. 2. FTMS of the pure C_{70} sample using positive ion mode, Q-switched laser desorption.

small, regularly spaced peaks which appeared in the high mass range (> 1000 m/z) were due to fullerene coalescence, a common phenomenon in the positive ion mass spectroscopy of fullerenes. More exact quantitation of C_{70} was impossible, since the amount created in the laser desorption process, and the relative detection cross sections of C_{60} and C_{70} under those conditions were only qualitatively known. In negative ion mode, no fullerenes other than C_{60} were discernible above the noise. As fullerenes were desorbed by the laser, positive fullerene ions from photoionization were to be expected if any fullerenes existed in the sample. Negative ion mode was much less sensitive, but did not suffer from the coalescence problem. The C_{70} sample (Fig. 2) showed the same level of purity using the same process.

The molar absorptivities for C_{60} and C_{70} in toluene across the visible region are shown in Figs. 3 and 4. Those for C_{60} and ethylcarbazole in hexane are shown in Figs. 5 and 6. These values were computed at 2 nm intervals on the even numbers. In all cases, the absorptivity data was computed beginning with the lowest wavelength

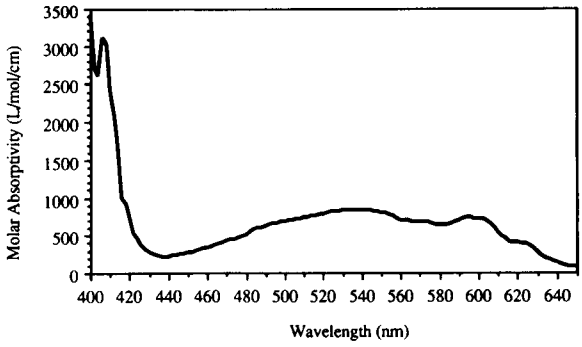

Fig. 3. Molar absorptivities of C_{60} in toluene. The thickness of the line well represents a one-standard-deviation error bar.

at which stable data could be obtained, limited by the cutoff value of the solvent. The thickness of the curve in each graph represents very well a one-standard-deviation error bar. The complete set of numerical values may be obtained from the author. A short list of absorptivities for both fullerenes in toluene, corresponding to easily discernible maxima and shoulders, is given in Table 1. Even though only one or the other of those fullerenes showed a feature at the given wavelength, both values must be known if the composition of the mixture were to be calculated. The wavelengths of Table 1 were selected because these features allowed easy matching of the monochromator of the spectrometer used in these experiments to the monochromators of future researchers. When this data was used to determine the compositions of the 7 known mixtures, the values calculated from the absorbance differed from the known values by between 0.2% and 2.0%, all indicating mass fractions of C_{70} lower than the known values.

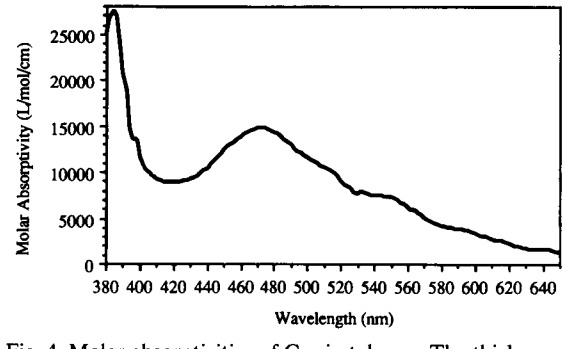

Fig. 4. Molar absorptivities of C_{70} in toluene. The thickness of the line well represents a one-standard-deviation error bar.

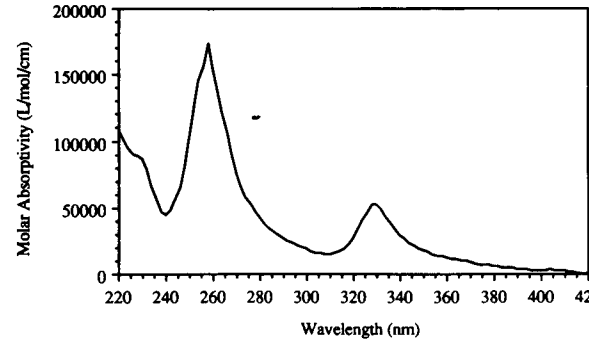

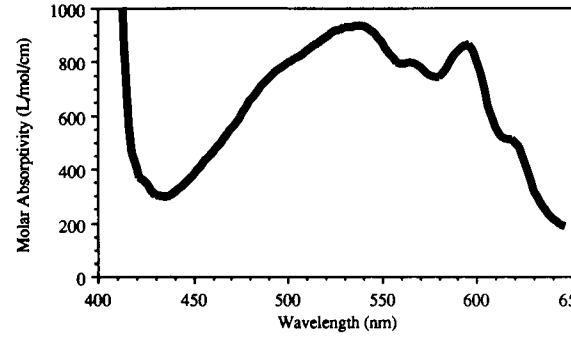

Fig. 5. Molar absorptivities of C_{60} in hexane. The thickness of the line well represents a one-standard-deviation error bar.

In the fullerene mixtures obtained from Diack and from ABC Labs., upon FTMS analysis with laser desorption in negative ion mode, higher fullerenes were perhaps detectable (with a little

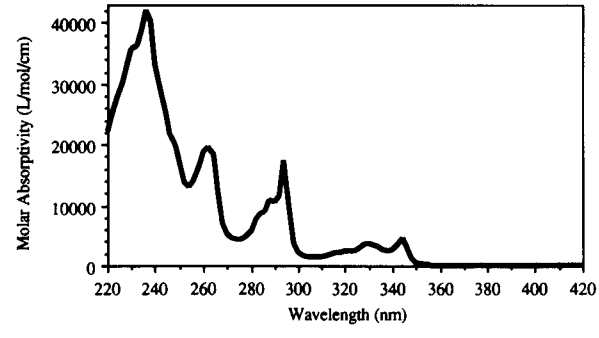

Fig. 6. Molar absorptivities of ethylcarbazole in hexane. The thickness of the line well represents a one-standard-deviation error bar.

Table 1
Molar absorptivities (l mol^{-1} cm^{-1}) at features of C_{60} or C_{70} in toluene

λ (nm)	ϵ_{60}	σ_{60}	ϵ_{70}	σ_{70}	Feature
384			27500	530	C_{70} peak
398			13500	370	C_{70} weak shoulder
407	3100	50	9570	160	C_{60} peak
474	457	9	14800	230	C_{70} major peak
498	683	10	11800	180	C_{60} weak shoulder
532	833	13	7890	220	C_{70} weak shoulder
538	838	13	7540	200	C_{60} major peak
548	816	12	7340	190	C_{70} strong shoulder
570	684	11	5050	90	C_{60} strong shoulder
580	642	10	4190	70	C_{70} weak shoulder
594	730	11	3670	60	C_{60} minor peak
614	464	8	2600	40	C_{70} shoulder
618	414	7	2430	50	C_{60} shoulder
640	128	5	1660	35	C_{70} minor peak

imagination) above the noise. In positive ion mode with 720 m/z ejected, C_{84}^+, C_{88}^+, and C_{94}^+ peaks became clearly visible. The tallest of the higher fullerenes, C_{88}^+, was slightly smaller than the C_{68}^+ and C_{56}^+ peaks in the Diack mixture, but slightly larger in the ABC mixture. Under the same conditions, the Aldrich mixture showed a larger percentage of C_{70}, but less of the higher fullerenes. The reaction mixture showed no detectable higher fullerenes and a depleted quantity of C_{70}.

The wavelengths of the three major visible spectral maxima of a mixed fullerene solution in a variety of solvents are given in Table 2, illustrating a small but marked solvent dependency as first noted by Heath from benzene (386.3 nm) to methylene chloride (386.0 nm) [5].

Table 2
Three spectral maxima of a mixed $C_{60:70}$ solutions appeared at slightly different wavelengths (nm) in different solvents

Solvent	C_{60}	C_{70}	C_{60}
Hexane	404	469	590
Aniline		469	
Methylene chloride	404	470	591
Cyclohexane[18]	404		598
tert.-Butylbenzene	406	474	597
Bromobenzene	406	473	593
Nitrobenzene		473	593
Benzene[19]	406	474	597
Toluene	407	474	594

None of the mixed fullerene solutions in toluene or *tert.*-butylbenzene showed any measurable decomposition over a period of 1 month. No epoxide peak [6] was discernible at 424 nm in the UV–visible spectra. However, all samples in methylene chloride lost approximately 4% of the 404 nm peak relative to the valley at 400 nm and a small maximum at 424 nm was apparent, indicating some epoxidation.

Bromobenzene showed the same spectrum as toluene after 3 h, but had completely lost its 406 nm maximum (the same feature as 404 nm for methylene chloride) after 3 days. Aniline and nitrobenzene lost the same peak within minutes. However, the mass spectra of the three solutions showed no fullerene adducts in either positive or negative ion mode.

4. Discussion

In a solution composed of a mixture of solutes, the absorbance of the whole can be attributed to the sum of the absorbances of the parts. Combining this in terms of Beer's Law with a function describing the mass fraction of one solute (and rearranging), the mass fraction may be found by

$$F_1 = \frac{A/M - K_2 + \Sigma F_i(K_2 - K_i)(i > 2)}{K_1 - K_2} \quad (1)$$

where F_i is the mass fraction of solute i, A is the absorbance, M is the total mass of all solutes in grams per liter of solution, and K_i is the molar absorptivity multiplied by the pathlength divided by the molar mass of solute i. The derivation uses $K = \epsilon b/\mathrm{MW}$, $F = m/M$, and $F_1 = 1 - \Sigma F_i$ $(i > 1)$ where ϵ is the molar absorptivity, b is the pathlength, MW is the molar mass, F is the mass fraction, and m is the mass per liter of one analyte. From Beer's Law, $A = \Sigma \epsilon_i b_i c_i = \Sigma K_i m_i = \Sigma K_i F_i M$. Since the system of interest contained two primary analytes, the first two terms were extracted as $A/M = K_1F_1 + K_2F_2 + \Sigma K_iF_i$ $(i > 2)$. Since $F_2 = 1 - F_1 - \Sigma F_i$ $(i > 2)$, $A/M = K_1F_1 + K_2(1 - F_1 - \Sigma F_i \ (i > 2)) + \Sigma K_iF_i \ (i > 2) = F_1(K_1 - K_2) + K_2 - \Sigma F_i(K_2 - K_i)$ $(i > 2)$. Solving for F_1 produces (Eq. 1).

If no significant contamination exists and the molar absorptivities at the same wavelength are known for all solutes, and if the mass of analyte per liter can be known accurately, the composition may be determined by a simple absorption measurement. The effects of slightly different contaminants and spectrometer baselines may be reduced by measuring the absorbance of successive dilutions, calculating a "relative molar absorptivity" to be used in place of the absorbance. Eq. 1 above becomes quite simple if only two solutes are present (e.g., C_{60} and C_{70}). A system of simultaneous equations is created for higher numbers of solutes.

Unfortunately, contamination by trace quantities of higher fullerenes and fragments of broken fullerenes accounts for some of the absorbance in nearly every fullerene mixture. Rearranging the formula above isolates the contamination term:

$$F_1 = \frac{A/M - \mu K_2 + \Sigma F_i(K_2 - K_i)(i > 2)}{K_1 - K_2} - \frac{K_c m_c}{M(K_1 - K_2)} \quad (2)$$

where K_c is the molar absorptivity multiplied by the pathlength divided by the molar mass of the contaminant, m_c is the mass of the contaminant in grams per liter, μ is the fraction of the mass which is not contaminant ($\mu = 1 - m_c/M$), and all other variable are as in Eq. 1 above. The contaminant is not included in the $\Sigma F_i(K_2 - K_i)$ $(i > 2)$ term. If the mass of the contaminants is thought to be less than 1% of the total mass of the dried solution, μ may be set to 1 without altering the results significantly.

Since the contribution to the absorbance by contaminants is presumed to be small but is essentially unknown, the reliability of the fraction obtained will be similarly unknown. If the calculation is repeated for several wavelengths, a collection of variously inaccurate F_1 values will be generated. Comparing Eq. 1 and Eq. 2, contamination will always cause F_1 of Eq. 1 to be too high if $K_1 > K_2$, and too low if $K_1 < K_2$. No evaluation is possible if the mass-weighted molar absorptivities are equal. By judicious choice of analytical wavelengths, a bracketing of the correct fraction may be obtained.

Unfortunately, the molar absorptivity of C_{70} is greater than the molar absorptivity of C_{60} at all visible wavelengths between 380 and 650 nm. At wavelengths longer than 650 nm, the absorptivity is too small to be statistically useful. At wavelengths shorter than 380 nm, the toluene absorbs so strongly that the transmitted photon counts in both the reference and sample paths are insufficient to yield stable values. But, if C_{70} is identified as solute 1, an upper bound may be obtained for the C_{70} mass fraction in toluene from the lowest computed value. To test this premise without the presence of significant contamination, seven solutions of varying composition were mixed from C_{60} and C_{70} standards. Considering that (1) the C_{60} and C_{70} concentrations were known only to 1.4% and 0.8%, respectively, (2) the absorbances were single measurements, and (3) some small measurement error was introduced in mixing, the values obtained from the mixtures were at the extreme of being within experimental error, although systematically low. Since no measurable contamination was present, a minimum tolerance of 2% must be assumed when applying this idea to unknown mixtures. At small concentrations of C_{70}, the relative error of measurement becomes very significant, so a quantitation limit of about 4% should be assumed.

Were this process performed in hexane solutions in the ultraviolet range, bracketing perhaps could be accomplished, since the molar absorptivity of C_{70} appears to be smaller than that of C_{60} in the regions of the C_{60} maxima at 329 nm and 257 nm [2,7]. If that were done, a bracketing $\pm 1\%$ could be expected as long as the mass fractions were above 4%.

If Eq. 1 were applied at many wavelengths for the same solution, the absorption profile of the contaminants would be generated. Taking the lowest mass fraction produced by Eq. 1 (assuming that bracketing is not possible) and knowing the dry mass of the sample (a critical but difficult measurement to be discussed subsequently) and the molar absorptivities of C_{60} and C_{70} across the spectrum, the absorbance of fullerenes may be subtracted from the absorbance of the mixture,

Table 3
Reported UV–visible absorption maxima and shoulders (nm) for the higher fullerenes

C_{2v}–C_{78} CH_2Cl_2	ϵ[l mol^{-1} cm^{-1}] (C_{78}: Ref. 3)	D_3–C_{78} CH_2Cl_2	C_{84}[a] $CHCl_3$
696	3400	820	912 sh
638	4000	768	760 sh
528	11500	757	668 sh
424	23800	734	616
390 sh	25500	700	566
368 sh	30300	472	476 sh
359	30800	362 sh	393
325	42700	356	380 sh
308	44400	322	320 sh
		276	280 sh

[a] Ref. 20.

yielding the absorbance of the contaminants. That profile may lead to identification of some of the sources of the contamination, which then may be included in the known portion of the equation, better bracketing the true fractional masses. Published absorption maxima and shoulders for some of the higher fullerenes are given in Table 3.

As mentioned, determining the mass of the analytes is a complex problem. Fullerene powders trap solvent molecules and broken pieces of fullerenes very well. The accepted method for determining the analyte mass is to dry the sample under vacuum and 200°C overnight. However, this use of time is inconvenient, even useless for those wishing to monitor chromatography columns. And the process itself is not without significant opportunity for error. If the mass of the contaminants (higher fullerenes, broken fullerenes, and solvent) were to increase to 10% of the whole, the estimate of C_{70} mass fraction from Eq. 1 would as much as double. Further, μ in Eq. 2 would no longer be insignificant, and M would be of doubtful accuracy. So, an alternate method was developed (a computer program) which does not require knowledge of the mass.

The program (the source code, parameter files, and help text are available from the author), usable on any mixture of substances, not just fullerenes, contains as reference files the molar absorptivities at 2 nm intervals of all target substances. The operator specifies regions of the spectrum which are characteristic of each substance, and the algorithm incrementally subtracts aliquots of each target substance until the residual absorbance in the specified regions is as linear as possible (using the correlation coefficient, r^2, as the indicator). The program is merely a fast way of investigating thousands of combinations of proposed analyte masses to find the optimum residual absorbance.

Testing for linearity in specified regions yields superior results compared to evaluating the linearity of the entire absorption spectrum. The background due to contaminants and the equipment may be nonlinear. Even a small contamination by higher fullerenes will produce a background with two distinct regions, breaking around 540 nm, with the shorter wavelength region rising and the longer wavelength region horizontal.

Better results are obtained by selecting broad maxima for the test regions rather than very narrow ones. Very narrow maxima (e.g., 407 nm for C_{60} in toluene) are very difficult to measure reproducibly due to the steep slope, the tolerance in the wavelength selection, and the somewhat arbitrary effects of grouping at 2 nm intervals. Misalignment of only 0.1 nm results in tremendous noise in the residual spectrum in that region. Wider peaks are much easier to measure because alignment is no longer critical. The maxima which gave the best results for fullerenes were those at 594 nm for C_{60} and 474 nm for C_{70}. The choice of 474 nm was obvious, since that was the strongest peak of C_{70} in the visible region. The 594 nm peak was chosen because, while it was not the strongest in the visible spectrum of C_{60}, it was better separated from other features. The maximum at 538 nm for C_{60}, while larger, was extremely broad, so linearity was difficult to detect.

The width chosen for each test region depends on the width of the peak and the presence of contaminant peaks. The C_{84} maximum at 616 nm and the C_{60} noise between 400 nm and 410 nm must be avoided. Since noise and unexpected contaminants may arise anywhere, a manual viewing function has been included in the program to aid in selection of the optimum region. In general, the ranges of 580 nm to 600 nm for C_{60} and 466 nm to 512 nm for C_{70} gave best results for

mixtures with significant higher fullerenes. Broader regions (540 nm to 600 nm and 440 nm to 540 nm) were better for situations with smaller contamination.

A negative residual absorbance is not reasonable. However, due to differences in baseline and noise, such may be necessary. A compromise was included in the program by disallowing negative absorbance only in the operator-specified regions. Thus, the noise of a misaligned narrow peak was allowed to go negative. Were negative absorbances allowed, a second set of maxima would appear in the program at absolutely impossible masses.

Discovering the optimum combination of masses is not trivial, as there is not always a single maximum. The three-dimensional plots in Fig. 7 illustrate the problem. (Such plots may be obtained from the program if exactly two analytes are specified, since any other number of analytes requires a different number of axes.) Except for the 540 nm to 600 nm plot for the pure C_{60} sample, each plot for each fullerene mixture had two distinct maxima and a pronounced valley. The pure C_{60} plot had no valley. Masses which yielded negative residual absorbances in the regions of interest were assigned correlation coefficients of zero, which was the source of the sharp cliff. The valley corresponded to the region where just enough of one analyte had been removed to give best definition to the peak of the other substance, drastically reducing linearity. The optimum was declared when both plots were on a maximum correlation for the same set of masses.

Adjusting the width of a region of interest has very little effect on the final result until the region begins to encompass (or fails to encompass) a contamination maximum or shoulder. Then, with only a small change in region width, a radically different optimum is found, but at an

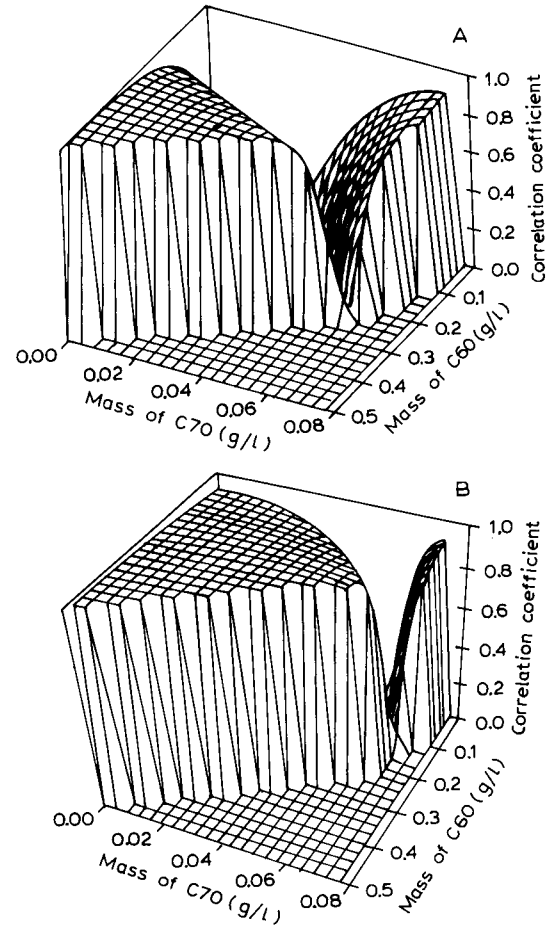

Fig. 7. Correlation coefficients as a function of fullerene mass for the Diack solution. (A) Wavelength region 580–600 nm for C_{60}. (B) Wavelength region 466–512 nm for C_{70}.

Table 4
Comparison of analyte masses from weighing dry fullerene powder, from Eq. 1 and from C_{60} and C_{70} masses from the global maximum of the correlation coefficients of the regions of interest

Source	Weighed C_{60} (g/l)	Weighed C_{70} (g/l)	Computed C_{60} (g/l)	Computed C_{70} (g/l)	C_{60} Region (nm)	C_{70} Region (nm)	Δ mass from weighed (%)
ABC	0.115	0.015	0.119	0.015	580–600	466–512	−3
Aldrich	0.140	0.011	0.127	0.011	580–600	466–512	+9
Diack	0.410	0.021	0.412	0.021	580–600	466–512	+0.5
Pure C_{60}	0.190	0.000	0.184	0.000	540–600	440–540	+3
Reaction			0.398	0.012	540–600	440–540	

unrealistic mass. For example, with the Diack mixture, changing one region limit from 580 nm to 586 nm resulted in an estimate of 75% contamination. Thus, reasonable regions were easily found.

For speed, a binarily decreasing step size was used. If the combination of masses chosen by the program had a larger correlation coefficient than both points one step to either side, the increment was divided by two and tried again. The maximum was declared when the step size reached a preset minimum. The initial step size used in the search must be large enough to step over the noise maxima, but not the same size as the noise frequency. For certain initial values, the program will oscillate across a valley indefinitely. If too small an initial value is chosen, the result will always be zero. Between those limits, an optimum value may be chosen for speed. The same results were found regardless of which substance was optimized first.

A comparison, summarized in Table 4, was made between results gained from Eq. 1 as opposed to those from the program. The samples for which the analyte mass was known showed an excellent agreement. Theoretically, the masses in the Computed C_{70} column will be systematically high. In addition, the fact that analyte absorbance could have been extracted from contaminants and baseline, the masses in both computed columns could be systematically high. The total of the computed fullerene masses, when subtracted from the sum of the weighed masses, indicated the amount of contamination (solvent, broken fullerenes and higher fullerenes), although a substantial portion of those values were within experimental error (±3%). The Aldrich sample indicated some contamination by solvent or broken fullerenes.

The residual spectra are shown in Fig. 8. Although the Diack and Aldrich samples appeared to still have a substantial maximum at the C_{70} feature location of 474 nm, closer inspection showed that this feature had disappeared and a new maximum at 470 nm had taken its place. It was possible to find mass combinations of C_{60} and C_{70} to eliminate this new maximum, but the contaminant mass needed to account for the now

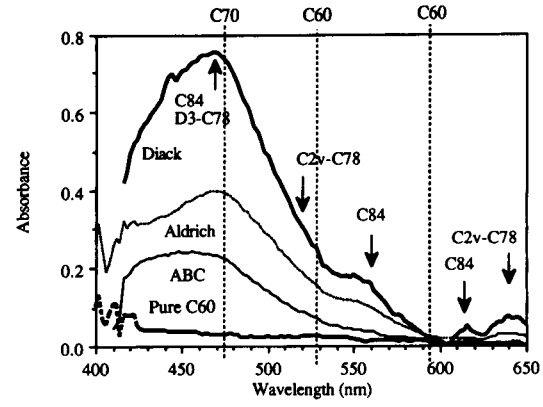

Fig. 8. Residual absorbances for three mixtures and pure C_{60} after subtraction of the fullerene masses shown in Table 4. The locations of maxima of higher fullerenes are given for reference.

nearly flat background became 34%. The markers in Fig. 8 are given only to emphasize the striking correspondence between the features of the residual spectrum and the spectra of higher fullerenes. While C_{84} was found in the FTMS spectra of the mixtures, C_{78} was not. Were absorption maxima experimentally known for C_{88} and C_{94} (which were found in the FTMS spectrum), they perhaps would be able to account for much of these residuals.

The molar absorptivities given herein were not corrected for the absorbance of the triplet state [8–10]. Thus, these coefficients may include a very small contribution from that source.

In spectrometers which use monochromatic excitation, very little deviation from the ground state absorbance generally is found, primarily because the excitation photon flux is small enough to keep multi-photon absorption to a minimum. Further, the greatest difference between the singlet and triplet state absorption spectra is at longer wavelengths, but absorption at those wavelengths is much less, making multi-photon absorption again unlikely.

However, in diode array spectrometers, white light excitation is used. The UV flux is almost entirely absorbed, fullerenes having huge absorptivities in that region, creating a sizable triplet population within nanoseconds. In addition, the total photon flux must be much higher in a diode

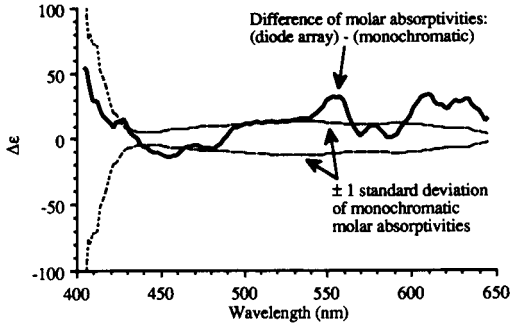

Fig. 9. Measurement of the same C_{60} sample on an HP 8452A diode array spectrometer (white light excitation) and a Perkin-Elmer 576 UV–visible spectrometer (monochromatic excitation) producing different absorbances.

array instrument in order to have enough photons to disperse to 256 (or more) detectors, greatly increasing the probability of two-photon absorption. Even so, for most molecules the probability of two-photon absorption is remote. But C_{60} and C_{70} have excited state lifetimes several orders of magnitude larger than usual. And, virtually all photons absorbed by C_{60} and a vast majority of those absorbed by C_{70}, result in that long-lived triplet, since fluorescence is negligible in fullerenes [1]. Fig. 9 shows the difference between the C_{60} absorbance generated from the same sample on the two types of spectrometers.

Considering the dearth of published molar absorptivities for fullerenes in toluene, of which there have been only two, the data given in this report is in reasonable agreement. In the literature, an estimate of the C_{60} absorptivity based on bracketing [1] included a rather large standard deviation [$\epsilon(S_0) = 400 \pm 200$ l mol^{-1} cm^{-1} at 480 nm], so the value reported herein ($\epsilon = 511 \pm 10$ l mol^{-1} cm^{-1}) fits with ease into the experimental error. A value determined through laser excitation ($\epsilon = 440$ l mol^{-1} cm^{-1} at 624 nm, no standard deviation specified) [11] was for a solution of unspecified purity. As little as 1% contamination by C_{70} would reduce that published e value to 406 l mol^{-1} cm^{-1}. Also, since the laser photon flux would maintain a significant percentage of the fullerenes in their long-lived triplet state, the absorbance would be increased; the triplet absorbance being several times larger [$\epsilon(T) \approx 2000$ l mol^{-1} cm^{-1}] [12] than the singlet at this wavelength. Thus, the value reported herein (384 ± 6 l mol^{-1} cm^{-1}), taken with a much smaller photon flux, is within reasonable agreement.

Finally, solvation and charge transfer effects were shown to cause the absorption spectrum to change in unusual ways. If the solvent molecules (or other solute molecules) have a region of high electron density, associations ranging from coordination spheres [13] to complexation to charge transfer [11,14,15] may occur. The high electron affinity [16] of fullerenes makes such associations highly likely. A valuable diagnostic for such charge influences may be found in a shrinking of the small but sharp maximum of C_{60} which appears between 404 nm and 407 nm, depending on the solvent. Since the wavelength shifts indicated by Table 2 have several anomalies, the suggestion that molar absorptivities may be generalized between solvents [17] may not be entirely valid.

5. Conclusion

Visible absorption spectroscopy promises to be a valuable tool in monitoring the output of separations columns and the progress of fullerene reactions. For separations, spectra may be taken digitally (even older model spectrometers may be quite easily interfaced to computers) and reduced to analyte concentrations rapidly, allowing automation of the separation process. For polychromatic excitation spectrometers, however, the molar absorptivities will need to be re-measured on each type of instrument (since photon flux varies considerably between instruments) to account for triplet absorbance. For monitoring the progress of reactions, the disappearance of analytes, the appearance of "contaminants," and a diagnostic for charge transfer may all be gained. Some caution must be observed even in this usually non-invasive analytical method, since fullerenes seem particularly susceptible to photo-initiated charge transfer reactions and photolysis of adducts.

While the absorptivity data presented in this report is of a mundane nature, the constants generated and reported herein were hitherto unavailable. The observations of solvent depen-

dency and an indicator of charge transfer were likewise not previously quantitated. Finally, software for deconvoluting absorbance spectra of mixtures has not been advertized. That software, which does not require prior knowledge of the total mass of analytes, has wide application in separations, synthesis, and kinetics.

6. Acknowledgement

This research was performed under appointment to the Environmental Restoration and Waste Management Fellowship program administered by Oak Ridge Institute for Science and Education for the U.S. Department of Energy.

7. References

[1] J.W. Arbogast, A.P. Darmanyan, C.S. Foote, Y. Rubin, F.N. Diedrich, M.M. Alvarez, S.J. Anz and R.L. Whetten, J. Chem. Phys., 95 (1991) 11.
[2] J.P. Hare, H.W. Kroto and R. Taylor, Chem. Phys. Lett., 177 (1991) 394.
[3] F. Diederich, R.L. Whetten, C. Thilgen, R. Ettl, I. Chao and M.M. Alvarez, Science, 254 (1991) 1768.
[4] S. Leach, M. Vervloet, A. Despès, E. Bréheret, J.P. Hare, T.J. Dennis, H.W. Kroto, R. Taylor and D.R.M. Walton, Chem. Phys., 160 (1992) 451.
[5] J.R. Heath, R.F. Curl and R.E. Smalley, J. Chem. Phys., 87 (1987) 4236.
[6] K.M. Creegan, J.L. Robbins, W.K. Robbins, J.M. Millar, R.D. Sherwood, P.J. Tindall and D.M. Cox, J. Am. Chem. Soc., 114 (1992) 1103.
[7] H. Aije, M.M. Alvarez, S.J. Anz, R.D. Beck, F. Diederich, K. Fostiropoulos, D.R. Huffman, W. Krätschmer, Y. Rubin, K.E. Schriver, D. Sensharma and R.L. Whetten, J. Phys. Chem., 94 (1990) 8630.
[8] N.M. Dimitrijevic and P.V. Kamat, J. Phys. Chem., 96 (1992) 4811.
[9] M. Terazima, N. Hirota, H. Shinohara and Y. Saito, J. Phys. Chem., 95 (1991) 9080.
[10] J.W. Arbogast, C.S. Foote and M. Kao, J. Am. Chem. Soc., 114 (1992) 2277.
[11] R.J. Sension, A.Z. Szarka, G.R. Smith and R.M. Hochstrasser, Chem. Phys. Lett., 185 (1991) 179.
[12] L. Bicsok, H. Linschitz and R.I. Walter, Chem. Phys. Lett., 195 (1992) 339.
[13] D. Dubois, G. Moninot, W. Kutner, M.T. Jones and K.M. Kadish, J. Phys. Chem., 96 (1992) 7137.
[14] P.N. Keizer, J.R. Morton, K.F. Preston and A.K. Sugden, J. Phys. Chem., 95 (1991) 7117.
[15] P.V. Kamat, J. Am. Chem. Soc., 113 (1991) 9705.
[16] L.-S. Wang, J. Conceicao, C. Jin and R.E. Smalley, Chem. Phys. Lett., 182 (1991) 5.
[17] D.K. Palit, A.V. Sapre, J.P. Mittal and C.N.R. Rao, Chem. Phys. Lett., 195 (1992) 1.
[18] T. Suzuki, Q. Li, K.C. Khemani, F. Wudi and Ö. Almarsson, Science, 254 (1991) 1186.
[19] R. Taylor, J.P. Hare, A.K. Abdul-Sada and H.W. Kroto, J. Chem Soc. Chem. Commun., (1990) 1423.
[20] F. Diederich, R. Ettl, Y. Rubin, R.L. Whetten, R. Beck, M. Alvarez, S. Anz, D. Sensharma, F. Wudl, K.C. Khemani and A. Koch, Science, 252 (1991) 548.

ELSEVIER

Analytica Chimica Acta 289 (1994) 69–78

ANALYTICA CHIMICA ACTA

Comparison of solid phase extraction with salting-out solvent extraction for preconcentration of nitroaromatic and nitramine explosives from water

Thomas F. Jenkins *[,a], Paul H. Miyares [a], Karen F. Myers [b], Erika F. McCormick [b], Ann B. Strong [b]

[a] *U.S. Army Cold Regions Research and Engineering Laboratory, Hanover, NH 03755-1290, USA*
[b] *U.S. Army Engineer Waterways Experiment Station, Vicksburg, MI 39180, USA*

(Received 2nd August 1993; revised manuscript received 2nd November 1993)

Abstract

Residues of high explosives are a significant pollution problem at U.S. military facilities. Because TNT, RDX and HMX, as well as several manufacturing impurities and environmental transformation products, are mobile in the soil and have caused groundwater pollution, there is an increasing demand for low-concentration analysis of these compounds in water from installation boundary wells. Because RDX and HMX are polar, conventional liquid–liquid extraction with nonpolar solvents yields poor recovery. Two techniques have been reported that appear to offer improved recovery and adequate preconcentration: solid phase extraction (SPE) and salting-out solvent extraction (SOE). This paper compares resin based cartridge-SPE, membrane-SPE, and SOE using fortified reagent grade water samples and a set of 58 groundwater samples from an explosives-contaminated military facility. The three methods were comparable with respect to low-concentration detection capability, which ranged from 0.05 to 0.30 μg/l. Percent recoveries generally exceeded 80%, except for HMX and RDX by membrane-SPE. Interferences were found in extracts from half of the groundwater samples preconcentrated using the two SPE procedures, but were not found in any of the extracts from the SOE. These interferences were traced to matrix interaction of the polymeric resins with low-pH groundwater containing high levels of dissolved solids.

Key words: Liquid chromatography; Explosives; Extraction; Ground water; Preconcentration; Waters

1. Introduction

TNT (2,4,6-trinitrotoluene) and RDX (hexahydro-1,3,5-trinitro-1,3,5-triazine), along with several of their manufacturing impurities and environmental degradation products, have been observed in groundwater at a number of U.S. Army installations [1–5]. Health Advisories have been issued by the U.S. Environmental Protection Agency (EPA) for many of these compounds (Table 1), with drinking water criteria at sub-μg/l concentrations for some. For this reason, the U.S.

* Corresponding author.

Elsevier Science B.V.
SSDI 0003-2670(93)E0623-F

Table 1
Proposed drinking water criteria for nitroaromatics and nitramines

Compound	Proposed drinking water limit (μg/l)	Ref.
HMX	400 [a]	[6]
RDX	2.0 [a]	[7]
TNT	2.0 [a]	[8]
2,4-DNT	50 [b]	[9]
	0.1	[10]
2,6-DNT	40 [b]	[9]
	0.007	[10]
1,3-DNB	1.0 [a]	[11]

[a] EPA Lifetime Health Advisory Number.
[b] EPA number for increased cancer risk of 1.0×10^{-6}.

Army has developed analytical methods to determine these compounds at trace levels in water. To detect these compounds at the sub-μg/l level, the first step has been preconcentration of the analytes using an extraction process.

Classical, batch liquid–liquid extraction of these analytes has been reported, but poor extraction efficiency has been found, particularly for RDX and HMX. Octanol–water partition coefficients (K_{ow}) for HMX and RDX are 1.15 and 7.24 [12] and methylene chloride–water partition coefficients are 12.5 and 59.6 [13], respectively, indicating the compounds are quite polar and difficult to extract from water using nonpolar solvents. Consequently, several alternative procedures were developed. The most successful of these have been the use of solid phase extraction (SPE) [14–16] and salting-out liquid–liquid extraction (SOE) [17–19]. SPE methods using organic polymer resins [14,15] provide much better recovery of HMX and RDX than those using reversed-phase silicas [16].

The objective of the work described here was to obtain a direct comparison of resin-based cartridge SPE [14] and membrane SPE methods [15] with the SOE method [19]. Aqueous test solutions of nitroaromatics and nitramines prepared in groundwater without the use of organic solvents allowed a realistic comparison at concentrations of analytes below the proposed drinking water criteria (Table 1). In addition, all three procedures were tested with a set of 58 groundwater samples from a military toxic waste site known to be contaminated with explosives.

2. Experimental

2.1. Salting-out solvent extraction / nonevaporative preconcentration procedure

This method was based on a salting-out solvent extraction procedure [19] in combination with a nonevaporative preconcentration technique [20] reported elsewhere. A 251.3-g portion of reagent grade sodium chloride was added to a one-l volumetric flask along with a 770-ml sample of water. A stir bar was added and the contents stirred at maximum speed (rpm) until the salt was completely dissolved. A 164-ml aliquot of acetonitrile (ACN) was added and stirred for 15 min. The stirrer was turned off and the phases allowed to separate. The ACN phase (about 8 ml) was removed and 10 ml of fresh ACN added. The flask was again stirred for 15 min, followed by phase separation. The ACN was removed and combined with the initial extract. For preconcentration, the combined extract was placed in a 100-ml volumetric flask, 84 ml of salt water (325 g NaCl per 1000 ml of water) was added and the contents stirred for 15 min. After allowing the phases to separate, the ACN phase was carefully removed and the aqueous layer extracted with an additional 1.0-ml aliquot of ACN. The resulting extract, about 5–6 ml, was diluted 1:1 with reagent grade water prior to analysis.

2.2. Cartridge solid-phase extraction

Porapak R (80/100 mesh) was obtained from Supelco and the bulk material precleaned by Soxhlet extraction. Two 300-ml portions of ACN were each used for a period of one day for 75 cc of polymer [13]. After precleaning, the material was air dried briefly and then oven-dried at 105°C for 2 h.

Empty 3-ml extraction cartridges were packed with 0.5 g of the precleaned Porapak R. The cartridges were placed on a Visiprep solid-phase extraction manifold (Supelco) and conditioned by

eluting with 30 ml of ACN followed by 50 ml of reagent grade water. A 500-ml aliquot of each water sample was pulled through a cartridge at about 10 ml/min. The cartridges were eluted by passing a 5-ml aliquot of ACN through the cartridge at about 2 ml/min and the eluate collected in a 10-ml graduated cylinder. The resulting extract, about 5 ml, was diluted 1:1 with reagent grade water prior to analysis.

2.3. Membrane solid-phase extraction

The extraction membranes used in this study were 47-mm Empore styrene–divinyl benzene (SDVB) disks which contain about 310 mg of SDVB. The disks were precleaned by soaking individual disks in 50 ml of ACN [13]. Each membrane was soaked for four 24-h periods using fresh ACN each day. Each disk was rinsed with ACN, then centered on a 47-mm vacuum filter apparatus and leached with a 20-ml portion of ACN and a 50-ml aliquot of reagent grade water. Just before the last of this water was pulled through the membrane, the vacuum was stopped and the reservoir filled with sample. The vacuum was turned on again and a 500-ml aliquot of a water sample was pulled through the membrane. This took from 5 to 7 min, with resulting flow rates ranging from 70 to 100 ml/min. Air was then drawn through the membrane for one minute to remove excess water. A 5-ml aliquot of ACN was used to extract the analytes from the disk and the extract was diluted 1:1 with reagent grade water prior to analysis.

2.4. RPLC analysis

All analyses were conducted using reversed-phase liquid chromatography (RPLC). Primary separations used a 25 cm × 4.6 mm i.d. LC-18 (5 μm) column eluted with methanol–water (1:1) at a flow rate of 1.5 ml/min [21]. Samples were introduced by overfilling a 100-μl loop. If primary analysis indicated that target analytes could be present, second column confirmation was obtained on a combined LC-8/LC-CN column using a ternary eluent composed of water–methanol–tetrahydrofuran (70.7:27.8:1.5, v/v/v) [18].

2.5. Preparation of standards and samples

Because we felt it was important that test samples be completely free of organic solvents, as would normally be the case for real samples, we prepared all test samples in a totally aqueous matrix. This was done by preparing individual aqueous analyte stock solutions by placing a few hundred milligrams of Standard Analytical Reference Material (SARM) of each specific analyte in individual 4-l brown glass bottles, filling with reagent grade water, adding a stir bar and stirring for two days at room temperature. Each solution was filtered through a 0.45-μm nylon-66 membrane (Supelco) into a clean brown glass bottle. Aliquots of each solution were then analyzed by RPLC against standards prepared in acetonitrile to estimate the concentration of analyte in each aqueous stock solution. A combined analyte spiking solution was prepared by combining known volumes of these individual stock standards.

2.6. Groundwater samples

Groundwater samples used for method comparisons were taken from the Rockeye site, Naval Surface Warfare Center, located primarily in Martin County, Indiana. Underlying sedimentary rocks date from the Pennsylvanian and Mississippian periods and consist of sandstone, coal and shale. Boring logs from the Rockeye wells show thin seams of coal, some containing pyrite. Water leaching through these formations can have low pH and high concentrations of dissolved iron.

3. Results and discussion

3.1. Certified reporting limit test

Spiked test solutions were used to conduct a 4-day Certified Reporting Limit (CRL) Test [13]. This test utilizes a series of fortified samples covering a 20-fold concentration range and allows

an estimation of low concentration detection capability, percent recovery, interferences and overall precision. A discussion of the CRL, and how results compare with the U.S. EPA Method Detection Limit, is presented elsewhere [22]. Chromatograms for samples containing target analytes at about 0.2 μg/l and preconcentrated by the three procedures are presented in Fig. 1.

The CRLs obtained are shown in Table 2. Overall the CRLs for a given analyte are quite similar for all three preconcentration techniques and were also quite similar to those reported by others [14]. None of the procedures are consistently superior to the others in low concentration

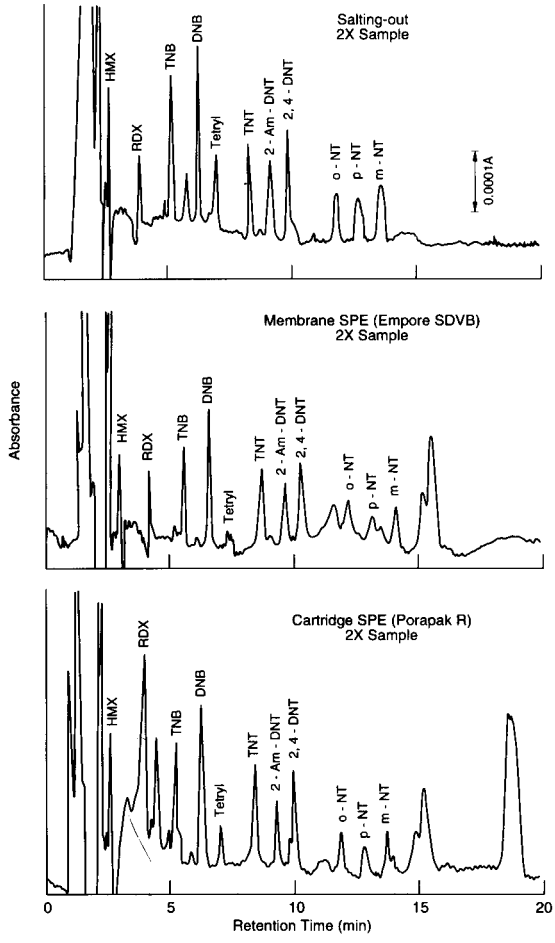

Fig. 1. LC-18 chromatograms for 0.2 μg/l sample preconcentrated by salting-out, cartridge-SPE and membrane-SPE methods.

Table 2
Certified reporting limits for various preconcentration techniques

Analyte	Salting-out	CRL (μg/l) Cartridge-SPE	Membrane-SPE
HMX	0.19	0.21	0.33
RDX	0.13	0.27	0.12
TNB	0.052	0.042	0.051
DNB	0.081	0.032	0.036
Tetryl	0.20	0.24	0.83
TNT	0.086	0.068	0.13
2-Am-DNT	0.10	0.046	0.055
2,4-DNT	0.083	0.085	0.044
o-NT	0.13	0.10	0.20
p-NT	0.22	0.12	0.23 [a]
m-NT	0.21	0.13	0.37

[a] One outlier removed for this analyte/method combination.

detection capability. CRL values range from a low of 0.032 μg/l for DNB using cartridge SPE, to a high of 0.83 μg/l for tetryl using membrane-SPE. All values for HMX, RDX, TNT, 2,4-DNT and 1,3-DNB are below the proposed drinking water limits for these compounds. We did not include 2,6-DNT in our study, because we did not expect to be able to routinely achieve the very low proposed drinking water criterion of 0.007 μg/l. CRLs of 0.074 μg/l and 0.123 μg/l for 2,6-DNT by cartridge-SPE and SOE, respectively, have been reported elsewhere [14]. A CRL of 0.006 μg/l for 2,6-DNT has been achieved using SOE followed by analysis of an 1100-μl subsample by RPLC, but the procedure used is not practical for routine use [19]. A CRL of 0.003 μg/l has been reported by GC-ECD [23], and this appears to be the most appropriate method if this detection criterion must be met. The only CRL value that seems out of line is the 0.83 μg/l value for tetryl using membrane-SPE. Inspection of the data indicates this high CRL is due to low recovery on one of the four days for this compound. High CRLs for tetryl were found by others who attribute this behavior to instability of tetryl in water [14]. Our experience indicates that instability of tetryl is due to photochemical decomposition.

Regression lines obtained from the plots of found vs. spiked concentrations were also examined for curvature using lack-of-fit testing. Linear

relationships adequately described the data at the 95% confidence level. The slopes of these linear regression lines are measures of the overall percent recoveries of these analytes using each preconcentration method. Recoveries (Table 3), in general, are quite good (near a theoretical value of 100%). Measured recoveries for the SOE procedure range from 93–119%. Likewise recoveries for cartridge-SPE and membrane-SPE range from 83–133% and 81–116%, respectively. *Y*-intercept values for the regression lines were tested (95% confidence level) to determine if they were significantly different from zero. Only RDX preconcentrated by cartridge-SPE showed a significant positive intercept larger than the corresponding CRL, indicating the presence of a positive interference. This interference can be seen in Fig. 1 for RDX preconcentrated using the cartridge-SPE method.

3.2. Comparison using groundwater samples

A further test was conducted using 58 ground water samples from the Rockeye site at the Naval Surface Warfare Center. All of the samples were analyzed without preconcentration and with preconcentration using the three procedures (SOE, cartridge-SPE and membrane-SPE). Table 4 summarizes the results for samples where the concentration of at least one nitroaromatic or nitramine analyte was high enough to be obtained using the direct method. Because the concentrations obtained by direct analysis are subject to fewer sources of error than those obtained using preconcentration, we treated these values as "true" values for purposes of comparison. We then compared the results from the various preconcentration techniques relative to these "true" values. Examination of Table 4 indicates that all three preconcentration procedures did a fairly good job of recovering these analytes. The membrane-SPE method, however, recovered only about 68% of HMX. Recovery of HMX, RDX and TNT by the cartridge-SPE and salting-out methods were greater than 80% in all cases.

For about half of the samples the chromatograms for the SOE method were blank with respect to target analytes and interferences, but the chromatograms for both SPE methods, at the same attenuation, showed large peaks at a number of retention times across the entire chromatogram (Fig. 2). Second column confirmation indicated that none of these peaks resulted from the presence of nitroaromatic or nitramine explosives. Their presence, however, interfered with the ability to detect nitroaromatic and nitramine analytes at concentrations well above the CRLs. These large interference peaks were not observed when these groundwater samples were analyzed without preconcentration, even though they should have been easily observable. Hence these interferences were introduced by the solid phases themselves. Since the Porapak R and the SDVB membranes were cleaned separately just prior to use and all the Porapak R cartridges were packed from material cleaned in the same batch, we do not believe these peaks were a result of poorly cleaned material. Rather, it appears that some components of these samples interacted with the solid phases to either degrade the polymer or release contaminants from within the polymer by either swelling or reorienting the polymer matrix. The release of contaminants from the interior of the resins is supported by our observation that

Table 3
Overall percent recovery and relative standard deviation (R.S.D.) from Certified Reporting Limit Test

Analyte	%Recovery [a] (%R.S.D.)					
	Salting-out		Cartridge-SPE		Membrane-SPE	
HMX	106	(10.5)	107	(9.6)	81	(14.0)
RDX	106	(8.7)	116	(22.0)	116	(11.1)
TNB	119	(7.6)	133	(8.7)	116	(10.3)
DNB	102	(6.6)	115	(2.6)	103	(6.5)
Tetryl	93	(16.4)	83	(32.8)	83	(46.4)
TNT	105	(7.6)	111	(7.5)	97	(10.5)
2-Am-DNT	102	(9.1)	113	(4.1)	103	(8.9)
2,4-DNT	101	(5.8)	109	(6.8)	94	(6.6)
o-NT	102	(9.1)	107	(8.1)	92	(15.6)
p-NT	96	(18.1)	104 [b]	(6.6)	89 [c]	(18.0)
m-NT	97	(12.4)	100	(7.3)	86	(17.2)

[a] Slope of regression line of spiked concentration vs. found concentration × 100.
[b] Lack-of-fit test indicates data not adequately described by linear relationship at the 95% confidence level.
[c] One outlier removed for this analyte/method combination.

contamination reappears in solvent cleaned resin cartridges and membranes after several weeks of storage.

3.3. Investigation of the source of SPE interferences

Additional water samples were obtained from four of the wells where large interferences were observed for samples preconcentrated using SPE. These samples were again analyzed without preconcentration and with preconcentration using cartridge-SPE on Porapak R. The results confirmed those given above: no interferences for the samples analyzed without preconcentration and large interferences when the samples were preconcentrated using SPE (Figs. 3 and 4). These water samples were also analyzed for pH, specific conductance, total organic carbon, and major anions and cations (Table 5) in an attempt to understand this phenomenon. All four samples had pH values below 3 and relatively high specific conductance. Sulfate values were very high, ranging from 490 to 1600 mg/l. The low pH in the groundwater solubilized large concentrations of aluminum, iron, and manganese, which produced

Table 4
Comparison of results for direct analysis of groundwater samples from the Rockeye site at the Naval Surface Warfare Center, Crane, Indiana, with the three preconcentration methods

Sample	Method [a]	Concentration (μg/l)				
		HMX	RDX	TNB	TNT	4A-DNT
20649	Direct	151	135		33	9.6
	SPE-M	98	121		32	11.2
	SPE-C	156	147		34	12.2
	SOE	161	138		38	13.7
20650	Direct	119	82		9.0	
	SPE-M	60	64		7.6	
	SPE-C	107	85		9.2	
	SOE	98	66		10.3	
20662	Direct	26	160		42	
	SPE-M	19	176		51	
	SPE-C	17	138		34	
	SOE	22	154		46	
20663	Direct	281	94		21	65
	SPE-M	153	89		22	75
	SPE-C	214	109		26	78
	SOE	232	90		26	78
20667	Direct	318	618	19.2	284	166
	SPE-M	199	488	19.5	317	216
	SPE-C	356	666	19.6	328	239
	SOE	319	558	18.6	320	217

[a] Membrane-SPE (SPE-M), Cartridge-SPE (SPE-C) and Salting-out (SOE).

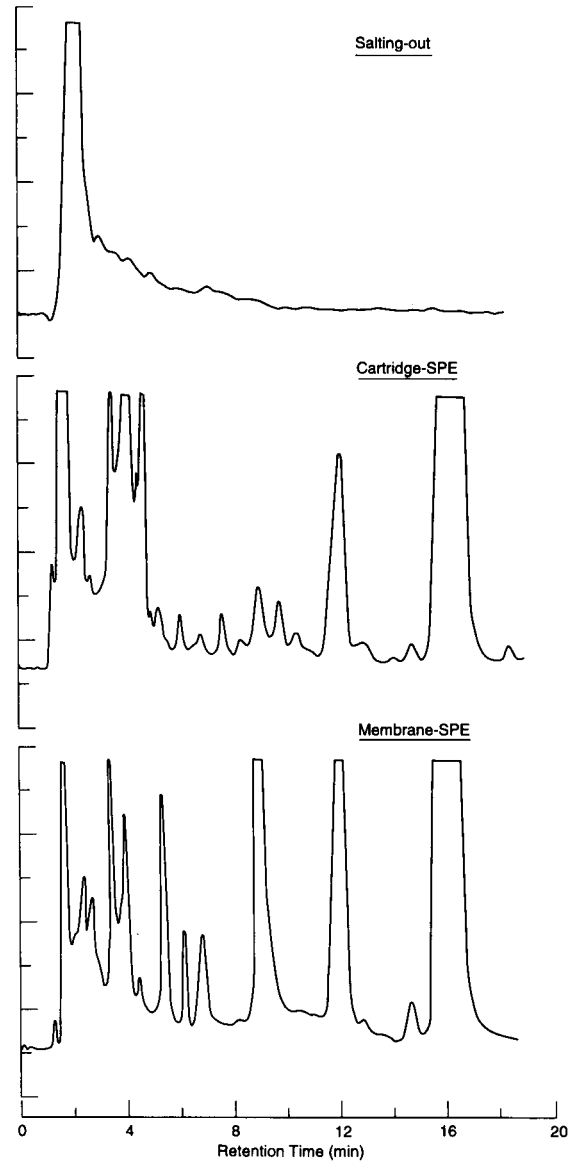

Fig. 2. LC-18 chromatograms for sample from well 10C40P2 Rockeye site, Naval Surface Warfare Center, preconcentrated by salting-out, cartridge-SPE and membrane-SPE methods.

a yellowish precipitate when the pH was raised. Background geological information seems to indicate that the low pH and high specific conductance may be due to naturally occurring phenomena. When neutralized water was preconcentrated using cartridge-SPE, the intensities of the

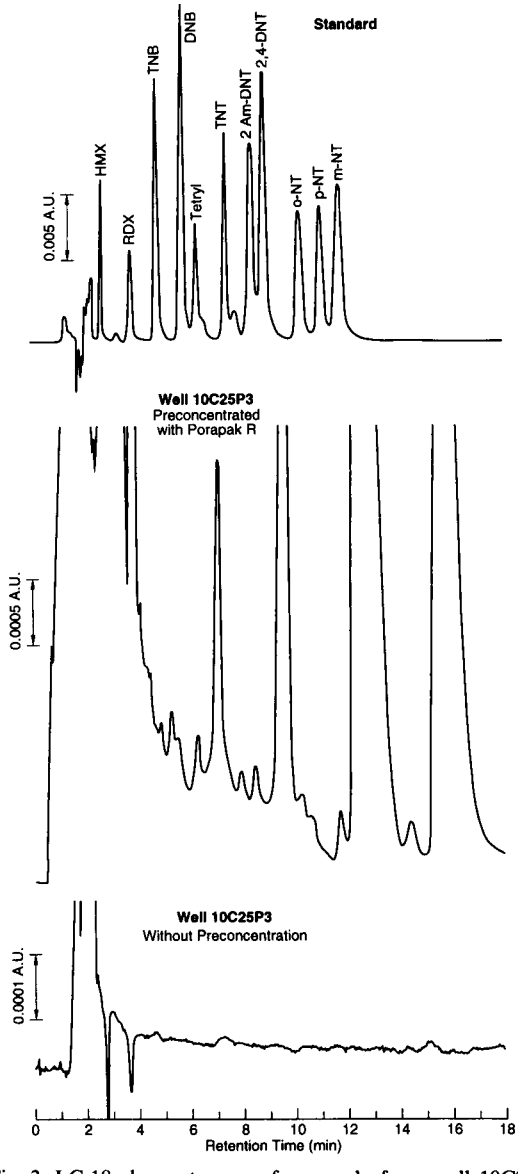

Fig. 3. LC-18 chromatograms for sample from well 10C25P3 without preconcentration and with preconcentration using SPE on Porapak R along with chromatogram of combined analyte standard.

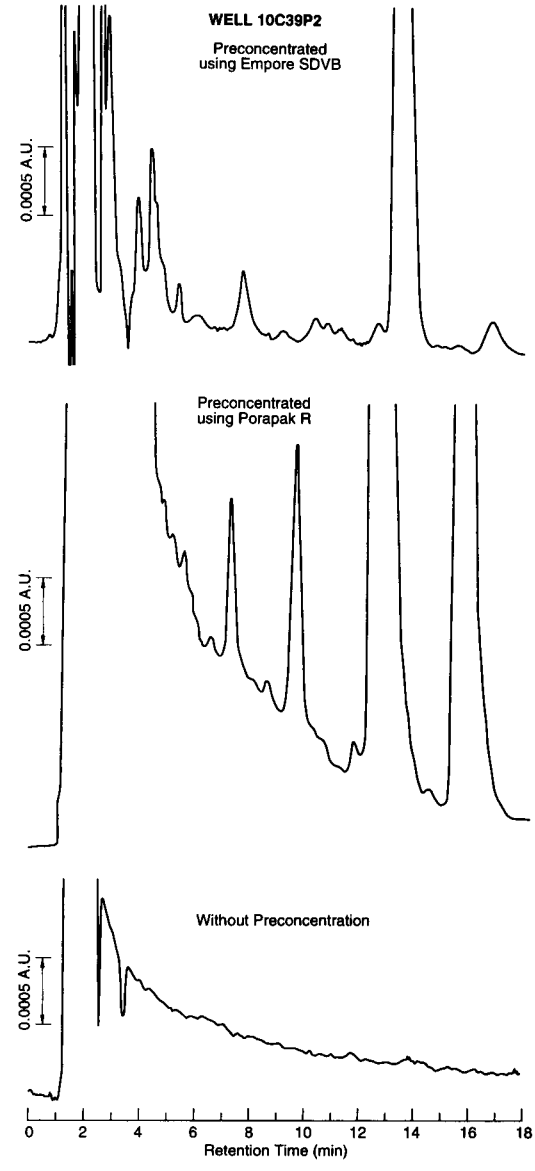

Fig. 4. LC-18 chromatograms for sample from well 10C39P2 without preconcentration and with preconcentration by SPE on Porapak R and Empore SDVB.

interference peaks were drastically reduced. Several of these low pH samples were fortified with a group of nitroaromatics and nitramines, the samples neutralized with aqueous NaOH, filtered and preconcentrated using cartridge-SPE as described above. Recovery of these analytes was nearly quantitative, indicating that the analytes

Table 5
Composition (mg/l) of several well waters from Crane Naval Surface Warfare Center

Monitoring well	pH	Conductivity (μmho/cm)	TOC	SO_4	Cl	Al	Fe	Mn	Ca	Mg	Na
1016	2.8	1760	4.2	800	34	31	11	8	100	92	114
10C39P2	2.8	2540	12.2	1600	137	81	11	12	189	154	175
10C46P2	2.6	1160	9.3	490	55	10	8	10	71	71	60
10C25P3	2.7	1780	4.5	950	31	67	110	10	88	88	59

did not associate with the precipitated hydrous iron–aluminum–manganese oxides. Thus pH adjustment prior to SPE preconcentration may be a useful pretreatment to reduce these unwanted interferences.

Several cartridges containing exhaustively cleaned Porapak R were obtained from Millipore. When these cartridges were used to preconcentrate these troublesome groundwater samples, only minor interferences were observed (Fig. 5), a major improvement over the results using commercially available material cleaned by us. This result indicates that these interferences are probably due to release of contaminants that have not been removed by the standard cleaning procedures used by the manufacturer or by the Soxhlet procedure used on site. Thus, if resins can be adequately precleaned, these interferences may no longer be a problem.

4. Conclusions

SOE and cartridge- and membrane-SPE were compared with respect to their ability to preconcentrate nitroaromatic and nitramine explosives from water prior to RPLC analysis. Both fortified reagent grade water and contaminated groundwater samples were used in this assessment. Low detection capability and overall precision were comparable among the three procedures. Recovery of HMX is better using cartridge-SPE and SOE than membrane-SPE. Recovery of the nitroaromatics was acceptable for all three procedures.

At present, one of the major problems associated with the use of resin-based SPE procedures is the inadequacy of the current cleaning proce-

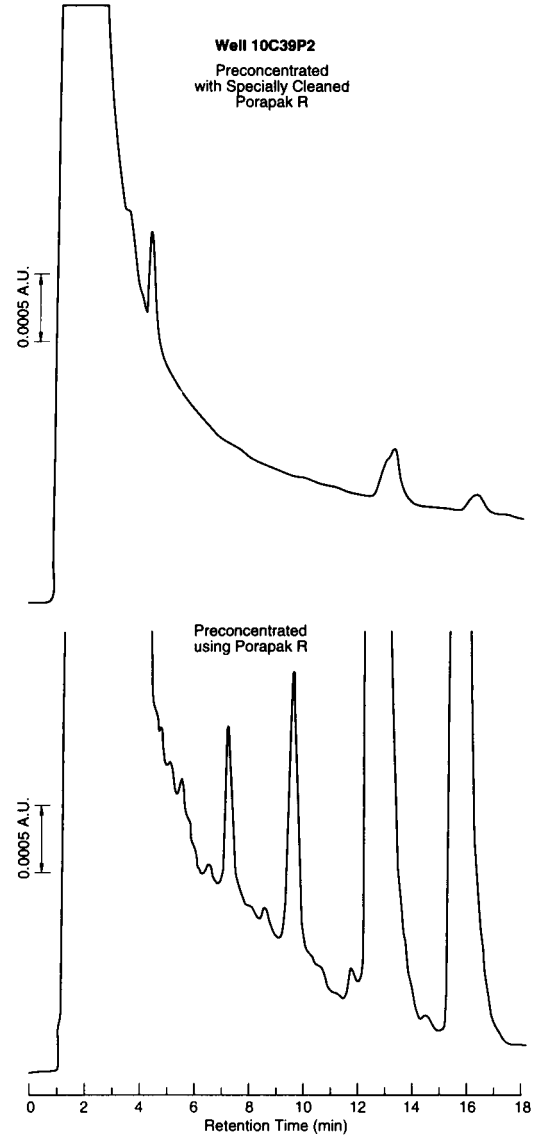

Fig. 5. LC-18 chromatograms for sample from well 10C39P2 preconcentrated by SPE on commercially available and specially cleaned Porapak R.

dures used by resin suppliers. This forces users to clean these materials with large volumes of solvent. While use of the Soxhlet procedure on a batch basis for the Porapak R material appears to be adequate for most samples, except perhaps for RDX, cleaning must be accomplished on site just before use or the contamination reappears. The cleaning procedure we used for the membranes is cumbersome and solvent-wasteful. Since one of the major advantages of SPE is reduced solvent usage, the need for this degree of cleaning was surprizing. For comparison, the SOE procedure uses 174 ml of acetonitrile and 278 g of sodium chloride per sample.

Even with these on-site cleaning procedures, problems with interferences were encountered using both the cartridge-SPE and membrane-SPE procedures for a number of actual groundwater samples. These interferences appeared to be similar to the compounds released from the solid phases during cleaning, but were apparently released from the SPE phases due to a matrix interaction. We believe these interferences result from release of resin impurities not completely removed during cleaning. When present in SPE extracts, these compounds interfere with determination of nitroaromatic and nitramine explosives even at reasonably high analyte concentrations.

Elimination of the need to use evaporative preconcentration with the SOE is a major improvement over the initial salting-out procedure which utilized a Kudena-Danish evaporator and was evaluated elsewhere [14]. We believe the SOE method evaluated here, which includes a nonevaporative preconcentration procedure, is more precise and less subject to error in routine use than the original method. It also reduces the possibility of analyte loss due to volatilization and thermal degradation of temperature sensitive analytes.

In summary, the SOE, cartridge-SPE and membrane-SPE preconcentration techniques are all capable of providing adequate analyte preconcentration of nitroaromatics and nitramines prior to RPLC determination. Of the three, the SOE method appears to be the least prone to interferences. The membrane-SPE method requires the least sample processing time, but its recovery of HMX is the poorest of the three methods. The cartridge-SPE method requires the least solvent per sample and provides adequate overall analyte recovery, but a small positive interference was observed for RDX.

5. Acknowledgements

The authors acknowledge Dr. C.L. Grant, Professor Emeritus, University of New Hampshire and M.E. Walsh of the U.S. Army Cold Regions Research and Engineering Laboratory (CRREL) for useful comments and suggestions on the manuscript. In addition, Roy Wade of the U.S. Army Engineer Waterways Experiment Station (WES) is acknowledged for groundwater sample collection, and S. Paige Pitts and Allyson H. Lynch of WES for assistance in groundwater extractions and Anne Halpenny-Weathersby for cation analysis. A.D. Hewitt (CRREL) and S.M. Golden of the Science and Technology Corporation are acknowledged for conducting experiments that were helpful in assessing the contaminant release problem from the solid phase materials. The authors also thank Dr. E.S.P. Bouvier of Waters Chromatography Division, Millipore Corporation, for useful discussions regarding the nature of the interferences observed for the solid phase extraction materials and for supplying us with several experimental cartridges packed with specially cleaned Porapak R. Funding for this research was provided jointly by the U.S. Army Environmental Center, Aberdeen Proving Ground, Maryland, Martin H. Stutz, Project Monitor, and the U.S. Army Engineer Waterways Experiment Station, Vicksburg, Mississippi, Ann B. Strong, Project Monitor.

6. References

[1] D.L. Pugh, U.S. Army Toxic and Hazardous Materials Agency, Report DRXTH-FS-FR-82131, Aberdeen Proving Ground, MD, 1982.
[2] D.H. Robenblatt, U.S. Army Medical Bioengineering Research and Development Laboratory Technical Report 8603, Fort Detrick, MD, 1986.
[3] R.F. Spaulding and J.W. Fulton, J. Contam. Hydrol., 2 (1988) 139.

[4] M.P. Maskarinec, D.L. Manning and R.W. Harvey, Oak Ridge National Laboratory, Report TM-10190, Oak Ridge, TN, 1986.
[5] D. Layton, B. Mallon, W. Mitchell, L. Hall, R. Fish, L. Perry, G. Snyder, K. Bogen, W. Malloh, C. Ham and P. Dowd, Lawrence Livermore Laboratory AD-A220 588, Livermore, CA, 1987.
[6] Environmental Protection Agency, Health Advisory for HMX. Criteria and Standards Division, Office of Drinking Water, Washington, DC, November 1988.
[7] Environmental Protection Agency, Health Advisory for RDX. Criteria and Standards Division, Office of Drinking Water, Washington, DC, November 1988.
[8] Environmental Protection Agency, Trinitrotoluene Health Advisory, Office of Drinking Water, Washington, DC, January 1989.
[9] Environmental Protection Agency, Dinitrotoluene Health Advisory, Criteria and Standards Division, Office of Drinking Water, Washington, DC, April 1992.
[10] E.L. Etnier, Oak Ridge National Laboratory, Report AD-ORNL 6312, Oak Ridge, TN, 1987.
[11] Environmental Protection Agency, Health Advisory for 1,3-Dinitrobenzene, Criteria and Standards Division, Office of Drinking Water, Washington, DC, January 1991.
[12] T.F. Jenkins, University of New Hampshire, Dissertation, Durham, NH, 1989.
[13] T.F. Jenkins, P.H. Miyares, K.F. Myers, E.F. McCormick and A.B. Strong, USA Cold Regions Research and Engineering Laboratory, Special Report 92-25, Hanover, NH, 1992.
[14] M.G. Winslow, B.A. Weichert and R.D. Baker, Proceedings of the EPA 7th Annual Waste Testing and Quality Assurance Symposium, July 8–12, Washington, DC, 1991.
[15] D.F. Hagen, C.G. Markell and G.A. Schmitt, Anal. Chim. Acta, 236 (1990) 157.
[16] M.A. Major, R.T. Checkai, C.T. Phillips, R.S. Wentsel and R.O. Nwanguma, Int. J. Anal. Chem., 48 (1992) 217.
[17] D.C. Leggett, T.F. Jenkins and P.H. Miyares, Anal. Chem., 62 (1990) 1355.
[18] P.H. Miyares and T.F. Jenkins, USA Cold Regions Research and Engineering Laboratory, Special Report 90-30, Hanover, NH, 1990.
[19] P.H. Miyares and T.F. Jenkins, USA Cold Regions Research and Engineering Laboratory, Special Report 91-18, Hanover, NH, 1991.
[20] T.F. Jenkins and P.H. Miyares, Anal. Chem., 63 (1991) 1341.
[21] T.F. Jenkins, M.E. Walsh, P.W. Schumacher, P.H. Miyares, C.F. Bauer and C.L. Grant, J. Assoc. Off. Anal. Chem., 72 (1989) 890.
[22] C.L. Grant, A.D. Hewitt and T.F. Jenkins, Am. Lab., Feb. (1991) 15.
[23] M. Hable, C. Stern, C. Asowata and K. Williams, J. Chromatogr. Sci., 29 (1991) 131.

ELSEVIER

Analytica Chimica Acta 289 (1994) 79–85

ANALYTICA CHIMICA ACTA

Continuous-flow determination of relative diffusion coefficients of iron complexes with ligands of the 1,10-phenanthroline family and with 3-(2-pyridyl)-5,6-diphenyl-1,2,4-triazine in acetonitrile–water solutions

Shaofeng Li, Horacio A. Mottola *

Department of Chemistry, Oklahoma State University, Stillwater, OK 74078-0447, USA

(Received 2nd August 1993; revised manuscript received 2nd November 1993)

Abstract

Relative diffusion coefficients for a series of iron(II) complexes with ligands containing the chelating moiety =N–C=C–N= have been determined by using a continuous-flow procedure based on the original work of Taylor taking into account dispersion by convection/diffusion processes in the hydrodynamic transport of a sample plug inside a narrow and sufficiently long tube. Two detection approaches (amperometric and photometric) are compared. In solutions consisting of 0.0360 M H_2SO_4 in water–acetonitrile (25 : 75), the diffusion coefficients follow a power dependence on molecular weight, MW [$D = 244(MW)^{-0.58}$ with photometric monitoring, and $D = 513(MW)^{-0.67}$ with amperometric monitoring]. The data point to qualitative agreement with the Stokes–Einstein relation, assuming that the radius of the unsolvated complexes is representative of their molecular size.

Key words: Flow systems; Complexometry; Diffusion coefficients; Iron complexes; 1,10-phenanthroline; 3-(2-Pyridyl)-5,6-diphenyl-1,2,4-triazine

1. Introduction

Diffusion is a mass transport of great relevance in contemporary analytical chemistry [1] and the diffusion coefficient characterizes this mass transport in a given medium. Diffusion plays a significant role, for instance, in electroanalytical techniques, chromatographic and electrophoretic separations, and in continuous-flow sample/reagent(s) processing. There are several methods that can be used for the determination of diffusion coefficients [2], such as the diaphragm cell method, the restricted diffusion method, optical methods, NMR spin-echo, electrochemical methods, and continuous-flow methods based on the original work of Taylor [3]. Diffusion coefficients for species of relevance in analytical chemistry are frequently determined by electrochemical methods (e.g. polarography, chronopotentiometry, chronoamperometry, and chronocoulometry) and only occasionally by continuous flow [4]. Con-

* Corresponding author.

0003-2670/94/$07.00 © 1994 Elsevier Science B.V. All rights reserved
SSDI 0003-2670(93)E0622-E

tinuous-flow determinations require more time than most of the other methods and may also need a reference standard of known diffusion coefficient in the given medium. These drawbacks, however, are counteracted by the simplicity and convenience of the approach and by its adaptability to different types of detection.

This paper reports the determination of diffusion coefficients in solution of a series of iron complexes with ligands containing the chelating moiety =N–C=C–N= present in 1,10-phenanthroline, its substituted derivatives, and some other analytical ligands and obtained by a continuous-flow approach. These determinations have been prompted by the need of such diffusion coefficient values in a study on the characterization of chemically modified conducting surfaces. Two detection approaches, amperometric and absorptiometric, have been employed and results compared.

2. Experimental

2.1. Reagents and solutions

All reagents used were of AR grade, except as noted. All ligands used, L, form complexes with iron(II) in a 3:1 ligand–metal ion ratio and were purchased from GFS Chemicals (Columbus, OH). Solochrome Violet RS was from K&K Labs. (Cleveland, OH). The complexes containing perchlorate as counterion were prepared by mixing stoichiometrically an aqueous solution of $Fe(NH_4)_2(SO_4)_2$ with the ligand dissolved in acetone and then precipitating the perchlorate salt, $FeL_3 \cdot 2ClO_4$, by addition of $NaClO_4$. Other complexes were directly purchased from GFS Chemicals and used as received.

The water used for solution preparation was deionized and further purified by distillation in an all-borosilicate-glass still with a quartz immersion heater. The carrier solution, 0.0360 M in H_2SO_4, was prepared with acetonitrile–water (74.6:25.4). Acetonitrile was required to solubilize some of the rather high molecular weight ligands and at the same time to provide a suitable conducting medium in electrochemical detection.

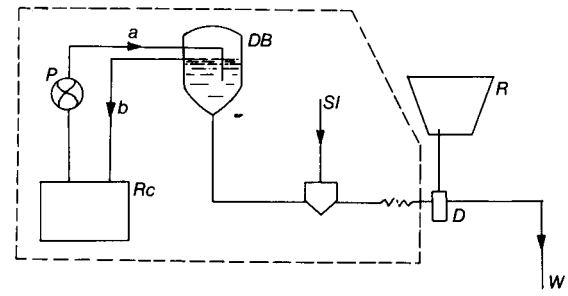

Fig. 1. Continuous-flow system. P = pump (Model 396, Laboratory Data Control/Milton Roy, Riviera Beach, FL) used to feed carrier solution into the delivery bottle DB; Rc = reservoir for carrier solution; a = feed line; b = overflow line to keep liquid level, and correspondingly the flow, constant; SI = sample intercalation valve (see text for details); D = detector (see text for details); R = recorder (see text for details); W = waste line. Components within the area delimited by the broken line were thermostated as indicated in the text.

All injected samples (4.20 μl) of iron(II) complexes were 1.00×10^{-3} M in complex and used the carrier as solvent.

2.2. Apparatus

A block diagram of the single-line continuous-flow system used in this work is shown in Fig. 1. The carrier solution was propelled by gravity flow (typically 0.30 ml min^{-1}). Gravitational flow provides a very effective pulse-free flow, essential for the preservation of laminar flow conditions and to eliminate detection artifacts with amperometric detection. The tubing manifold defining the residence time was 400 cm long and coiled (25 cm coil diameter). All tubing was PTFE and of 0.06 cm i.d. (Cole-Parmer, Chicago, IL). Photometric detection was accomplished with a Spectronic 21 spectrophotometer (Bausch and Lomb, Rochester, NY) equipped with a quartz ultra-micro flow cell of 20 μl volume (NSG Precision Cells, Farmingdale, NY). The wavelengths used for detection are listed in Table 1. Amperometric detection (applied potentials listed in Table 1) was accomplished at a thin-layer cell equipped with a glassy carbon sensing surface (Bioanalytical Systems, West Lafayette, IN) in a three-electrode system reported earlier [5]. Cyclic voltammetric data ob-

Table 1
Wavelength and applied potential used for each of the iron(II) complexes with the listed ligands

Ligand	Wavelength (nm)	Applied potential (V)
1,10-Phenanthroline	520	1.000
5-Methyl-1,10-phenanthroline	524	1.000
5-Chloro-1,10-phenanthroline	510	1.150
5-Nitro-1,10-phenanthroline (in 0.036 M H_2SO_4–CH_3CN–H_2O)	510	1.300
5-Nitro-1,10-phenanthroline (in 1.00 M KCl)	510	1.000
5-Phenyl-1,10-phenanthroline	512	1.100
3,4,7,8-Tetramethyl-1,10-phenanthroline	512	0.800
4,7-Diphenyl-1,10-phenanthroline	532	1.000
4,7-Diphenyl-1,10-phenanthroline disulfonate	549	0.950
3-(2-Pyridyl)-5,6-Diphenyl-1,2,4-Triazine, PDT	560	1.300
3-(2-Pyridyl)-5,6-bis(4-phenyl-sulfonic acid)-1,2,4-triazine, Ferrozine	560	1.300
Data for species other than iron(II) complexes		
Solochrome Violet RS	532	0.800
Hexacyanoferrate(III)	410	0.180

tained with a BAS 100 unit (Bioanalytical Systems) were used to select the applied potential.

Sample injection was performed with a rotary four-way valve Rheodyne Type 50 (Rheodyne, Cotati, CA). Recording conditions (Hewlett Packard HP 7128 strip chart recorder) were adjusted as to obtain peaks with heights of 21.6 ± 1.3 cm. All measurements were performed at 25.0 ± 0.1°C by use of a thermostat-water circulator Lauda K-2/R (Brinkman Instruments, Westbury, NY).

2.3. Polarographic determinations of the diffusion coefficient, D, for Solochrome Violet RS and cadmium ion

Current–potential data were obtained with a Metrohm Herisau Polarecord E 506 equipped with an E 505 Polarographic stand. A mercury pool electrode was used as reference and a platinum wire as auxiliary electrode in determining D for Solochrome Violet RS; a saturated calomel electrode (SCE) was used as reference in the determination of D for Cd^{2+}.

Polarographic measurements were performed using a 0.0040 M Cd^{2+} solution prepared from a $CdCl_2$ stock solution diluted with 0.20 M HCl as supporting electrolyte. An aliquot of the resulting solution was subject to N_2(g) bubbling for 15 min and the polarogram recorded between −0.20 and −1.10 V vs. SCE at a sensitivity of 2.5×10^{-7} A mm^{-1}.

Aqueous solutions containing 0.271 mM Solochrome Violet RS were prepared in 0.072 M and 0.037 M H_2SO_4 as supporting electrolyte. A volume of 0.40 ml of a 0.0050% Triton X-100 was added per 100 ml of each dye solution. An aliquot of the resulting solutions was subjected to N_2(g) bubbling for 15 min and polarograms were obtained between 0 and −0.60 V vs. a mercury pool electrode at a sensitivity of 1.5×10^{-8} A mm^{-1}. The determination in acetonitrile–H_2SO_4–H_2O was performed similarly.

Measurements to find the rate of flow of mercury and drop time were performed between −0.30 and −0.50 V.

The values for D were extracted from Ilkovic's equation, from measurements of the average diffusion current, and with a value of 2 for the number of electron equivalents per molar unit, both for Cd^{2+} and for Solochrome Violet RS. All measurements were performed at 25.0 ± 0.1°C.

3. Background for the determination of *D* by continuous flow

According to hydrodynamics, for a liquid flowing under laminar flow conditions through a narrow tube, there is a parabolic distribution of velocities over any cross-section normal to the tube axis. The liquid at the center of the tube is moving at twice the average flow velocity. As first observed by Griffiths [6], when a plug of liquid of different chemical composition is intercalated into the laminar stream, the plug shape is distorted by the stream into a parabolic bolus. Taylor [3] later explained the parabolic shape as the result of

both convection and diffusion contributing to mass transport. Taylor has shown that if

$$L/u \gg \left[2r^2/(3.8)^2 D\right] \quad (1)$$

where L = tube length, u = average flow velocity, r = tube radius and D = diffusion coefficient of species in the intercalated plug, diffusion controls the dispersion of the species out of the plug boundaries. In such a case the concentration distribution with time in the region defined by the leading and tailing fronts of the plug should be, ideally, Gaussian and characterized by a variance given by:

$$\sigma^2 = (2D\mathbf{t}/u^2) + (r^2\mathbf{t}/24D) \quad (2)$$

in which $\mathbf{t}$ is the time elapsed from the point of intercalation to the point of detection of the maximum concentration in its distribution. Usually the values of D for solutes are in the order of 10^{-5} cm^2 s^{-1} or even less. If in a given experiment, u is sufficiently low (long residence times) and r very small, the first term in Eq. 2 can be neglected, and:

$$\sigma^2 = r^2\mathbf{t}/24D \quad (3)$$

Since in a perfectly Gaussian peak, the peak width at half height, $w_{1/2}$, corresponds to 2.354 σ:

$$\sigma^2 = (w_{1/2})^2/5.54 \quad (4)$$

Combining Eqs. 3 and 4 we obtain:

$$(w_{1/2})^2 = 5.54r^2\mathbf{t}/24D \quad (5)$$

Experimentally, $\mathbf{t}$ and $w_{1/2}$ can be obtained by changing flow rate. A plot of $(w_{1/2})^2$ vs $\mathbf{t}$, in turn, allows calculation of D from the slope of the resulting straight line. The calculation of D, however, requires knowledge of r, a value that can be obtained by calibration against standards.

In a significant contribution to the description of dispersion under laminar flow conditions, Vanderslice et al. [7] adapted the approach of Anantharkrishnan et al. [8] by numerically solving Taylor's diffusion/convection equation to account for the dispersion occurring at both boundaries of an injected sample plug. The numerical solution is based on the method of *alternating direction implicit finite difference approximation* [9]. In Vanderslice's first paper [6a], the following empirical equation can be found which permits the determination of D by unsegmented continuous-flow sample processing:

$$\partial\mathbf{t}_b = (35.4r^2 f/D^{0.36})(L/u)^{0.64} \quad (6)$$

where $\partial\mathbf{t}_b$ is the baseline-to-baseline peak width of the Gaussian peak and f is a correction factor (concentration and detector sensitivity factor). If r, L, f and u are kept constant, Eq. 6 reduces to:

$$\partial\mathbf{t}_b = X/D^{0.36} \quad (7)$$

where X is a calibration factor that can be obtained with the help of a standard. If X is known, an unknown D can be calculated using:

$$D = (X/\partial\mathbf{t}'_b)^{2.778} \quad (8)$$

in which $\partial\mathbf{t}'_b$ is the baseline-to-baseline peak width for the species under study. Eq. 8 is valid if all experimental parameters used to calculate X with a standard are duplicated in determining D for the species of interest.

4. Results and discussion

4.1. Determination of D for reference standard

Solochrome Violet RS (as the sodium salt of 5-sulfo-2-hydroxy[*a*]benzene-azo-2-naphthol) was chosen as reference standard. Values of D for this chemical species in different supporting electrolytes are available in the literature [10] and were used to validate the determination in the

Table 2
Diffusion coefficients for Solochrome Violet RS (temperature 25 ± 1°C)

Supporting electrolyte	Diffusion coefficient, cm^2 s^{-1}	
	Literature value [a]	This work [b]
0.0720 M H_2SO_4	4.06×10^{-6}	$4.0 \pm 0.1\times10^{-6}$
0.0370 M H_2SO_4	4.25×10^{-6}	$4.20\pm0.05\times10^{-6}$
0.0360 M H_2SO_4 in water–acetonitrile (25:75)	–	$6.20\pm0.20\times10^{-6}$

[a] Values taken from Ref. 8.
[b] Uncertainties based on 10 replicate measurements.

Table 3
Diffusion coefficients (25.0±0.1°C) for a series of iron(II) complexes with the listed ligands[a]. Solochrome Violet RS as standard (0.036 M H_2SO_4 in 25.4:74.6, v/v, H_2O–CH_3CN)

Ligand	$D \times 10^6$, $cm^2\ s^{-1}$	
	Photometric monitoring [a]	Amperometric monitoring [b]
1,10-Phenanthroline	6.13±0.40	5.56±0.06
5-Methyl-1,10-phenanthroline	5.66±0.02	6.17±0.13
5-Chloro-1,10-phenanthroline	5.49±0.28	6.41±0.26
5-Nitro-1,10-phenanthroline	5.24±0.28	7.26±0.30
5-Phenyl-1,10-phenanthroline	5.01±0.17	10.2 ±0.10
3,4,7,8-Tetramethyl-1,10-phenanthroline	5.16±0.43	6.54±0.24
4,7-Diphenyl-1,10-phenanthroline	4.24±0.08	5.85±0.12
4,7-Diphenyl-1,10-phenanthrolinedisulfonate	3.25±0.09	3.23±0.01
3-(2-Pyridyl)-5,6-diphenyl-1,2,4-triazine, PDT	4.45±0.18	4.22±0.64
3-(2-Pyridyl)-5,6-bis-(4-phenylsulfonic acid-1,2,4-triazine), Ferrozine	3.59±0.03	3.45±0.11
Hexacyanoferrate(III) as standard (1.00 M KCl)		
5-Nitro-1,10-phenanthroline	2.13±0.01	3.46±0.08

[a] Uncertainties based on 7 to 12 replicate measurements.
[b] Uncertainties based on 6 replicate measurements.

media used in the work reported here. Table 2 summarizes the results obtained in experiments described in the Experimental section. The value of $D = 6.20 \pm 0.20 \times 10^{-6}$ $cm^2\ s^{-1}$ was used as standard value to calibrate the continuous-flow system used for determination of the diffusion coefficients of the metal chelates under study. The polarographic system was previously tested by determining D for Cd^{2+} in 0.20 M HCl as supporting electrolyte. A value of $0.65 \pm 0.01 \times 10^{-5}$ $cm^2\ s^{-1}$ was obtained which coincides with the literature value of 0.65×10^{-5} $cm^2\ s^{-1}$ [11].

4.2. Determination of D for a series of iron(II) complexes with ligands of the 1,10-phenanthroline family and 3-(2-pyridyl)-5,6-diphenyl-1,2,4-triazine

Triton X-100, used as a maximum suppressor in the polarographic work with Solochrome Violet RS, was found to have no effect on the determination of D values for the iron complexes under study, at least at the concentration level used in this work. Table 3 summarizes the values of the diffusion coefficients determined by use of Vanderslice's approach and as described above. Fig. 2 displays the correlation of D values listed in Table 3 with the molecular weight of the iron(II) complexes. In most cases, higher values were obtained with amperometric detection than with photometric detection. Verification of this

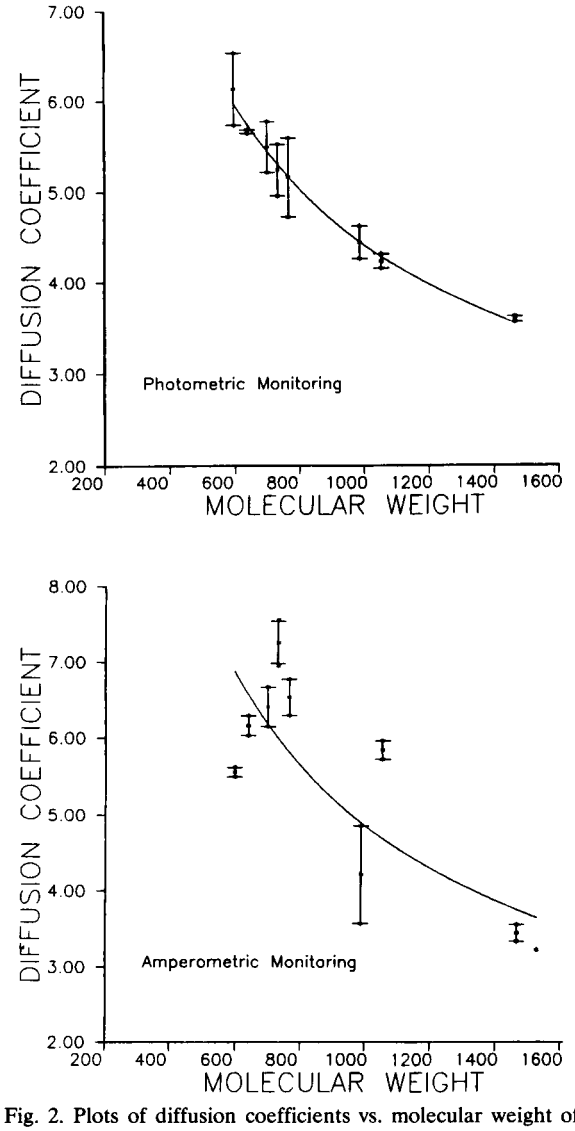

Fig. 2. Plots of diffusion coefficients vs. molecular weight of the iron(II) complexes. Values in the y-axis have been multiplied by 10^6 and have units of $cm^2\ s^{-1}$. Error bars based on the sample standard deviations as reported in Table 3.

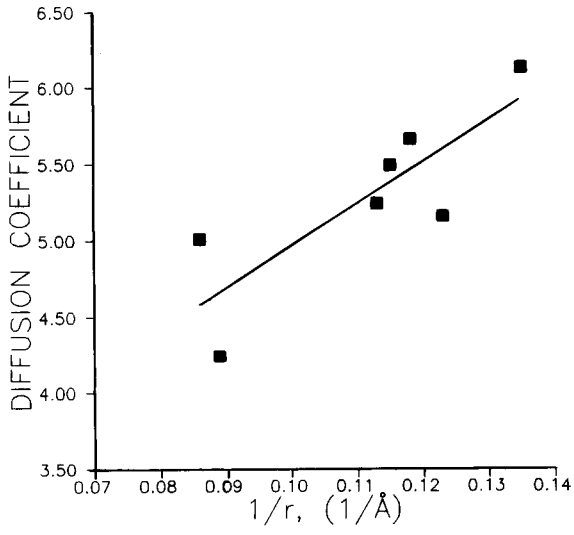

Fig. 3. Trend in diffusion coefficients illustrated as a plot vs. the reciprocal of the corresponding cross-sectional radius of the unsolvated complex (Stokes-Einstein plot). Values in the y-axis have been multiplied by 10^6 and have units of $cm^2\ s^{-1}$.

trend was further established by determining the D for the iron(II) complex with 5-nitro-1,10-phenanthroline in aqueous medium and using hexacyanoferrate(III) as standard (see Table 3). The values of the diffusion coefficients obtained with both detection approaches are power related to the molecular weight and decrease according to: $D = 244(\text{molecular weight})^{-0.58}$, with photometric monitoring, and $D = 513(\text{molecular weight})^{-0.67}$, with amperometric monitoring.

Excluded from these plots are the values for 5-phenyl-1,10-phenanthroline as ligand since the difference between values obtained with amperometric and photometric detection differ considerably more than with the other ligands. For the doubling in the value of D obtained by amperometric detection, unfortunately, we cannot offer an explanation.

The overall trend observed in the relative values obtained, seems in agreement with the Stokes-Einstein relation [12], if the radii of the unsolvated complexes are considered to be directly proportional to their molecular size. Fig. 3, for instance, illustrates the trend as a plot of D (obtained using photometric detection) as a function of the reciprocal of the cross sectional radius for the unsolvated complexes of the 1,10-phenanthroline family used in this work. The value of the radius for each complex was obtained by molecular computer graphics (Poly Graf from Molecular Systems, Burlington, MA).

5. Conclusions

The results reported here point to the relative validity of the data obtained within a family of related complexes rather than in the validity of absolute values, as well as to the sensitivity of the approach to changes in detection means. The data with photometric detection appear more reliable than the data obtained with amperometric detection as evidenced by the correlation observed in Fig. 2. Although the in-method precision is comparable with the two detection modes, adsorption of the complexes on the glassy carbon surface and electroreaction of impurities (all the oxidation currents measured required relatively very high positive potentials) may be responsible for the greater scatter of values obtained with electrochemical detection (Fig. 2). The data trend is in qualitative agreement with the Stokes-Einstein relationship:

$$D = (RT)/6\pi\mu Nr$$

in which R, T and π have the usual meaning; μ is the solvent viscosity, N is Avogadro's number, and r the spherical radius of the molecule.

6. Acknowledgement

The authors thank Rhea Howard for the polarographic determinations as well as for the calculation of the cross sectional radii of the unsolvated iron(II) complexes with ligands of the 1,10-phenanthroline family.

7. References

[1] H.A. Mottola, Kinetic Aspects of Analytical Chemistry, Wiley, New York, 1988, pp. 238–240.

[2] H.J.V. Tyrrell and K.R. Harris, Diffusion in Liquids. A Theoretical and Experimental Study, Butterworths, London, 1984, Chap. 5.
[3] G. Taylor, Proc. R. Soc. London, Ser. A, 219 (1953) 186; 225 (1954) 473.
[4] (a) D. Betteridge, W.C. Cheng, E.L. Dagless, P. David, T.B. Goad, D.R. Deans, D.A. Newton and T.B. Pierce, Analyst, 108 (1983) 17; (b) G. Gerhardt and R.N. Adams, Anal. Chem., 54 (1982) 2618.
[5] M. Bonakdar, J. Yu and H.A. Mottola, Talanta, 36 (1989) 219.
[6] A. Griffiths, Proc. Phys. Soc., 219 (1911) 190.
[7] (a) J.T. Vanderslice, K.K. Stewart, A.G. Rosenfeld and D. Higgs, Talanta, 28 (1981) 11; (b) J.T. Vanderslice, A.G. Rosenfeld and G.R. Beecher, Anal. Chim. Acta, 179 (1986) 119.
[8] V. Ananthakrishnan, W.N. Gill and A.J. Bardhun, AIChE J., 11 (1965) 1063.
[9] B. Carnahan, H.A. Luther and O.J. Wilkes, Applied Numerical Methods, Wiley, New York, 1969, pp. 270–272.
[10] D.S. Turnham, in G.J. Hills (Ed.), Polarography 1964, Vol. 1, Macmillan, London, 1966, pp. 535–545.
[11] I.M. Kolthoff and J.J. Lingane, Polarography, Interscience, New York, 2nd edn., 1952.
[12] P.W. Atkins, Physical Chemistry, Freeman, New York, 3rd edn., 1986, p. 612.

ELSEVIER

Analytica Chimica Acta 289 (1994) 87–95

ANALYTICA CHIMICA ACTA

Automated flow-injection serial dynamic dialysis technique in the study of drug binding with cyclodextrins

E.E. Sideris [a], C.A. Georgiou [b], M.A. Koupparis *[,b], P.E. Macheras [a]

[a] *Department of Pharmacy, University of Athens, Panepistimiopolis, Kouponia, Athens 15771, Greece*
[b] *Department of Chemistry, University of Athens, Panepistimiopolis, Kouponia, Athens 15771, Greece*

(Received 23rd June 1993; revised manuscript received 2nd November 1993)

Abstract

A flow-injection dynamic dialysis technique is presented for the determination of binding parameters of drugs to cyclodextrins (CDs). The automated system consists of a flow-injection unit, the sample loop of which is the receiving compartment of a dialyser unit, and a home made timing module for operation control through two flow switching solenoid valves. The procedure of binding studies is rapid and yields reproducible results. Binding parameters of CD–micromolecule complexes were calculated using the Scatchard model. Typical examples of the binding of *p*-nitrophenol with α-CD ($K_{as} = 1.58 \times 10^3$ M^{-1} at pH 7.4 and 2.06×10^3 M^{-1} at pH 9.0), salicylic acid with β-CD ($K_{as} = 3.8 \times 10^2$ M^{-1} at pH 1.5 and 51 M^{-1} at pH 7.4) and ibuprofen with β-CD ($K_{as} = 2.2 \times 10^2$ M^{-1} at pH 2.5) are presented and the binding constants obtained are compared to literature values. 1 : 1 stoichiometry was found in all cases and within run precision ranged from 2 to 14% R.S.D. The between run precision for the binding of *p*-nitrophenol to α-CD was 2% ($n = 3$).

Key words: Flow injection; Automated serial dynamic dialysis technique; Cyclodextrins; Drug binding to cyclodextrins; Ibuprofen; *p*-Nitrophenol; Salicylic acid; Scatchard model

1. Introduction

Cyclodextrins (CDs) are torroidally shaped, cyclic oligosaccharides, consisting of six, seven, or eight glucopyranose units (α-, β- and γ-cyclodextrin, respectively), which are linked with α-1,4-glycosidic bonds. CDs form inclusion complexes of the "host-guest" type with a wide variety of ionic and molecular species, the main requirement being that the guest fits entirely, or partly, in the CD cavity [1,2]. The intermolecular interactions involved in the formation of these complexes are non-covalent, consisting mainly of Van der Waals forces, hydrophobic interactions and, when possible, hydrogen bonding [1,2].

The enclosure of a molecule in the CD cavity causes considerable modification of its physical, chemical and biological properties. In addition, upon dissociation of the complex the molecule regains its former properties. These characteristics, and their insignificant per os toxicity, have resulted in a large number of applications for CDs in pharmaceutical technology [2–4], analyti-

* Corresponding author.

0003-2670/94/$07.00 © 1994 Elsevier Science B.V. All rights reserved
SSDI 0003-2670(93)E0633-I

cal chemistry [5], chemical technology [6] and various industrial uses [7].

Increasingly important is the capability of CDs to form complexes with drug molecules, as various properties of the guest drug molecule are altered upon complexation. These properties can thus be modified and the biopharmaceutical and pharmacokinetic behaviour of a drug can be improved. The solubility and dissolution rate are usually increased, the absorption rate is improved and the bioavailability of the drug is enhanced; also, stability is usually increased and the use of CDs in drug formulation has been extensively reported [2–4].

The binding of CDs to various molecules has been studied by various techniques, including phase solubility, spectroscopy (spectrophotometry, circular dichroism, fluorimetry, NMR), chromatography, and electrochemistry (potentiometry) [1,2]. In the so-called "direct methods, the measurement of the analytical signal is performed in the micromolecule–CD mixture under study, while the "indirect methods" require a separation step of the complexes from the free micromolecules. Equilibrium and dynamic dialysis methods are the most common methods in the latter group.

In the present paper, a technique based on the principle of dynamic dialysis in conjunction with the flow-injection (FI) concept is introduced for studying binding parameters of CD complexes. Dynamic dialysis methods [8–10] have been used for in vitro studies of drug–protein interactions, offering the advantages of relatively increased speed (in comparison with the time-consuming equilibrium dialysis methods) and measurement of drug–protein binding over a range of drug concentrations in a single experiment. These methods are based on the principle that the macromolecule–drug complex reaches rapid equilibrium with free macromolecule and diffusible drug in a macromolecule compartment, which is separated from a sink compartment by a semipermeable (dialysis) membrane. The rate of diffusion across the membrane is directly proportional to the free drug concentration in the macromolecule compartment. Sampling of dialysed drug is accomplished by periodical removal of a volume from the sink compartment which is replaced with fresh buffer solution in order to maintain sink conditions. Measurement is usually accomplished using UV-spectrophotometry.

The coupling of dynamic dialysis with the flow-injection concept results in an advantageous

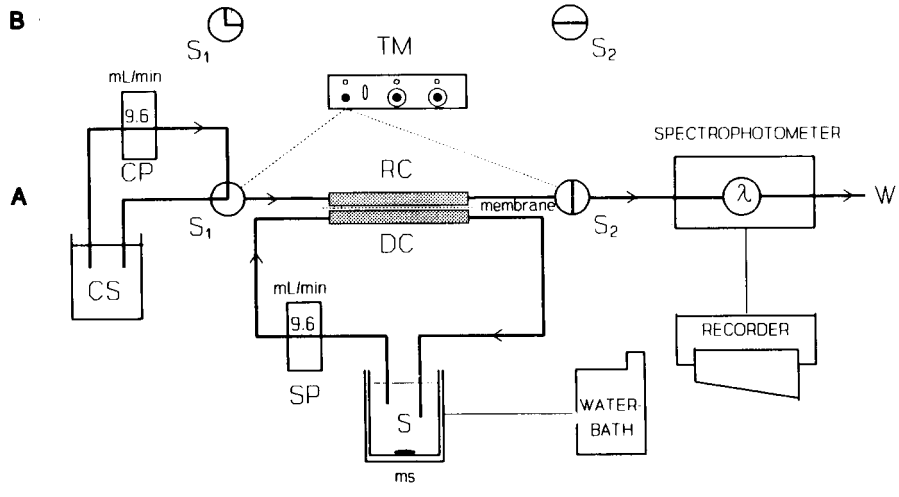

Fig. 1. Schematic diagram of the FISDD system used. CS, carrier solution; CP, carrier pump; RC, receiving compartment; DC, donor compartment; SP, sample pump; S, sample (cyclodextrin–micromolecule) solution; W, waste; S_1, S_2 three- and two-way solenoid valves, respectively; TM, timing module; ms, magnetic stirrer. B, sampling-washing and A, dialysis position of solenoid valves, respectively.

automated fast technique for binding studies. By inserting a dialyser unit in an FI system, the receiving compartment of the former functioning as a sample loop, the binding experiment can be accomplished automatically through a successive series of dynamic dialysis runs. This concept, called flow-injection serial dynamic dialysis (FISDD), has been exploited in protein binding studies [11] and dissolution studies of drug formulations in milk [12], by use of an automated FI analyzer.

In this paper a very simple timing module is used for operation control through two flow switching solenoid valves, and the technique is applied to the recently interesting topic of cyclodextrin–micromolecule binding studies. The performance of the system and the technique were evaluated in the study of the binding of *p*-nitrophenol with α-CD, and salicylic acid and ibuprofen with β-CD. The Scatchard model for one class of binding sites (the CD cavity) was used in order to calculate the binding parameters. This model, frequently used in binding studies of drugs to proteins, has been previously used in the determination of binding constants of drugs to CDs [13].

2. Experimental

2.1. Apparatus

The home-made FISDD apparatus used, shown in Fig. 1, was a simplified version of the system devised previously in our laboratory [11]. In this study, the sample injection rotary valve and the microcomputer were replaced by a home-made timing module, a three-way (S_1) and an on-off (S_2) flow switching 6V DC solenoid valves (Angar).

The dialyser unit, constructed from plexiglas, had a dialysis surface of 670 mm^2 with two identical chambers of 1.0 ml volume each. The two chambers were separated by a semipermeable membrane with 20 μm pores (Cuprophan, Technicon Chemicals), which was hydrated for a short time before assembling the unit. The donor compartment was connected to the sample pump (Masterflex, Cole Palmer), which circulated the cyclodextrin–micromolecule solutions from a thermostatted (25 $\pm$ 0.5°C) cell of 100 ml volume. The inlet of the receiving compartment was connected to the carrier pump via the three-way solenoid valve and the outlet to the UV–visible

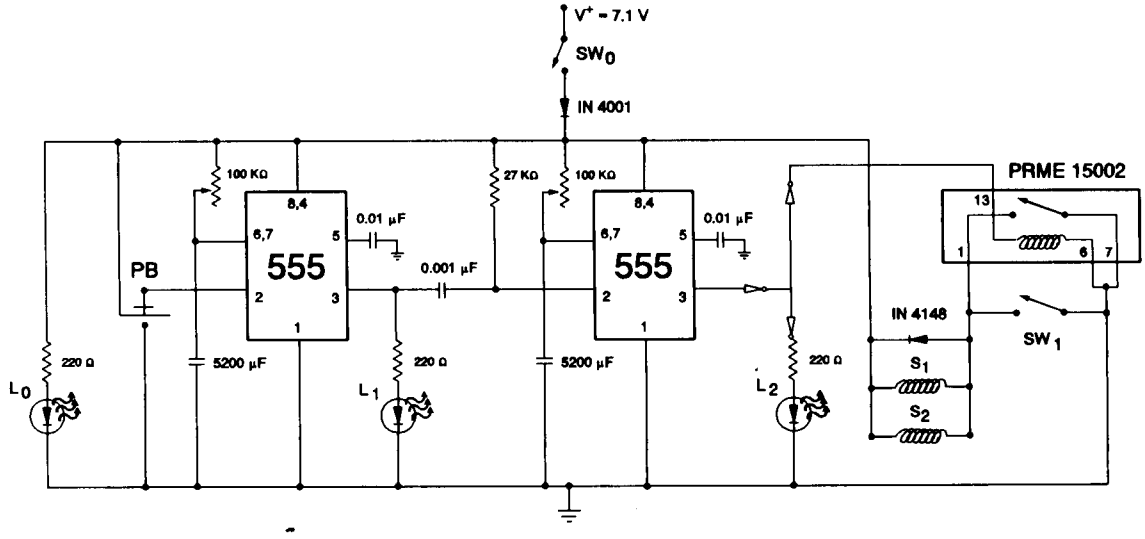

Fig. 2. Circuit diagram of the timing module. SW_o, voltage supply switch; S_1 and S_2 solenoid valves; SW_1, manually operated switch turning S_1 and S_2 to the sampling-washing position overriding timer control; PB, push button triggering timing sequence; L_o, voltage supply indication LED; L_1 and L_2 dialysis and sampling-washing time indication LEDs, respectively.

spectrophotometer (UV-120-02, Shimadzu) equipped with a 400-μl flow cell (Hellma) via the on-off solenoid valve. The absorbance peaks were recorded on a chart recorder (Model 7334, Knauer).

The circuit of the home made timing module (Fig. 2) consists of two cascaded 555 (National Semiconductor) integrated circuit (IC) timers that are configured in the monostable (one-shot) mode and a solid state relay (Clare, PRME 15002) controlled by the second 555 IC. This relay controls the solenoid valves by opening and closing their common power supply. Light emitting diodes (LEDs) connected to the timer's output indicate timing sequence to the operator. The timing element in the 555 ICs is an RC circuit and the time measured is 1.1RC (s). Fixed 5200 ($\pm$10%) μF capacitors were used and the time was set by two 100 ($\pm$5%) kΩ ten-turn potentiometers (Sectrol mod-534) that are linear within $\pm$0.25%. Triggering of the timing sequence was achieved by pressing a push button.

Binding experiments were carried out at constant temperature, flow-rates, and dialysis and sampling times. Data (concentration of free micromolecule calculated from a calibration curve) were treated using the Statgraphics statistical graphics system on an IBM PS/2 computer.

2.2. Reagents

p-Nitrophenol binding study

Concentrated stock solutions of 0.100 M *p*-nitrophenol (Merck) and 5.00×10^{-4} M α-CD (Fluka) were prepared in (a) phosphate buffer 0.010 M, pH 7.4 or (b) borate buffer 0.010 M pH 9.2.

Salicylic acid binding study

Concentrated stock solutions of 0.0100 M sodium salicylate (Ferak) and 1.00×10^{-3} M β-CD (Sigma) were prepared in (a) water and the pH was adjusted to 1.5 by H_2SO_4 2 M (final H_2SO_4 concentration about 0.1 M) or (b) phosphate buffer 0.10 M, pH 7.4.

Ibuprofen binding study

Concentrated stock solutions of 0.010 M ibuprofen (kindly donated by a local manufacturer) and 3.00×10^{-4} M β-CD were prepared in 50% (v/v) methanol in water and adjusted to a phenomenal pH 2.5 with concentrated HCl.

The carrier solution in all cases was the same buffer used in the binding experiment.

The reagent solutions used (0.10 M $NaH_2PO_4 \cdot H_2O$, 2.0 M H_2SO_4 and 50% (v/v) methanol) were prepared from analytical grade reagents. Deionized water was used throughout.

2.3. System set up and operation

In the FISDD system the receiving compartment of the dialyser unit is the "sample loop" of the FI analyzer. Carrier solution is enclosed in the "sample loop" to receive the dialysable micromolecule (drug) of the donor compartment (cyclodextrin compartment) through which the CD–micromolecule (drug) solution is continuously circulated. Periodically this "sample zone" is transferred to a UV–visible spectrophotometer for measurement, and fresh carrier solution is enclosed in the "sample loop". The change of the total concentration of the micromolecule in the donor compartment was achieved by successive manual additions of small volumes of a concentrated standard micromolecule solution.

The dialysis time (3 min for *p*-nitrophenol, and 2 min for salicylic acid and ibuprofen) and sampling time (25 s for all experiments) are set on the timing module and the appropriate wavelength is set on the spectrophotometer (399 nm for *p*-nitrophenol, 237 nm for salicylic acid in pH 1.5, or 296 nm in pH 7.4, and 220 nm for ibuprofen). Then 50.0 ml of the appropriate buffer (for the construction of the calibration curve) or buffered CD solution (for the binding experiment) are pipetted into the beaker, and the carrier and sample pumps are started at the appropriate flow-rate (9.6 ml/min in all experiments). The valves are set, by a manually operated switch overriding timer control, to the sampling-washing position (Fig. 1B), diverting the carrier flow through the receiving compartment, and 100% transmittance and recorder baseline are set. The first portion of the standard stock solution of the micromolecule (drug) under test is added and the timing module is activated after a 2 min mixing/

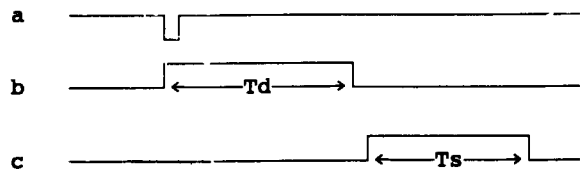

Fig. 3. Timing sequence of the timing module. a, triggering pulse; b and c, output of first and second 555 IC, respectively. Td and Ts, dialysis and sampling-washing time, respectively.

incubation time. During the preset dialysis period, the solution in the beaker is recycled through the donor compartment. Carrier solution is trapped in the receiving compartment and the carrier flow is recycled through the S_1 valve (as shown in Fig. 1A). Then, the timing module initiates the sampling-washing period, switching the S_1 and S_2 valves to the positions shown in Fig. 1B, so that carrier solution flows through the receiving compartment transferring the dialysate to the spectrophotometer, where an absorbance peak corresponding to the dialysed drug concentration is recorded. The next portion of the standard stock solution is added and the cycle is repeated. The timing sequence is shown in Fig. 3.

By using the procedure of successive additions in the selected buffer, calibration curves (absorbance peaks vs. free micromolecule concentration (D_F)) were obtained in a concentration range of $1.0–10 \times 10^{-4}$ M for *p*-nitrophenol and $1.0–30 \times 10^{-4}$ M for salicylic acid and ibuprofen. From the absorbance peaks obtained in the binding experiments the concentration of the free (unbound) micromolecule can be obtained from the constructed calibration curves.

In order to obtain the dialysis–time profiles, a standard solution of the drug under study in the appropriate buffer is placed in the sample beaker, and a series of dialysis-measurement experiments are conducted varying the dialysis time within a range of 1–10 min. The data obtained from this procedure were used to calculate the experimental dialysis rate constants, and thus to optimize the dialysis time chosen.

3. Results and discussion

3.1. System evaluation

Before using the timing module a calibration curve of the potentiometer turns (settings) versus time was constructed for each 555 IC. The time range found was 0.65 s to 10 min with a resolution of 0.65 s. The 555 ICs calibration curves were stable within 2% for six months of operation. These two calibration curves were used in order to set the dialysis and sampling-washing time. The flow-rate used (9.6 ml/min) was selected on the basis of fast donor recycling and low sampling-washing time. The second solenoid (S_2) was included to prevent a small flow of the solution in the receiving compartment to the waste, due to the force of the hydrodynamic pressure gradient during the dialysis period.

Since α- and β-CD are not large macromolecules (MW 973 and 1135, respectively), experiments had to be conducted to assure that they do not diffuse through the membrane under the experimental conditions used during the binding experiments. Buffered solutions of CDs were dialysed for a time period equal to that used in binding experiments. Then the dialysates were collected in test tubes containing phenolphthalein (for β-CD) or methyl-orange (for α-CD) solution, and the absorbances were measured and compared to those of blank experiments (the dialysate was substituted with an equal volume of buffer). No difference in the absorbance was detected, therefore CDs did not diffuse through the membrane under the experimental conditions used. This test is based on the resulting decoloration of phenolphthalein or methyl orange solutions upon addition of β- or α-CD, respectively, due to the formation of the corresponding inclusion complexes [2].

3.2. Determination of dialysis rate constants

The selection of the dialysis time for the micromolecules studied was based on the dialysis rate constants. The experimental dialysis rate constant (k_d) can be calculated according to Eq. 1 [11]

$$\ln[(D_f - D_i)/D_f] = -k_d t \quad (1)$$

where D_f is the concentration of the free (unbound) micromolecule in the donor compartment and D_i is the micromolecule concentration in the receiving compartment after dialysis for a period of time t. D_i is calculated from absorbance measurements using experimentally determined molecular absorptivities. D_f remains practically constant during the experiment, due to the large volume of the solution in the cell (50 ml), as compared to the volume trapped in the receiving compartment (1.0 ml), and can be considered as equal to D_{fo}, which is the initial free micromolecule concentration in the donor compartment. Then the dialysis time required to attain a specified percent of dialysis is calculated according to Eq. 2 [11]

$$t = -\ln[1 - (\%D_i/100)]/k_d \quad (2)$$

The calculated experimental dialysis rate constants for *p*-nitrophenol, salicylic acid and ibuprofen, along with the percent of dialysed micromolecule during the dialysis time chosen and their pK_a values are shown in Table 1. The good within run precision and the correlation coefficients found verify the validity of Eq. 1.

Due to the hydrophobic character of the cuprophan membrane, the non-ionised form of *p*-nitrophenol and salicylic acid diffuse at a higher rate than their corresponding anions (Table 1). As ibuprofen has the highest molecular weight, its k_d value was found to be the lowest one.

3.3 Determination of binding constants

Typical absorbance peaks recorded during the binding study of ibuprofen are shown in Fig. 4. Dashed-line peaks obtained from solutions of pure ibuprofen in various concentrations are shown superimposed to the corresponding (solid-line) ones obtained in the presence of a constant β-CD concentration. It is very clear that binding lowers the amount of ibuprofen dialysed by decreasing the free ibuprofen concentration.

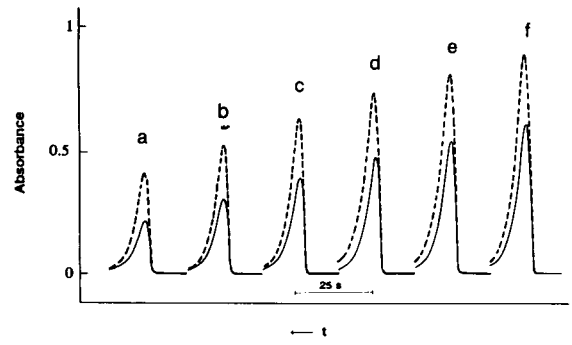

Fig. 4. FIA peaks for a typical binding study of ibuprofen. Dashed line, calibration curve; Solid line, same experiment in the presence of 3.00×10^{-3} M β-CD. Dialysis time 2 min. Total (free plus bound) drug concentration in donor compartment: (a) 1.07, (b) 1.47, (c) 1.86, (d) 2.25, (e) 2.64 and (f) 3.03×10^{-3} M.

The binding parameters were estimated by the use of the well-known Scatchard equation (Eq. 3.), for one class of binding sites

$$(r/D_f) = nK_{as} - K_{as}r \quad (3)$$

where $r = D_b/CD_t$, D_b being the concentration of the bound micromolecule (drug) ($D_b = D_t - D_f$) and CD_t the total cyclodextrin concentration, n the number of cyclodextrin molecules complexed with each micromolecule and K_{as} the association constant of the complex. The parameters n and K_{as} were calculated by linear regres-

Table 1
Calculation of experimental dialysis rate constants at 25°C

Compound	C ($M \times 10^4$)	pK_a	pH	$k_d \pm$ S.D. (min^{-1})	r [a]	dialysed % [b]
p-Nitrophenol	1	7.10	7.4	0.075 ± 0.003	0.996	20.1
	1		9.2	0.056 ± 0.002	0.995	15.5
Salicylic acid	4	2.97	1.5	0.093 ± 0.006	0.993	17.0
	1		7.4	0.058 ± 0.003	0.99	10.9
Ibuprofen	2	5.20	2.5	0.041 ± 0.002	0.996	7.9

[a] Correlation coefficient for the fitting of experimental data to Eq. 1.
[b] Calculated using Eq. 2 and the dialysis times listed in system setup and operation.

Table 2
Binding data for the studied compounds to cyclodextrins [a]

Compound	C_{CD} ($M \times 10^4$)	pH	n	K_{as} (M^{-1}x10)
p-Nitrophenol	5.00	7.4	0.77 ± 0.01 [b]	158 ± 3 [b]
	10.0	9.0	0.82 ± 0.07 [b]	206 ± 16 [b]
Salicylic acid	10.0	1.5	1.07 ± 0.03 [b]	38 ± 1 [b]
Salicylate	30.0	7.4	1.3 ± 0.2 [b]	5.1 ± 0.7 [b]
Ibuprofen	30.0	2.5	0.96 ± 0.09 [b]	22 ± 2 [b]

[a] α-CD for *p*-nitrophenol, β-CD for the others; temperature, 25°C.
[b] Within run standard deviation.

sion of r/D_f versus r values. Examples of Scatchard plots obtained for the three model molecules studied are shown in Fig. 5. Binding data calculated from Eq. 3 is presented in Table 2 and a comparison to literature values is shown in Table 3. As expected, $n = 1$, i.e. the cavity of

Table 3
Comparison of determined binding constants with literature values at 25°C

K_{as} (M^{-1})	pH	Medium, method	Ref.
p-Nitrophenol–α-CD			
2230 [a]	11.0	0.5 M phosphate, spectrophotometry	[14]
2200		pH–Potentiometry	[15]
2500	11.0	Phosphate, spectrophotometry	[16]
2700	11.0	Phosphate, NMR	[16]
1590	11.0	Phosphate, optical rotation	[16]
1890	11.0	0.1 M Phosphate, spectrophotometry	[24]
2408		pH–Potentiometry	[19]
3550	10.0	0.1 M Na_2CO_3, gel filtration	[25]
1770	9.0	0.01 M Borate, ISE–potentiometry	[13]
1579	7.4	0.01 M Phosphate	This study
2060	9.0	0.01 M Borate	This study
Salicylic acid–β-CD			
700	2.5	Water [b], phase-solubility	[26]
378	1.5	0.1 M H_2SO_4	This study
51	7.4	0.1 M Phosphate	This study
Ibuprofen–β-CD			
10800 [c]	7.0	1/15 M Phosphate, spectrophotometry	[27]
10000 [c]	5.0	Water [b], phase-solubility	[26]
410	2.0	Phase-solubility	[23]
221	2.5	Methanol 50% (v/v) [b]	This study

[a] Original measurement for 20°C; calculated for 25°C by Connors and Lipari [15].
[b] Adjusted to pH value by addition of HCl solution.
[c] Complexation stoichiometry 2:3 (drug to CD) was detected.

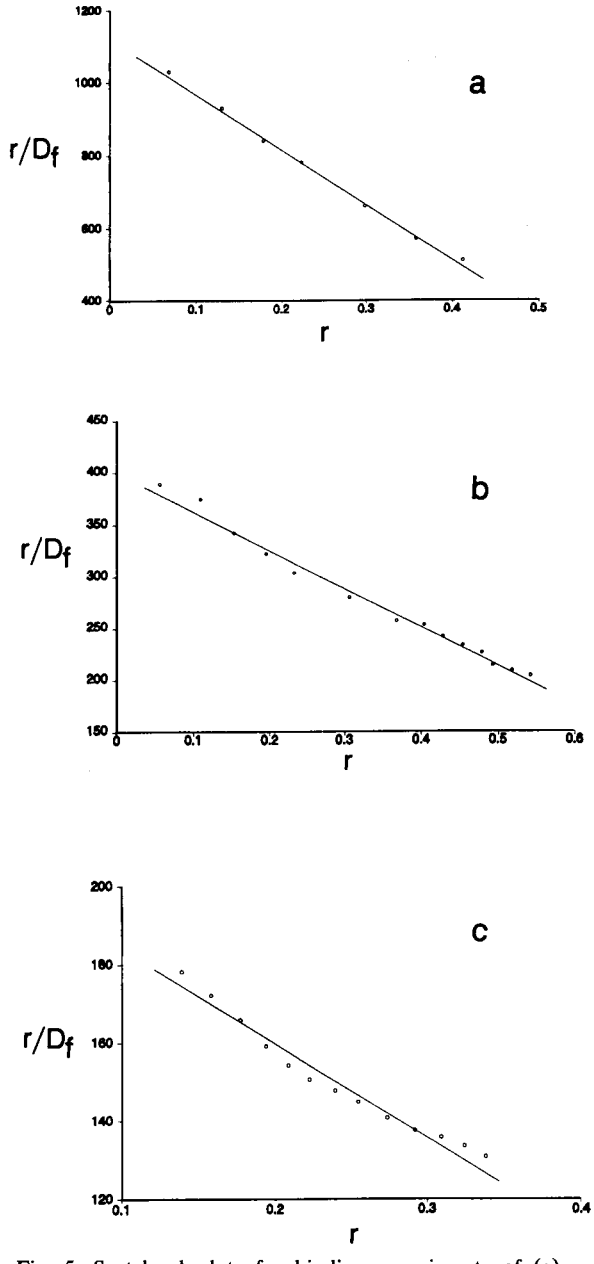

Fig. 5. Scatchard plots for binding experiments of (a) *p*-nitrophenol, (b) salicylic acid and (c) ibuprofen.

the cyclodextrin. Within run precision ranged from 2 to 14% R.S.D., while the between run precision for the binding of *p*-nitrophenol to α-CD was 2% ($n = 3$).

The reactions of micromolecules with CDs in solution are fast enough and completed in a few seconds, as was revealed by in situ monitoring with ion-selective electrodes [13]. The 2 min mixing/incubation time after each successive addition of the micromolecule solution, in conjunction with the 2–3 min dialysis time, ensures that equilibrium is reached.

While the estimated value of K_{as} for *p*-nitrophenol at pH 9.0 is within the range of previously reported estimates (Table 3), at pH 7.4 the K_{as} value is lower. This can be explained on the basis of the degree of ionization of *p*-nitrophenol at the two pH values. At pH 7.4 *p*-nitrophenol is only partially (66%) ionized. It is well-established that *p*-nitrophenolate is bound much stronger than *p*-nitrophenol to α-CD, as proven by a negative change of its pK_a upon complex formation with α-CD ($\Delta pK_a = -0.94$) [14–19].

In contrast to phenols, carboxylic acids are bound to CDs much stronger than their conjugate bases, resulting in a positive change of their pK_a values upon complex formation [15–17,20,21]. This is clearly shown by the two estimates of K_{as} as obtained for salicylic acid at pH 1.5 and 7.4. Although the K_{as} found (378 M^{-1}) at pH 1.5 is in the same order of magnitude with the literature value (700 M^{-1}) at pH 2.5, the difference shows the effect of pH and the method used on the K_{as} values.

Methanolic medium was used to solubilize ibuprofen, which is sparingly soluble in water at pH 2.5. Ethanolic medium was also tried as a solvent, but the dialysis rate was found to be negligible compared to that of the methanolic one. Ethanol was also found to affect complex formation to such a degree, that no useful binding data could be obtained. Various methanol concentrations in the range of 10 to 60% (v/v) were tried and the 50% (v/v) concentration was found to be adequate. The effect of organic solvents on inclusion complex formation with CDs has been studied [22] and it has been shown that methanol is bound much weaker than ethanol in the CD cavity due to its smaller size [2]. However the weak binding of methanol may account for the somehow lower K_{as} of ibuprofen compared to that found by Orienti et al [23].

4. Conclusion

The serial dynamic dialysis technique offers the advantage of separation of free from bound drug and diminishes the long times usually required in static experiments (equilibrium dialysis, phase-solubility studies). The combination with the flow-injection technique results in automated measurements utilizing an exceptionally simple and low-cost system based on two solenoid valves and a home made timing module. The detection scheme used in this study was a direct UV measurement. To improve sensitivity, or when studying drugs that do not absorb in the UV–visible range, the carrier stream leaving the receiving compartment could be merged with appropriate reagent stream(s), allowed to react for a limited time period in a reaction coil and afterwards measured in the appropriate wavelength. Drug ion-selective electrodes, fluorimetry and other detection principles could also be adapted to this system without any modifications. It was also shown that the FISDD technique can be used in the binding studies of cyclodextrins with micromolecules.

5. Acknowledgements

Support from the Greek National Drug Organization through a research contract is gratefully acknowledged. The donation of the IBM PS/2 computer used in this work by IBM Hellas is gratefully acknowledged.

6. References

[1] F. Hirayama and K. Uekama, in D. Duchene (Ed.), Cyclodextrins and their Industrial Uses, Editions de Sante, Paris, 1987, pp. 133–174.
[2] J. Szejtli, Cyclodextrin Technology, Kluwer, Dordrecht, 1988.
[3] D. Duchene, in D. Duchene (Ed.), Cyclodextrins and their Industrial Uses, Editions de Sante, Paris, 1987, pp. 213–257.
[4] O. Bekers, E.V. Uijtendal, J.H. Beijnen, A. Bult and W.J.M. Underberg, Drug. Dev. Ind. Pharm., 17 (1991) 1503.
[5] J. Szejtli, B. Zsaden and T. Cserhati, in W.L. Hinze and D.W. Armstrong (Eds.), Ordered Media in Chemical Separations, ACS Symposium Series 342, ACS, Washington, DC, 1987, pp. 201–234.
[6] W. Saenger, Coll. Ges. Biol. Chem., 32 (1981) 33.
[7] C. Vation, M. Hutin, F. Glomot and D. Duchene, in D. Duchene (Ed.), Cyclodextrins and their Industrial Uses, Editions de Sante, Paris, 1987, pp. 297–350.
[8] M.C. Meyer and D.E. Guttman, J. Pharm. Sci., 57 (1968) 1627.
[9] M.C. Meyer and D.E. Guttman, J. Pharm. Sci., 59 (1970) 33.
[10] K.A. Connors, Binding Constants – The Measurement of the Molecular Complex Stability, Wiley, New York, 1987.
[11] P. Macheras, M. Koupparis and C. Tsaprounis, Int. J. Pharm., 30 (1986) 123.
[12] P. Macheras, M. Koupparis and C. Tsaprounis, Int. J. Pharm., 33 (1986) 125.
[13] G.N. Valsami, P.E. Macheras and M.A. Koupparis, J. Pharm. Sci., 79 (1990) 1087.
[14] F. Cramer, W. Saenger and H.C. Spatz, J. Am. Chem. Soc., 89 (1967) 14.
[15] K.A. Connors and J.M. Lipari, J. Pharm. Sci., 65 (1976) 379.
[16] R.J. Bergeron, M.A. Channing, G.J. Gibeily and D.M. Pillor, J. Am. Chem. Soc., 99 (1977) 5146.
[17] R.J. Bergeron, M.A. Channing and K.A. McGovern, J. Am. Chem. Soc., 100 (1978) 2878.
[18] R.I. Gelb, L.M. Schwartz, B. Cardelino, H.S. Fuhrman, R.F. Johnson and D.A. Laufer, J. Am. Chem. Soc., 105 (1981) 1750.
[19] S.F. Lin and K.A. Connors, J. Pharm. Sci., 72 (1983) 1333.
[20] R.I. Gelb, L.M. Schwartz, R.F. Johnson and D.A. Laufer, J. Am. Chem. Soc., 101 (1979) 1869.
[21] K.A. Connors, S.F. Lin and A.B. Wong, J. Pharm. Sci., 71 (1982) 217.
[22] R.I. Gelb, L.M. Schwartz, M. Radeos, R.B. Edmonds and D.A. Laufer, J. Am. Chem. Soc., 104 (1982) 6283.
[23] I. Orienti, C. Cavallari and V. Zecchi, Arch. Pharm., 322 (1989) 207.
[24] A. Cooper and D.D. McNicol, J. Chem. Soc. Perkin Trans. II, (1978) 760.
[25] T.K. Korpela and J.P. Himanen, J. Chromatogr., 290 (1984) 351.
[26] H. Vromans, A.C. Eissens and C.F. Lerk, Acta Pharm. Technol., 35 (1989) 250.
[27] D.D. Chow and A.H. Karara, Int. J. Pharm., 28 (1986) 95.

ELSEVIER

Analytica Chimica Acta 289 (1994) 97–104

ANALYTICA CHIMICA ACTA

Simultaneous speciation determination of vanadium(IV) and vanadium(V) as EDTA complexes by liquid chromatography with UV detection

Jen-Fon Jen *, Shih-Ming Yang

Department of Chemistry, National Chung-Hsing University, Taichung, 40227, Taiwan

(Received 7th June 1993; revised manuscript received 2nd November 1993)

Abstract

A liquid chromatographic (LC) method for the simultaneous determination of the speciation of vanadium(IV) and vanadium(V) was developed by using reversed-phase ion-pair liquid chromatography. Vanadium(IV) and vanadium(V) were complexed with EDTA in a precolumn, then a C_8 column was used to separate the vanadium–EDTA complexes from other species with an eluent containing acetonitrile, EDTA and tetrabutylammonium ion. The separated species were monitored at 245 nm with a UV detector. Factors affecting the chromatographic behaviour, complex stability and possible interferences were investigated. The proposed LC–UV detection method provides a simple procedure for the determination of vanadium speciation. The detection limits were 1.0 ng for both species with a 20-μl injection. The relative standard deviations for vanadium(IV) and vanadium(V) were 0.69% and 0.43%, respectively, for a 20 μg ml^{-1} (20-μl) injection ($n = 5$).

Key words: Ion chromatography; Liquid chromatography; Speciation; Vanadium

1. Introduction

Speciation analysis of trace metals has been focused on the interpretation of their roles in environmental and biological studies recently [1–3]. The chemical and physical properties of a metal species depend very much on its oxidation state, hence an accurate determination of each species is important to evaluate the potential risk of some metals. Vanadium is considered as an essential element for cell growth at the μg ml^{-1} concentration level, but can be toxic at higher μg ml^{-1} levels [4]. In surface waters, it usually exists as V^V and V^{IV} [5]. It is recognized that the biological function of the element depends on its oxidation state [6] and V^V as vanadate is more toxic than V^{IV} present as vanadyl ions [7]. Therefore, it is essential to differentiate V^V from V^{IV} in environmental and biological samples for a better understanding of the toxicity of vanadium.

The contents of vanadium species in aquatic samples have rarely been measured individually [8–11]. In most previous studies, the total content of vandium was determined by atomic spectrometry or spectrophotometry [12–16]. Patel et al. [8]

* Corresponding author.

0003-2670/94/$07.00 © 1994 Elsevier Science B.V. All rights reserved
SSDI 0003-2670(93)E0632-H

determined vanadium speciation by using a flow-injection system that incorporated a strong anion-exchange resin and was coupled to flame atomic absorption spectrometry (AAS). Hirayama et al. [10] applied a two-column system and inductively coupled plasma atomic emission spectrometry to speciate vanadium ions. Sugijama and Hori [11] used air-segmented continuous-flow analysis based on a catalytic reaction to determine vanadium species. However, these methods still do not satisfy the requirements for routine analysis because of their complicated process design, time consumption and the need for a sophisticated detection system.

Application of liquid chromatography (LC) to the determination of the speciation of metal ions has increased rapidly. However, with regard to vanadium(V) and (IV), so far only Komarova et al. [9] have studied the ion chromatographic behaviour of their anionic EDTA complexes. However, with ion chromatography, a high pH buffer is required to elute the anionic species, which might destroy the $[VO_2Y]^{3-}$ complex, and the high acidity in suppressor column could cause the protonation of the $[VO_2Y]^{3-}$ complex to form $[VO_2HY]^{2-}$, $[VO_2H_2Y]^{-}$ and $[VO_2H_3Y]$ [9]. These would affect the chromatogram and lead to difficulties in obtaining a chromatogram with sufficient resolution.

In this study, the simultaneous determination of V^{IV} and V^{V} as EDTA complexes was achieved successfully by using reversed-phase ion-pair LC with a conventional UV detector. This method has sufficient selectivity and sensitivity for the determination of the speciation of vanadium within an acceptable analysis time.

2. Experimental

2.1. Apparatus

The LC system used for these studies was an LC-9A (Shimadzu, Kyoto) equipped with a Rheodyne Model 7125 injection valve with a 20-μl sample loop and a Supelcosil LC-8 (3 μm) reversed-phase column (25 cm × 4.6 mm i.d. 3) (Supelco, Bellefonte, PA). A Soma Model S-3702 UV–visible detector and a Shimadzu C-R6A Chromatopac integrator were used.

A Model Z-8100 polarized Zeeman-effect atomic absorption spectrometer (Hitachi) was used to analyse the effluent from the LC column.

2.2. Reagents

Distilled, deionized water was used to prepare all solutions. Stock standard solutions of 1000 ppm VO^{2+} and VO_2^+ were prepared by dissolving 0.42 g of analytical-reagent grade $VOSO_4 \cdot 3H_2O$ (Fluka) in 100 ml water and 0.229 g of analytical-reagent grade NH_4VO_3 (Riedel-de Haën) in 5 ml of concentrated H_2SO_4 and dilution to 100 ml with water, respectively. Fresh working standard solutions of VO^{2+} and VO_2^+ (single or mixed) were prepared daily by appropriate dilution of the stock solutions. Ethylenediaminetetraacetate disodium salt (Na_2EDTA) was obtained from Merck and tetrabutylammonium hydroxide (TBAOH) was purchased from Riedel-de Haën. The LC eluent was prepared from LC-grade acetonitrile (Mallinckrodt), water, TBAOH and EDTA. Sulphuric acid (0.01 M) was used to adjust the pH. All eluents were filtered through a 0.45-μm PVDF membrane filter and degassed ultrasonically.

2.3. Procedure

A 50-ml volume of sample solution containing VO^{2+} and/or VO_2^+ was pipetted into a 100-ml beaker and the pH was adjusted to 6.0. After adding excess EDTA (1.5 times equimolar proportions), the solution was kept for 20 min for complete chelation, and then transferred into a 100-ml volumetric flask followed by dilution to the mark with water. The sample was injected into the LC system throught a 20-μl sample loop after filtration through a membrane filter. The eluent was 12% (v/v) acetonitrile prepared in 0.05 M TBA aqueous solution containing 0.002 M EDTA at pH 6.0. The flow-rate was 1.2 ml min^{-1}. The eluent composition and the elution conditions were adjusted to obtain an optimum separation of vanadium complexes from other species in a real sample.

3. Results and discussion

3.1. Vanadium chelate formation and UV detection

Complexation of EDTA with V^{IV} and V^{V} forms $[VOY]^{2-}$ and $[VO_2Y]^{3-}$ (where Y represents the deprotonated EDTA species), respectively. This makes it possible to separate the vanadium species as anionic EDTA complexes by ion chromatography [9]. As vanadium species are separated with the complex form of EDTA, the retention of the former depends on the extent of chelation. In order to ensure the completeness of chelation, vanadium species were chelated with EDTA on a precolumn. The formation constants were calculated [17,18] based on several earlier studies on the chelation between vanadium ions and EDTA [9,18–21]. The pH is the most important factor in the chelation because the condensation of vanadium species occurs at pH > 10 and the protonation of V^{V} chelates occurs at pH < 5 [9]. Therefore, the pH in chelation and in elution was maintained at 6.0.

Although the formation of the V^{V} complex was very fast, with a high formation constant ($10^{18.05}$ [17] or $10^{15.55}$ [18]), the complex was unstable in the elution system until EDTA was added to the eluent. Only the V^{IV} complex peak appeared stably on the chromatogram if there was no EDTA in the eluent. Fig. 1 (solid lines) shows the influence of EDTA on the detection of V^{V}–EDTA and V^{IV}–EDTA. The peak area of V^{V}–EDTA increases as the EDTA concentration in eluent increases. This indicates the instability of V^{V}–EDTA in the elution system. Hence a sufficient amount of EDTA in the eluent is necessary to increase the sensitivity of detection. In contrast, the detection sensitivity of V^{IV}–EDTA did not change with increase in the concentration of EDTA in the eluent. This indicates that V^{IV}–EDTA is stable in the elution. In this study, with 0.002 M EDTA added to the eluent, a 102.3% recovery of V^{V} and a 97.9% recovery of V^{IV} were obtained [detected by graphite furnace AAS after fractional collection] from a 20 μg ml^{-1} (20-μl) injection.

The sensitivity is also affected by the selection of the wavelength. The UV spectra of V^{V}–EDTA and V^{IV}–EDTA complexes are shown in Fig. 2. Although separation of vanadium species was achieved by an ion-pair mechanism with tetra-

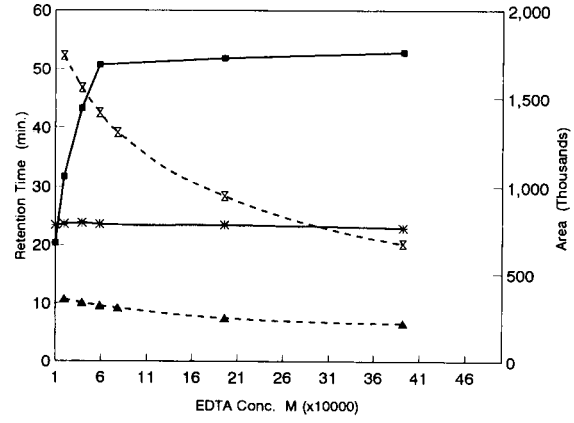

Fig. 1. Influence of EDTA on quantitative detection and retention time. Eluent, 0.005 M TBA and x M EDTA in 12% (v/v) acetonitrile at pH 6.0; RP-C_8 column for 20 μg ml^{-1} $[VOY]^{2-}$ and $[VO_2Y]^{3-}$. Flow-rate, 1.2 ml min^{-1}. Retention times: ▲ = V^{IV}; ⧖ = V^{V}. Areas: * = V^{IV}; ■ = V^{V}.

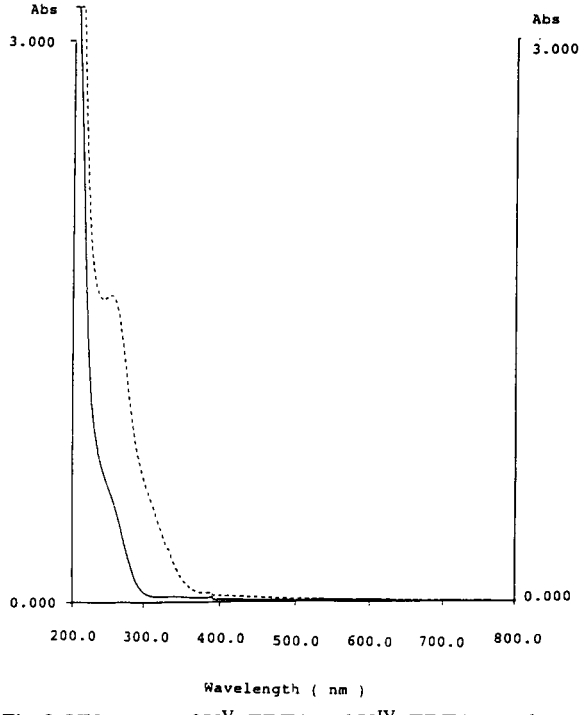

Fig. 2. UV spectra of V^{V}–EDTA and V^{IV}–EDTA complexes. Operation conditions: scan speed, 120.0 nm min^{-1}; band pass, 2.00 nm. Solid line = 20 μg ml^{-1} V^{IV}–EDTA and dashed line = 20 μg ml^{-1} V^{V}–EDTA at pH 6.0.

butylammonium ion, there was no significant difference between the absorption spectra of the ion pair and complex anion. Because a worse baseline was obtained with detection at lower wavelengths and the sensitivity decreased as the wavelength increased, 245 nm was selected for monitoring both species under the specified experimental conditions.

3.2. Separation and identification of species

The V^{IV}–EDTA and V^{V}–EDTA complex ions were separated in the reversed-phase C_8 column and detected with a UV detector under the conditions described earlier. Chromatograms of the vanadium complexes are shown in Fig. 3a. To identify these species, their retention behaviours

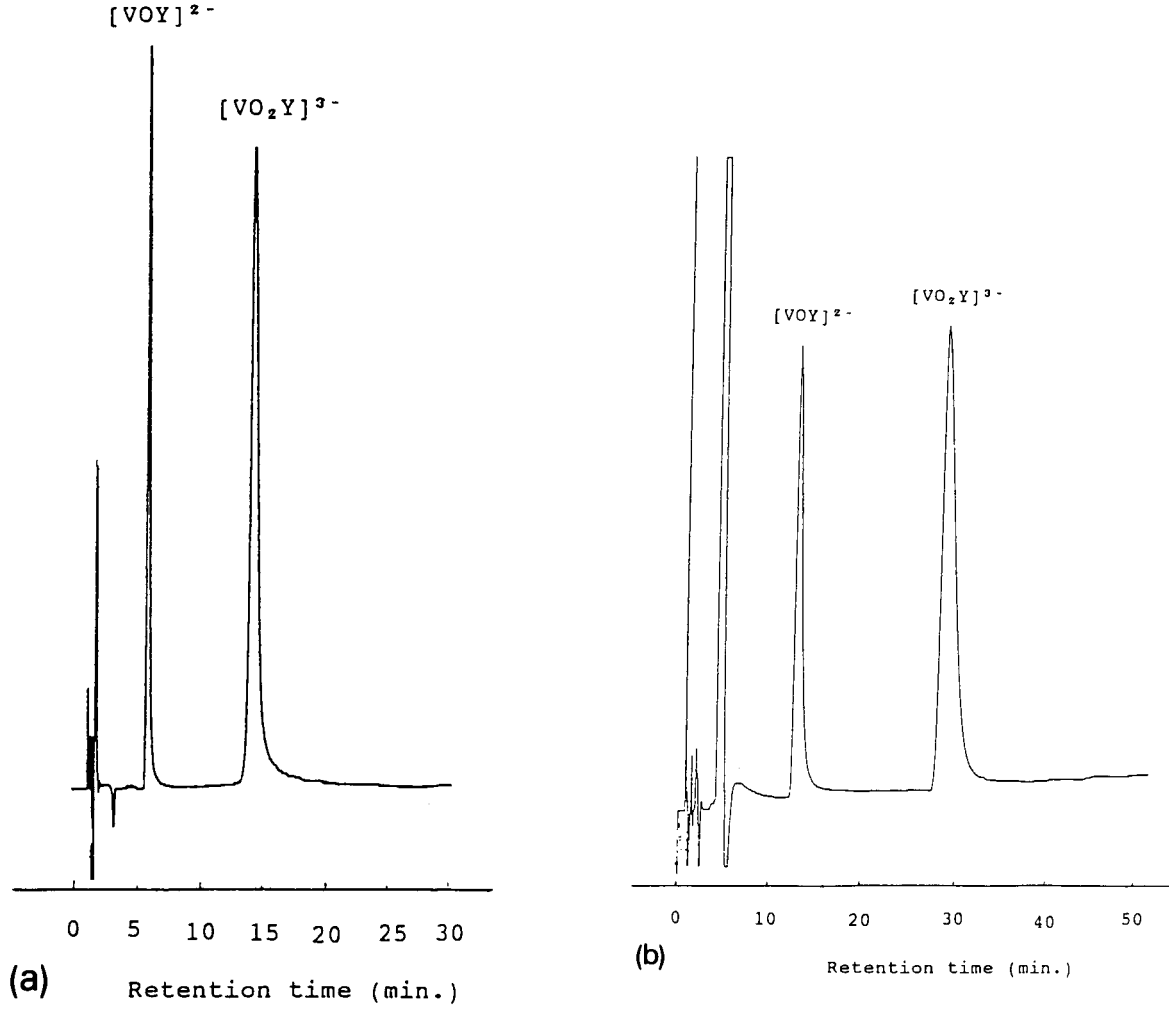

Fig. 3. Chromatograms of V^{V}–EDTA and V^{IV}–EDTA complexes. (a) Eluent, 0.05 M TBA and 0.002 M EDTA in 12% (v/v) acetonitrile at pH 6.0; RP-C_8 column for 20 μg ml^{-1} standards of $[VOY]^{2-}$ and $[VO_2Y]^{3-}$. Flow-rate, 1.2 ml min^{-1}. (b) Eluent, 0.05 M TBA and 0.002 M EDTA in 0.01 M sodium acetate solution at pH 6.0; RP-C_8 column for a leachate sample. Flow-rate, 2.0 ml min^{-1}.

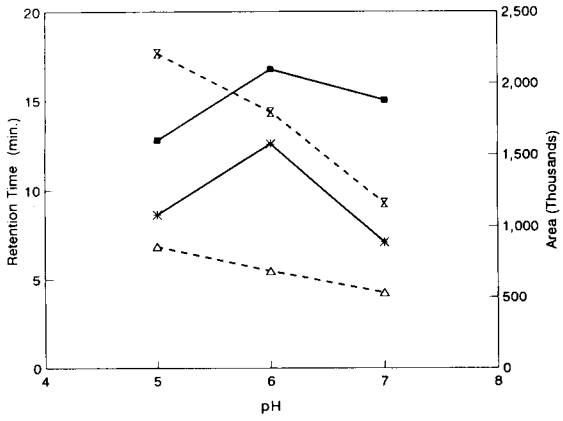

Fig. 4. Influence of pH on chromatographic behaviour. Eluent, 0.005 M TBA and 0.002 M EDTA in 12% (v/v) acetonitrile at pH 5, 6 or 7; RP-C_8 column for 20 μg ml^{-1} of $[VOY]^{2-}$ and $[VO_2Y]^{3-}$. Flow-rate, 1.2 ml min^{-1}. Retention times: $\Delta = V^{IV}$; $\boxtimes = V^{V}$. Areas: $* = V^{IV}$; $\blacksquare = V^{V}$.

were compared with those of standards, and also AAS and UV–visible spectrophotometry were used for confirmation following fraction collection. As shown in the chromatogram for standard species, the V^{IV}–EDTA and V^{V}–EDTA complexes are obviously well separated. The separation is due to the charge difference between V^{IV}–EDTA (as $[VOY]^{2-}$) and V^{V}–EDTA (as $[VO_2Y]^{3-}$).

3.3. Effect of pH

Because the stabilities of the vanadium complexes, the EDTA chelation and the TBA ion pairing are all affected by pH, the eluent should be adjusted carefully to the appropriate pH. Fig. 4 shows the influence of pH on the retention and quantitative detection of the vanadium complexes. As can be seen, the retention time decreases significantly as the pH increases from 5 to 7; the retention of $[VO_2Y]^{3-}$ decreases more rapidly than that of $[VOY]^{2-}$. This can be explained by considering the pK_b of TBA and the pK_a of EDTA. A lower pH favours the dissociation of TBA and disfavours EDTA ionization. Generally, the dissociation of TBA aids ion-pair formation, which enhances the retention of vanadium species. Conversely, the ionization of EDTA increases the ionic strength in eluent and shortens the retention time of species. Hence the retention times of $[VO_2Y]^{3-}$ and $[VOY]^{2-}$ decreased as the pH increased. Concerning the influence of pH on quantitative detection, an increase in pH supplies more Y^{4-} for complexation and enhances the stability of $[VO_2Y]^{3-}$ and $[VOY]^{2-}$. However, there is a risk of precipitation [22] ($V_{18}O_{42}^{12-}$ for V^{IV} and $V_{10}O_{28}^{6-}$ for V^{V}) at pH > 10. Overall, elution at pH 6 gave the optimum sensitivity of detection and was applied throughout the studies.

3.4. Effect of ion-pair reagent

In a reversed-phase ion-pair chromatographic column, the sorption of TBA^+ offers dynamic ion-exchange sites. Thus, the retention of $[VO_2Y]^{3-}$ and $[VOY]^{2-}$ is directly related to the surface charge arising from the absorbed TBA^+ (TBA_s^+) and an adsorption equilibrium of TBA is established between the eluent and the stationary phase. In the ion-exchange mechanism, the retention should increase with increasing amount of TBA_s^+ until saturation. However, Fig. 5 (dashed lines) shows that the retention of $[VO_2Y]^{3-}$ only increases with increase in TBA concentration in the low concentration range and then decreases

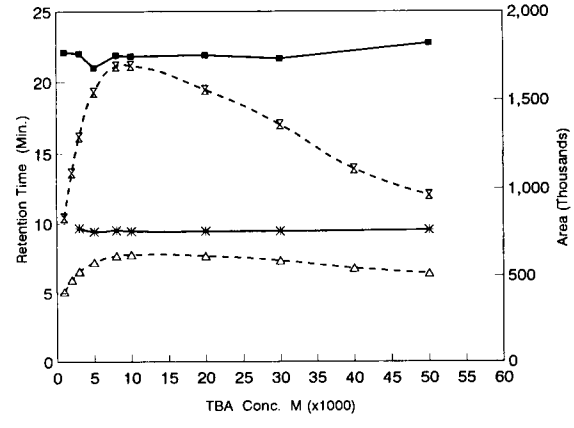

Fig. 5. Influence of TBA concentration on retention time. Eluent, x M TBA and 0.002 M EDTA in 12% (v/v) acetonitrile at pH 6.0; RP-C_8 column for 20 μg ml^{-1} $[VOY]^{2-}$ and $[VO_2Y]^{3-}$. Flow-rate, 1.2 ml min^{-1}. Retention times: $\Delta = V^{IV}$; $\boxtimes = V^{V}$. Areas: $* = V^{IV}$; $\blacksquare = V^{V}$.

after an optimum addition. On the other hand, the TBA effect on the retention of $[VOY]^{2-}$ is negligible. This aspect is worthy of further investigate. Concerning the influence of TBA on quantitative detection (solid lines), the TBA concentration did not affect the detection signal.

3.5. Effect of organic modifier

The in situ-formed neutral ion pairs, $(TBA_s^+)_3 \cdot (VO_2Y)^{3-}$ and $(TBA_3^+)_2 \cdot (VOY)^{2-}$ tend to be firmly adsorbed on the surface of a reversed-phase column because of the large size of the ion pair. In order to shorten the elution time, an organic modifier is needed in the eluent to compete with the TBA_s or ion pairs in the adsorption equilibria. Acetonitrile was selected as the organic modifier throughout the studies. The capacity factor, k', decreased rapidly as the content of acetonitrile increased and the good resolution was maintained up to a 30% addition. Moreover, no significant change in the detection sensitivity was observed with the addition of organic modifier. Hence appropriate amounts of organic modifier can be added to adjust the retention behavior for optimum separation.

3.6. Effect of EDTA in eluent

The action of EDTA in the eluent was described earlier. Because EDTA dissolves and forms several ionic species in the eluent, the ionic strength of eluent increases with increasing EDTA concentration. Thus, the retention behaviours of $[VO_2Y]^{3-}$ and $[VOY]^{2-}$ were influenced by the addition of EDTA. As shown in Fig. 1 (dashed lines), addition of EDTA decreases the retention of $[VO_2Y]^{3-}$ greatly, but that of $[VOY]^{2-}$ only slightly.

3.7. Calibration graphs and detection limits

In order to test the applicability of the method for the simultaneous determination of $[VO_2Y]^{3-}$ and $[VOY]^{2-}$, calibration graphs were constructed for both over the concentration range 0.1–80 $\mu g\ ml^{-1}$. The linear relationship between the peak areas and the injected amounts was excellent for both species. The correlation coefficients were all above 0.9999. The reproducibilities were examined with five replicate injections of 20 $\mu g\ ml^{-1}$ (20 μl) of each complexion. Peak areas were measured and the relative standard deviations (R.S.D.s) were calculated. The R.S.D.s were 0.69% and 0.43% for $[VOY]^{2-}$ and $[VO_2Y]^{3-}$, respectively. The detection limits were 1 ng (20 μl) for both based on three times the average background noise level.

Table 1
Retention times of possible interferents

Ion (50 $\mu g\ ml^{-1}$)	Retention time (min)
Sn^{4+}-EDTA	1.26
Mn^{2+}-EDTA	2.72
Pb^{2+}-EDTA	2.83
Ni^{2+}-EDTA	2.86
Co^{2+}-EDTA	2.95
Cu^{2+}-EDTA	3.10
Cr^{3+}-EDTA	4.19
Zn^{2+}-EDTA	4.21
NO_3^-	4.34
CrO_4^{2-}	4.98
$[VOY]^{2-}$	6.54
Fe^{3+}-EDTA	8.01 [a]
I^-	10.15
$[VO_2Y]^{3-}$	17.43
Br^-, Cl^-, SO_4^{2-}	– [b]
Ca^{2+}, Mg^{2+}, Cd^{2+}-EDTA	– [b]

Elution conditions: mobile phase, 0.05 M TBA and 0.002 M EDTA in 12% (v/v) acetonitrile at pH 6.0; flow-rate, 1.1 ml min^{-1}.

[a] Broad and tailing interference for $Fe^{3+} > 20\ \mu g\ ml^{-1}$; with elution at lower pH or with no EDTA in eluent, no interference occurred.

[b] No signal response.

3.8. Interferences

EDTA could chelate with other metal ions to form complex anions and then some anions could form ion pairs in the elution. Therefore, possible interferences by various species were studied. Table 1 gives the retention time of these species. Fortunately, no serious interference occurred in the elution except for iron(III) ions at concentrations $> 20\ \mu g\ ml^{-1}$. Even though the interference could not be removed by adding KCN, it could be decreased by using a lower pH for

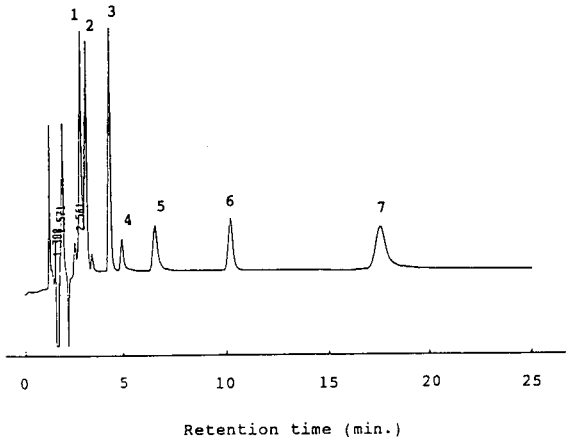

Fig. 6. Chromatograms of V^{V}–EDTA and V^{IV}–EDTA complexes with some potential interferences. Eluent, 0.05 M TBA and 0.002 M EDTA in 12% (v/v) acetonitrile at pH = 6.0; RP-C_8 column for 20 μg ml^{-1} standards of $[VOY]^{2-}$ and $[VO_2Y]^{3-}$. Flow-rate, 1.1 ml min^{-1}. Peaks: 1 = PbY^{2-}; 2 = CuY^{2-}; 3 = NO_3^-; 4 = CrO_4^-; 5 = $[VOY]^{2-}$; 6 = I^-; 7 = $[VO_2Y]^{3-}$ (50 μg ml^{-1}).

elution (pH 4). Fig. 6 shows the chromatogram of $[VOY]^{2-}$, $[VO_2Y]^{3-}$ and some possible interferences. Peaks 1–7 agreed with those of PbY^{2-}, CuY^{2-}, NO_3^-, CrO_4^-, $[VOY]^{2-}$, I^- and $[VO_2Y]^{3-}$, respectively. As can be seen, $[VOY]^{2-}$ and $[VO_2Y]^{3-}$ can be freed from interferences by using appropriate elution conditions. This indicates that the proposed method can be used to analyse aqueous samples with lower iron(III) contents. Hence the elution conditions should be modified if the method is applied to the determination of vanadium in a sample with a high iron(III) content.

3.9. Analysis of vanadium species in the leachate from an oil-refining waste site.

Because the matrix of a leachate sample from an oil-refining waste site was complex, serious tailing occurred in the separation of vanadium species using the conditions described above. Therefore, the eluent composition and elution conditions were adjusted to obtain a better separation of vanadium species from the matrix. Acetonitrile was removed in order to increase the retention times of the vanadium species relative to the matrix components, sodium acetate was added to decrease peak tailing and the flow-rate was increased to shorten all the retention times. Fig. 3b shows the chromatogram of the leachate analysed using the above conditions. Calibration graphs were linear over the range 1.0–30 μg ml^{-1} for both vanadium–EDTA complexes (r = 0.9996 and 0.9998 for $[VOY]^{2-}$ and $[VO_2Y]^{3-}$, respectively). The concentrations of V(IV) and V(V) in the sample were 12.2 and 16.5 μg ml^{-1}, respectively, as compared with the total vanadium concentration (29.1 μg ml^{-1}) determined by AAS.

4. Conclusion

This study has shown the potential of the simultaneous determination of vanadium(IV) and vanadium(V) by using a simple LC–UV system after EDTA complexation for a simple matrix sample. The study of real sample study analysis showed that the method is applicable to the simultaneous determination of vanadium species in a leachate of waste catalyst after modification of the eluent and elution conditions.

5. Acknowledgement

The authors thank the National Science Council of the Republic of China for financial support under grant NSC 82-0208-M-005-054.

6. References

[1] T.M. Florence and G.E. Batley, CRC Crit. Rev. Anal. Chem., 9 (1980) 219.
[2] T.M. Florence, Analyst, 111 (1986) 489.
[3] E. Nakayama, Y. Suzuki, K. Fujiwara and Y. Kitano, Anal. Sci., 5 (1989) 129.
[4] F.H. Nielsen, Clin. Biochem. Nutr. Aspects Trace Elem., 6 (1982) 379.
[5] B. Wehrli and W. Stumm, Geochim. Cosmochim. Acta, 53 (1989) 69.
[6] B. Lagerkvist, G.F. Nordberg and V.B. Vouk, in L. Friberg, G.F. Nordberg and V.B. Vouk (Eds.), Handbook on the Toxicology of Metals, Vol. II, Elsevier, Amsterdam, 1986, pp. 638–663.

[7] G.R. Willsky, D.A. White and B.C. McCabe, J. Biol. Chem., 259 (1984) 13273.
[8] B. Patel, G.E. Henderson, S.J. Haswell and R. Grzeskowiak, Analyst, 115 (1990) 1063.
[9] T.V. Komarova, O.N. Obrezkov and O.A. Shpigun, Anal. Chim. Acta. 254 (1991) 61.
[10] K. Hirayama, S. Kageyama and N. Unohara, Analyst, 117 (1992) 13.
[11] M. Sugiyama and T. Hori, Anal. Chim. Acta. 261 (1992) 189.
[12] R.W. Collier, Nature, 309 (1984) 441.
[13] Y. Nojiri, T. Kawai, A. Otsuki and K. Fuwa, Water Res., 19 (1985) 503.
[14] Y. Sato and S. Okabe, Kaiyo Kagaku, 17 (1985) 552.
[15] M. Sugiyama, O. Fujino, S. Kihara and M. Matsui, Anal. Chim. Acta, 181 (1986) 159.
[16] M. Sugiyama, J. Geochem., 23 (1989) 111.
[17] J.A. Dean, Lange's Handbook of Chemistry, McGraw-Hill, New York, 11th edn., 1976, Table 5-15, p. 5-56.
[18] L. Przyborowski, G. Schwarzenbach and Th. Zimmermann, Helv. Chim. Acta, 48 (1965) 1556.
[19] J.L. Hoard, W.R. Scheidt and C.-C. Tsai, J. Am. Chem. Soc., 93 (1971) 3867.
[20] J.L. Hoard, W.R. Scheidt and D.M. Collins, J. Am. Chem. Soc., 93 (1971) 3873.
[21] D.T. Sawyer and L.W. Amos, Inorg. Chem., 11 (1972) 2692.
[22] G.K. Johnson and E.O. Schlemper, J. Am. Chem. Soc., 100 (1978) 3645.

ELSEVIER

Analytica Chimica Acta 289 (1994) 105–111

ANALYTICA CHIMICA ACTA

Mercaptoethanesulphonic acid as a protecting and hydrolysing agent for the determination of the amino acid composition of proteins using an elevated temperature for protein hydrolysis

János Csapó *,[a], Zsuzsanna Csapó-Kiss [a], Staffan Folestad [b], Anna Tivesten [b]

[a] *Faculty of Animal Science, PANNON Agricultural University, P.O. Box 16, Dénesmajor 2, H-7401 Kaposvár, Hungary*
[b] *Department of Analytical and Marine Chemistry, University of Göteborg, and Chalmers University of Technology, S-412 96 Gothenburg, Sweden*

(Received 23rd July 1993)

Abstract

Mercaptoethanesulphonic acid (MES-OH) (3 M) was used for the hydrolysis of different samples (pure proteins, free tryptophan and milk powder with a high sugar content). Different temperatures (160, 170 and 180°C) and time periods (15–90 min) were compared under standard conditions to minimize side-reactions in order to obtain the best recovery of the amino acids (especially tryptophan and methionine). The materials used for testing the hydrolysis methods were bovine ribonuclease, lysozyme, cytochrome *c*, free tryptophan and mare's milk powder. Hydrolysis at high temperature was successfully applied for the amino acid analysis of milk powder with high contents of carbohydrate and pure proteins. In some instances, such as in tryptophan and methionine determination at 160–170°C for 15–30 min, the results were better than those obtained by the original MES-OH method. A disadvantage of the MES-OH hydrolysis method is that it reduces cystine to cysteine, which co-elutes with proline from the ion-exchange column used to separate the released amino acids and it may interfere with the determination of proline in high-cystine proteins.

Key words: Sample preparation; Amino acids; Mercaptoethanesulphonic acid; Methionine; Protein hydrolysis; Tryptophan

1. Introduction

The problems associated with the rapid and accurate determination of the tryptophan content of polypeptides, food and feed proteins have not yet been completely solved. Tryptophan can be determined indirectly in intact proteins by spectrophotometric methods if the amount of tyrosine is known [1,2]. The tryptophan content can also be determined directly after basic hydrolysis of proteins [3,4], but this method is time consuming. Such a hydrolysate is not suitable for total amino acid analysis because some amino acids (especially arginine) are damaged under the conditions of hydrolysis. During acid hydrolysis of proteins, tryptophan is partly or, in the presence of carbohydrates, totally decomposed.

* Corresponding author.

0003-2670/94/$07.00 © 1994 Elsevier Science B.V. All rights reserved
SSDI 0003-2670(93)E0641-J

In the last 20 years, attempts have been made to eliminate the destruction of tryptophan residues. Matsubara and Sasaki [5] performed the hydrolysis of proteins with 6 M HCl containing 0.5–5% thioglycolic acid, Liu and Chang [6] used 3 M *p*-toluenesulphonic acid containing 0.2% tryptamine, Simpson et al. [7] introduced the non-volatile 4 M methanesulphonic acid containing 3-(2-aminoethyl)indole and Penke et al. [8] and Csapó et al. [9] used 3 M mercaptoethanesulphonic acid for the mild acid hydrolysis of peptides and proteins in order to increase the precision of determination for tryptophan.

More recently, some hydrolysis methods at elevated temperature [10] or using microwave techniques [11–13] were developed. With the help of microwave irradiation, the temperature in the hydrolysis vessels is > 150°C, and this offers the advantage of shortening the hydrolysis time from 24–72 h to 15–45 min. The use of a mixed acid solvent of hydrochloric acid and trifluoroacetic acid [14] or hydrochloric acid and propionic acid [10] at temperatures > 150°C has been reported. In this work, 3 M mercaptoethanesulphonic acid at 160, 170 or 180°C was used for the amino acid analysis of pure proteins, free tryptophan and milk powder with a high sugar content. Different temperatures and different hydrolysis times were compared under standard conditions. The aims were to minimize side-reactions during the mercaptoethanesulphonic acid hydrolysis for in order to obtain an efficient recovery of the individual amino acids (especially tryptophan and methionine), and to establish a rational hydrolysis method for the amino acid analysis of food and feed samples. A further objective was to develop a hydrolysis method that permits the accurate and very rapid hydrolysis of proteins.

2. Experimental

2.1. Hydrolysis and processing of the hydrolysate

Reusable Pyrex hydrolysis tubes of 8 mm i.d. (Pierce, Rockford, IL) were used for the hydrolysis of proteins or for treating free tryptophan. The tubes can contain up to 8 ml of hydrolysing agent without contact with the PTFE sealing cup. In each instance, 1 ml of 3 M mercaptoethanesulphonic acid (MES-OH) (Pierce) was added to the tubes for the preparation of protein and peptide hydrolysate. Each tube had two PTFE sealing caps to achieve complete leak-free operation during heating at 160, 170 or 180°C.

A 1-mg amount of peptide, protein or free tryptophan or 20 mg of fat-free milk powder was weighed into Pyrex tubes previously washed with hydrochloric acid and deionized water. A 1-ml volume of 3 M MES-OH was added to each sample and nitrogen was bubbled for 5 min through the contents by a glass capillary. The Pyrex tubes were then immediately closed, and placed in the oven at 160°C for 15, 30, 45, 60 or 90 min at 170°C for 30, 45, 60 or 90 min or at 180°C for 15, 30, 45, 60 or 90 min. One sample of each material examined was hydrolysed at 110°C for 24 h, according to the method of Moore and Stein [15], with 6 M HCl, and one sample with 3 M MES-OH at 125°C for 24 h as suggested by Liu and Chang [6]. After hydrolysis, the tubes were cooled to room temperature and the pH of the samples was adjusted to 2.2 with 4 M NaOH. During neutralization, the temperature was held below 30°C with the help of a sodium chloride–ice mixture. After dilution with citrate buffer (pH 2.2), the hydrolysates were filtered and applied to an automatic amino acid analyser (based on ion-exchange chromatography).

2.2. Materials tested

The materials used for testing the hydrolysis methods were bovine ribonuclease, lysozyme, cytochrome *c*, free tryptophan and mare's milk powder. The protein content of the milk powder (22.7%) was determined using a Kjel-Foss 16200 rapid nitrogen analyser (Foss Electric, Hillerød, Denmark). The protein content was calculated from the percentage of nitrogen using a conversion factor of 6.38.

2.3. Amino acid analysis

The peptides and proteins were hydrolysed at different temperatures for different times, and

Table 1
Amino acid composition of bovine ribonuclease hydrolysed by MES-OH at 160°C for different times

Amino acid	Theoretical value	6 M HCl, 110°C for 24 h	3 M MES-OH, 125°C for 24 h	3 M MES-OH, 160°C for				
				15 min	30 min	45 min	60 min	90 min
Asp	12.54	12.40	13.03	15.16	14.32	13.35	13.46	12.83
Thr	7.48	7.19	7.63	8.15	8.11	7.65	6.64	7.46
Ser	9.90	9.73	10.13	9.76	9.81	9.99	10.16	9.91
Glu	11.11	12.18	12.30	12.73	11.84	11.38	11.32	11.10
Pro	2.89	2.96	5.00	4.43	4.53	4.70	5.03	5.22
Gly	1.41	1.64	1.49	2.37	2.22	2.06	1.70	1.70
Ala	6.71	6.92	6.92	7.81	7.84	7.27	7.29	7.08
Cys	6.08	5.15	–	4.25	4.02	3.89	2.22	1.42
Val	6.62	6.66	6.82	4.10	4.32	5.24	6.02	6.78
Met	3.75	3.26	3.86	3.87	3.85	3.93	3.95	3.86
Ile	2.47	2.52	2.54	0.84	1.71	2.15	2.42	2.56
Leu	1.65	1.75	1.68	1.37	1.54	1.66	1.70	1.68
Tyr	6.83	6.78	7.02	5.84	6.32	6.51	6.69	6.98
Phe	3.11	3.36	3.42	2.69	2.93	3.05	3.15	3.34
Lys	9.18	9.18	9.54	9.67	9.72	9.81	9.60	9.45
His	3.90	3.83	4.05	2.87	2.95	3.17	3.23	4.13
Arg	4.37	4.49	4.57	4.09	4.06	4.19	4.42	4.50

Data are expressed as g amino acid per 100 g protein. The values are the means of triplicate determinations. Hydrolysis conditions, 3 M MES-OH 125°C for 24 h and 160°C for different times using Pyrex No. 9826 tubes. The theoretical values for different amino acids were calculated from the protein sequence.

the amino acid contents of the hydrolysates were determined with an LKB 4101 automatic amino acid analyser (LKB Biochrom, UK) using a Merck amino acid calibration standard. Otherwise the analyses were carried out as described by Csapó et al. [16].

Table 2
Amino acid composition of bovine ribonuclease hydrolysed by MES-OH at 170 and 180°C for different times

Amino acid	170°C for				180°C for			
	30 min	45 min	60 min	90 min	15 min	30 min	45 min	60 min
Asp	13.44	13.40	12.68	13.04	13.73	13.28	12.93	12.96
Thr	7.69	7.70	7.55	7.68	7.77	7.50	7.52	7.53
Ser	10.03	10.04	9.84	7.94	10.16	9.94	9.94	9.81
Glu	11.27	11.21	10.88	11.32	11.70	11.46	11.61	11.81
Pro	4.73	5.99	6.14	6.55	5.93	5.94	6.08	6.35
Gly	2.06	1.70	1.71	1.76	2.11	1.70	1.64	1.67
Ala	7.27	7.13	6.99	7.08	7.42	6.99	6.88	6.93
Cys	3.87	2.20	1.44	0.91	2.40	1.99	0.84	0.15
Val	5.22	5.89	6.63	6.89	4.51	5.72	6.64	6.78
Met	3.93	3.92	3.80	3.66	4.04	3.70	3.73	3.61
Ile	2.16	2.41	2.52	2.62	1.35	2.21	2.51	2.58
Leu	1.64	1.66	1.64	1.71	1.64	1.62	1.67	1.68
Tyr	6.47	6.70	6.93	6.98	6.63	6.86	6.87	6.85
Phe	3.05	3.12	3.32	3.46	3.11	3.09	3.16	3.24
Lys	9.80	9.37	9.45	9.72	9.99	9.47	9.28	9.31
His	3.17	3.23	4.03	4.11	3.22	4.13	4.13	4.17
Arg	4.20	4.33	4.45	4.58	4.29	4.40	4.57	4.57

Data expressed as in Table 1.

3. Results and discussion

3.1. Amino acid composition of bovine ribonuclease

Bovine ribonuclease was hydrolysed with 6 M HCl at 110°C for 24 h, 3 M MES-OH at 125°C for 24 h and 3 M MES-OH at 160, 170 and 180°C for different times (15–90 min). The amino acid compositions of ribonuclease after the two 24-h hydrolyses and at elevated temperatures for shorter times are given in Tables 1 and 2. The results in Table 1 shows that the conventionally used 6 M HCl at 110°C and the MES-OH hydrolysis method at 125°C gave very similar results, except for the two very sensitive amino acids (threonine and methionine). For these amino acids, the 3 M MES-OH method gave higher results than the 6 M HCl method. Using the MES-OH hydrolysis method, it was found that the cystine content of the sample was reduced to cysteine and the free SH group of cysteine can react with the SH group of MES-OH, resulting in the formation of a small amount of 2-amino-3-(2-sulphoethylthio)propionic acid. A further finding was that, using MES-OH hydrolysis, the cysteine (formed from the cystine) appeared in the chromatogram in the place of proline and, particularly with proteins of high cystine content, this resulted in incorrect proline determinations.

As can be seen from the results in Table 1, 45 min was not a sufficient time to hydrolyse all of the peptide bonds, shorter hydrolysis times yielded incomplete recoveries of several amino acids (valine, leucine, isoleucine) and 60 min at 160°C was not sufficient for total cleavage of the peptide bonds adjacent to valine. The results of hydrolysis at 160°C for 60 min were very similar (except for valine) to those of conventionally used hydrolysis methods. The recovery of valine was close to 100% only with hydrolysis at 160°C for 90 min. At 170 and 180°C, 60 and 45 min, respectively, were needed for the total hydrolysis of peptide bonds. The higher temperatures did not yield decreased amounts of threonine and methionine.

In summary, it can be stated that the optimum hydrolysis times for all amino acids were 90, 60 and 45 min at 160, 170 and 180°C, respectively. With shorter times, the recoveries of valine and isoleucine were much lower, but those of threonine and methionine did not change.

3.2. Recovery of free tryptophan

In Table 3, the recoveries of free tryptophan after treatment with 3 M MES-OH at various temperatures for various times are shown. The tryptophan completely decomposed during acidic hydrolysis, but 93.2% of tryptophan remained unchanged after hydrolysis at 125°C for 24 h. This is very similar to the results obtained with hydrolysis at 160°C for 90 min, 170°C for 60 min and 180°C for 45 min. With increasing temperature and hydrolysis time, the decomposition of free tryptophan increased. However, at the highest temperature and longest hydrolysis time (180°C for 60 min), 91.2% of free tryptophan remain unchanged. Accordingly, the decomposition rate of tryptophan at lower temperatures and longer times is very similar to that at higher temperatures and shorter times.

Table 3
Recovery (%) of free tryptophan

Hydrolysis conditions	Hydrolysis time	Recovery of tryptophan (%) [a]
6 M HCl, 110°C	24 h	–
3 M MES-OH, 125°C	24 h	93.2
3 M MES-OH, 160°C	15 min	99.8
	30 min	98.3
	45 min	96.4
	60 min	95.2
	90 min	93.1
3 M MES-OH, 170°C	30 min	96.2
	45 min	95.3
	60 min	94.8
	90 min	92.1
3 M MES-OH, 180°C	15 min	94.3
	30 min	94.1
	45 min	93.1
	60 min	91.2

Theoretical value tryptophan content = 7.41 g per 100 g protein.
[a] Mean of three runs.

Table 4
Tryptophan contents of lysozyme using various hydrolysis methods

	160°C for			170°C for			180°C for		
	45 min	60 min	90 min	30 min	45 min	60 min	15 min	30 min	45 min
Tryptophan content found (g per 100 g protein) [a]	7.18	7.03	6.94	7.09	6.94	6.82	7.08	6.91	6.74
Tryptophan recovery (%) [a]	96.9	94.9	93.7	95.7	93.7	92.0	95.5	93.3	90.9

Theoretical value tryptophan content = 7.41 g per 100 g protein.
[a] Mean of three runs.

Table 5
Tryptophan contents of cytochrome *c* using various hydrolysis methods

Hydrolysis	160°C for			170°C for			180°C for		
	45 min	60 min	90 min	30 min	45 min	60 min	15 min	30 min	45 min
Tryptophan content found (g per 100 g protein) [a]	1.49	1.44	1.40	1.42	1.39	1.37	1.38	1.36	1.29
Tryptophan recovery (%) [a]	96.1	92.9	90.3	91.6	89.7	88.4	89.0	87.7	83.2

Theoretical value tryptophan content = 1.55 g per 100 g protein.
[a] Mean of three runs.

Table 6
Amino acid composition of milk powder hydrolysed by MES-OH at different temperatures for different times

Amino acid	6 M HCl, 110°C for 24 h	3 M MES-OH, 125°C for 24 h	MES-OH, 160°C for			MES-OH, 170°C for		MES-OH, 180°C for	
			30 min	45 min	60 min	45 min	60 min	30 min	45 min
Asp	10.4	9.2	9.5	9.4	9.2	9.3	9.7	9.6	9.7
Thr	4.3	4.3	4.6	4.4	4.3	4.4	4.3	4.3	4.2
Ser	6.2	6.4	6.6	6.4	6.4	6.4	6.2	6.3	6.2
Glu	21.2	20.1	21.0	20.6	20.5	21.1	20.8	20.5	20.8
Pro	7.7	8.1	8.0	8.0	8.0	8.2	8.1	8.1	8.2
Gly	1.9	1.7	1.8	1.7	1.7	1.8	1.8	1.9	1.8
Ala	3.2	3.3	3.3	3.2	3.3	3.2	3.2	3.3	3.3
Cys	0.7	–	0.4	0.1	–	0.2	–	–	–
Val	4.1	4.5	3.7	4.3	4.5	4.3	4.4	4.4	4.5
Met	1.8	2.2	2.3	2.3	2.2	2.2	2.1	2.2	2.1
Ile	3.8	4.6	3.7	4.2	4.5	4.3	4.5	4.4	4.6
Leu	9.7	9.7	9.3	9.5	9.6	9.5	9.6	9.6	9.4
Tyr	4.3	4.8	4.9	4.7	4.7	4.7	4.8	4.8	4.6
Phe	4.7	4.6	4.8	4.8	4.7	4.7	4.7	4.7	4.7
Lys	8.4	8.2	8.2	8.2	8.1	8.0	8.0	8.1	8.0
His	2.4	2.6	2.3	2.6	2.6	2.3	2.5	2.4	2.4
Arg	5.2	4.4	4.2	4.3	4.5	4.1	4.2	4.3	4.5
Trp	–	1.30	1.34	1.29	1.27	1.29	1.14	1.09	1.01
Recovery (%) [a]									
Trp	0	100	103.1	99.2	97.7	99.2	87.7	83.9	77.7
Met	81.0	100	104.5	104.5	100	100	95.4	100	95.4

Results expressed in Table 1.
[a] Hydrolysis at 125°C for 24 h with 3 M MES-OH = 100%.

3.3. Analysis of tryptophan-containing pure proteins

Lysozyme and cytochrome *c* were hydrolysed with 3 M MES-OH at various temperatures and for various times and the results are given in Tables 4 and 5. In the higher tryptophan-containing lysozyme, the recovery of tryptophan was higher than that found for cytochrome *c*. Similarly to the results for the recovery of free tryptophan, it can be stated that, with increasing temperature and hydrolysis time, the decomposition of tryptophan will be higher. It seems that the optimum hydrolysis conditions for tryptophan determination would be a shorter time and a lower temperature, such as 160°C for 45 min or 170°C for 30 min. The recovery of tryptophan from cytochrome *c* with hydrolysis at 180°C for 15 min was only 89.0%. When choosing the optimum hydrolysis time and temperature, one must consider that a lower temperature and a shorter hydrolysis time may not be sufficient to cleave the peptide bonds between hydrophobic amino acids.

3.4. Analysis of milk powder

The tryptophan contents of milk powder following various methods of hydrolysis are presented in Table 6. The 6 M HCl (110°C for 24 h) and the 3 M MES-OH (125°C for 24 h) hydrolysis methods gave very similar results for the amino acid composition of milk powder except for methionine and cystine. The methionine content of milk powder is higher after 3 M MES-OH hydrolysis owing to the reducing effect of MES-OH. The cystine content of milk powder cannot be determined by the MES-OH hydrolysis method because the cystine content of the milk protein will be reduced to cysteine and this amino acid appears in the chromatogram in the same position as proline. Fortunately, with milk powder the very low cystine content does not seriously affect the determination of proline. The reduction of cystine to cysteine is influenced by the time and temperature of hydrolysis. With hydrolysis at 160°C for 30 and 45 min and at 170°C for 45 min, part of the cystine can be determined after 3 M MES-OH hydrolysis. After longer times and/or higher temperatures of hydrolysis, most of the cystine will be converted into cysteine.

As can be seen from the results in Table 6, 30 or 45 min is not sufficient to hydrolyse the peptide bonds adjacent to valine and isoleucine. The results of hydrolysis at 160°C for 60 min are very similar to those with 6 M HCl at 110°C for 24 h and 3 M MES-OH at 125°C for 24 h. The recoveries of aliphatic amino acids were also very good. The methionine and threonine contents of milk protein decreased with increasing hydrolysis time and/or temperature. These decreases were small and the methionine content of milk protein was higher at the highest temperature and longest hydrolysis time than the values obtained by the 6 M HCl hydrolysis method. The recovery of methionine with hydrolysis at elevated temperature for a short time was higher than that obtained with hydrolysis at 125°C for 24 h.

The recovery of tryptophan was lower with a longer hydrolysis time and/or higher temperature than with hydrolysis at 125°C for 24 h. It seems that 180°C is too high for tryptophan determination. The optimum hydrolysis conditions for tryptophan determination are 160°C for 30, 45 or 60 min or 170°C for 45 min.

In conclusion, high-temperature hydrolysis with 3 M MES-OH was successfully applied to the amino acid analysis of pure proteins and milk powder with high carbohydrate content. The aim of these investigations was to introduce a rapid method that is suitable for the complete hydrolysis of protein and with a hydrolysate that is suitable for complete amino acid determination, including tryptophan. In the original method proposed by Penke et al. [8], the protein was hydrolysed with 3 M MES-OH at 110°C for 24 and 72 h, similarly to the conventionally used 6 M HCl hydrolysis. In this work, it was found that a higher temperature and shorter time yielded results that were very similar to those in the original methods. In some instances (such as tryptophan and methionine determination with hydrolysis at 160 or 170°C for 15–80 min), the results were superior to those obtained with the original method. The great disadvantage of this method is that MES-OH reduces cystine into cysteine, which appears in the chromatogram at the position of

proline and this, particularly with proteins with a high cystine content, may give false results for proline determination.

4. Acknowledgement

The authors greatly appreciate the editorial assistance of Dr. Truman G. Martin (Visiting Professor at PANNON Agricultural University, Kaposvár, and Professor of Animal Science at Purdue University).

5. References

[1] T.W. Goodwin and R.A. Morton, Biochem. J., 40 (1946) 628.
[2] W.L. Bencze and K. Schmid, Anal. Chem., 29 (1957) 1193.
[3] A. Dreze, Bull. Soc. Chim. Biol., 38 (1956) 243.
[4] F.J. Oelshlegel, J.R. Schroeder and M.A. Stahmann, Anal. Biochem., 34 (1970) 331.
[5] H. Matsubara and R.M. Sasaki, Biochim. Biophys. Res. Commun., 35 (1969) 157.
[6] T.Y. Liu and Y.H. Chang, J. Biol. Chem., 246 (1971) 2842.
[7] R.J. Simpson, M.R. Neuberger and T.Y. Liu, J. Biol. Chem., 251 (1976) 1936.
[8] B. Penke, R. Ferenczy and K. Kovács, Anal Biochem., 60 (1974) 45.
[9] J. Csapó, B. Penke, I. Tóth-Pósfai and Zs. Csapó-Kiss, Acta Aliment., 15 (1986) 227.
[10] S.H. Chiou and K.T. Wang, J. Chromatogr., 448 (1988) 404.
[11] S.T. Chen, S.H. Wu and K.T. Wang, Int. J. Pept. Protein Res., 33 (1989) 73.
[12] S.T. Chen, S.H. Chiou, Y.H. Chu, and K.T. Wang, Int. J. Pept. Protein Res., 30 (1987) 572.
[13] M.V. Pickering and P. Newton, BioSeparations, 3 (1992) 10.
[14] A. Tsugita, and J.J. Scheffler, Eur. J. Biochem., 124 (1982) 585.
[15] S. Moore and W.H. Stein, J. Biol. Chem., 211 (1954) 893.
[16] J. Csapó, Zs. Csapó-Kiss and I. Tóth-Pósfai, Acta Aliment., 15 (1986) 3.

ELSEVIER

Analytica Chimica Acta 289 (1993) 113–120

ANALYTICA CHIMICA ACTA

Imaging and space-resolved spectroscopy in the Xe–Cl laser ablation of noble metals with charge-coupled device detection

J.J. Laserna *, N. Calvo, L.M. Cabalín

Department of Analytical Chemistry, Faculty of Sciences, University of Málaga, E-29071 Málaga, Spain

(Received 27th July 1993; revised manuscript received 10th November 1993)

Abstract

Spatially resolved emission spectra of laser-produced plasmas from metal samples are reported. A pulsed XeCl excimer laser delivering fluences in the range 2.3–4.7 J cm^{-2} at 308 nm was used. Line emission was detected using a charge-coupled device. The effect of laser parameters on the plasma morphology was investigated for silver, copper and mercury targets. The emission spectrum of a 18-carats gold sample is discussed.

Key words: Lasers; Metals; Noble metals; Plasmas; Space-resolved spectroscopy

1. Introduction

Laser ablation is receiving increased attention as an alternative to conventional plasma sources (i.e., inductively coupled plasma, direct-current plasma, glow discharge plasma, etc.) for the spectrochemical analysis of solid materials. This interest derives from the advantages of the technique, which include the ability to sample a diverse range of substances such as metals [12], biological materials [3], ceramics and minerals [4–7] and non-conducting materials [8–10], the capability to achieve spatially resolved or bulk analyses [11], and a high sample throughput as little or no sample preparation is usually required. These advantages are tempered by the difficulties of calibration, which in turn depend upon the use of standard materials and matrix effects.

A description of laser/solid interactions and compressive reviews of analytical spectroscopy techniques have been published by several authors [12–15]. The interaction between a laser beam and a metal is a complicated process, and depends on many characteristics of both the laser and the solid metal. Numerous factors affect ablation, including the laser pulse properties (pulse width, laser frequency and repetition rate and fluence deposited on the metal) and the metal characteristics (heat capacity, heat of vaporization, vaporization temperature and reflectivity). In a plasma, matter breaks apart into atoms, ions, and electrons, at temperatures above 10000 K. Visible flash and an audible popping sound due to the acoustical shock wave generated by the sudden, high-velocity expansion of matter outward from the plasma volume is produced.

* Corresponding author.

0003-2670/94/$07.00 © 1994 Elsevier Science B.V. All rights reserved
SSDI 0003-2670(93)E0637-M

In this work spatially resolved emission spectra of laser-produced plasmas from silver, copper and mercury are reported. The study was performed using a pulsed XeCl excimer laser at 308 nm. The performance of the CCD-based detection system is discussed. The shot-to-shot variability of the emission intensity was between 3.1 and 5.5% (relative standard deviation). The dependence of plasma size and emission intensity with incidence angle of the laser on the substrate was established.

2. Experimental

A pulsed XeCl-excimer laser (Lambda Physik, Model Lextra 200, wavelength 308 nm, pulse duration 28 ns) was used to irradiate metal samples. Laser fluence in the range of 2.3–4.7 J cm^{-2} was employed. The laser beam was focused onto the sample surface with a plano-convex quartz lens with a focal length of 100 mm and $f = 4$. The laser-ablated plasma emission was collected onto the entrance slit of a triple indexable grating spectrograph (Acton Research, SpectraPro 275, Czerny-Turner; $f = 3.8$) fitted with gratings of 300, 600 and 1800 grooves/mm. Collection was performed with a biconvex glass lens with focal length of 25.4 mm and $f = 1$. The reciprocal linear dispersion of the spectrometer is 12 nm/mm with the 300 grooves/mm grating giving a spectral coverage of 116.4 nm for the detector used. The spectrometer entrance slit was 15 mm high by 10 μm wide. The metal sample was placed approximately 12.5 cm from the collection lens, with the distance from the entrance slit to the lens being 5.5 cm. Thus the optical magnification was ca. 0.5. A solid-state two-dimensional charge-coupled device (CCD) (EG&G PAR, Thomson CSF, THX-31159A) was used to detect the plasma image. The CCD consists of 512 × 512 elements each being 19 μm × 19 μm. The active area is 9.7 mm × 9.7 mm. This CCD system has a quantum efficiency of 32% at 550 nm. The CCD was cooled to −60°C by a Peltier system. When cooled to −60°C, this detector exhibits a dark current of 10 photoelectrons/pixel/second and a readout noise of 4–5 electrons per scan. Calibration of the detector system was conducted with a mercury pen lamp. Operation of the detec-

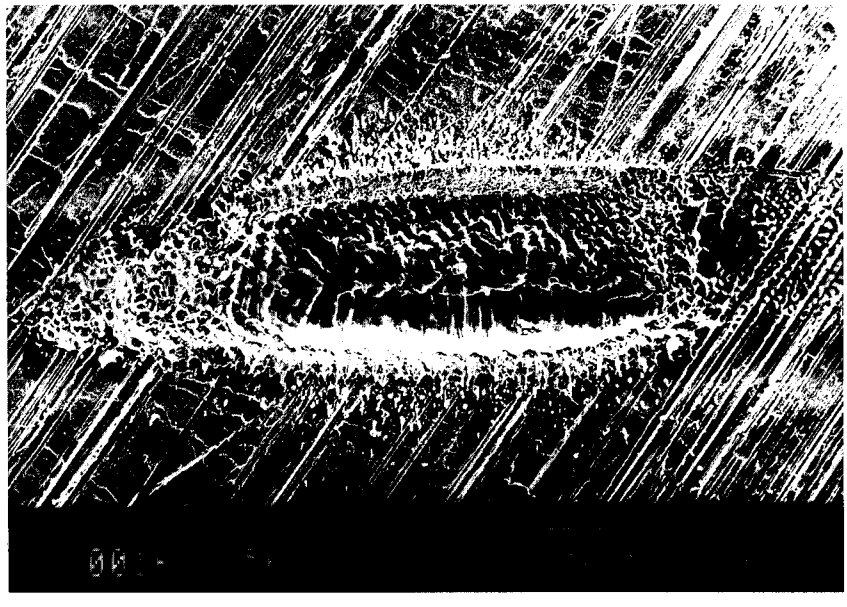

Fig. 1. SEM photograph showing an ablation hole generated on a silver foil by 20 laser pulses of 2.35 J cm^{-2}. The laser beam area was 0.004 cm^2.

tor is controlled by a personal computer with OMA Spec 4000 software. The spectrometer is connected to the controlling PC by a conventional IEEE-488 general-purpose interface bus (GPIB). The metal samples used in this study were copper and silver foils and mercury, purchased from Alfa. The purity of metals was > 99%. Ag and Cu were cleaned with methanol (Merck), before irradiation and mounted on a *xyz* translational stage to allow fine positioning of the sample. Hg was cleaned with nitric acid (Merck), and demineralized water (Millipore) and placed inside a square glass cuvette. Except otherwise noted, the image of the plasma was recorded for a single laser shot and acquisition time of 2 s.

3. Results and discussion

Laser ablation is a thermal process by which material is removed from the target through a phase change that may include melting and vaporization. The predominant process will depend on the laser fluence (energy per unit area) deposited onto the surface. Fig. 1 shows an electron micrograph of the crater produced by 20 XeCl-laser shots in a silver foil target. The laser fluence was 2.35 J cm^{-2}, equivalent to an irradiance of 8.4×10^8 W cm^{-2}. No attempts were made to improve the spatial distribution of the energy. As shown, a certain amount of molten material surrounds the crater, although most of the metal has been ejected as a vapor.

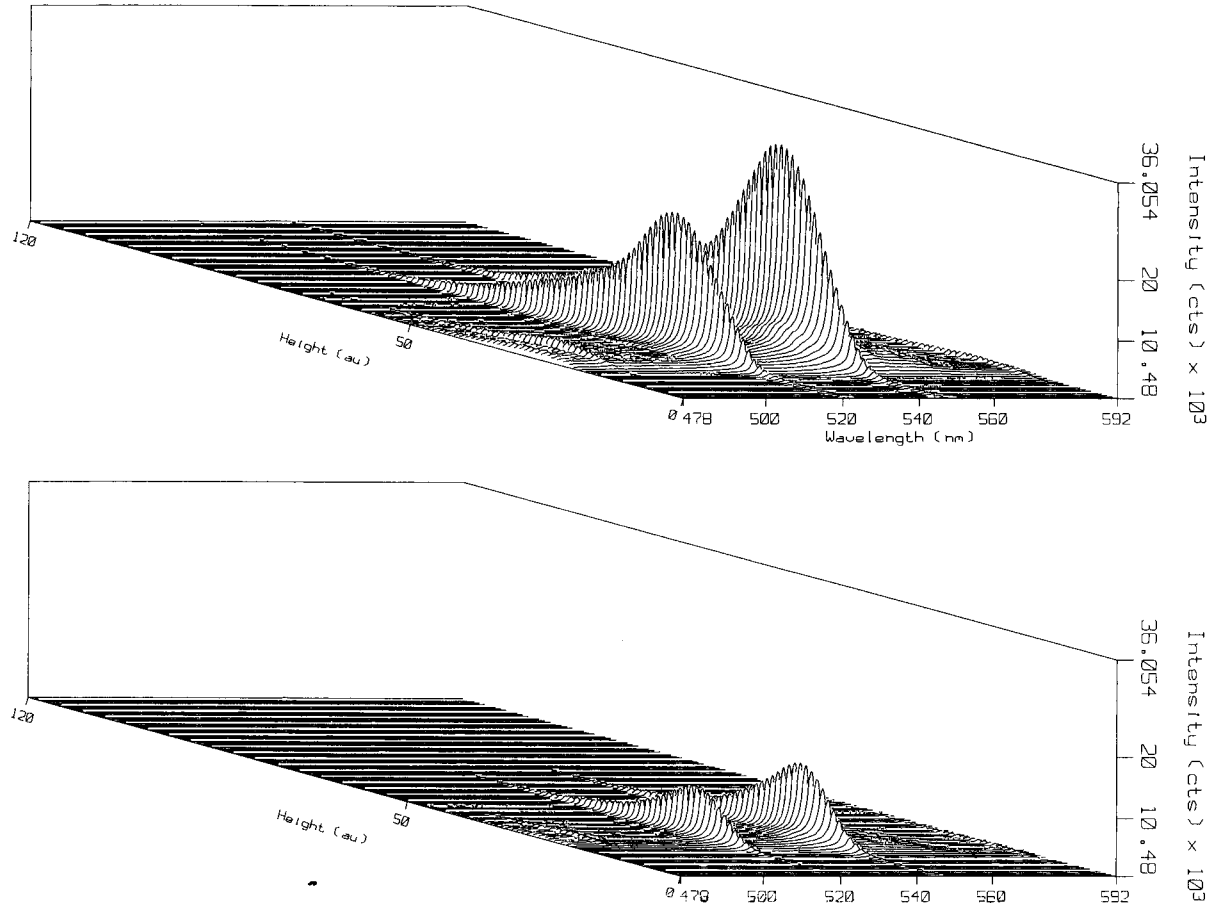

Fig. 2. Space-resolved spectra of laser-ablated plasma with silver at 760 Torr in air at (top) 4.76 J cm^{-2}, (bottom) 2.35 J cm^{-2}.

3.1. Instrument performance

Charge-coupled devices are ideal detectors for the spectroscopy of laser-produced plasmas because of their imaging capability. Fig. 2 shows spectrograms of plasmas generated from silver at laser fluences of 4.76 J cm^{-2} (top) and 2.35 J cm^{-2} (bottom). The target was at room temperature in air at atmospheric pressure. The height dimension in the figure corresponds to the axial distance taken from the metal surface. Each unit corresponds to a row of pixels, each 19 μm high. Since the optical magnification in this experiments was ca. 0.5, each unit represents about 40 μm of actual plasma size. The silver lines at 520.9 nm and 546.5 nm can be easily identified. The intensity reaches a maximum at 0.8 mm above the surface for a fluence of 4.76 J cm^{-2} and at 0.6 mm for 2.35 J cm^{-2}. After this maximum, the intensity drops monotonically in both cases. It should be noted that the total acquisition time needed for each of these images is only 2 s.

A further advantage of CCDs for plasma imaging is their extremely low dark current. In the system used here, the synchronization between laser firing and data acquisition was made manually. The CCD acquisition time was adjusted to the desired value, the acquisition sequence was started and a number of laser shots previously selected was integrated in the detector. The maximum number of plasma images integrated depended on the laser repetition rate. A study of the peak intensity of silver plasmas at 546.5 nm vs. the acquisition time in the detector was performed between 0.5 s and 8 s, by averaging 12 independent signals generated with a single laser shot at 2.35 J cm^{-2}. The relative standard deviation for the intensities was 3.1–5.5%. This precision level is compatible with most practical analytical situations. It should be noted that these values represent shot-to-shot variability, and could be improved by integrating a number of laser shots prior to read out of the generated charge. The background signal was mostly due to read out noise. Because of the extremely low dark current of this detector when cooled at −60°C, both the averaged silver signal and the background signal were virtually independent of the total acquisition time in the range studied. This is of interest since it allows the integration of a

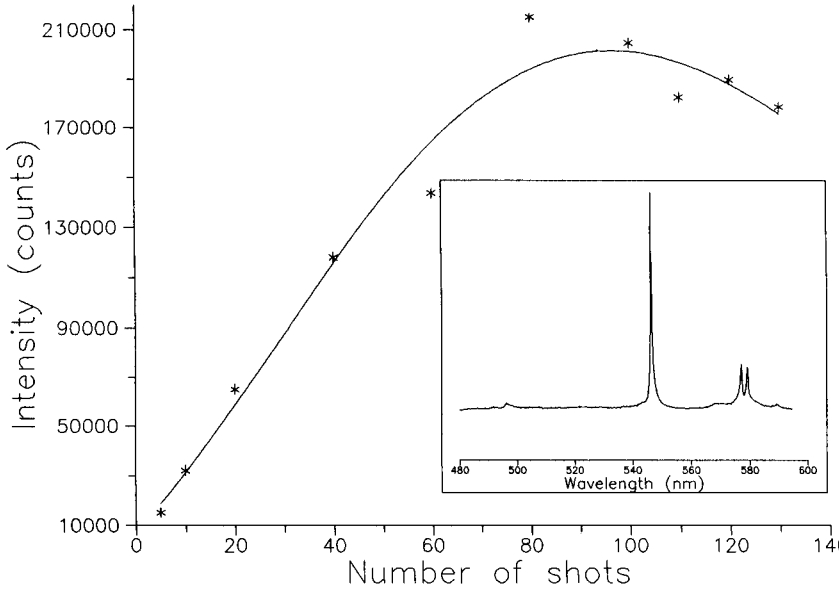

Fig. 3. Intensity of the laser plasma generated on mercury vs. the number of laser shots. Fluence was 2.35 J cm^{-2}, laser repetition rate 30 Hz. Inset: mercury emission spectrum in the range 480–600 nm taken 1 mm above the mercury surface.

large number of samples (plasmas) without detector saturation due to build up of background signal. Thus the full dynamic range of the detector (18 bit) is available for signal integration.

3.2. Plasma morphology and laser parameters

The size and spectral intensity of the laser-ablated plasma depends on a number of laser parameters. Fig. 3 shows the intensity of the laser plasma generated on mercury vs. the number of laser shots. The inset represents the mercury emission spectrum in the range 480–600 nm taken 1 mm above the mercury surface. The intensity measurements were performed at 546.1 nm. As expected, the intensity linearly increases with the number of plasmas integrated. Above 80 laser shots the curve saturates and the intensity tends to decrease as the number of laser shots increases. This effect can be due to an increase in the reflectivity of the cuvette walls as a result of deposition of the ablated mercury.

The size of the plasma and its emission intensity depend on the angle of incidence (α) of the laser on the target. Fig. 4 shows this effect for silver. The inset shows the geometry of the experiment. As shown the maximum intensity is obtained for 40° incidence. It should be noted that the plasma height remains roughly uniform at 4 mm from normal incidence to 85° incidence. The intensity, however, drops dramatically for incidence above 40°. Although it is not obvious the reason for this angular dependence, we consider an optic theory to explain it. Propagation of a plane-polarized electromagnetic wave across an interface with a transparent dielectric medium, induces a dipole in the material, which oscillates with the same frequency of the incident field. Considering a wave that is incident on a surface and polarized so that its electric-field vector lies in the plane of incidence, there will be an angle of incidence called Brewster's angle, for which the refracted and reflected waves propagate at right angle to one another. At Brewster's angle, there is no wave reflected, and all the incident intensity is transmitted to the dielectric.

The reflectance of metals varies with incidence, much as that of dielectrics. Light polarized with its electric-field vector parallel to the plane of incidence passes through a principal angle that

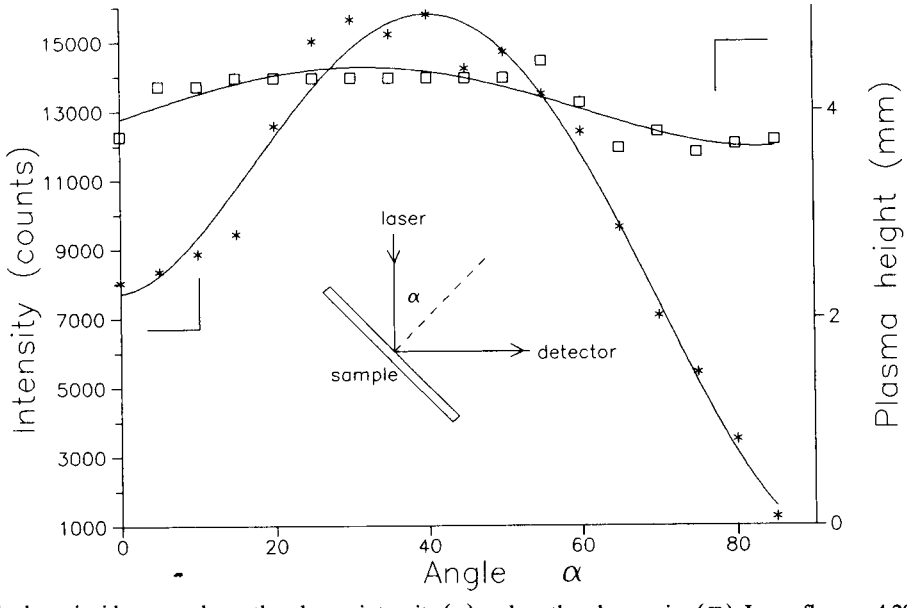

Fig. 4. Effect of the laser incidence angle on the plasma intensity (*) and on the plasma size (□). Laser fluence 4.29 J cm^{-2}. Single laser shot. The inset represents the geometry of the experiment.

is analogous to Brewster's angle. At the principal angle, the coupling of the incident wave with the metal is maximum, with virtually no reflected beam. Thus, the amount of ablated material would be maximum at this incidence, in this case 45°, resulting in maximum emission intensity.

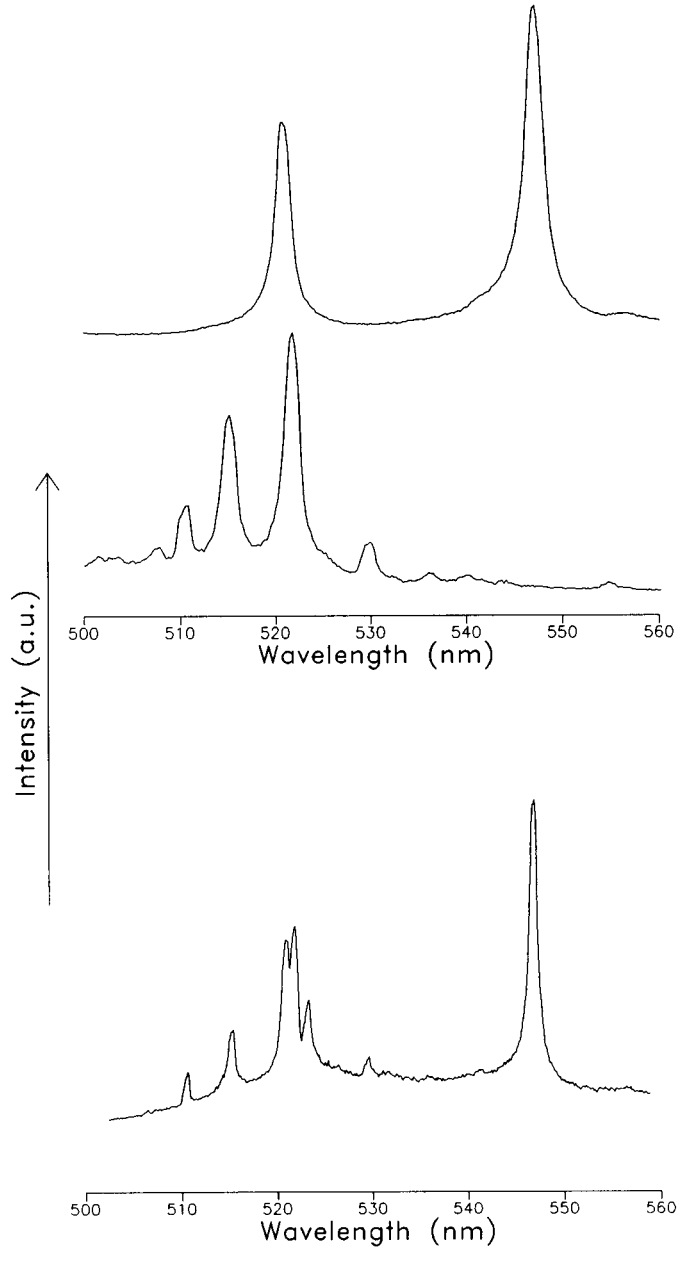

Fig. 5. Spectrum of net silver (top), spectrum of net copper (middle), and spectrum of a 18-carats gold sample used in jewelry works (bottom). Laser fluence was 2.35 J cm^{-2} and incidence was 0°.

The maximum amount of material, m (g), that can be vaporized by a single laser pulse of energy E (J) is given by [16]:

$$m = \frac{E}{C(T_b - T_0) + H}$$

where C is the heat capacity (J g^{-1} K^{-1}), and H is the heat of vaporization (J g^{-1}). T_b (K) and T_0 (K) are the vaporization and starting temperature of the target, respectively. Thus for a single laser shot of 10 mJ, the calculated maximum amount of mercury vaporized is 28 μg. The respective amounts for silver and copper are 3 and 1.5 μg. The actual amount of vaporized metal must be significantly smaller than the calculated amount because of the reflexion of the laser beam on the metal surface and since the plasma formed in front of the sample absorbs part of the laser energy within the duration of the pulse. The ejected amount of silver estimated from Fig. 1 is about 0.3 μg per shot. The small amount of vaporized metal is however able to produce line emission intense enough for the characterization of the target constituents.

A spectrum from an 18-carats gold sample used in jewelry works is shown in Fig. 5 (bottom). For comparison purposes the spectra of net silver and copper are also shown (top spectra). These spectra were obtained with the 300 grooves mm^{-1} grating of the spectrograph, and thus 116 nm can be simultaneously detected with the current detector. Unfortunately, the resolution provided by this grating is insufficient for resolving the silver peak at 520.9 nm from the copper peak at 521.8 nm. Thus for the gold sample the 600 grooves mm^{-1} grating was used. The emission spectra of the laser produced plasma clearly identify silver and copper in the 18-carats gold. The identification of Cu and Ag is simplified in this case since gold, the major component in the sample, produces no intense emission in the spectral region of 500–560 nm. The presence of copper on the gold sample is indicated by the three peaks at 510.5, 515.3 and 521.8 nm whose positions can be easily compared with the spectrum of pure copper in top of the figure. The silver peaks at 520.9 and 546.5 nm can be also identified. The line at 523.2 nm in the gold sample must be due to a weak emission of gold. It should be noted that a single laser shot was used for the gold spectrum, and thus an insignificant damage to the sample was produced.

4. Conclusions

Charge-coupled devices have several advantages over more conventional detectors for the spectroscopy of laser produced plasmas. Spatially resolved spectroscopy along the axial direction of the plasma can be performed without realignment of the sample. Their extremely low dark current when cooled results in background signals virtually independent of the total acquisition time. Single-shot elemental analysis with acceptable precision can be conducted, thus allowing sample inspection with essentially no physical damage. At present, read out times of standard CCD detectors are larger than those required for time resolved spectroscopy of the plasmas. Configurations using microchannel plate technology allowing gating in the ns range could be combined with charge-coupled devices to construct an extremely powerful instrument for the spectroscopy of laser-produced plasmas.

5. References

[1] I.S. Borthwick, K.W.D. Ledingham and R.P. Singhal, Spectrochim. Acta, 47B (1992) 1259.
[2] A. Vertes, R.W. Dreyfus and D.E. Platt, Research Report, IBM Research Division, 1992.
[3] D.M. Schieltz, C.W. Chou, C.W. Luo, R.M. Thomas and P. Williams, Rapid Commun. Mass Spectrom., 6 (1992) 631.
[4] N.J.G. Pearce, W.T. Perkins and R. Fuge, J. Anal. Atom. Spectrom., 7 (1992) 595.
[5] S. Chenery, A. Hunt and M. Thompson, J. Anal. Atom. Spectrom., 7 (1992) 647.
[6] N. Imai, Anal. Chim. Acta, 269 (1992) 263.
[7] P.C. Smalley, C.N. Maile, M.L. Coleman and J.E. Rouse, Chem. Geol., 101 (1992) 43.
[8] J. Kleinschmidt and J.U. Walther, Phys. Stat. Sol., 131 (1992) 167.
[9] M. Späth and M. Stuke, Appl. Surf. Sci., 54 (1992) 237.
[10] I. Steffan and G. Vujicic, Spectrochim. Acta, 47B (1992) 61.

[11] W. Marine, J.M. Scotto, D'Aniello and J. Marfaing. Appl. Surf. Sci., 46 (1990) 239.
[12] K. Dittrich and R. Wennrich, Prog. Anal. Atom. Spectrosc., 7 (1984) 179.
[13] R.J. Radziemski and D.A. Cremers, in L.J. Radziemski and D.A. Cremers (Eds.), Laser-Induced Plasmas and Applications, Marcel Dekker, New York, 1989, p. 295.
[14] E.H. Piepmeier, in E.H. Piepmeier (Ed.), Analytical Applications of Lasers, Wiley, New York, 1986, p. 627.
[15] K. Laqua, in N. Omenetto (Ed.), Analytical Laser Spectroscopy, Wiley, New York, 1979, p. 47.
[16] D.A. Cremers and L.J. Radziemski, in L.J. Radziemski, R.W. Solarz and J.A. Paisner (Eds.), Laser Spectroscopy and its Applications, Dekker, New York, 1987, p. 361.

ELSEVIER

Analytica Chimica Acta 289 (1994) 121–124

ANALYTICA CHIMICA ACTA

Abolition of the equivalent. Rule of equal amount of substance

Mengyue Zhao *, Lingcui Lu

Department of Chemical Engineering, Zhengzhou Institute of Technology, Zhengzhou, Henan 450002, China

(Received 29th September 1993)

Abstract

According to provisions of IUPAC, SI and ISO the concept of equivalence should be abandoned, due to its shortcomings. The equivalent weight of a substance cannot be uniquely defined. The equivalence law applies only to acid–base and oxidation–reduction titrations, and does not apply to complexometric and precipitation titrations. This paper presents a rule of equal amount of substance to solve the problems of the equivalence law.

Key words: Equivalence, concept of

1. Introduction

For a long time, equivalence and the equivalence law ($N_1V_1 = N_2V_2$, where N_i denotes the "normality" or equivalent concentration and V_i the volume of component i) have been the foundation of titrimetric analysis in analytical chemistry. However, equivalence has many shortcomings. First, equivalence is not coincident with the SI unit. Secondly, the equivalent weight of a substance does not have a unique definition. Thirdly, it is quite hard to calculate the equivalence in some situations. In addition, the equivalence law applies to acid–base and oxidation–reduction titrations but not to complexometric and precipitation titrations. Therefore, chemical quantities and units recommended by IUPAC [1–5] or ISO 31/8 (International Standards) [6] do not contain equivalence. In order to fulfil SI and international standards, equivalence must be abolished. Here, a rule of equal amount of substance is presented which will be helpful to standardize analytical calculations.

2. Superiority of amount-of-substance concentration

The concentration of substance refers to the amount of the substance per unit of volume in a solution. Its SI unit is mol m^{-3}, while the commonly used unit is mol dm^{-3}. The SI system stipulates that the elementary entity must be indicated by use of its mole. It is very flexible to choose an elementary entity which may be real or imaginary or a special combination of some particles if necessary. This, therefore, makes the application of concentration flexible and has a precise meaning without any misunderstanding.

For example, in order to express the concentration of MnO_4^-, we can choose $2MnO_4^-$, MnO_4^-,

* Corresponding author.

0003-2670/94/$07.00 © 1994 Elsevier Science B.V. All rights reserved
SSDI 0003-2670(93)E0665-T

$(1/3)MnO_4^-$ or $(1/5)MnO_4^-$ as an elementary entity. Its concentration can be expressed as $c(MnO_4^-)$, $c(2MnO_4^-)$, $c[(1/3)MnO_4^-]$ or $c[(1/5)MnO_4^-]$. If $c(MnO_4^-) = 1$ mol dm^{-3}, then for the solution $c(2MnO_4^-) = 0.5$ mol dm^{-3}, $c[(1/3)MnO_4^-] = 3$ mol dm^{-3} and $c[(1/5)MnO_4^-] = 5$ mol dm^{-3}.

From this example, we can see that no matter how the concentration is expressed, its meaning is accurate and not confusing. The relationship is clear. Generally, for the same substance B, if its elementary entities are B and bB (b, either integer or fraction), the relationship between concentrations is as follows:

$$c(b\mathrm{B}) = (1/b)c(\mathrm{B}) \quad (1)$$

It is suggested that the customary c(B) (corresponding to molar concentration) should used on the label of a reagent bottle. In calculation, if necessary, c(B) may be converted into $c(b$B) according to Eq. (1). For example, if $c(MnO_4^-)$ is known while $c[(1/5)MnO_4^-]$ is needed, Eq. 1 gives

$$c[(1/5)MnO_4^-] = 5c(MnO_4^-)$$

Equivalent concentration may also be expressed in amount-of-substance concentration. For example, $c[(1/5)MnO_4^-]$ corresponds to the "equivalent concentration" of MnO_4^- in acidic medium as an oxidizing agent. Since "equivalent concentration" could be replaced by a more explicit specification $c[(1/5)MnO_4^-]$, it is not necessary to retain the term equivalent concentration.

3. Rule of equal amount of substance

Some chemists believe that equivalent concentration should not be abandoned because the equivalence rule and the formula $N_1V_1 = N_2V_2$ standardize calculations in acid–base and oxidation–reduction titrations. The application of amount-of-substance concentration is as convenient as above. Furthermore, the amount-of-substance concentration can enlarge the standardization process to the whole of titrimetry.

For any titration method, a calculation can be made in accordance with the following procedure.

If a test is made by means of the following reactions:

$$a\mathrm{A} + b\mathrm{B} \rightarrow c\mathrm{C} + d\mathrm{D} \quad (2)$$

$$c\mathrm{C} + t\mathrm{T} \rightarrow g\mathrm{G} + h\mathrm{H} \quad (3)$$

the following reaction is obtained by combing reactions 2 and 3:

$$a\mathrm{A} + b\mathrm{B} + t\mathrm{T} \rightarrow d\mathrm{D} + g\mathrm{G} + h\mathrm{H} \quad (4)$$

where A is the test substance, B is another reactant and T is the titrant.

If these special combinations aA, bB, tT, dD and hH are regarded as elementary entities, then in reaction 4, 1 mol aA, 1 mol tT and 1 mol bB will produce 1 mol dD, 1 mol gG and 1 mol hH, In other words, the elementary entities have been chosen in such a way that each reactant consumed is equal to every product in the amount of substance at any time in the reaction. This is the rule of equal amount of substance in reactions.

Suppose $c(t\mathrm{T})$ is the concentration of a standard solution and the consumed volume of standard solution is V(T), the amount of substance of the standard substance which participates the reaction is:

$$n(t\mathrm{T}) = c(t\mathrm{T})V(\mathrm{T})$$

The amount of substance of the test substance in solution is:

$$n(a\mathrm{A}) = c(a\mathrm{A})V(\mathrm{A})$$

According to the rule of equal amount of substance:

$$c(a\mathrm{A})V(\mathrm{A}) = c(t\mathrm{T})V(\mathrm{T}) \quad (5)$$

Suppose the concentration of the test substance is c_1 and its is volume V_1, the concentration of the standard solution is c_2 and the consumed volume of standard solution is V_2. Eq. 5 changes to

$$c_1V_1 = c_2V_2 \quad (6)$$

Eqs. 5 and 6 are the expressions of the rule of equal amount of substance, so the equivalence rule $N_1V_1 = N_2V_2$ can be replaced.

For the convenient use of the literature data which were obtained by the application of equiva-

lence, the elementary entity of standard substance should be chosen according to the following principle so that the molar mass of these elementary entities is equal to the gram equivalence in the numerical value.

For acid–base titrations, the elementary entity is the particle or specified combination of particles which gains or loses a proton in the titration reaction. For example, NaOH or HCl is chosen as the elementary entity.

For oxidation–reduction titrations, the elementary entity is the particle or specified combination of particles which gains or loses an electron in the titration reaction. For example: $(1/5)KMnO_4$ is chosen as the elementary entity in a permanganate titration; $(1/6)K_2Cr_2O_7$ is chosen as the elementary entity in a dichromate titration; $Na_2S_2O_3$ is chosen as the elementary entity in an iodimetric titration.

For a complexiметric titration with EDTA, (where the titration reaction is between equal numbers of molecules), Na_2H_2Y, which expresses EDTA, is chosen as the elementary entity. For argentimetric (precipitation) titration, $AgNO_3$ is chosen as the elementary entity.

4. Application

The use of the rule brings a unified procedure for calculation in titrimetry and avoids the shortcomings of equivalence.

4.1. Example 1. Iodimetric titration for determination of lead

The determination reactions are as follows:

$$Pb^{2+} + CrO_4^{2-} \rightleftharpoons PbCrO_4(s)$$

$$2PbCrO_4(s) + 2H^+ \rightleftharpoons Cr_2O_7^{2-} + 2Pb^{2+} + H_2O$$

$$Cr_2O_7^{2-} + 6I^- + 14H^+ \rightleftharpoons 3I_2 + 2Cr^{3+} + 7H_2O$$

$$I_2 + 2S_2O_3^{2-} \rightleftharpoons 2I^- + S_4O_6^{2-}$$

From these equations, each original Pb^{2+} leads to the eventual consumption of $3S_2O_3^{2-}$, so if $S_2O_3^{2-}$ is chosen as the elementary entity of thiosulphate, $(1/3)Pb^{2+}$ should be chosen as the elementary entity of lead. According to the rule of equal amount of substance, we can get

$$n(1/3Pb^{2+}) = n(S_2O_3^{2-})$$

or

$$c(1/3Pb^{2+})V(1/3Pb^{2+}) = c(S_2O_3^{2-})V(S_2O_3^{2-})$$

which avoids calculating the abstruse equivalent of Pb^{2+} because Pb^{2+} does not gain or lose any electrons in the above reactions.

For a disproportionation reaction, it is more difficult to calculate the equivalent. However, the use of the new rule can make the calculation as simple as that in a reaction without disproporationation, as in Example 2.

4.2. Example 2. Determination of the mass fraction of MnO_2 in a manganite ore

Sample mass is m. MnO_4^{2-} is obtained after alkaline fusion of MnO_2, which disproportionates to MnO_2 and MnO_4^- on acidification. The MnO_2 is filtered off and the MnO_4^- titrated with Fe^{2+}. The reactions are as follows:

$$Na_2O_2 + MnO_2 \rightleftharpoons MnO_4^{2-} + 2Na^+$$

$$4H^+ + 3MnO_4^{2-} \rightleftharpoons 2MnO_4^- + MnO_2 + 2H_2O$$

$$MnO_4^- + 5Fe^{2+} + 8H^+ \rightleftharpoons 5Fe^{3+} + Mn^{2+} + 4H_2O$$

Therefore, if Fe^{2+} is chosen as an elementary entity, $(3/10)MnO_2$ should be chosen as an elementary entity. According to the rule of equal amount of substance,

$$n(Fe^{2+}) = n(3/10\ MnO_2)$$

$$n(3/10\ MnO_2) = c(Fe^{2+})V(Fe^{2+})$$

The mass fraction of MnO_2 is

$$W(MnO_2) = n(3/10\ MnO_2)M(3/10\ MnO_2)/m = c(Fe^{2+})V(Fe^{2+})M(3/10\ MnO_2)/m$$

The concept of equivalence, therefore should be abandoned and the equivalence law should be replaced by the rule of equal amount of substance. This not only avoids many difficulties in calculating equivalent concentration, but also standardizes the concept of concentration across

the whole of titrimetry. In addition, the method simplifies the teaching process for calculation of concentrations by titrimetry.

5. References

[1] IUPAC Manual of Symbols and Terminology for Physicochemical Quantities and Units, Pure Appl. Chem., 51 (1979) 1–36.

[2] H.M. Irving, H. Freiser and T.S. West, Compendium of Analytical Nomenclature, Definitive Rule 1977, Pergamon Press, Oxford, 1978.

[3] H. Freiser and G.H. Nancollas, Compendium of Analytical Nomenclature, Definitive Rules 1987, Blackwell, Oxford, 1988.

[4] IUPAC, Analytical Chemistry Division, Pure Appl. Chem., 50 (1978), 325–338.

[5] I. Mills, T. Cvitas, K. Homann and K. Kuchitsu, IUPAC Quantities, Units and Symbols in Physical Chemistry, Blackwell, Oxford, 1988 and 1993.

[6] Internal Organization of Standarddization (ISO) 31/8, Quantities and Units of Physical Chemistry and Molecular Physics, Jilang Press, China, 1993.

HPLC '94

18th International Symposium on Column Liquid Chromatography

May 8-13, 1994

Minneapolis, Minnesota, USA

[Chairmen: Professor Peter W. Carr and Professor Larry D. Bowers]

We would like to issue you a personal invitation to attend the largest meeting and exhibit dedicated to HPLC '94, to be held May 8-13, 1994, at the Minneapolis Convention Center in Minneapolis, Minnesota, USA. Several new features have been added to the meeting such as short courses, vendor seminars, and panel discussions. We hope you will find these new opportunities interesting and useful. ***For further information, please contact Mrs. Janet Cunningham, HPLC '94 Symposium and Exhibit Manager, 10120 Kelly Road--BOX 279, Walkersville, Maryland 21793 USA (phone 301-898-3772; fax 301-898-5596).***

— PRELIMINARY PROGRAM —

SUNDAY — MAY 8, 1994

- Registration & Welcome Reception

MONDAY — MAY 9, 1994

- **Plenary Session I** *(W.S. Hancock, R.F. Browner, E.L. Cussler)*
- **Exposition Opens**
- **Poster Sessions on Clinical, Forensic, & Biological Analysis; HPLC/MS and CE/MS**
- **Approaches to HPLC/MS and CE/MS** *(J. Henion, L.D. Bowers, K.L. Busch, T.W. Hutchens)*
- **Bioanalysis with HPLC and Capillary Electrophoresis – I** *(L.S. Ramos, H.C. Greenblatt, J. Haginaka, D. Westerlund)*
- **Practical Characterization of Stationary Phase Materials** *(T.H. Walter, J.R. Jezorek, B.A. Olsen, J.J. Kirkland)*
- **Panel Discussion on Characterization of Stationary Phase Materials — How Helpful is it in Predicting Analytical Success?**

TUESDAY — MAY 10, 1994

- **HPLC/MS and CE/MS** *(M.D. Beeson, F. Banks, Jr., S. W. Preece, A.J. Tomlinson, P. Thibault)*
- **Enantiomeric Separations** *(W.H. Pirkle, W.L. Hinze, T. Beesley, T.J. Ward, D.W. Armstrong)*
- **Advances in Detection Systems** *(M. Spraul, M.B. Smalley, L.J. Nagels, C.A. Monnig, D.C. Johnson)*
- **Exposition**
- **Poster Sessions on Enantiomeric Separations; Optimization, Chemometrics, & Methods Development; Planar Chromatography, Supercritical Chromatography, & Selected Topics**
- **Selected Topics** *(E. Grushka, H.A.H. Billiet, R. Freitag, S.M. Cramer)*
- **Molecular Recognition in Peptide / Protein Separations** *(M.T.W. Hearn, J. Frenz, M. Kempe, F.E. Regnier)*
- **Capillary Zone Electrophoresis** *(K. B. Sentell, R. Kaliszan, J.P. Foley, G.G. Yowell)*
- **Discussion Sessions on Tayloring Stationary Phases for Molecular Recognition; Enantiomeric Separations with HPLC, CE or GC: Will One Technique Solve all of the Problems; Chromatographic Characteriza-tion of Glycoproteins; Supercritical Fluid Extractions and Chromatography**

WEDNESDAY — MAY 11, 1994

- **Advances in Packing Materials** *(P.W. Carr, F. Švec, K.-S. Boos, N. Tanaka, R. Ranis-Jansen)*
- **Capillary Electrophoresis – II** *(Y. Baba, P. Shieh, A.S. Cohen, W.J. Warren, J.G. Dorsey)*
- **Supercritical Fluid Extraction** (A.A. Clifford, H.J. Cortes, J.A. Field, J.W. King, S.B. Hawthorne)
- **Exposition**
- **Poster Sessions on Advances in Detection; Capillary Electrophoresis; Macromolecular Separations**
- **Novel Stationary Phases** *(H. Poppe, D.A. Whitman, S.V. Olesik, K. Jinno)*
- **Laser Detection** *(A.E. Bruno, R.E. Synovec, J.A. Koropchak, E.S. Yeung)*
- **Supercritical Fluid Chromatography** *(A. Malik, M.E.P. McNally, K. Anton, T.L. Chester)*
- **Seminars** — *One-hour sessions on the scientific basis of commercially available technology and hardware will be presented in parallel sessions. This is an opportunity to learn about the latest offerings from the corporate community*

THURSDAY — MAY 12, 1994

- **Preparative Chromatography** *(G. Guiochon, S.H. Hobbs, A.M. Katti, M.R. Schure, G. Carta)*
- **Separation Science in Glycobiology** *(R. O'Neill, R.J. Linhardt, M. Stefansson, B. Gillece-Castro, M.V. Novotny)*
- **Enantiomeric Separations by HPLC** *(H. Engelhardt, A.M. Stalcup, T.C. Pinkerton, J.L. Glajch, A.-F. Aubry)*
- **Exposition Closes**
- **Poster Sessions on Advances in Column Technology; Characterization of Mobile Phase Interactions; Environmental Analysis / Biological Analysis II**
- **Polymer Analysis & Characterization** *(J.C. Giddings, J.C. Kraak, E.M. Fujinari, P.D. DePhillips)*
- **Selected Topics** *(C.E. Lunte, D.S. Hage, H. Wang, J.-P. Chervet)*
- **Sample Preparation** *(J.S. Fritz, J.M. Rosenfeld, I.S. Krull, H. Lingeman)*
- **Discussion Sessions on Chromatographic Characterization & Isolation of Glycoproteins; Sample Preparation for HPLC; Future Directions for Capillary Electrophoresis; Preparative Scale Separations**

FRIDAY — MAY 13, 1994

- **Capillary Zone Electrophoresis** *(D.J. Harrison, S.C. Jacobson, J.W. Jorgenson, B.L. Karger)*
- **Fundamentals of Retention** *(A.J. Dallas, M. Jaroniec, J. Ståhlberg, C.M. Roth)*
- **Electrochemical Detection** *(S.G. Weber, A.C. Ewing, R.P. Baldwin, R. Townsend)*
- **Plenary Session II** — *(Cs. Horvath, W. Lindner)*

Analytical Applications of Circular Dichroism

Edited by **N. Purdie** and **H.G. Brittain**

Techniques and Instrumentation in Analytical Chemistry Volume 14

Circular dichroism is a special technique which provides unique information on dissymmetric molecules. Such compounds are becoming increasingly important in a wide variety of fields, such as natural products chemistry, pharmaceutics, molecular biology, etc. The content of this book has been selected in order to feature the unique aspects of circular dichroism, and how these strengths can be of assistance to workers in the field.

Substantial discussions have been provided regarding the particular phenomena associated with dissymmetric compounds which give rise to the circular dichroism effect. Reviews are also given of the type of instrumentation available for the measurement of these effects. A number of chapters cover the wide range of applications illustrating the power of the method.

Owing to its broad appeal, the book will be of interest to workers in all areas of chemistry and pharmaceutical science.

Contents:

© 1994 360 pages Hardbound
Price: Dfl. 355.00 (US $ 202.75)
ISBN 0-444-89508-6

ORDER INFORMATION

For USA and Canada
ELSEVIER SCIENCE INC.
P.O. Box 945
Madison Square Station
New York, NY 10160-0757
Fax: (212) 633 3880

In all other countries
ELSEVIER SCIENCE B.V.
P.O. Box 330
1000 AH Amsterdam
The Netherlands
Fax: (+31-20) 5862 845

US$ prices are valid only for the USA & Canada and are subject to exchange rate fluctuations; in all other countries the Dutch guilder price (Dfl.) is definitive. Customers in the European Community should add the appropriate VAT rate applicable in their country to the price(s). Books are sent postfree if prepaid.

ELSEVIER SCIENCE B.V.

PUBLICATION SCHEDULE FOR 1994

	S'93	O'93	N'93	D'93	J	F	M	A	M			
Analytica Chimica Acta	281/1 281/2 281/3	282/1 282/2 282/3	283/1 283/2	283/3 284/1 284/2	284/3 285/1–2 285/3	286/1 286/2 286/3	287/1–2 287/3 288/1–2	288/3 289/1 289/2	289/3 290/1–2 290/3			
Vibrational Spectroscopy		6/1			6/2		6/3		7/1			

INFORMATION FOR AUTHORS

Detailed "Instructions to Authors" for *Analytica Chimica Acta* was published in Volume 256, No. 2, pp. 373–376. Free reprints of the "Instructions to Authors" of *Analytica Chimica Acta* and *Vibrational Spectroscopy* are available from the Editors or from: Elsevier Science B.V., P.O. Box 330, 1000 AH Amsterdam, The Netherlands. Telefax: (+31-20) 5862459.

Manuscripts. The language of the journal is English. English linguistic improvement is provided as part of the normal editorial processing. Authors should submit three copies of the manuscript in clear double-spaced typing on one side of the paper only. *Vibrational Spectroscopy* also accepts papers in English only.

Rapid publication letters. *Letters* are short papers that describe innovative research. Criteria for letters are novelty, quality, significance, urgency and brevity. Submission data: max. of 2 printed pages (incl. Figs., Tables, Abstr., Refs.); short abstract (e.g., 3 lines); *no* proofs will be sent to the authors; submission on floppy disc; *no* revision will be possible.

Abstract. All papers and reviews begin with an Abstract (50–250 words) which should comprise a factual account of the contents of the paper, with emphasis on new information.

Figures. Figures should be prepared in black waterproof drawing ink on drawing or tracing paper of the same size as that on which the manuscript is typed. One original (or sharp glossy print) and two photostat (or other) copies are required. Attention should be given to line thickness, lettering (which should be kept to a minimum) and spacing on axes of graphs, to ensure suitability for reduction in size on printing. Axes of a graph should be clearly labelled, along the axes, outside the graph itself. All figures should be numbered with Arabic numerals, and require descriptive legends which should be typed on a separate sheet of paper. Simple straight-line graphs are not acceptable, because they can readily be described in the text by means of an equation or a sentence. Claims of linearity should be supported by regression data that include slope, intercept, standard deviations of the slope and intercept, standard error and the number of data points; correlation coefficients are optional.

Photographs should be glossy prints and be as rich in contrast as possible; colour photographs cannot be accepted. Line diagrams are generally preferred to photographs of equipment. Computer outputs for reproduction as figures must be good quality on blank paper, and should preferably be submitted as glossy prints.

Nomenclature, abbreviations and symbols. In general, the recommendations of IUPAC should be followed, and attention should be given to the recommendations of the Analytical Chemistry Division in the journal *Pure and Applied Chemistry* (see also *IUPAC Compendium of Analytical Nomenclature, Definitive Rules*, 1987).

References. The references should be collected at the end of the paper, numbered in the order of their appearance in the text (*not* alphabetically) and typed on a separate sheet.

Reprints. Fifty reprints will be supplied free of charge. Additional reprints (minimum 100) can be ordered. An order form containing price quotations will be sent to the authors together with the proofs of their article.

Papers dealing with vibrational spectroscopy should be sent to: Dr J.G. Grasselli, 150 Greentree Road, Chagrin Falls, OH 44022, U.S.A. Telefax: (+1-216) 2473360 (Americas, Canada, Australia and New Zealand) or Dr J.H. van der Maas, Department of Analytical Molecular Spectrometry, Faculty of Chemistry, University of Utrecht, P.O. Box 80083, 3508 TB Utrecht, The Netherlands. Telefax: (+31-30) 518219 (all other countries).

© 1994, ELSEVIER SCIENCE B.V. All rights reserved.

0003-2670/94/$07.00

No part of this publication may be reproduced, stored in a retrieval system or transmitted in any form or by any means, electronic, mechanical, photocopying, recording or otherwise, without the prior written permission of the publisher, Elsevier Science B.V., Copyright and Permissions Dept., P.O. Box 521, 1000 AM Amsterdam, The Netherlands.

Upon acceptance of an article by the journal, the author(s) will be asked to transfer copyright of the article to the publisher. The transfer will ensure the widest possible dissemination of information.

Special regulations for readers in the U.S.A.–This journal has been registered with the Copyright Clearance Center, Inc. Consent is given for copying of articles for personal or internal use, or for the personal use of specific clients. This consent is given on the condition that the copier pays through the Center the per-copy fee for copying beyond that permitted by Sections 107 or 108 of the U.S. Copyright Law. The per-copy fee is stated in the code-line at the bottom of the first page of each article. The appropriate fee, together with a copy of the first page of the article, should be forwarded to the Copyright Clearance Center, Inc., 27 Congress Street, Salem, MA 01970, U.S.A. If no code-line appears, broad consent to copy has not been given and permission to copy must be obtained directly from the author(s). The fee indicated on the first page of an article in this issue will apply retroactively to all articles published in the journal, regardless of the year of publication. This consent does not extend to other kinds of copying, such as for general distribution, resale, advertising and promotion purposes, or for creating new collective works. Special written permission must be obtained from the publisher for such copying.

No responsibility is assumed by the publisher for any injury and/or damage to persons or property as a matter of products liability, negligence or otherwise, or from any use or operation of any methods, products, instructions or ideas contained in the material herein.

Although all advertising material is expected to conform to ethical (medical) standards, inclusion in this publication does not constitute a guarantee or endorsement of the quality or value of such product or of the claims made of it by its manufacturer.

This issue is printed on acid-free paper.

PRINTED IN THE NETHERLANDS

Send your article on floppy disk!

All articles may now be submitted on computer disk, with the eventual aim of reducing production times and improving the reliability of proofs still further. Please follow the guidelines below.

With revision, your disk plus one final, printed and exactly matching version (as a printout) should be submitted together to the editor. **It is important that the file on disk to be processed and the printout are identical.** Both will then be forwarded by the editor to Elsevier.

The accepted article will be regarded as final and the files will be processed as such. Proofs are for checking typesetting/editing: only printer's errors may be corrected. No changes in, or additions to the edited manuscript will be accepted.

Illustrations should be provided in the usual manner and, if possible, on a **separate** floppy disk as well.

Please follow the general instructions on style/arrangement and, in particular, the reference style of this journal as given in the "Guide for Authors".

The preferred storage medium is a 5¼ or 3½ inch disk in MS-DOS or Macintosh format, although other systems are also welcome.

Please label the disk with your name, the software & hardware used and the name of the file to be processed.

For further information on the preparation of compuscripts please contact:

Elsevier Science B.V.
Analytica Chimica Acta
P.O. Box 330
1000 AH Amsterdam, The Netherlands
Phone: (+31-20) 5862 791 Fax: (+31-20) 5862459

ELSEVIER SCIENCE

0003-2670(19940420)289:1;1-7